Pumping of Concrete Mixtures: Rheology, Lubrication Layer Properties and Pumping Pressure Assessment

by

Jan Vosahlik

B.S., Czech Technical University in Prague, 2012
M.S., Kansas State University, 2014

AN ABSTRACT OF A DISSERTATION

submitted in partial fulfillment of the requirements for the degree

DOCTOR OF PHILOSOPHY

Department of Civil Engineering
College of Engineering

KANSAS STATE UNIVERSITY
Manhattan, Kansas

2018

Abstract

Pumping is the most utilized placement technique to deliver fresh concrete from the concrete mixer to the formwork on construction site. Compared to other available placement methods, such as bucket-and-crane or conveyor belts, pumping offers superior placement rates while reducing the required labor cost. Despite the fact that concrete pumping has been utilized on job sites around the world since the early 1960s, there is still a lack of knowledge, supported by research evidence, as to what affects concrete pumpability and how pumping changes concrete properties both in the plastic and hardened state.

A four-phase research study was carried out to: (1) improve the existing methodology of rheological characterization of the lubrication layer formed during pumping, (2) evaluate the effect of concrete mixture constituents and proportioning on rheological properties of concrete and the lubrication layer, (3) asses the effect of pumping and pumping pressure on concrete fresh properties and the air void system under controlled conditions, and (4) to evaluate the effect of pumping on concrete fresh properties and the air void system in the field conditions.

In the first phase of this research program, a correction procedure was developed evaluating 3D flow at the bottom of the cylindrical concrete interface rheometer. Results showed that the correction procedure can be successfully used for characterization of lubrication layer properties, and that the bottom of the cylinder can cause measurement error of up to 10% depending on concrete rheological properties and the interface rheometer geometry.

The second phase of this research program consisted of a laboratory study to evaluate rheological properties and properties of the lubrication layer of large variety of concrete mixtures. Considered mixture proportion variables included air void content, water-to-cement ratio, paste volume, fly ash replacement ratio, fine-to-coarse aggregate ratio, aggregate shape,

use of viscosity-modifying admixture, and use of nano-clay particles. Results indicated that the changes in rheological properties of the lubrication due to mixture proportioning adjustments corresponded in most cases to changes of the bulk concrete rheological properties.

In the third phase of the study, a full-scale controlled pumping experiment was conducted. During the experiment, three different concrete mixtures were pumped and both fresh and hardened properties of concrete were determined. Additionally, the pumping circuit was equipped with a system to monitor pumping pressures. The obtained results revealed that concrete pumping can significantly modify concrete fresh properties. Additionally, it was shown that changes in the fresh properties as well as in the concrete air void system are independent of applied concrete pressure.

Finally, the forth phase of this research program consisted of field evaluation of concrete pumping. Six concrete bridge project sites were visited and concrete samples were collected before and after pumping. Analysis results indicated that the changes in concrete properties appear to be influenced not only by mixture characteristics but also by discharge conditions in the formwork.

Pumping of Concrete Mixtures: Rheology, Lubrication Layer Properties and Pumping Pressure Assessment

by

Jan Vosahlik

B.S., Czech Technical University in Prague, 2012
M.S., Kansas State University, 2014

A DISSERTATION

submitted in partial fulfillment of the requirements for the degree

DOCTOR OF PHILOSOPHY

Department of Civil Engineering
College of Engineering

KANSAS STATE UNIVERSITY
Manhattan, Kansas

2018

Approved by:

Co-Major Professor
Christopher A. Jones

Approved by:

Co-Major Professor
Kyle A. Riding

Copyright

Abstract

Pumping is the most utilized placement technique to deliver fresh concrete from the concrete mixer to the formwork on construction site. Compared to other available placement methods, such as bucket-and-crane or conveyor belts, pumping offers superior placement rates while reducing the required labor cost. Despite the fact that concrete pumping has been utilized on job sites around the world since the early 1960s, there is still a lack of knowledge, supported by research evidence, as to what affects concrete pumpability and how pumping changes concrete properties both in the plastic and hardened state.

A four-phase research study was carried out to: (1) improve the existing methodology of rheological characterization of the lubrication layer formed during pumping, (2) evaluate the effect of concrete mixture constituents and proportioning on rheological properties of concrete and the lubrication layer, (3) asses the effect of pumping and pumping pressure on concrete fresh properties and the air void system under controlled conditions, and (4) to evaluate the effect of pumping on concrete fresh properties and the air void system in the field conditions.

In the first phase of this research program, a correction procedure was developed evaluating 3D flow at the bottom of the cylindrical concrete interface rheometer. Results showed that the correction procedure can be successfully used for characterization of lubrication layer properties, and that the bottom of the cylinder can cause measurement error of up to 10% depending on concrete rheological properties and the interface rheometer geometry.

The second phase of this research program consisted of a laboratory study to evaluate rheological properties and properties of the lubrication layer of large variety of concrete mixtures. Considered mixture proportion variables included air void content, water-to-cement ratio, paste volume, fly ash replacement ratio, fine-to-coarse aggregate ratio, aggregate shape,

use of viscosity-modifying admixture, and use of nano-clay particles. Results indicated that the changes in rheological properties of the lubrication due to mixture proportioning adjustments corresponded in most cases to changes of the bulk concrete rheological properties.

In the third phase of the study, a full-scale controlled pumping experiment was conducted. During the experiment, three different concrete mixtures were pumped and both fresh and hardened properties of concrete were determined. Additionally, the pumping circuit was equipped with a system to monitor pumping pressures. The obtained results revealed that concrete pumping can significantly modify concrete fresh properties. Additionally, it was shown that changes in the fresh properties as well as in the concrete air void system are independent of applied concrete pressure.

Finally, the forth phase of this research program consisted of field evaluation of concrete pumping. Six concrete bridge project sites were visited and concrete samples were collected before and after pumping. Analysis results indicated that the changes in concrete properties appear to be influenced not only by mixture characteristics but also by discharge conditions in the formwork.

Table of Contents

List of Figures

List of Tables

Acknowledgements

I want to express my sincere gratitude to my advisor, Dr. Kyle Riding, for giving me the opportunity and financial support to pursue my PhD studies under his supervision. Without his mentorship, guidance, encouragement and patience I would have not been able to accomplish what I have. Thank you for always supporting me, creating a fun working environment and your willingness to put up with my time management skills (or lack thereof). I am also forever grateful for your help with starting my post-academia professional career.

I want to thank to Dr. Dimitri Feys for his always well-thought advice and feedback, technical expertise he brought to the subject and his willingness to travel to Kansas when needed. Our collaboration was certainly something I truly enjoyed during my PhD program.

I want to thank my co-major professor, Dr. Christopher Jones, for his help pushing me across the finish line. I would also like to thank to my other supervisory committee members – Dr. Robert Peterman, Dr. Matthew Brueseke and Dr. Vinod Kumarappan – for their help and willingness to serve on the committee.

I would like to acknowledge the financial support of my research that was provided by the Kansas Department of Transportation. I want to thank to ACI Concrete Pumping and Fordyce Concrete Company for their support and help with our pumping experiments.

None of the research presented in dissertation would be possible without the help of many K-State undergraduate and graduate students. Thank you Abe Fangman, Ahmad Ghadban, Aref Shafiei, Cale Armstrong, Casey Keller, Hossein Mosavi, Jason Kane, Kirk Pfannenstiel, Koby Daily, Mohammed Albahttiti and Yadira Porras. Thank you K-State research technologists Ryan Benteman and Cody Delaney for your help with the equipment and labs.

Thank you to all my friends who made living 5,000 miles away from home enjoyable experience. Pablo, Lauren, Meghan, Marta, Kevin, Erica, and many others – thank you for keeping me sane.

Above all, I want to thank my parents for making me understand how important the education is in one's life. Without their emotional and financial support none of this would be possible. Mom, I am sorry I did not become a lawyer – concrete is much more fun!

Chapter 1 - Introduction

The need for a suitable concrete placement technique stems from the inherent nature of concrete production process. Concrete is a composite material that, in its most basic form, consists of four constituent materials: cement, water, fine aggregate (sand), and coarse aggregate (rock). However, modern concrete mixtures typically require more than the four basic ingredients, and products such supplementary cementitious materials (SCM), chemical admixtures, plastic or metallic fibers, saturated lightweight aggregates, super-absorbent polymers and many others are also often used. Upon completion of mixing, concrete must be placed into formwork to attain its final shape and begin the process of hardening, primarily facilitated by the cement hydration and pozzolanic reactions. Concrete pumping is often the placement technique of choice for many construction projects due to its versality, high placement rates compared to other placement techniques and low demand on human labor. Although concrete pumps became a common accessory of a construction site in the 1960s, there still exist significant gaps of evidence-based knowledge related to the concrete pumping process. In this dissertation, research aimed on filling some of these gaps is presented.

A robust experimental research program was developed and conducted both in laboratory and field conditions in order to investigate concrete pumping and how it affects concrete properties both in the plastic and hardened states. More specifically, the work presented in this dissertation had the following objectives:

(1) to assess and improve the existing methodology of rheological characterization of the lubrication layer in the laboratory;

(2) to evaluate the effect of concrete mixture constituents and proportioning on rheological properties of concrete and the lubrication layer;

(3) to determine the effect of concrete mixture constituents on pumping pressures through laboratory tools;

(4) to quantify pumping pressures generated in the pumping circuit during typical field pumping operation;

(5) to assess the effect of pumping and pumping pressures on concrete fresh properties, rheology and the air void system in controlled field conditions, and

(6) to evaluate the effect of pumping on concrete fresh properties, rheology and the air void system on real-world job sites.

This dissertation is comprised of seven chapters. In Chapter 2, the current state-of-the-art review of research literature on concrete pumping is provided. In Chapter 3, efforts leading to the development and evaluation of correction procedure for a concrete interface rheometer are discussed. Chapter 4 describes a laboratory study that was designed to evaluate rheological and other properties of the lubrication layer for a large variety of concrete mixtures. Mixture proportioning variables such as air void content, water-to-cement ratio, paste volume, fly ash replacement ratio, fine-to-coarse aggregate ratio, aggregate shape, use of viscosity-modifying admixture, and use of nano-clay particles and their effect on pumping pressure were all considered. In Chapter 5, a full-scale controlled pumping experiment is discussed. During the experiment, different concrete mixtures were pumped and both fresh and hardened properties of concrete were determined, in addition to active monitoring of pumping pressures during the experiment. Chapter 6 describes a field investigation campaign that was conducted to complement the full-scale experiment and provide additional insights into pumping of concrete in field conditions. Lastly, a summary of conclusions from each phase of this research work is provided in Chapter 7.

Chapter 2 - Literature Review

2.1 Introduction

2.1.1 Concrete Placement

Arguably, two primary concrete production approaches can be differentiated in the current concrete world: (1) precast and (2) ready-mixed concrete. The United States Geological Survey (USGS) data reveals that in 2016, approximately 83 million tons (75 metric tons) of portland cement was produced in the United States; 70% of which is used by the ready-mix industry [1]. Precast concrete products, such as girders, pipes, walls, barriers, etc., are fabricated in plants where concrete is mixed, placed into molds, cured, and finally transported to its destination. Since both mixing, placing and curing of concrete occurs at the same location, the need for sophisticated placement techniques is essentially eliminated. However, this is not the case for ready-mixed concrete. Ready-mixed concrete is primarily produced in a concrete plant, although exceptions such as portable on-site batch plants exist. Subsequently, concrete is transported to the construction site and placed into the formwork where it attains its final shape and is cured.

Commonly utilized concrete placement techniques include the use of buckets (Figure 2.1), hoppers, buggies, conveyor belts, paving equipment (Figure 2.2), tremies and finally pumps (Figure 2.3) [2]. Each of the listed placement techniques has distinguishing characteristics that serve specific purposes. For instance, buckets, hoppers or buggies are used for low-volume concrete placements such as driveways, floor slabs, etc.; concrete pavers are used to construct concrete pavements with low-slump concrete; conveyor belts are utilized for large-volume placements with concrete mixtures that are not suitable for pumping; and tremie pipes are used for under-water and underground placements. Concrete pumps were specifically developed for

large-volume, large placement rate concrete placements where no of the previously discussed techniques could be used. Additionally, the pumping approach is not used solely for ready-mixed concrete placements. Specialized cement-based materials, such as grout or shotcrete are also routinely pumped. Moreover, additive manufacturing with cement-based materials (i.e. 3D printing) that have recently gained a significant traction within the concrete industry also relies in many cases on hydraulic pumps to move concrete from a mixer through the printer nozzle.

Selection of an appropriate concrete placement technique requires consideration of various factors: construction site arrangement (is there enough space for placement equipment on the job site?), concrete volume to be placed, workability window of a concrete mixture that can be used for placement, fresh concrete properties, desired long-term properties of concrete, construction personnel availability, financial cost, etc.

Source: Crane bringing in the concrete by the bucket load by Washington State Department of Transportation, licensed under CC BY-NC-ND 2

Figure 2.1 – Bucket and crane

Source: WIRTGEN Slipform Paver, by Natalia Brandt, licensed under CC BY-SA 4.0

Figure 2.2 – Concrete paver

Source: NASA Photo / Tony Landis, Press Release

Figure 2.3 – Concrete pump

2.1.2 Concrete Pumping History

Although some sources suggest that concrete pumps were used during construction of the New York City subway as early as 1903 [3], the exact date of a concrete pump's first use is unknown. The first U.S. concrete pump patent application, however, was filled in 1913 and accepted in 1914 [4]. Since that time, concrete pumping has become a widely utilized and popular means of concrete transport worldwide.

Concrete pump design has also significantly evolved in the ensuing years since the initial patent. In the 1930s, a German company, Torkret, developed a single-cylinder concrete pump equipped with plate valves that replaced older ball valves and significantly improved pump performance. The product increased in popularity, with approximately 1,000 of the pumps produced by 1945. Torkret also sold commercial production licenses for these pumps to Milwaukee-based firm Rex, consequently allowing successful introduction to the American market in 1933 [3], [5].

Throughout the 20th century, German manufacturers led the progress in the pumping industry. Post-war periods of the 1950s and 1960s were marked with concrete pumping expansion due to increased construction activity associated with rebuilding infrastructure damaged during World War II. Immediately after the war, concrete pumps remained primarily mechanically driven; however, transition from a mechanical drive to hydraulic systems occurred throughout the following decades [6].

Since the early days of concrete pumping, concrete pumps and the pumping industry have faced many challenges. For example, in 2008, a highly flowable concrete mixture was pumped to a height of 1988 ft (606 m) as a part of the construction project to build the world's tallest building, the 2722 ft (830 m) high Burj Khalifa Tower [7]. In the same region, the largest

continuous concrete placement was achieved in 2017. In order to place 28,226 yd^3 (21,580 m^3) of concrete in over 35 hours, 18 concrete pumps had to be employed. An average placement rate of 799 yd^3/h (611 m^3/h) was achieved [8]. None of these record placements would be possible with traditional concrete placement techniques.

Companies such as Schwing or Putzmeister retain the status of leaders of the pumping industry, however, many U.S. companies have expanded their share of the market (Reed, Concord, or Alliance). Many pump producers in the United States collaborate in the Concrete Pump Manufacturers Association (CPMA). In addition, the American Concrete Pumping Association (ACPA) members include concrete pump owners, pump manufactures, and distributors of pumps and pumping accessories.

2.2 Pumping Equipment

2.2.1 Concrete Pumps

As mentioned, concrete pump design has changed noticeably since concrete pump invention in the 1930s. Mechanically driven pumps have been almost completely replaced by hydraulic systems and many improvements have been made in valve design [6]. Several types of concrete pumps and flow-controlling valves are discussed in this section.

2.2.1.1 Piston Pump

Currently, the most common type of concrete pump is a high-capacity dual piston pump [9]–[11]. Many piston concrete pumps that vary in detail are available for purchase, but they are conceptually identical. The three major parts of a piston pump are: (1) a concrete receiving hopper, (2) a valve system, and (3) a power transmission system [6], [9], as shown in Figure 2.4.

The hopper is commonly equipped with an agitator that prevents aggregate segregation and allows the fresh concrete to flow smoothly into the pistons. The pump performs in two

cycles: during the first cycle, concrete is drawn into one of the cylinders, utilizing suction created by the retreating piston, while the second piston moves in the opposite direction and discharges concrete into the pipeline. In the second cycle, pistons reverse their roles from the first cycle. Most pumps are driven by cylinders powered by hydraulic pumps, however some models of piston pumps are still driven by a mechanical system [9].

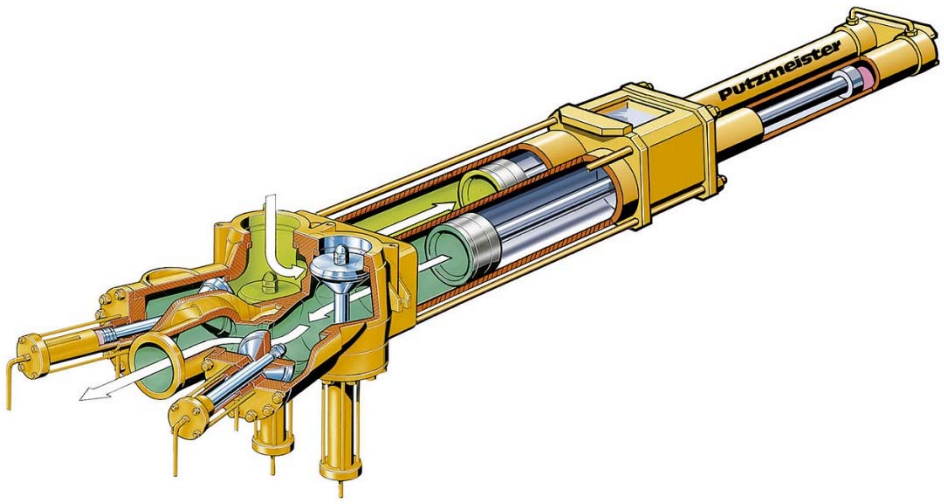

Figure 2.4 – Concrete hydraulic piston pump details

Source: Sitzventilpumpe, by Putzmeister Solid Pumps GmbH, licensed under CC BY-SA 3.0 DE

2.2.1.2 Worm Pump

A less common type of pump, though still widely used in the industry, is a worm pump, also referred to as a screw pump. The worm pump utilizes the principle of a screw that pushes concrete forward through a rubber stator. Worm pumps are used to pump workable mortars and highly flowable mixes with small aggregate sizes, such as shotcrete or flowable fill mixes, because these pumps typically operate at significantly lower pressures than standard piston pumps. For example, Putzmeister SP 11 Worm Pump is recommended for mixes with aggregate particle sizes up to 0.25 in. Cooke reported that a typical working range of a worm pump is approximately 145 to 220 psi (1 to 1.5 MPa) [6]. Technical simplicity of these pumps, and low

working pressures, makes them durable, long-lasting construction machines. A disadvantage of the worm-pump is that it cannot be used to facilitate pumping of stiff mixes with large aggregate particles.

2.2.1.3 Peristaltic pump

A peristaltic pump is another concrete pumping machine with a primary component consisting of a rotational device with rollers that squeezes a rubber hose in the pump body to create a suction that pushes concrete through the pump and to the pumping line. This pump also operates at low pressures and is highly reliable, however, similar to the worm pump, a peristaltic pump is not capable of pumping stiff concretes, consequently preventing its utilization on many job sites.

2.2.2 Pump Types Based on Mobility

Concrete pumps can be classified on the basis of their drive (mechanical/hydraulic), type of valve (hollow-core tube, ball, gate), or mobility. The three most common types of a concrete pump based on mobility are boom pumps, truck-mounted line pumps, and trailer pumps.

2.2.2.1 Boom Pumps

Boom pumps are commonly deployed for large projects in which big volumes of concrete must be pumped typically for long distances, such as a bridge deck or residential building construction. Modern boom pumps are state-of-the-art machines that require well-trained operators to oversee the pumping process. One of the biggest and most powerful concrete pumps currently available on the market, the Putzmeister 70Z, can pump 210 yd^3 (161 m^3) of concrete per hour, utilizing pressures up to 1,230 psi (8.5 MPa) [12].

A boom pump typically consists of a hopper, a pumping unit, and a flexible robotic arm (boom), as shown in Figure 2.5. The entire assemblage is mounted on a truck equipped with

outriggers for additional stability that allows the pump to be moved effortlessly to and around the construction site. Boom length starts from 6 ft (20 m), while the largest pumps on market offer booms that are more than 21 ft (70 m) long. The major advantages of boom pumps include their ability to pump large volumes of concrete over a short period of time, good maneuverability, flexibility, and the prevention of a necessary external pumping line for concrete because the pump is equipped with a boom.

Figure 2.5 – Boom pump

2.2.2.2 Truck-mounted pumps

Truck-mounted line pumps are essentially boom pumps without a long boom and corresponding pumping line. These pumps offer high power (the most powerful Putzmeister pump CP 2116H claims to have a capacity of 209 yd^3 (160 m^3) per hour), and thus are can be utilized at a large-scale construction site while providing higher mobility than traditional boom pumps. The disadvantage of truck-mounted pump is that these machines require installation of conventional pipelines to distribute the concrete on the site, hence use of a truck-mounted pump is more labor intensive than utilization of a boom pump. However, in limited working conditions

such as cities, parks, and dense housing developments, the smaller truck-mounted pumps are very often used to accommodate for these limitations.

2.2.2.3 Trailer pump

The least powerful type of concrete pump is a trailer pump, or a pump that is not mounted or attached to a transportation vehicle, thereby requiring means a semi-truck or a similar transportation to move the pump. An example of a trailer pump is shown in Figure 2.6. A trailer pump is typically utilized on jobs in which pumping speed is not essential because this pump's capacity is significantly lower than boom or truck-mounted pumps. For example, Putzmeister TK-70 offers pumping rate of only 74 yd^3 (57 m^3) per hour. However, trailer pumps maintain high working pressures, e.g. TK-70 specifications claim maximum concrete pressure to be 1130 psi (7.8 MPa). Trailer pumps are used to deliver concrete on small job sites, such as urban housing developments, or less traditional concrete applications, such as on shotcrete or grout pumping jobs. Trailer pump usage requires a stand-alone pipeline to transport concrete to its final location. These pumps are advantageous because they can be used in spatially restricted working conditions, and they have relatively low cost of operation compared to truck-mounted or boom pumps.

Figure 2.6 – Trailer pump

Source: Trailer pump by Judgefloro licensed under CC0 1.0

2.2.3 Valves

An essential element of each piston pump is a valve system that can be used to distinguish one type of pump from another. The valve ensures that concrete coming from two cylinders can be pushed through one line while providing a constant flow rate of concrete for the entire pumping circuit [9]. However, concrete pressure has been proven to fluctuate as piston position in the cylinders changes [10], [13]. In some instances, negative pressure in the system was also observed when the piston retreated immediately before the controlling valve opened for the discharging piston [11].

2.2.3.1 Gate valve

Many types of valves or valve systems are available on the market [14]. One of the earliest but still widely implemented valves in modern concrete pumps [6] is the gate valve, or the sliding gate valve or rotating visor valve. This valve consists of two distinct valves: one valve

that controls concrete flow from the hopper to the system and one valve that is responsible for concrete discharged to the pipeline. If the hopper valve is open, the output of the circuit is closed. Since both valves are perfectly synchronized, one piston is allowed to push concrete out to the pipes while the other valve draws concrete in from the hopper.

2.2.3.2 Flapper valve

The main component of flapper valve is a flapper blade. It is located in a flapper valve chamber where it swings rapidly from left to right, diving the chamber into two isolated compartments. One compartment is then allocated for the incoming concrete, while the outgoing concrete is allotted space in the second compartment. Although this valve system suffers significant wear over time, it can be easily reconditioned as its design is very simple from the mechanical point of view.

2.2.3.3 Hollow tube valve

The most commonly used valves are hollow transfer tube valves [6]. These valves can be divided into the following subcategories: rock valves, S-valve (or swing tube), and C valve. These valves incorporate a hollow pipe-like element into their designs. Variation in design details of hollow transfer tube valves occurs because many pump manufacturers have developed unique devices to be used only in their concrete pumps.

Rock valve

The rock valve is a registered trademark of Schwing [15]. This valve utilizes a single Y-shaped component that pivots so that the intake cylinder is always open to the hopper and the output piston is connected to the line. This type of valve is believed to provide a high sealing efficiency because the cutting ring maintains consistent contact with the wear plate.

S-valve

An S-valve, or swing valve, is a valve composed of a single tube that swings around the axis of the line from one cylinder to another, leaving one of the pistons always open for incoming concrete while the other cylinder is simultaneously connected to the pumping line. This type of valve has only small reduction in the valve body, translating into lower pumping pressures when the S-valve is used in the pump. Lower pressure also means that less friction is imposed on wear parts of the pump [14].

C-valve

Due to the swing motion of the tube, a C-valve is very similar to an S-valve. It is often referred to as an elephant trunk because of its distinct shape. A C-valve is a single-tube valve that swings from one piston to another; however, the valve tube has two bends that allow concrete transfer to the pipeline that is oriented in the opposite way to the all the other valves.

2.2.3.4 Ball valves

Historically, ball valves have been frequently used in concrete pumps, primarily in low-volume pumping units with pumping capacity less than 30 yd^3 (23 m^3) per hour [16]. A steel ball whose position is actuated by concrete flow drives the opening and closing of cylinders. Two types of pumps principally use ball valves: mechanically driven valves and pumps that use hydraulics as their primary driving force. In a ball valve, the ball, or set of balls moves with the concrete flow inside the pump, allowing concrete move only either to the intake piston or into the discharge cylinder. Although ball valves were once very popular in concrete pumps, to the author's best knowledge, they are not currently used in any industry-standard pumping machine.

2.2.4 Pipeline and Pumping Accessories

In addition to the concrete pump, other parts of the pumping circuit greatly influence the quality and safety of concrete pumping. Once concrete leaves the pump, it is transported through a pumpline, very often referred to as "line," to its final destination, usually flowing through a system of bends, reducers, and fittings. The entire assemblage interacts with pumped concrete and significantly influences pumping quality (rate, pressure loss) as well as properties of concrete after pumping (slump, air content, and rheological properties). This subsection provides an overview of frequently utilized pumping accessories, compiled using information gathered from commercial manufacturers of pumping equipment [17], [18].

2.2.4.1 Pumping line

The pumping line is composed of tightly connected pipe segments to provide an airtight system for transportation of the pressurized concrete. Standard material for a concrete pipe is steel, and it must be rated to sustain a pressure of 1,230 psi (8.5 MPa) according to current CPMA standards. Pipe diameter varies from 3 to 6 in. (76 to 152 mm), however, 4-in. (102-mm) and 5-in. (127-mm) diameter pipes are the most common sizes currently used on job sites. Two types of pipe are available: boom pipes and deck pipes. Boom pipes are specifically designed to fit into the system of a boom pump; deck pipes are generic pipes that can be deployed when stand-alone pumping circuit must be assembled on the construction site, such as when a truck-mounted or a trailed pump is used.

Each pipe is equipped with two coupling ends to allow for a smooth assemblage of the pipeline. These ends are welded to the pipe body. Weld quality is essential to pumping operation safety because working pressures in the pipeline can reach as high as 1,230 psi (8.5 MPa), and therefore any fracture in the weld could cause serious problems.

2.2.4.2 Other accessories

The pumping circuit contains many parts that have distinct functions. Standard concrete pumping accessory items are summarized in Table 2.1.

Table 2.1 – Concrete pump accessories

Accessory Type	Purpose
Couplings	Used to connect individual circuit pipes
Gasket	A seal placed into the coupling to prevent a loss of pressure
Elbows	Bends that allow directional change in the pumping circuit
Reducers	Incorporated if two (or more) sizes of pipes are used
Discharge hoses	A flexible end-part of the system, typically made from steel-reinforced rubber or a fabric-like material
Devices to slow concrete	Double S-bend elbow ("Rams horn") or other similar devices are sometimes used at the end of the pumping circuit to slow down discharging concrete. However, these devices are not recommended for use due to safety concerns [19].

2.3 Rheology of Concrete

2.3.1 Introduction

Rheology[1] is defined as "*the science of the deformation and flow of matter*" [20]. When applied to concrete, rheology deals with deformation and flow of concrete in the plastic state, i.e.

[1] The word "*rheology*" was first derived in the 1920s from the Greek term *rheos*, meaning stream.

before setting. Understanding concrete rheology is the key to understanding concrete behavior at early stages of its life cycle. Rheology directly affects how concrete is mixed, transported, placed and finished. However, rheology of fresh concrete can also impact concrete long-term properties: for instance, poor consolidation due unsatisfactory concrete workability[2] can lead to honeycombing, which can subsequently reduce concrete compressive strength. As concrete is pumped in the fresh state, concrete rheology is a significant factor affecting the overall performance of the pumping process.

2.3.2 Basic Principles

Concrete is a combination of several constituent materials in various states. Cement, SCM, fine and coarse aggregates, fibers, and others are solid materials, whereas water, chemical admixtures and air are fluids. Therefore, fresh concrete is a system of solid particles dispersed in a liquid medium, i.e. a suspension. Fresh concrete is a complex suspension with constantly changing properties due to both chemical (i.e. cement hydration and pozzolanic reaction) and physical (i.e. thixotropy) processes occurring simultaneously, hence it is extremely difficult to characterize it as either a pure fluid or a solid, and a more intricate approach is often required. When determining whether the concrete fresh system acts more as a solid or as a liquid, the so-called Deborah number can be useful. This concept, originally proposed by a famous Israeli scientist Reiner[3] is defined as a ratio of the time of relaxation to the time of observation [21], as shown in Eq. 2-1:

---

[2] Workability - property of freshly mixed concrete or mortar that determines the ease with which it can be mixed, placed, consolidated, and finished to a homogenous condition [84].

[3] Marcus Reiner (1886 - 1976), together with Eugene Bingham, are considered to be founders of the modern science of rheology. Reiner is known, among others, for formulations of the Buckingham-Reiner and the Reiner-Riwlin equations.

$$D_e = \frac{t_R}{t_0} \quad \text{Eq. 2-1}$$

where D_e is the Deborah number, t_R is the relaxation time and t_0 is the time of observation. The relaxation time refers to the time it takes the substance to reach an equilibrium state (i.e. how long it flows) whereas the observation time refers to the time domain of the observer (i.e. how long we measure the flow). The difference between solid-like and fluid-like behaviors is then defined by the magnitude of the number. When the number is close to zero (i.e. $t_0 >> t_R$), the material exhibits a liquid-like (plastic) behavior, when $t_R << t_0$, the material acts solid-like (i.e. it is elastic). Finally, when it approaches unit (i.e. $t_0 \sim= t_R$), the material exhibits both solid-like and liquid-like (viscoelastic) behavior [22]. This is typically the case for a fresh cementitious system. Hence, to understand fresh concrete rheology, deformation characteristics of all constituent phases and their respective behaviors, i.e. solids and fluids, must be studied.

2.3.2.1 Solids

Solid materials have specific characteristics that make them clearly distinguishable from liquids: they retain a fixed volume and shape, they are not compressible, and they do not flow. These macro-properties reflect the internal arrangement of particles that form solids (atoms, molecules, ions); these particles are tightly packed, often in a regular pattern. Coussot distinguished five groups of solid materials based on their microscopical structure: (a) crystalline solids, (b) glasses, (c) reticulated polymers, (d) colloidal aggregates, and (e) concentrated foams or emulsions [23]. Crystalline solids are the basic form of solid materials, and the behavior of such solids under deformation is very well understood.

When a small load is applied, most solid materials experience a deformation that is linearly proportional to the magnitude of stress and, upon removal of the load, the material

reverts to its original shape. This deformation regime, referred to as elastic, is defined by Hooke's Law, described in its general form by Eq. 2-2 and Eq. 2-3:

$$\sigma = E\epsilon \quad \text{Eq. 2-2}$$

$$\tau = G\gamma \quad \text{Eq. 2-3}$$

where σ and τ are principal and shear stress, respectively, ε and γ are corresponding normal and shear strains, and E and G are material constants that define the amount of deformation for a corresponding load (i.e. Young's and shear moduli).

When the solid material micro-structure is under applied load, one can observe that the atoms were slightly displaced from their original positions. Before the deformation, all the atoms were in equilibrium at their lowest potential energy levels. The applied load caused these particles to transform to a new state of equilibrium on a higher energy level, but once the load is removed, atoms assume their initial position (assuming only small deformation was induced in the material). This behavior is described as *elastic* [23].

As the load level reaches a certain point, typically called the yield point, a fraction of the material's atoms receive a large amount of energy and move far enough from their original position to cause a dislocation in the crystalline structure. Remaining atoms, however, take advantage of these dislocations and change their position; therefore, the material persists in an arranged structure. This process corresponds to *plastic* behavior at a macroscopic scale typical for many materials; plastic deformation is non-reversible deformation. In fact, no purely linear-elastic materials exist because all materials yield permanent deformations upon the load removal, although these deformations are often neglected for engineering purposes [23].

If loading continues, all atoms are separated, and the material exhibits fracture on a macroscopic scale. A combination of elastic and plastic responses under an external load defines the *elasto-plastic* deformational model. This model is characteristic of many material types,

including reinforced concrete. However, concrete in a fresh state cannot be characterized as a crystalline solid, therefore the term "soft solid" is sometimes used. A soft solid typically does not have an organized internal structure, but it still demonstrates some solid-like behavior. This is obvious when poured into a container; pure fluid has a perfectly leveled horizontal surface in a container, whereas a soft solid material is uneven and often retains its shape. It is difficult to characterize behavior of soft solid systems due to their nature; they are often composed of different size particles, such as coarse and fine aggregate grains in cement paste that cause development of various interactions between these elements [23].

2.3.2.2 Fluids

Unlike solids, fluids do not retain a fixed shape. Their deformation characteristics defines them very well: they have zero shear modulus, in other words, continually flow under applied shear stress as long as the applied shear stress is greater than yield stress of the fluid. Newtonian fluids and non-Newtonian fluids are two groups of commonly distinguished fluids [24]. To be able to discuss these fluid types, basic terms must be defined.

The elasticity theory defines stress as a force divided by the area over which the stress is applied, and the strain is relative deformation caused by the stress. For shear deformation, this can be mathematically expressed as:

$$\tau = \frac{P}{A} \qquad \text{Eq. 2-4}$$

where τ is shear stress, P is applied force, and A is the area over which the force is applied, and

$$\gamma = \frac{x}{d} \qquad \text{Eq. 2-5}$$

where γ is shear strain, x is relative element deformation of the element and d is element height, as shown in Figure 2.7.

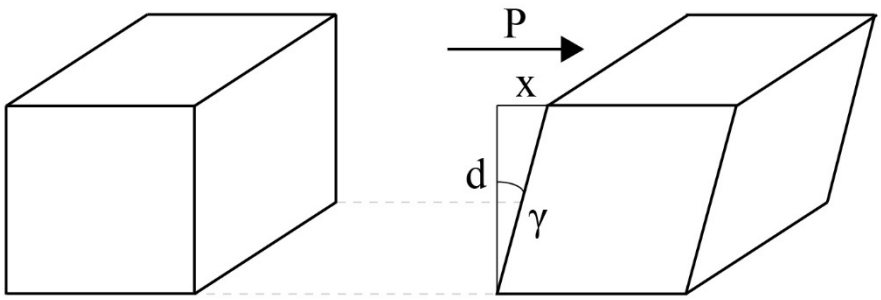

Figure 2.7 – Shear deformation

Consider two solid parallel plates with fluid filling the space between plates, as shown in Figure 2.8.

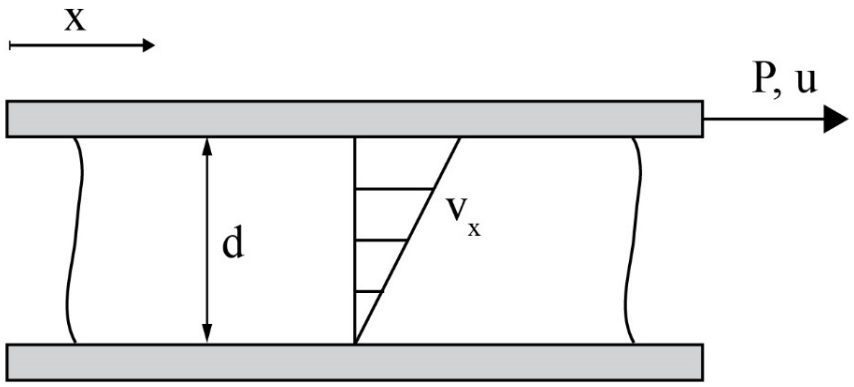

Figure 2.8 – Shear rate, adapted from [24]

Assuming no slip occurs between surfaces and force *P* action on the upper plate, strain produced over an increment of time *dt* is defined by Eq. 2-5.

Recall that velocity *u* can be defined as the first derivative of displacement *x* with respect to time *t*, as shown in Eq. 2-6:

$$u = \frac{dx}{dt} \qquad \text{Eq. 2-6}$$

Therefore, the rate of shear strain $d\gamma$ with respect to time *t* becomes

$$\frac{d\gamma}{dt} = \frac{dx}{ddt} \quad \text{Eq. 2-7}$$

which can be rewritten as

$$\dot{\gamma} = \frac{u}{d} \quad \text{Eq. 2-8}$$

The term $\dot{\gamma}$ is a basic deformation parameter of a fluid matter, referred to as rate of strain, velocity gradient, or shear rate.

Newtonian fluids

The relationship between shear stress τ and shear rate $\dot{\gamma}$ is linear for a Newtonian fluid[4]. The slope in the equation that describes this relationship is viscosity, also designated as apparent or shear viscosity, and typically denoted κ, η or μ[5]. The fundamental unit of viscosity is Pa.s. Because it represents resistance of a fluid to flow, viscosity can be visualized as internal friction between fluid layers. Outside of the academic world, viscosity is referred to as thickness; water is considered to be thin while honey is considered to be thick. Shear behavior of a Newtonian fluid can be formulated by Eq. 2-9:

$$\tau = \mu\dot{\gamma} \quad \text{Eq. 2-9}$$

However, constant viscosity under different shear rates is not the only requirement for a fluid to be characterized as Newtonian. Barnes [24] defined additional requirements for Newtonian behavior:

1. Shear viscosity is constant and does not vary with shear rate.

[4] Named after Isaac Newton (1642 – 1726/7) who defined the relationship between shear stress, strain and viscosity in the second book of his *Philosophiae Naturalis Principia Mathematica* (1687).

[5] μ is used throughout this dissertation

2. The only stress generated in simple shear flow is shear stress, the two normal stresses are zero.
3. Viscosity is constant with respect to time of shearing, and stress in the liquid falls to zero immediately when shearing stops.
4. Viscosities measured in various types of deformation are always in proportion to one another. For example, the viscosity measured in uniaxial extensional flow is always three times the value measured in simple shear flow.

Typical representations of a Newtonian fluid includes water with viscosity of 10^{-3} Pa.s at room temperature or glycerol with viscosity of 1.5 Pa.s.

Non-Newtonian fluids

Fluids that do not meet one of the requirements for Newtonian fluids are considered to be non-Newtonian liquids [24]. These types of fluids often fail to meet the first requirement of Newton fluids that viscosity is independent of shear rate. Shear stress for non-Newtonian fluid can be expressed after Wallevik as [25]:

$$\tau = \mu_{(\dot{\gamma})}\dot{\gamma} \qquad \text{Eq. 2-10}$$

Viscosity can develop according to two scenarios. In the first scenario, viscosity increases with shear rate, causing liquids to demonstrate behavior consistent with shear-thickening materials, such as Silly Putty, a silicone polymer-based toy. When viscosity decreases with an increase in shear rate, the fluid experiences shear-thinning. Modern paints or ketchup are both

shear-thinning fluids. The power-law model (or Ostwald–de Waele[6] relationship) is often used to characterize non-Newtonian fluids, and its general relationship is described by Eq. 2-11.

$$\tau = \mathrm{K}(\dot{\gamma})^n \qquad \text{Eq. 2-11}$$

where *K* is flow consistency index (Pa.s^n), and *n* is the flow behavior index. For $n = 1$, the fluid becomes Newtonian. For $n < 1$, shear-thinning behavior is observed, and for $n > 1$, shear thickening behavior can be expected.

Many fluids, including fresh concrete, must overcome an initial value of stress in order to flow. This behavior is described by the Bingham[7] fluid model. Bingham fluid does not flow until yield stress τ_0 is exceeded; once yield stress is achieved, the fluid is characterized by a constant value of plastic viscosity μ_p. In a mathematical form, Bingham fluid can be defined according to Eq. 2-12:

$$\tau = \tau_0 + \mu_p \dot{\gamma} \qquad \text{Eq. 2-12}$$

2.3.2.3 Suspensions

Suspension, according to McNaught, is a "*dispersion of solid particles in a liquid.*" [26] In fresh concrete, cement, coarse aggregate and fine aggregates represent solid particles dispersed in a liquid (combination of water, air and chemical admixtures). Some suspension definitions require solid particles to be sufficiently large so that if the suspension is left undisturbed, solids eventually settle down. However, this condition is not applicable to majority of fresh concrete mixtures because it can behave as suspension only for a limited time that does

[6] Reiner named the model in 1933 [133] after two papers published on the same topic by Wilhelm Ostwald (1853 – 1932) [134] and Armand de Waele (1887 – 1966) [135].

[7] Named after Eugene C. Bingham (1878-1945), American scientist who proposed its formulation in 1916 [31].

not allow for particle sedimentation, unless the mixture is unstable and prone to aggregate segregation. If left undisturbed, concrete eventually hardens and transforms into the solid phase.

If a suspension is subjected to shear deformation, three types of interactions that defines its rheological characteristics occur in the structure matter: hydrodynamic, solid interactions, and colloidal interactions [27]. Hydrodynamic interactions occur in the liquid phase of suspension and dominate behavior of liquid materials. Solid interactions (slippage, friction) are typical for solid matters and colloidal interactions such as inter-particle forces and Brownian motion are characteristic for the colloidal system. Therefore, solid volume concentration Φ, i.e. ratio of volume of solid elements to volume of the sample, and particle size distribution of the solids greatly affect the contribution of each kind of interaction to suspension behavior.

Figure 2.9 illustrates the effect of the solid volume concentration on viscosity of the suspension. The vertical axis in the figure represents relative viscosity, which is a ratio of suspension viscosity to viscosity of the Newtonian fluid that constitutes the suspension. As shown in the figure, when the number of solid particles is relatively low, viscosity of the suspension is very similar to the viscosity of the fluid (i.e. μ/μ_p is close to 1). As the particle concentration rises, the relative viscosity increases. When solid volume concentration reaches a critical value of Φ_m, solid interactions become dominant and the suspension experiences predominantly a solid-like behavior. Suspensions with high concentration of solid particles may exhibit density heterogeneities because particles can slightly migrate within the phase, creating regions with both high and low levels of solid particles concentration. Subsequently, regions with low solid volume concentration can exhibit fluid-like behavior, while zones with high solid volume concentration values can behave as solids, thereby increasing the complexity of rheological characteristics of the material because two dissimilar flow regimes must be

considered. Although this example considers Newtonian fluid to be the liquid medium in the suspension, similar behavior can be observed in fresh concrete. Mixtures with high water content (low Φ) are more "fluid," while “stiff” mixtures (low water content and high Φ) have higher resistance to flow, i.e. viscosity.

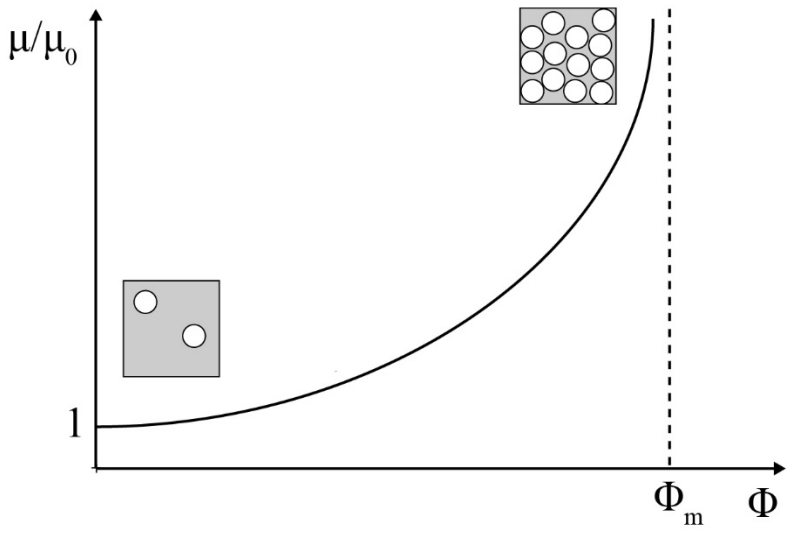

Figure 2.9 – Relative viscosity of a suspension in a Newtonian liquid, adapted from [23]

2.3.3 Rheological Models of Cement-Based Systems

Many rheological models describe the behavior of concrete under shear flow. The Bingham fluid model is the most commonly used, as discussed in Section 2.3.2. However, the Bingham model is not a universal tool and it might be quite problematic to implement to characterize behavior of all existing types of concrete. For example, a non-linear, shear-thickening behavior of fresh SCC was reported previously [28]–[30]. To model this behavior, the Herschel-Bulkley model is often utilized. It is based on the general power-law model and enhanced by addition of the yield stress component, as shown in Eq. 2-13.

$$\tau = \tau_0 + \mathrm{K}(\dot{\gamma})^n, \tau \geq \tau_0 \qquad \text{Eq. 2-13}$$

A comprehensive list of rheological models utilized for cement-based systems is listed in Table 2.2. Coefficients *A*, *B*, and *C* in represent constants, which in some cases include material parameters. The choice of an appropriate model for rheological characterization of concrete is critical. Although the Bingham model is the model of choice for majority of concretes, it can produce inaccurate results, or even results that are physically impossible such as negative yield stress values for concrete mixtures that do not exhibit linear behavior over the whole shear rate domain.

Table 2.2 – Flow models of cement-based materials, adapted [22]

Model	Governing Equation	Reference
Bingham	$\tau = \tau_0 + \mu(\dot{\gamma})$	[31]
Herschel-Bulkley	$\tau = \tau_0 + \mathrm{K}(\dot{\gamma})^n, \tau \geq \tau_0$	[32]
Robertson-Stiff	$\tau = A(\dot{\gamma} + \mathrm{B})^C$	[33]
Modified Bingham	$\tau = \tau_0 + \mu(\dot{\gamma}) + B\dot{\gamma}^2$	[34]
Casson	$\sqrt{\tau} = \sqrt{\tau_0} + \sqrt{\mu\dot{\gamma}}$	[35]
Yahia and Khayat	$\tau = \tau_0 + 2\sqrt{\tau_0 \mu\dot{\gamma} e^{-A\dot{\gamma}}}$	[34]
Quemada	$\tau = \left(\frac{1+\sqrt{A\gamma}}{B + C\sqrt{A\gamma}}\right)^2 \dot{\gamma}$	[36]
Vom Berg	$\tau = \tau_0 + Asinh^{-1}(B\dot{\gamma})$	[37]

2.3.4 Concrete Rheometry

Rheometry is a discipline that focuses on experimental determination of mechanical properties of substances classified as fluids [38]. For concrete, the primary objective of rheometry is to measure rheological parameters of fresh concrete, especially viscosity and yield stress, or Bingham parameters.

Ovarlez [39] stated that the relationship between general stress tensor σ_{ij} and strain rate tensor d_{ij} must be known in order to successfully characterize the general flow of fluid matter. However, obtaining this relationship is a complex problem, so the objective of rheometry is to simplify this relationship. The relationship is measured by subjecting the fluid only to simple shear, i.e. when only one component of the strain rate tensor remains non-zero. In addition, if shear rate $\dot{\gamma}$ is constant along the y-direction, simple shear is homogeneous. Theoretically, ideal homogeneous simple shear can be achieved by inserting fluid matter between two plates of an infinite surface area and imposing different velocities on each plate.

Various geometries have been used to simulate homogeneous shear on finite geometries. The three main geometries are (1) parallel plates, (2) cone and plate, (3) and Couette (or coaxial or concentric) cylinder, as shown in Figure 2.10 [39]. Parallel plate and coaxial cylinder geometries were successfully incorporated in concrete rheometers [40], [41].

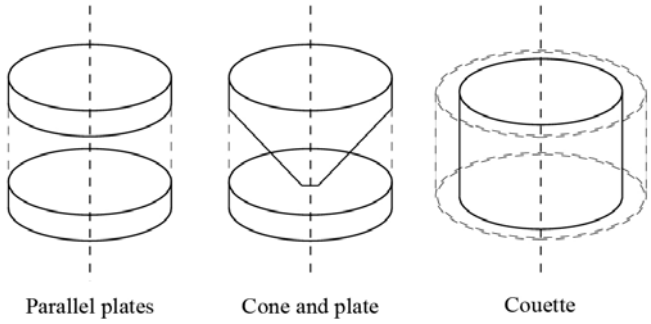

Figure 2.10 – Rheometer geometries, adapted from [39]

2.3.4.1 Principles of Rheological Measurements

No matter the rheometer geometry, virtually all devices that have been developed for rheological characterization of cement-based suspensions are not capable of directly measuring the basic viscoelastic quantities of shear stress and shear rate. Typically, device-specific quantities such as torque, force, and linear or rotational velocities are registered, and

transformation equations are needed to obtain shear stress and rate values. In this section, principal transformation equations for concentric cylinder rheometers are introduced.

Consider the concentric cylinder rheometer with geometry as shown in Figure 2.14 with a rotating inner cylinder.

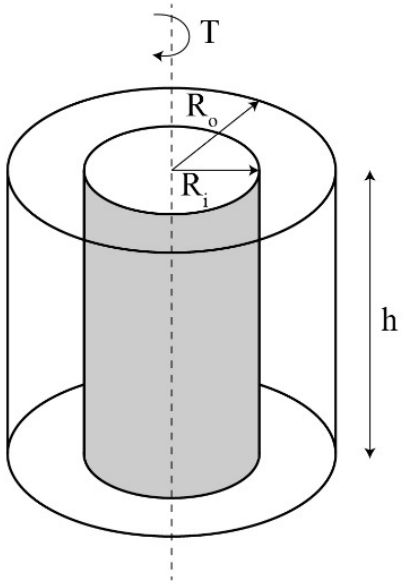

Figure 2.11 – Concentric cylinder rheometer

Shear stress can be calculated directly from the registered torque *T* using Eq. 2-14 [24], [42]:

$$\tau(r) = \frac{T}{2\pi R_o^2 h} \qquad \text{Eq. 2-14}$$

where *r* is a radial parameter that corresponds to the distance between inner cylinder radius R_i and outer cylinder radius R_o (as shown in Figure 2.14), and *h* is height of the cylinder.

Determining shear rate becomes much more complicated. Based on the rheometer geometry, two scenarios are possible:

(1) For a rheometer with a very small gap between the inner and outer cylinder (R_i/R_o > 0.99), it is assumed that the shear rate is constant over the gap, and the shear rate can be calculated as follows [43]:

$$\dot{\gamma}(R_i) \cong \dot{\gamma}(R_o) = \frac{2\omega_i \bar{R}}{R_o - R_i} \quad \text{Eq. 2-15}$$

where $\bar{R} = R_o + R_i/2$ is the mean radius and ω_i is the angular velocity of the rotating (inner) cylinder. However, it is not realistic to assume a small gap for concrete rheometry, particularly due to coarse aggregate size that must fit in the gap to truly measure concrete rheology.

(2) When the small gap condition is not met, the shear rate is not constant over the gap, and Eq. 2-16 can be used [24]:

$$\dot{\gamma} = \frac{2\omega_i}{n(1 - b^{2/n})} \quad \text{Eq. 2-16}$$

where b is the ratio of the inner and outer cylinder radius (R_i/R_o), and the coefficient n can be calculated as follows [43]:

$$n = \frac{d \ln T}{d \ln \omega_i} \quad \text{Eq. 2-17}$$

This coefficient is a slope of the torque-rotational velocity curve on log-log scale and corresponds to the n factor in the power-law model (see Section 2.3.3).

However, the use of Eq. 2-16 is not straight-forward due to its complexity and the fact that the n factor depends on rotational velocity [44].

Therefore, an alternative transformation procedure using the Reiner-Riwlin[8] equation can be used to obtain basic rheological quantities [45]. Yield stress and plastic viscosity can be determined according to Eq. 2-18 and Eq. 2-19, respectively [44], [45].

$$\tau_0 = \frac{\frac{1}{R_i^2} - \frac{1}{R_o^2}}{4\pi h ln\left(\frac{R_o}{R_i}\right)} G \qquad \text{Eq. 2-18}$$

$$\mu_p = \frac{\frac{1}{R_i^2} - \frac{1}{R_o^2}}{8\pi^2 h} H \qquad \text{Eq. 2-19}$$

where H is a slope of the torque-rotational velocity relationship and H is an intercept of the same relationship.

The Reiner-Riwlin transformation is also available for the modified Bingham and Herschel–Bulkley models [46].

Finally, for non-Newtonian fluids, the obtained results must be evaluated and adjusted for the presence of plug flow [44]. For coaxial rheometry, it is assumed that material between both cylinders is sheared. However, it is possible that the shear stress (that decreases by the power of 2 with increasing distance from the rotating cylinder) can be lower than yield stress of tested material, i.e. the material is not entirely sheared, as shown in Figure 2.14.

[8] This equation is often misspelled "Reiner-Rivlin" and confused with the Reiner-Rivlin fluid formulation. However, there is an interesting connection between these two. Reiner-Rivlin fluid is a non-Newtonian fluid which constitutive equations were independently developed by a British-American scientist Ronald Samuel Rivlin (1915 – 2005) and the famous Marcus Reiner (1886 – 1976) [136], [137]. Both scientist never worked together, however, their areas of interest overlapped to some extent, eventually leading to formulation of the so-called Reiner-Rivlin fluid. On the other hand, the Reiner-Riwlin equation was developed in 1927 by the same M. Reiner, however, the co-author of this work was Rassa Riwlin (PhD University of Utrecht, 1923). In this case, Reiner and Riwlin actually worked together on solving the problem. The fascinating part of this story is that Rassa Riwlin was in fact an aunt of Ronald Rivlin. She died very young in a car accident, therefore is not as known as her famous nephew.

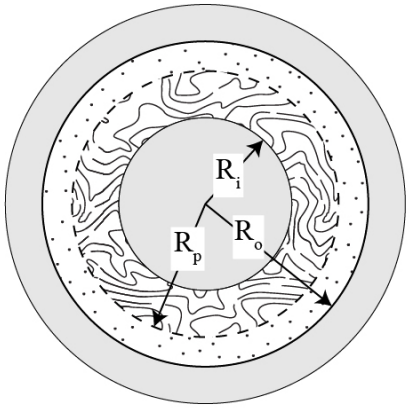

Figure 2.12 – Concentric cylinder rheometer – plug flow

The no-shear zone is called the plug, and its radius R_p can be calculated as [44]:

$$R_p = \sqrt{\frac{T}{2\pi\tau_0 h}} \qquad \text{Eq. 2-20}$$

If the plug radius is greater that the radius of the outer cylinder (i.e. $R_p > R_o$), all material in the rheometer is sheared. If that is not the case, a plug exists in the rheometer and the shear rate can be calculated (for Bingham fluid) using the following equation based on the Reiner-Riwlin relationship [44]:

$$\dot{\gamma} = \frac{2}{R_i^2}\left(\frac{1}{R_i^2} - \frac{1}{R_p^2}\right)^{-1}(\omega + \frac{\tau_0}{\mu_p}\ln\frac{R_p}{R_i}) - \frac{\tau_0}{\mu_p} \qquad \text{Eq. 2-21}$$

It is apparent from Eq. 2-20 that the plug radius depends on applied torque and can be only calculated when yield stress of the tested material is known. Similarly, Eq. 2-21 contains values of the yield stress and plastic viscosity that are not known at the time of measurement. Therefore, an iterative procedure assuming initial values of yield stress and plastic viscosity is required to obtain real rheological properties.

2.3.4.2 Thixotropy

Thixotropy is a decrease of apparent viscosity under shear stress, followed by gradual recovery when stress is removed [38]. Therefore, thixotropy is a reversible process, as shown in Figure 2.13. The thixotropic effect in fresh concrete is associated with the colloidal nature of the suspension. When concrete is left undisturbed, attracting forces acting on the particles result in a formation of connections between these particles. A flocculation effect can be observed, leading to an increase in viscosity. If energy is supplied to the system, such as a shear force, connections are broken, the suspension de-flocculates, and viscosity decreases [47] . This time-dependent phenomenon must be taken into account for rheological testing of fresh concrete because incorrect results could be obtained in absence of time-dependent consideration. Concrete must be "pre-sheared" before rheological tests to eliminate the thixotropy effect and achieve equilibrium.

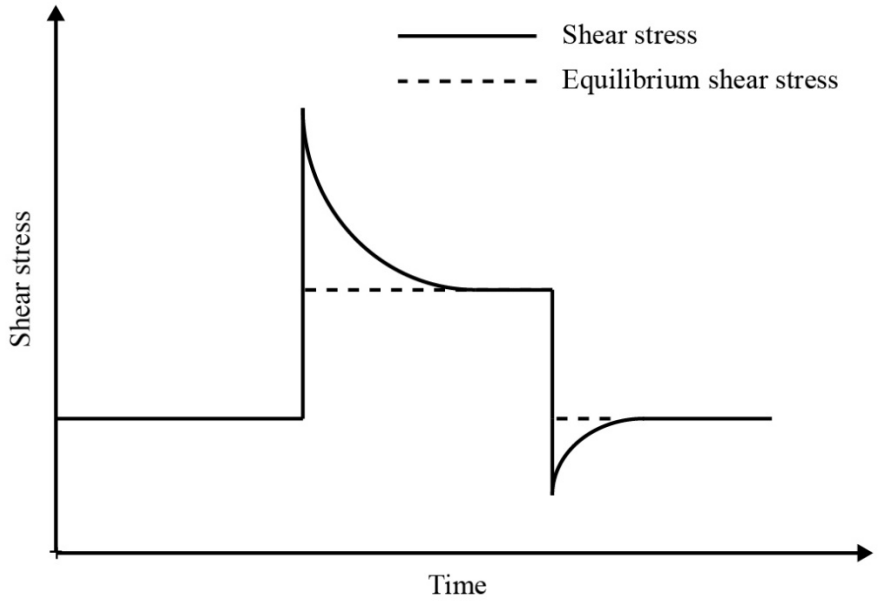

Figure 2.13 – Thixotropy

2.3.4.3 Structural breakdown

The term "structural breakdown" refers to a phenomenon in which connections formed by the hydration process of cement are broken [47]. Within a few seconds of initial contact between cement and water, a calcium silicate hydrate (CSH) membrane is formed around the cement particles. When more than one particle comes into contact with water, a membrane forms and covers all particles at once. However, as soon as the cement paste is agitated, this bridging membrane breaks. No recovery of those membranes was measured, therefore, in contrast to thixotropy, this process is considered irreversible [47].

2.3.4.4 Loss of workability

Loss of workability is a phenomenon characterized by reduction of fresh concrete workability over time due to formation of permanent connections in the concrete matrix. These connections are either chemical bonds created by hydration of cement grains, or they are connections formed by flocculation processes. Workability loss is influenced by many factors, including the mixing procedure, use and time of addition of water-reducing admixtures and reactivity of the cementitious system [48].

2.3.4.5 Concrete Rheometers

Numerous models of concrete rheometers were developed and are used to characterize rheological properties of fresh concrete. The following list provides an overview of several concrete rheometers that have been widely used in research and practice.

Tattersall two-point device

G. H. Tattersall has developed a series of rheometers (Mk I, Mk II and Mk III) that were reportedly first devices that measured concrete as a Bingham fluid [49]. His devices were based on the Hobart food mixers and utilized various impellers that sheared the concrete sample either

in axial or planetary motion. The torque was indirectly measured by recording input power required for shearing the sample at a certain rotational speed [50].

IBB Rheometer

The IBB rheometer is a modified version of Tattersall's Mk III device. This rheometer was originally developed to study rheology of shotcrete, however, was successfully used for other types of concrete mixtures [51]. The geometry of the rheometer is identical to the Mk III device, i.e. H-shaped impeller (inner cylinders) that moves in a planetary motion in a cylindrical bowl (i.e. outer container).

ConTec viscometers

ConTec has developed a family of rheometers that can be used to evaluate rheological properties of fresh concretes and mortars. This series of rheometers are also referred to as BML viscometers in the literature [41]. Several ConTec devices available on the market, including ConTec Viscometer 4, ConTec Viscometer 5, ConTec Viscometer 6, ConTec Rheometer-4SCC, etc. All these devices utilize two concentric cylinders to perform the measurement. The outer cylinder is defined by the steel container in which the tested concrete is placed, while the inner cylinder is a vane positioned in the center of the container. Both cylinders are equipped with vertical ribs to prevent concrete slipping along the cylinder walls. The inner cylinder is composed of an upper and lower part. The upper part registers torque; the lower part, which does not participate in measurement, is implemented in the system only to eliminate three-dimensional flow at the bottom of the inner cylinder [52]. During the testing procedure, the inner cylinder remained stationary and the outer cylinder rotates around its vertical axis.

BTRHEOM

The BTRHEOM is a French parallel plate rheometer capable of testing concretes with aggregate sizes up to 0.25 in (6.35 mm) [53]. The BTRHEOM consists of a reservoir with an outer radius of 120 mm and a top plate mounted on a rotational shaft (connected to the torque-registering device) located in the center of the container. The bottom of the container and the top plate are equipped with blades that prevent the slip of material on the plate-concrete interface. Additionally, to avoid concrete slipping on the container wall-concrete boundary, a portion of the vertical wall rotates with the concrete. According to Feys [52], container wall rotation disturbs the velocity profile near the edges of the container and potentially causes discrepancies in the measurements. However, ConTec and BTRHEOM showed some agreement in simultaneous rheological measurements [41].

ICAR Rheometer

The International Center for Aggregate Research (ICAR) in Austin, Texas recently developed a new portable rheometer [54]. This rheometer was used in experimental work that is described by this dissertation, therefore, operational aspects of this device are discussed in detail here.

ICAR Rheometer is a coaxial, portable rheometer consisting of five major components: a container with vertical ribs to prevent concrete slippage, a driver head equipped with an electric motor and torque meter, a four-blade vane, a frame to attach the driver head to the container, and a laptop to control the test. The rheometer utilizes concentric cylinder (Couette's) geometry: shear flow is induced by the vane evolving around its longitudinal axis while the container remains in still position during the test. Multiple container sizes are available for various maximum aggregate sizes.

Static and dynamic tests can be performed using the ICAR Rheometer. A static test is performed under a constant vane speed, and the increase in torque is recorded to calculate static yield stress. A dynamic test must be employed to measure Bingham parameters of fresh concrete (dynamic yield stress and plastic viscosity). At the beginning of the dynamic test, the vane is rotated at a high speed (typically 0.5 rev/sec) in order to pre-shear the concrete, reach the equilibrium state, and avoid thixotropic distortion of the measurement. After the initial "breakdown" stage, a set of decreasing vane velocities (the manufacturer recommends at least six steps) is imposed on the concrete sample, and corresponding values of torque for each step are recorded. Rheometer software then analyzes the measured values and flow curve, and Bingham parameters are reported.

Unfortunately, all concrete rheometers produce inconsistent results when testing the same concrete mixture [43]; therefore, the real rheological properties of concrete are still, to some extent, unknown. However, values of Bingham parameters obtained from these rheometers are still valuable and can be used as relative parameters when attempting to understand behavior of various types of concrete. Differences in rheological measurements obtained during a round-robin study conducted in France in 2000 using various rheometers are shown in Figure 2.14.

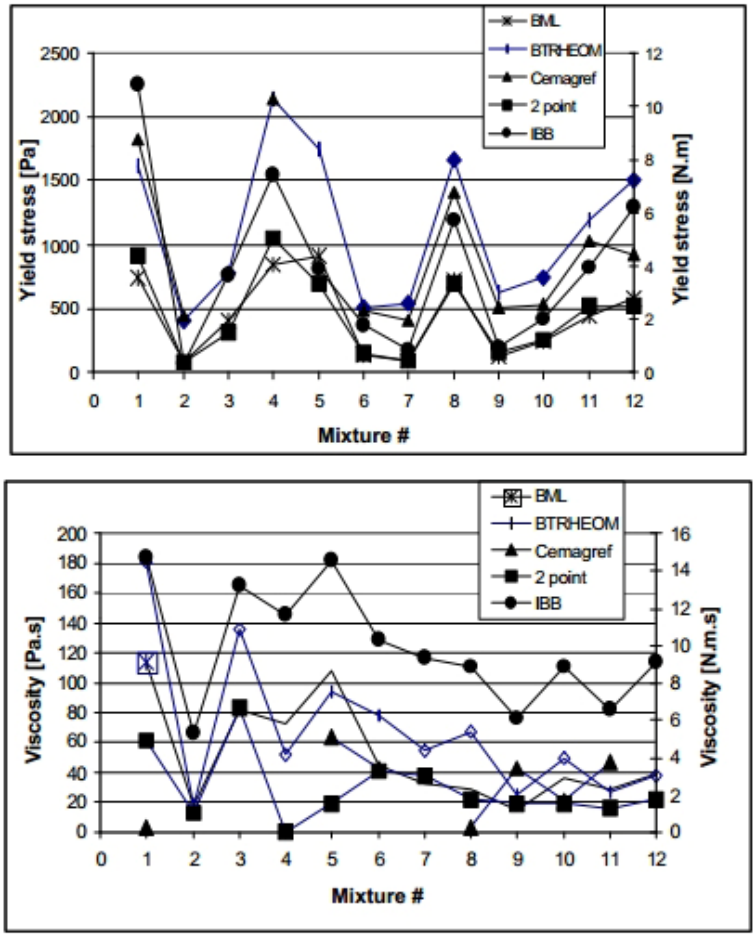

Figure 2.14 – Results of concrete rheometers round-robin experiment, from [41]

2.4 Concrete Flow in Pipes

Fresh concrete can be characterized as a suspension of rock and sand particles in cement paste, or as a suspension of rock particles in grout, as discussed in Section 2.3.2. Particle size, shape, and ratio of solid particles to overall volume of the suspension are critical parameters that determine fresh concrete behavior. Fresh concrete can be distinguished in two states: unsaturated concrete and saturated concrete [55].

When concrete is unsaturated, the concentration of solid particles relative to the content of the liquid phase is such that the particles form a network through direct contacts. The stress transfer is frictional. In this stress regime, stress transfer is dominated by inter-particle forces and

their contact. The Coulomb's Law of Friction (friction force is proportional to the friction coefficient and normal force acting on the surface) must be applied for unsaturated concrete, resulting in a nonlinear pressure loss in pipelines during pumping.

On the other hand, saturated concrete contains enough paste to lubricate all solid particles so that the particles are not in a direct contact. If solid particles do come into direct contact, we consider the stress transfer mode to be hydrodynamic. In the hydrodynamic stress regime, concrete flow is dependent on the shear rate in the interstitial liquid (mortar or grout) that fills the space between particles. Rheological properties of liquids in this mode (without normal force present during flow) are independent of applied pressure, thereby allowing application of rheology. For saturated concrete, pressure loss in the pipeline is linear (assuming no variations in pipe geometry, shape, or material), as shown in Figure 2.15.

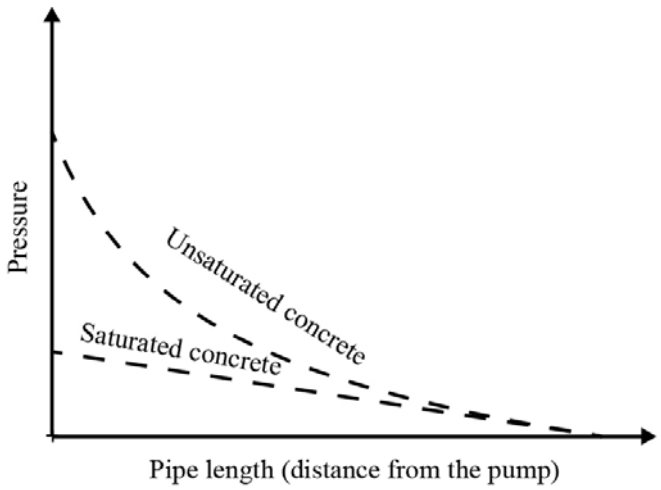

Figure 2.15 – Pressure loss for saturated and unsaturated concrete, after [55]

The saturation state of concrete is the fundamental parameter that determines whether concrete can be pumped. Figure 2.16 shows the difference in required axial pressure between saturated and unsaturated concrete. In a pioneering study on pumpability by Browne and Bamforth [55], analytical formulas for saturated and unsaturated concrete were developed in

order to calculate the distance concrete can be pumped, taking into account various parameters such as mixture properties, pipeline length, and pump pressure. An example calculation in their paper showed that concrete mixture in saturated state can be pumped approximately 250 meters, while the same mixture in unsaturated flow mode can be pumped only 1 meter. Therefore, the unsaturated flow must be avoided for concrete to be pumpable.

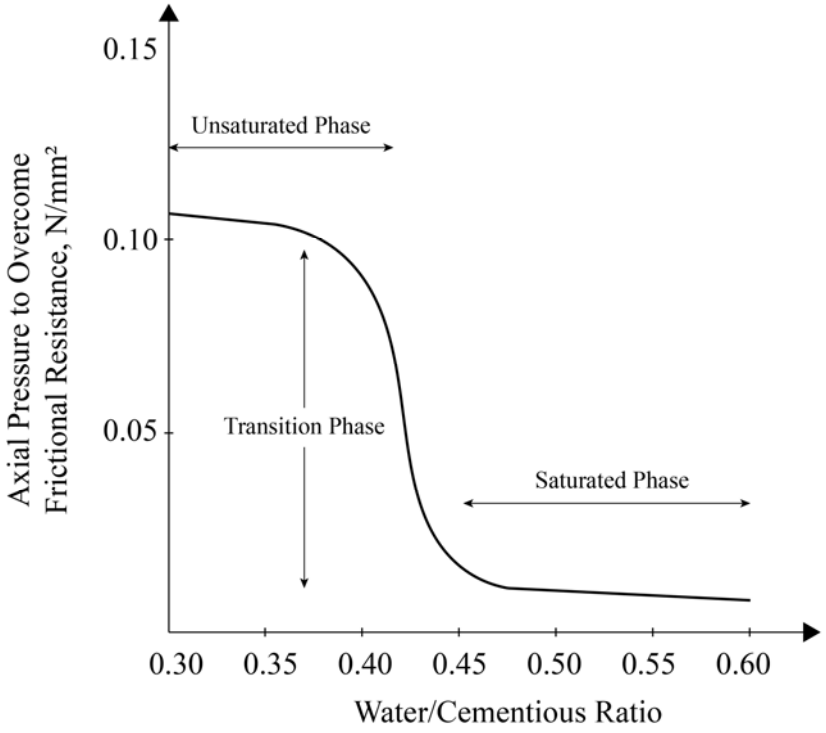

Figure 2.16 – Axial pressure for saturated and unsaturated concrete, adapted from [56]

2.4.1 Flow Characterization of Cement-Based Materials in Pipes

The science of hydraulics and fluid mechanics allows for numerous classifications of fluid flows. Typically, two types of flow are distinguished for a flow within a closed conduit: open channel flow and pipe flow. Primary difference in these flow types are summarized in Table 2.3 [57].

Table 2.3 – Flow types in a conduit

Open Channel Flow	Pipe Flow
Fluid upper surface exposed to atmosphere	A pipe is a close conduit. True pipe flow only occurs when the pipe is completely filled with the fluid and there is no free surface.
The flow is due to gravity	The flow is due to pressure
Hydraulic grade line coincides with the fluid surface	Hydraulic grade line does not coincide with the fluid surface
The maximum velocity occurs right beneath the fluid surface	The maximum velocity occurs at the pipe center

For purposes of this work, primarily pipe flow will be considered since concrete pumping is pressure-driven flow in a closed pipeline. However, fresh concrete can often flow in the open channel regime, for instance when sliding down the chute of a concrete truck.

Based on the Reynolds number[9] R_e, as defined in Eq. 2-22 [57], laminar, turbulent and/or transient (or transitional) type of flows can be distinguished:

$$R_e = \frac{\rho u L}{\mu} \qquad \text{Eq. 2-22}$$

where ρ is fluid density, u is fluid velocity, L characteristic linear dimension, and μ is viscosity. Concrete flow is typically considered to be laminar, however, it has been shown that at certain conditions (e.g. pumping of self-consolidating concrete (SCC) at high flow rates), transient or turbulent flow regimes can occur [58]. Laminar flow is characterized by fluid flow in parallel layers with no disruption, such as swirls or eddies, between the layers, and by the fact that the

[9] This number was first formulated by George Stokes (1819 – 1903) [138] but was later named by Osborne Reynold (1842 – 1912) who extensively studied pipe fluid transitions.

kinetic energy of the system can be neglected compared to all other sources of energy dissipation in the system [57], [58].

Mathematical models that describe rheological properties of fresh concrete, as described in Section 2.3.3, are valid only if the steady-state flow is reached. These models assume that concrete properties do not change with time. However, transient states always exist between two successive steady states [58]. For example, the initial seconds of concrete testing in a rheometer is a transient state between two boundary states: concrete at rest and concrete subjected to constant rotational velocity. Three phenomena that are typical of the transient flow of fresh concrete: thixotropy, structural breakdown, and loss of workability, as discussed in Section 2.3.4 [11].

2.4.2 Flow Zones

If saturated concrete is pumped through a pipeline, two or three zones, depending on the concrete type, of different properties and behavior can be observed [56]. A general model with three flow zones is presented in Figure 2.17. As shown in the figure, the first zone, the plug, is formed closest to the pipe center. This zone is comprised of concrete that is not shared during pumping because shear stress τ did not exceed the value of yield stress τ_0. Recall that the same phenomenon can occur in a concentric cylinder rheometer, as discussed in Section 2.3.4.1. In the second zone, the value of shear stress is equal or higher to yield stress of the mixture; therefore, concrete is sheared as it moves in this zone. Pumped material in the third zone is also sheared, but rheological properties of this zone, the lubrication layer, differ from sheared concrete in the second zone.

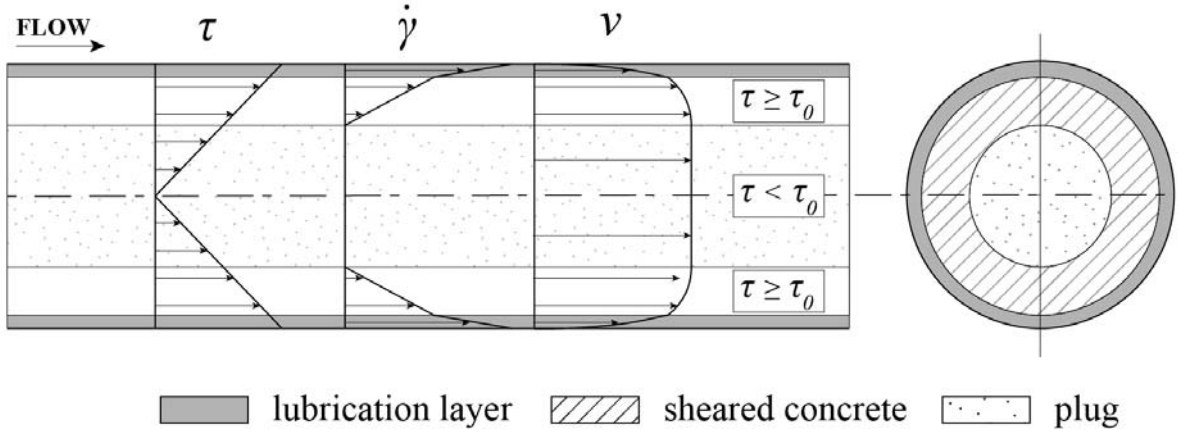

Figure 2.17 – Concrete flow zones in a pipe

2.4.3 Pressure Prediction

Pressure prediction is an important task related to pumpability of concrete mixtures. If one can accurately predict required pressure for pumping of a concrete mixture based on its properties, and accurately evaluate other aspects of pumpability such as static and dynamic stability, concrete mixtures can be adjusted in the laboratory for optimized pumping performance.

2.4.3.1 Energy Equilibrium

Similar to other physical processes that take place in our world, concrete pumping must obey the law of energy conservation. For flow in a pipe, this law is described by Bernoulli's equation:

$$\frac{v^2}{2} + gh + \frac{p}{\rho} = constant \qquad \text{Eq. 2-23}$$

where v fluid velocity at a chosen point, g is gravitational acceleration, h is the elevation of the point above the reference plane, p is pressure at the chosen point, and ρ is fluid density.

This equation can be extended to account for energy exchange in the pipe, yielding the steady flow energy equation (SFEE):

$$\left(h_1 + \frac{v_1^2}{2g} + \frac{p_1}{\rho g}\right)_{in} = \left(h_2 + \frac{v_2^2}{2g} + \frac{p_2}{\rho g}\right)_{out} + \Delta F - h_{pump} \qquad \text{Eq. 2-24}$$

where $v1$ and $v2$ are fluid velocities, p_1 and p_2 are absolute pressures, h_1 and h_2 are elevations above the reference level, ΔF is sum of minor and friction pressure losses, and h_{pump} is the pump head.

Eq. 2-24 states that pumping pressure must balance for pressure change, elevation change, kinetic energy (velocity), and pressure losses. Pressure losses can be categorized as minor and friction losses. Minor losses in pumping circuits, frequently associated with bends and elbows (see Section 2.2) are typically converted to pressure losses in an equivalent straight section. However, these approximations are non-consistent for various pumping application, therefore their applicability is questionable [13], [59]. Estimating friction (or pressure) losses can be quite challenging, and several models to relate concrete flow and pressure have been recently proposed. These models are discussed in Section 2.4.3.3.

2.4.3.2 Pressure Losses

For Newtonian fluids, the Hagen-Poiseuille[10] equation can be used to predict pressure required for fluid to flow through a pipeline, assuming the following conditions are met:

- Fully developed, isothermal, and steady flow in the pipe;
- One-dimensional flow (no radial or tangential flow component);
- Incompressible and homogeneous liquid;
- No slippage at the wall;
- Laminar flow condition.

[10] This equation was independently formulated by Gotthilf Hagen (1797 – 1884) and Jean Léonard Marie Poiseuille (1797 – 1869), and published by Poiseuille in 1846 [60].

The Hagen-Poiseuille can be expressed as follows:

$$Q = \frac{\Delta P \pi r^4}{8 \mu_p L} \quad \text{Eq. 2-25}$$

where Q is volumetric flow rate, ΔP is the pressure loss, L is length of the pipe, and r is a radius of the pipe. Full derivation of the equation can be found elsewhere [52], [60].

Eq. 2-25 was later expanded by Buckingham for Bingham fluids, resulting in the so-called Buckingham-Reiner equation [61], [62]:

$$Q = \frac{3r^4 \Delta P^4 + 16\tau_0^4 L^4 - 8\tau_0 L r^3 \Delta P^3}{24 \Delta P^3 L \mu_p} \quad \text{Eq. 2-26}$$

Overestimation of pumping pressures at certain flow rates was recorded by various researchers when the Buckingham-Reiner equations were utilized [59], [63], [64]. This is primarily due to the fact that one of the assumptions required for validity of the Hagen-Poiseuille formula, homogeneity of the material, is not applicable. As discussed in Section 2.4.2, a lubrication layer forms along the pipe wall, and therefore, the material does not remain homogenous during pumping.

2.4.3.3 Models Developed for Concrete

To address the inhomogeneous nature of concrete in the pipeline, several pressure prediction models were recently developed. These models incorporate not only rheological properties of the bulk concrete, but also rheological properties of the lubrication layer. Available models are presented in the following section, and an overview of techniques available to characterize lubrication layer properties is discussed in Section 2.5.1.

Kaplan's model [64], [65]

Kaplan utilized a 486-ft long (148-m) experimental pumping circuit to investigate conventional concrete behavior. His model was based on the basic assumption that the total flow

Q_{total} through the pump piston must equal to the flow in the pipeline. The total flow can be therefore expressed as (Eq. 2-27):

$$Q_{total} = v_p \pi R_p^2 k_r 3600 \quad \text{Eq. 2-27}$$

where v_p is the speed imposed by the piston, R_p is radius of the piston, and k_r is the filling coefficient. Moreover, he observed that two diverse flows are present in a pipe when concrete is sheared after yield stress of concrete τ_0 is reached: a slip flow Q_g and a shear flow Q_c. Since the total flow in the pump Q_{total} must remain constant, Kaplan noted that a regulation phenomenon exists: the shear flow is compensated by reduction in the slip flow. The model assumed that these flows are related to the total flow in the pump Q_{total} as follows:

$$Q_{total} = \begin{cases} Q_g, & if\ \tau_i \leq \tau_0 \\ Q_c, & if\ \tau_i > \tau_0 \end{cases} \quad \text{Eq. 2-28}$$

Subsequently, Kaplan's concept of two flows (or materials) resulted in a formation of a model that is based on the Buckingham-Reiner equation and momentum conservation law at the wall interface, while incorporating rheological properties of both the bulk concrete (plastic viscosity μ_p and yield stress τ_0) and properties of the lubrication layer (viscous constant η and interface yield stress τ_{0i}). According to his model, the pumping pressure for the imposed flow Q_{total} (Eq. 2-27) can be calculated as follows (Eq. 2-29):

$$P = \frac{2L}{R}\left[\frac{\frac{v_p R_p^2}{R^2} - \frac{R}{4\mu}\tau_{0i} + \frac{R}{3\mu}\tau_0}{1 + \frac{R}{4\mu}\eta}\eta + \tau_{0i}\right] \quad \text{Eq. 2-29}$$

where R is the radius of the pipe and L is the length of the pipe.

For slip flow only the Eq. 2-29 becomes:

$$P = \frac{2L}{R}\left[\frac{Q}{3600\pi R^2 k_r}\eta + \tau_{0i}\right] \quad \text{Eq. 2-30}$$

Where Q is the theoretical flow of the pump. This equation corresponds to the portion 1 of the pressure-flow curve, as shown in Figure 2.18. The implication of this equation is very important when considering pumping of conventional concretes, especially at slow flow rates. When only the slip flow is present (i.e. all shearing is done by the lubrication layer and the bulk concrete moves as a plug), rheological properties of concrete are to some extent irrelevant to the pressure development in the pipeline.

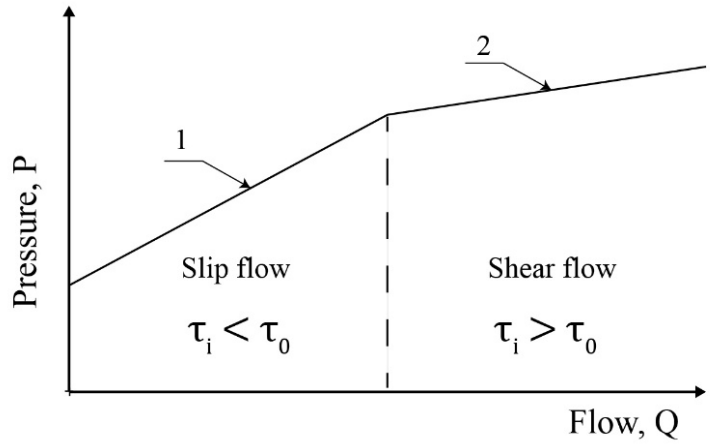

Figure 2.18 – Pressure-flow curve, adapted from [65]

Kaplan successfully verified the validity of his model by comparing pressure data obtained during the pumping experiment to real-world job site measurements. Other researchers also experimentally verified validity of Kaplan's model [66].

Kaplan's research was groundbreaking because he demonstrated and proved, analytically and experimentally, that CVC is often not sheared during pumping but is slipped in the pipe because of the lubrication layer. His model and subsequent experimental data also showed that friction loss is not dependent on pumping pressure; all his rate/pressure curves showed a linear character, proving that pumping pressure is a function of the slip rate.

Choi's model [64], [65]

Choi, as opposed to Kaplan, developed his model on assumed properties of the lubrication layer. In his research program, he evaluated wet-screened concrete mixtures and concluded that the lubrication layer rheology is similar to that of mortar obtained through the screening process. Based on ultrasonic velocity measurements, he assumed that the thickness of the lubrication layer was 0.08 in. (2 mm). His model was developed for and is therefore limited to concrete mixtures with low yield stresses (less than 180 Pa), i.e. self-consolidating or highly-flowable concretes.

Choi's analytical model can be expressed as:

$$\frac{\Delta P}{L} = \frac{2\mu_{pl}V_0}{R\left(\delta + \frac{R\mu_{pl}}{2\mu_p}\right)} \qquad \text{Eq. 2-31}$$

Where ΔP is the pressure loss, L is pipe length, V_0 is average concrete velocity, δ is thickness of the lubrication layer, R is pipe radius μ_{pl} is plastic viscosity of the wet-screened mortar and μ_p is concrete plastic viscosity.

Kwon's model [67]

Kwon approached the problem similarly to Choi by assuming thickness of the lubrication layer to be 0.08 in. (2 mm). He measured rheological properties of the lubrication layer using an interface rheometer (see Section 2.5.2.4), however, by assuming thickness of the layer he avoided the need for use of the viscous constant η (viscosity-to-thickness ratio of the lubrication layer) and was able to directly implement rheological parameters of the layer in his mode. Kwon's analytical model can be expressed as (Eq. 2-32):

$$Q = 3600\frac{\pi}{24\mu_s\mu_p}\left[3\mu_p\Delta P(R_P^4 - R_L^4) - 8\tau_{s,0}\mu_p(R_P^3 - R_L^3) + 3\mu_s\Delta P(R_L^4 - R_G^4) - 8\tau_0\mu_s(R_L^3 - R_G^3)\right] \qquad \text{Eq. 2-32}$$

Where Q is the flow rate, ΔP is the pressure loss, μ_p is concrete plastic viscosity, τ_0 is concrete yield stress, μ_s is plastic viscosity of the lubrication layer, $\tau_{s,0}$ is yield stress of the lubrication layer, R_P is radius of the pipe, R_L is (R_P – *thickness of the lubrication layer (assumed)*) and R_G is radius of the plug which can be expressed as (Eq. 2-33):

$$R_G = \frac{2\tau_0}{\Delta P} \qquad \text{Eq. 2-33}$$

2.5 Lubrication Layer

The presence of the lubrication layer in the pipeline was first postulated in the 1930s [68]. This layer, often also referred to as a slippage or boundary layer, facilitates the pumping by reducing the friction between the pipeline wall and pumped concrete. Morinaga [69] suggested that without the presence of this layer, pumping of concrete would not be possible, which was later confirmed using numerical flow simulations [70]. It was shown that without the lubrication layer presence, approximately three times greater pressure would be required to pump concrete. The existence of the slip layer was verified based on experiments with flow of colored concrete in various pipe types [10].

It was suggested that the lubrication formation can be attributed to several mechanisms that occur simultaneously:

(1) due the presence of high (wall of the pipe) and low shear (center of the pipe) zones in pumped concrete, large aggregate particles tend to migrate towards the low shear zone, thus leaving behind a paste-rich zone [71], [72];

(2) the packing density of large aggregates is limited in the near-wall region, resulting in locally increased paste and/or mortar volume in this zone [10], [49], as shown in Figure 2.19.

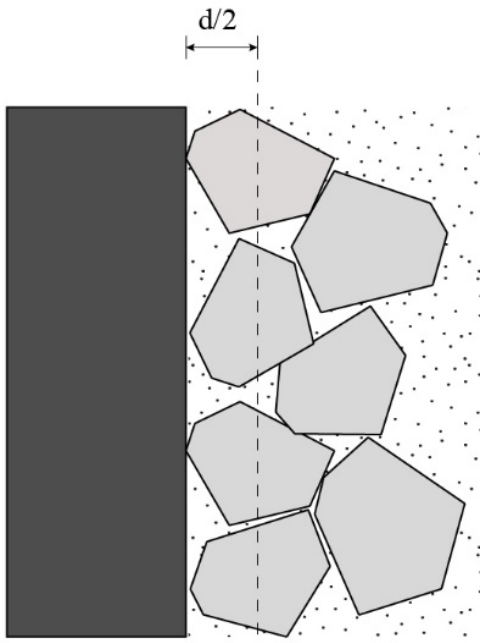

Figure 2.19 – The wall effect

It is generally agreed that the slip layer is composed of cement paste and a limited fraction of fine aggregate [65], [73], [74]. Additionally, it was suggested that only aggregate particles of diameter less than 0.25 mm contribute to the formation of the lubrication layer [75].

The size of the layer has been widely debated and there is no consensus in the literature as to its thickness. Several ranges of lubrication layer thickness were reported: 1-9 mm [75], 1-5 mm [71], and 2 mm [74].

Additionally, the opinion of the research community is not unified on the factors that affect the thickness of the lubrication layer. Some have suggested that layer thickness is independent of the flow rate or velocity profile of the concrete in the pipeline [70] while others have postulated that the layer thickness is influenced by the concrete's flow rate [71], [75]. Other pumping parameters, such as pipe diameter or length can have an effect on the thickness of the layer [74]. Lastly, several studies have shown that a connection exists between the composition,

thickness and properties of the layer and the initial concrete composition and properties of its constituent materials [66], [74], [76].

2.5.1 Rheological Characterization of the Lubrication Layer

In order to characterize rheological properties of the lubrication layer, a new class of rheometer-like devices has been successfully utilized [63], [65], [66], [75]. These devices have been commonly called tribometers, however, it was pointed out[11] that this name can be misleading as tribology is a science that studies friction of surfaces in relative motion, whereas no frictional behavior occurs in the lubrication layer during pumping [77]. Therefore, the term *interface rheometer* is used in this dissertation. Various interface rheometers designs were explored to be able to mimic as closely as possible the condition in the near-wall zone in laboratory conditions. Although design parameters of each device were different, the underlying principle of these devices is identical: a smooth cylinder is spun in a container containing fresh concrete mixture, allowing formation of the lubrication layer. This slip phenomenon is unwanted in traditional rheometers; however, it is very much needed in concrete interface rheometers. Subsequently, rotational velocity (*N, rps*) of the cylinder and torque (*T, N.m*) are recorded.

Since the thickness of the lubrication layer in the interface rheometer is not known, it is impossible to obtain its plastic viscosity using the rotational velocity-torque to shear rate-stress transformation that is typically used for rotational rheometers. Therefore, the concept of viscous constant (*η, Pa.s/m*), i.e. viscosity-to-thickness ratio of the layer, is used [65]. Viscous constant,

---

[11] As pointed out by De Schutter and Feys [77], the term *tribology* is incorrect when used in connection with the lubrication layer. *Tribology* is derived from the Greek word *tribos* meaning rubbing, therefore the literal translation is the *science of rubbing*, and commonly used English definition is the *science of friction and wear* [139]. Since no friction behavior occurs in the lubrication layer, this term is technically incorrect.

together with the interface yield stress of the lubrication layer ($\tau_{0,LL}$, Pa), can be obtained from the linear velocity-shear stress curve.

2.5.2 Concrete Interface Rheometers

Various devices were developed to simulate pumping conditions by letting concrete flow through a pipe [69], [78]. However, these devices have not been suitable for use in the field due to their size or issues have been raised regarding their accuracy. Therefore, a family of new interface rheometer types have been recently introduced.

2.5.2.1 Kaplan's interface rheometer

Kaplan developed an interface rheometer that utilizes rotational movement of a steel cylinder, a principle successfully used in rheometers [64], [65]. Kaplan's interface rheometer used a motor, an acquisition device, and a primary cylindrical container from a BTRheom rheometer (see Section 2.3.4.5). Another steel cylinder (diameter of 150 mm) was placed in the center of the container and connected to the driving block, assuring rotational movement of the cylinder. Because the driving block was placed under the main rheometer body, a rubber seal was required to ensure that concrete did not leak from the space between the inner cylinder and the steel container. For the testing procedure, the inner cylinder was rotated at a series of various speeds and corresponding values of the torque were recorded. Because steel surfaces in the devices were smooth, the concrete remained motionless during the test as long as stress at the steel-concrete interface did not exceed concrete yield stress. The interface rheometer proved to be a practical tool that could be used in the field, but the rubber seal on the bottom of the device was problematic because the resulting torque in the device is not caused solely by friction between the inner cylinder and concrete, but also by friction between the cylinder and the rubber

[66]. Although formulae to account for this friction have been introduced, a certain bias in the measurements is inevitable.

2.5.2.2 Chapdelaine's interface rheometer

Chapdelaine adopted an approach similar to Kaplan's interface rheometer when he modified an IBB rheometer (see Section 2.3.4.5) to allow interface rheology investigations [63]. The inner H-impeller of the rheometer was replaced with a smooth, open rubber or steel cylinder. Contrary to Kaplan's device, however, the main container of this tool was equipped with longitudinal ribs to prevent relative motion of the bowl and concrete. The lubrication layer was formed on both surfaces of the inner cylinder, causing complex flow conditions in the interface rheometer with various shear rates in concrete on both sides of the cylinder. Chapdelaine avoided the issue of additional friction caused by sealing the bottom surface of the steel bowl. In his device, a constant distance of 50 mm is maintained between the rotating cylinder and the main container.

2.5.2.3 Ngo's interface rheometer

Ngo developed a portable interface rheometer implementing the principle of a rotational inner cylinder [75]. However, his device incorporated a closed cylinder instead of an open cylinder used in Chapdelain's interface rheometer. Use of the closed cylinder helped eliminate complexity of the concrete flow because only two surfaces of the cylinder were in direct contact with concrete. The testing procedure consisted of two subsequent steps:

- The cylinder was placed in the container so that only the cylinder's base touched the concrete. A set of various rotational velocities was imposed, and friction parameters were measured.

- The inner cylinder was immersed in the concrete sample to the level of its top surface and the same rotational velocities that were imposed in the first step were applied and torque was registered.

The two obtained datasets were subtracted from each other so that only friction between the wall of the cylinder and concrete was considered. This type of interface rheometer provided accurate results for CVC, but problems related to the different flow regimes in Steps 1 and 2 of the testing procedure were identified when SCC was tested [66].

2.5.2.4 Kwon's interface rheometer

Kwon developed an interface rheometer similar to the interface rheometer introduced by Ngo [67]. The primary difference was an increased size of the rotary cylinders; Kwon's interface rheometer implemented a cylinder that was 9.4 in. (240 mm) tall and had a diameter of 5.1 in. (130 mm). To account for the 3D flow effect of the bottom of the cylinders, a testing protocol involving performing the test at two various filling heights was incorporated.

2.5.2.5 Feys' interface rheometer

Based on shortcomings of interface rheometers discussed in the previous section, Feys designed a new type of interface rheometer suitable for CVC and SCC [66]. Feys' interface rheometer was also based on a concrete rheometer, but he introduced a new shape of the inner cylinder. The conical shape of the cylinder allowed smooth insertion into the concrete because only a single step procedure was used. The distance between the cone tip and the bottom of the steel container was approximately 0.4 in. (10 mm), compared to 2 in. (50 mm) in Ngo's interface rheometer, and the height of the cylinder was 7.8 in. (200 mm). As a result of the height adjustments, the effect of the complex 3-D flow under the cone was significantly reduced but not fully restricted.

2.5.3 Determination of Lubrication Layer Properties

Rheological properties of the lubrication layer can be characterized similarly to rheological properties of bulk concrete. Different flow conditions in the interface rheometer, as shown in Figure 2.20, must be considered when the shear stress is calculated.

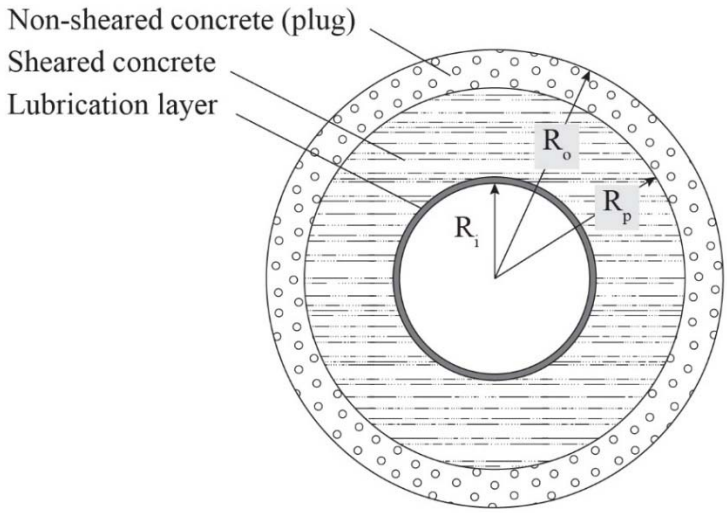

Figure 2.20 – Flow zones in the interface rheometer

Based on concrete yield stress τ_0, a value of plug radius (i.e. boundary distance from the rotational cylinders axis at which concrete is no longer sheared) can be calculated (Eq. 2-34):

$$R_p = \sqrt{\frac{T}{2\pi\tau_0 h}} \qquad \text{Eq. 2-34}$$

Where h is height of the rotational cylinder and T is recorder torque. Three flow conditions can be observed in the interface rheometer based on the plug flow radius, rotational cylinder radius R_i and outer cylinder (i.e. container) radius R_o:

1. *The lubrication layer is sheared while the concrete is not sheared ($R_p<R_i$):*

In this scenario, the measured torque can be transformed into a shear stress based on dimensional characteristics of the cylinder, as shown in Eq. 2-35, and no further correction is needed:

$$\tau = \frac{T}{2\pi Ri^2 h} \quad \text{Eq. 2-35}$$

2. Both lubrication layer and concrete are sheared ($R_p > R_o$):

If the entire mass of concrete in the interface rheometer is sheared, a correction must be made to the measured rotational velocity value [66]. Using Eq. 2-36, the value of N_i *(rps)* can be calculated. The rotational velocity N_i corresponds to the rotational velocity that would have to be imposed on the concrete mixture in a standard rheometer of the same cylinder size to register a torque value of *T*.

$$N_i = \frac{T}{8\pi^2 h\mu}\left(\frac{1}{R_i^2} + \frac{1}{R_o^2}\right) - \frac{\tau_0}{2\pi\mu}\ln\left(\frac{R_o}{R_i}\right) \quad \text{Eq. 2-36}$$

3. Lubrication layer is sheared while concrete is partially sheared ($R_o > R_p > R_i$):

Eq. 2-36 can be still used to correct the rational velocity for the effect of sheared concrete, however, the outer cylinder radius R_o must be replaced with the plug radius R_p. The value of linear velocity *V* can be calculated using the value of viscous constant, and interface yield stress can be calculated using Eq. 2-37:

$$V = 2\pi R_i N_{LL} \quad \text{Eq. 2-37}$$

Where N_{LL} is equal to measured rotational velocity *N* when concrete is not sheared, or $N_{LL} = N - N_i$ when concrete is fully or partially sheared. Shear stress at the surface of the inner cylinder can be calculated as (Eq. 2-38):

$$\tau = \frac{T}{2\pi R_i^2 h} \quad \text{Eq. 2-38}$$

Finally, values of viscous constant η and interface yield stress τ_{LL} can be obtained (Eq. 2-39):

$$\tau_{LL} = \tau_{0,LL} + \eta V \quad \text{Eq. 2-39}$$

2.6 Concrete Pumping

2.6.1 Basic Pumpability Requirements

When concrete pumping is utilized on a construction site, the concrete mixture must be capable of being transported via the pipeline. Pumpability is a flexible term with many interpretations, but when considering pumpable concrete, pumpability refers to a concrete that can flow through a pipeline with help of a pressure pump without unpredictable changes in its properties.

Kaplan defined pumpability as “the aptitude of concrete to be placed using a pump. The concept of pumpability therefore relates to the formation of blockages and does not refer to such pumping parameters as flow and pressure.” [79]

Jacobsen stated that two basic properties of pumpability are "sufficient paste content so that there is enough grout for a slip layer, and suitable grout consistency and structure between aggregate grains to hinder forced or pressurized bleeding due to pump pressure." [80]

Numerous parameters determine whether concrete mixture is pumpable, including maximum pressure of the pump, geometry of the pumping circuit, and rheology and performance under pressure of the concrete mixture. In this section, a breakdown of factors effecting concrete pumpability is presented.

2.6.2 Concrete Rheology

As discussed in Section 2.4.3, rheological parameters of pumped concrete mixture (i.e. yield stress τ_0 and plastic viscosity μ_p) and corresponding parameters of the lubrication layer

have a significant influence on pressure loss in the pumpline, and thus are essential to determination of required pump power to successfully pump concrete. Since the science of concrete rheology has not been adopted yet in the practice, indirect rheology measurements, such as slump, are typically used to account for concrete rheology when predicting required pump pressure.

Several empirical guidelines are available to relate slump and pumping pressure [9], [81]. An example of such a guideline is a nomograph available in the ACI 304.2R guide. This chart allows the user to estimate the pumping pressure based on slump, pipe diameter, and pumpline length. Besides the fact that this chart provides only limited range of slump values and completely disregards SCC, its limitations are defined by its empirical nature and not necessarily a mechanistic understanding of the pumping process.

2.6.3 Lubrication Layer

Concrete can be pumped only if the lubrication layer facilitating the pumping process is created [65], [82]. For successful formation of the lubrication layer, enough cement paste/mortar must be available in the mixture to create this layer, and the shear-induced particle migration mechanism must be available to form this layer. In order to promote the formation of the lubrication layer, the pumpline is typically primed with cement grout prior to initiation of concrete pumping. Concerns have been brought up for special types of concrete mixtures, such as ultra-high performance concrete (UHPC), where internal friction and Coulomb forces govern the flow characteristics and the lubrication layer cannot be formed [77]. Efforts have been made to create the layer artificially, for instance by imposing an external magnetic field on the pumping circuit [83].

2.6.4 Mixture Design

As a consequence of concrete behavior in a pipeline under pressure, aggregate selection and paste content are two mixture design parameters that are crucial for design of a pumpable concrete.

2.6.4.1 Aggregate

Several aggregate-related rules have been proposed in order to design a problem-free pumping mixture. The goal of aggregate optimization when designing a pumpable mixture is to reduce solid-solid interactions between aggregate particles. With increasing aggregate size, less cement paste is needed to coat the particles to allow for shearing, and similarly, the total amount of paste required to coat all aggregate particles increases with an increase content of aggregate fines (aggregate particles passing the No. 200 sieve (0.074 mm)). An optimum gradation of coarse aggregate has been suggested by various researchers for pumpable mixes. For fine aggregate, it is recommended that grading meets the requirements of ASTM C33 [9].

In addition to optimal gradation, the maximum aggregate size is an important parameter for pumpable concrete. Maximum size of crushed coarse aggregate has been recommended to be less than one-third of the pipe diameter ($D_{max} < 1/3\ D_{pipe}$) [9].

2.6.4.2 Cementitious materials

Balancing the total amount of cementitious materials for optimum pumpability is a complex task. High paste volume helps reduce concrete viscosity. This results in a reduction in the required pumping pressure and enables formation of the lubrication layer that is essential for a successful pumping operation [9]. The optimum paste content for good pumpability has been found to be unique for each concrete mixture [11]. It has been suggested that the optimum amount of fines (cement + aggregate particles smaller than 0.01 in. (0.25 mm)) is approximately

759 lb/cy (450 kg/m³) [80]. However, if this optimum paste volume is exceeded, the pressure demand at a given flow rate might be increased [80], and the chances of aggregate segregation in the mixture (and other concrete instability issues) dramatically rise [11].

Binns [56] reported that the use of fly ash and silica fume can positively contribute to concrete cohesion, thereby improving pumpability of concrete, especially in low-cement content mixes, and that granulated furnace slag and metakaolin have shown no significant effect on pumpability of concrete.

2.6.4.3 Chemical admixtures

Pumping aids are thickening agents that can be used to enhance pumpability of a general concrete mixture without any further modification. However, the current industry trend is to address deficiency in the concrete mixture rather than deploy another chemical admixture. Pumping aids are useful when pumping is carried out over a long distance, or when mixes with lightweight concrete are pumped [56].

Use of water reducers and superplasticizers has been recommended to reduce the amount of used cement, although enough cement paste must be present in concrete in order to maintain the lubrication layer and to reduce the risk of concrete bleeding that could lead to blockage in the pumping circuit [80].

Retarding admixtures are advisable, especially when pumping in hot temperatures. In addition, because the danger of pumping interruptions always exists, concrete that can potentially remain stationary in the pipeline without setting retarder should not be pumped [56].

2.6.5 Geometry of the Pumping Circuit

The length of pumping circuit and number of bends can have significant effect pumpability of concrete mixtures. Besides the very basic assumption that the pressure exerted by

the pump on concrete must overcome losses caused by friction over the whole length of the pumping circuit for successful pumping operation, bends and elbows were proposed to have further effect on the pressure loss. Traditionally, pumping guides have suggested that 90-degree elbow can cause pressure loss equivalent to a 9.8-ft (3-m) long straight pipe [81]. However, it was recently found through experimental research that bends in the pumping circuit do not increase pressure loss during pumping of CVC, which is contrary to practical pumping guidelines [63], [64]. On the other hand, research program investigating pressure losses for SCC found that the effect of bends on increased pressure loss exists, and in some cases its magnitude even exceeded the original empirical assumption based on the equivalent length of a straight pipe [59].

2.6.6 Stability under Pressure

It is essential that concrete remains homogenous in the pumpline throughout for successful pumping operation. The homogeneity requirement is never fully fulfilled due to the lubrication layer formation, as discussed in Section 2.5, however, the bulk part of the pumped concrete must remain stable in order to avoid blockages in the pumping circuit, and subsequently maintain the fluid-like behavior of the mixture. Therefore, the first and the utmost requirement for pumpable concrete is its ability to resist both static and dynamic segregation, especially when highly-flowable concrete or SCC is pumped [59]. Various test methods are available to test concrete for both static and dynamic segregation [84].

Kaplan analyzed the concrete pumping blockage mechanism and recommended precautions that should be taken to avoid pipeline blockage during concrete pumping [79]. Blockages are undesirable because they can delay the construction process, thereby increasing

the construction costs. Four different scenarios when of concrete blockage in the pipeline were proposed:

1. *Blockages that occur during priming*

Priming is the initial stage of concrete pumping in which grout is pumped through the pipeline to lubricate the steel walls and prepare them for future concrete flow. It was reported that blockages during priming are common, even for concretes that do not exhibit problems during steady-state pumping. During Kaplan's experimental testing, 15 blockage events during the priming stage were recorded. Analysis of these events revealed that the primary reason for a blockage is the fact that aggregate particles accumulate in front of the cement paste, causing a barrier that prevents the entire pumped mass from moving. Aggregate accumulation in front of the cement paste is explained by the fact that aggregates have greater inertia then cement, so they move farther than cement grains with every stroke of the pump. If the number of strokes is high enough or the pumping line is long, large aggregate particles will outrun the cement paste and cause blockage. In order to avoid the blockage, recommendations were made to (1) prime the circuit at the slowest possible pumping rate and (2) to use mortar as an additional intermediate stage before priming the line with grout.

2. *Blockages during pumping*

Blockage during concrete pumping is a common phenomenon. Kaplan highlighted common causes of blockage during pumping:

- Exceeding the maximum recommended aggregate size $D_{pipe}/3$
- Significant increase in pumping rate that causes blockages in tapered sections;
- Blockage due to a minor localized disruption in the pumping circuit (i.e., presence of a rubber hose, two pipes with significant differences in the amount of wear, etc.);

- Segregation of concrete in the pump hopper resulting in changes of the coarse/fine aggregate ratio in the pumped concrete;
- Mixtures with high coarse-to-fine aggregate ratio that cause large quantities of air to enter the pumping circuit. As pressure drops along the line, this air is decompressed, forming air pockets that cause uncontrolled motion in the pipes and potentially leading to blockages; and
- A foreign body in the concrete (i.e., stone or a piece of wood).

3. *Blockages when stopping and restarting pumping*

Stopping and restarting pumping is inevitable throughout the pumping procedure. Sometimes the circuit must be cleaned, the discharge boom must be redirected, or a delayed concrete truck requires interruption of the procedure. If concrete remains stationary in the pipe, two scenarios are possible: (1) concrete sets in the pipes if it does not contain sufficient dosage of a retarding admixture, making it impossible to restart the process, and (2) concrete remains in plastic state during the stationary period. When concrete stops moving, aggregate particles are driven down by the gravity force, disturbing the lubrication layer. When pumping is restarted, additional pressure is required to overcome aggregate-steel (solid/solid) friction until the lubrication layer is restored, and concrete thixotropy. When an unstable mixture (prone to segregation) is used, although this mixture can be perfectly pumpable under steady flow conditions, if pumping must be interrupted, the mixture can cause a blockage.

4. *Blockages during cleaning*

Three techniques are used to clean the pipeline after pumping: cleaning with compressed air, cleaning with water, and/or a combination of both. Blockages rarely occur when cleaning with compressed air but blockages are possible when water is used to clean the circuit. A

hardball is pushed through the pipeline to clean the pipe wall when water technique is utilized. If this plug is not tight, water can leak in front of the hardball, mixing with concrete and causing a blockage. This type of blockage is difficult to clean because additional cleaning increases concrete compaction. Therefore, the quality of the hardball is essential in order to avoid blockages during pumping.

2.6.7 Pumpability Tests

Gray developed a pumpability test apparatus that evaluated required pressure for concrete to move through curved, 6-in. (152-mm) steel pipe by action of a steel piston. This device was developed specifically as a reference tool to evaluate relative pumpability of various mixtures. It was never calibrated with field data as the intention of the researcher was to create a test that could be used in the laboratory to characterize pumpability, and not to create field or quality control test [85]. Browne and Bamforth have developed a test that evaluated resistance of a concrete mixture to water emittance under pressure, i.e. their pumpability test primarily focused on the requirement that concrete must remain in the saturated state during pumping [55]. The test measured cohesiveness of a concrete mixture under pressure by the means of water bleeding. The concrete sample was put into a container and subjected to 500 psi (3.4 MPa) and the amount of water that was emitted was recorded. Subsequently, they developed a nomochart that allows of determination of pumpability on the basis of the test results and concrete slump.

Similarly to Browne and Bamforth, Kaplan further developed the bleed test as an indicator of concrete pumpability [79]. His test apparatus is based on a standard ASTM C173 [86] air void meter, and the bleed test is performed using tetrachloroethylene. Correlation between the bleed rate and pumpability was found for some of the concrete mixtures that were tested in full-scale pumping trials.

2.6.8 Effect of Pumping on Concrete Properties

2.6.8.1 Slump

Several studies showed that slump of fresh concrete decreases after pumping [87], [88]. Slump loss after pumping is often expected by concrete practitioners, and construction guidelines typically recommend testing concrete fresh properties at the point of discharge to account for possible loss of slump due to pumping [89]. Water is assumed to migrate under pressure, and if the aggregate is not at or above the saturated-surface-dry condition, it is likely that the aggregate will absorb some of the water that is pressure driven from the paste, which subsequently translates into slump loss [90]. Additionally, slump is, to some extent, related to the total air void content of fresh concrete; because the air void system can experience significant changes due to pumping, slump is also expected to change after pumping. Lastly, pumping happens over a period of time, and although the time concrete spends in the pipeline is relatively short, the hydration reaction might cause stiffening of the mixture and subsequent slump loss [9]. Although plenty of anecdotal evidence is available among practitioners, a research-based literature explaining slump changes after pumping is not available. This is mainly a consequence of a rheology-based approach to pumpability that has been adopted by majority of researchers investigating concrete pumping. However, since slump is still extensively used as a quality control and acceptance/rejection criteria on construction sites, more research into this area is warranted.

2.6.8.2 Air void system

The effect of pumping on changes in the concrete air void system has been extensively investigated in the past [64], [91]–[96]. The general belief within the North American concrete industry is that pumping reduces air content by two or three percent [97]. However, numerous

studies have shown that the behavior of the air void system is not well predicted, and pumping can increase, decrease or have no effect on the air content or the air void system in terms of air void size distribution. Changes in the air content ranging from -5% (air loss) to 5% (air gain) were previously reported for ordinary portland cement concrete (OPC). However, most of the data in the literature suggest that air loss can be expected after pumping. Several research studies have shown that behavior of the air void system in HWC or SCC is different from OPC, that is the air content may increase after pumping [11], [52], [92]. Additionally, it has been concluded that the overall quality of the air void system can be compromised due to pumping, as the overall amount of fine air bubbles can be reduced. Hence, the freeze-thaw performance of concrete mixtures can be negatively affected [92]. Particularly, it was proposed that air voids smaller than 50 microns tend to vanish from the mixture after pumping [98].

A unified theory that would explain air system behavior during pumping has not yet been developed. Many factors can contribute to change in air void system. Pumped concrete first experiences a drop from the concrete truck to the hopper. It is pressurized, transported through the pipeline, and eventually de-pressurized after leaving the pumping system. In most cases, the concrete undergoes another drop from the pipeline to the form-work. At least three concurrent mechanisms have been proposed to partially explain processes that affect the air void system while in the pipeline.

Jolin [99] suggested that a negative pressure (i.e. vacuum) can be present in pump pistons when the mixture is drawn into the pump cylinder. Additionally, negative pressure was also reported in vertical sections of the pipeline if free fall is allowed [63], [92]. Because of the suction effect caused by the vacuum presence, air bubbles increase in size and may coalesce into

larger air bubbles. These larger air bubbles are easier to be removed by means of (self-) consolidation.

As concrete starts moving forward in the pipeline, large pressures are applied on the mixture. Dyer [100] proposed that due to the large pressure, small air voids dissolve in the mixing water, according to Henry's Law. This law states that the maximum amount of dissolved gas in a liquid is proportional to the partial pressure on the gas, which in the case of concrete pumping is typically the same as the applied pressure on the material. Secondly, as smaller bubbles have larger surface area, they are more prone to dissolution under pressure than larger bubbles. Once the pressure is removed, the dissolved air reappears, however, some of the bubbles resurface as a part of large, existing air voids, and small-diameter air voids are lost, as illustrated in Figure 2.21. This hypothesis is supported by the observed increase in the spacing factor after pumping in several studies [92], [101].

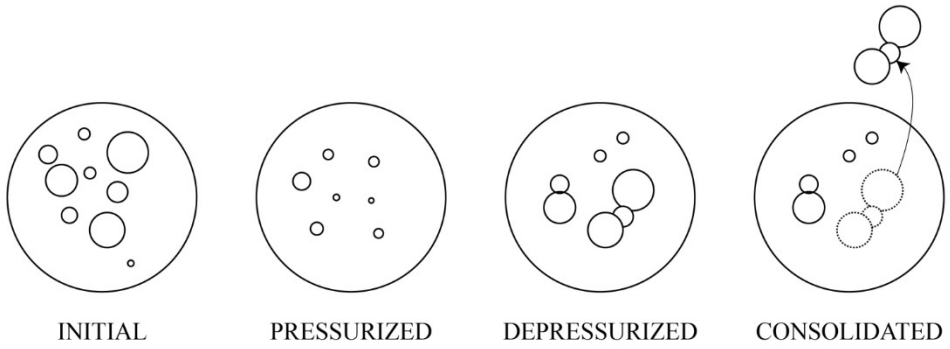

Figure 2.21 – Pressure-dissolution mechanism, adapted from [100]

With the discharge from the pipeline, the pumped concrete mixture will inevitably experience a sudden decrease in its velocity. It was hypothesized [93] that the impact force exerted by the moving concrete is responsible for bursting some of the air voids present in the mixture. The suggestion was also made that the drop from mixing truck to pump reservoir could potentially increase the air content [52].

2.6.8.3 Temperature

The phenomenon of temperature change in pumped concrete mixtures is not fully understood, however, it was shown that pumping can result in increased concrete temperature at discharge [52]. It demonstrated temperature change is a time-dependent property. Concrete temperature increased as the required travel time through the pipeline increased. It was also observed that small, sometimes even negative temperature changes for low pumping rates (or low pressure losses) can occur in SCC mixtures. In addition to pumping rate, aggregate particle size determines how the temperature of a mixture will change due to pumping. It was proposed that the relationship between temperature increase per time unit of time and pressure loss per unit of length is a constant material property [52]. Similar conclusions were confirmed for conventional concrete [11].

2.6.8.4 Rheological properties

In addition to changes in "traditional" fresh concrete properties described in previous paragraphs, alteration of rheological parameters has been observed in concrete because of pumping. Kwon has suggested, based on experimental evaluation of 7 concrete mixtures, that both concrete rheological properties and properties of the lubrication layer can both decrease or increase after pumping [102]. Jacobsen conducted pumping experiments on series of mortars, and observed that pumping process acts as a remixing procedure, keeping concrete workable for longer period of time than if it was not pumped [80].

For SCC, Feys analyzed results of two experimental programs conducted in Europe and Canada [103]. He observed substantial decrease in plastic viscosity with increasing time and increasing flow rate, and contributed this to shearing that SCC is subjected to during pumping, eventually leading to re-dispersion and additional dispersion of cement particles. The effect of

pumping on yield stress was also investigated, and no trend was observed – yield stress of analyzed SCC mixtures decreased, remained the same or increased after pumping. Although changes in the bubble structure of dilute suspensions have been documented to have influence on viscosity of such suspensions [104], Feys concluded that changes in the air void content are not the major cause of variations in both yield stress or plastic viscosity.

Khatib pointed out that the effect of temperature cannot be neglected when attempting to understand rheological changes in concrete due to pumping. As pumped matter heats up, decreased viscosity and increased yield stress can be observed [11].

Chapter 3 - A Correction Procedure to Characterize the Bottom Effect of a Rotational Cylinder during Interface Rheology Measurements of the Lubrication Layer

3.1 Research Significance

Rheological properties of the lubrication layer have been shown to significantly influence pressure development during concrete pumping. Although various devices have been used to characterize interface rheology of pumped mixtures and determine viscosity/viscous constant and yield stress of the lubrication layer, none of them were able to do so precisely and with a high level of accuracy. One of the major shortcomings of existing interface rheometers is the complicated phenomenon of three-dimensional flow that inevitably occurs around the cylinder bottom-concrete interface that subsequently distorts the torque measurements. In this chapter, an effort to improve a correction procedure to characterize the effect of the bottom of interface rheometer cylinders is described.

3.2 Introduction

An accurate characterization of rheological properties of the lubrication layer is a crucial task when one is attempting to predict concrete pumping pressures, as discussed in Section 2.5. Various interface rheometers have been developed to take on this task, however, each of the utilized designs had certain limitations when it comes to the accuracy of the measurements. All interface rheometers discussed in Section 2.5.2 were found to have issues when used with SCC [66], and it is reasonable to assume that similar issues can be expected when CVC is tested. In Kaplan's interface rheometer [64] shown in Figure 3.2a, a complex three-dimensional effect might occur at the interface of the stationary bottom plate and the inner cylinder, in addition to

unintentional friction between the rubber seal and the cylinder. In order to eliminate the friction effect at the bottom of the container, Chapdelaine's interface rheometer shown in Figure 3.2b [63] uses a hollow open cylinder, resulting in formation of two lubrication layers on the inner and outer wall of the cylinder. Both layers are, however, subjected to different shear rates which may yield to different thixotropic behavior of tested concrete. Furthermore, a third lubrication layer is likely to form at the ribs in the center of the device. Ngo [75] suggested using a two-step procedure to correct for the effect of the bottom of the cylinder in the interface rheometer shown in Figure 3.2c. In the first step, the cylinder is placed on the sample so that only its bottom is in contact with the concrete sample, and the test is performed. In the second step, the test is repeated with the whole cylinder immersed in concrete. To obtain the result, data from the Step 1 are subtracted from the Step 2 measurements. Finally, Feys [66] designed a interface rheometer to be used with SCC as shown in Figure 3.2d. In this interface rheometer, the flat bottom cylinder was replaced with a conical-shaped bottom cylinder to eliminate the 3-D flow phenomena that is typically present at the bottom of the container.

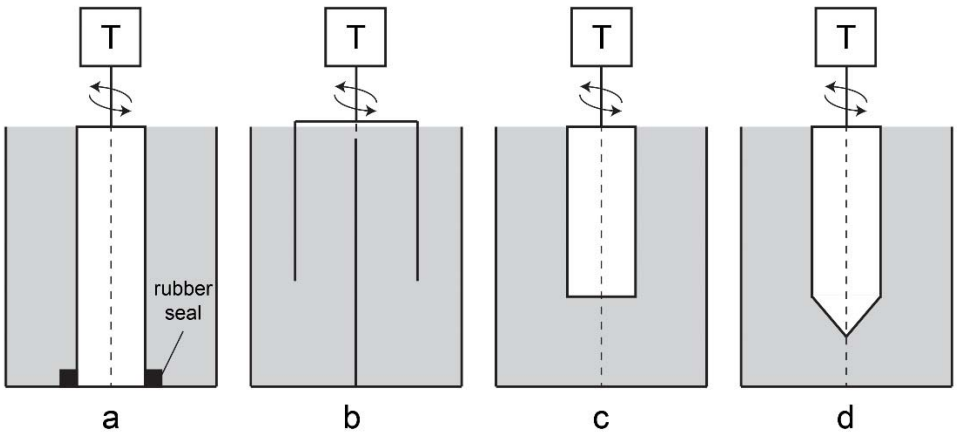

Figure 3.1 – Concrete interface rheometers by a) Kaplan, b) Chapdelaine, c) Ngo and d) Feys, adapted from [66]

In this chapter, a further development of the correction procedure to characterize the bottom effect of the inner cylinders developed for Feys' interface rheometer is introduced. The proposed procedure suggests that the test is performed multiple times, each time with different volume of concrete in the container [43]. By finding the relationship between the filling height of the container and registered torque, one can calculate the level of torque at filling height equal to zero, i.e. the effect of the bottom of the cylinder. However, this procedure did not deliver a successful correction procedure for the bottom of the cylinder. This is most likely attributed to the lack of cleaning the cylinder and the non-remixing of the concrete in between measurements. An experimental study was conducted to address these issues.

3.3 Experimental Methods

In this study, three different interface rheometers were utilized in an attempt to improve the accuracy of characterization of the lubrication layer rheological parameters. The developed correction procedure was tested on five concrete and one mortar mixtures.

3.3.1 Rheometers and Interface Rheometers

Three concrete interface rheometers based on the ICAR portable rheometer were used in this study. The standard four-blade vane for rheological measurements was replaced by an aluminium cylinder with a conical-shaped bottom in interface rheometer M to determine properties of the lubrication layer. Two different cylinders made of stainless steel were used in interface rheometer K; one with conical-shaped bottom (similar to interface rheometer M) and one with a flat bottom. Exact dimensions of interface rheometer cylinders are summarized in Table 3.1 and illustrated in Figure 3.2.

Table 3.1 – Interface rheometer cylinder dimensions

Interface Rheometer	M	K	
Cylinder bottom shape	*Cone*	*Cone*	*Flat*
Cylinder diameter, in. (mm)	4.9 (125)	5 (127)	5 (127)
Straight portion height, in. (mm)	7.9 (201)	8 (203)	10 (254)
Conical part height, in. (mm)	2.4 (62)	2 (51)	--

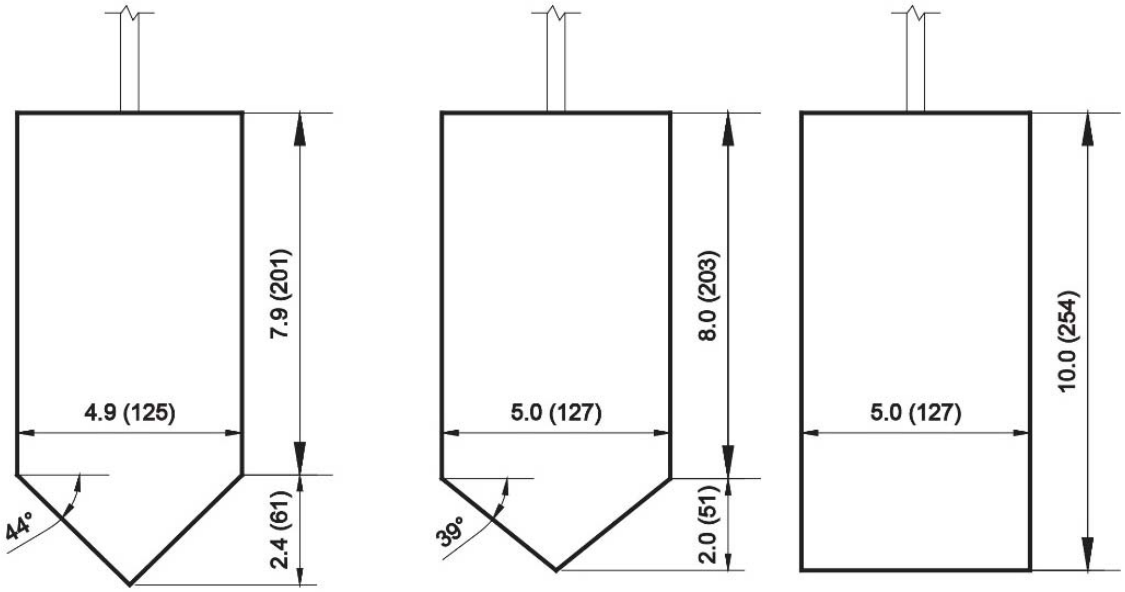

Figure 3.2 – Interface rheometer cylinders design: *M* (left), *K – cone* (middle), *K – flat* (right)

Each interface rheometer head was mounted on the ICAR rheometer when the lubrication layer rheology was measured, and two ICAR rheometers were available for this study (therefore interface rheometer M and interface rheometer K). For interface rheometer M, a standard ICAR rheometer container with diameter of 11.25 in. (286 mm) was utilized during interface rheology measurements. For interface rheometer K, a slightly larger container with a diameter of 13 in. (330 mm) was used. Both containers were equipped with vertical ribs to prevent slippage of concrete (and possible formation of a second lubrication layer) along the container wall. As a result of slightly different cylinder geometries, container sizes and the design of the fixture that

holds the ICAR device in place during the measurement, different distance between the bottom of the cylinder and the bottom of the container were used for interface rheometers M and K. For interface rheometer K, this distance was approximately 2 in. (50.8 m) whereas for interface rheometer M, this distance was approximately 1.6 in. (40 mm). The interface rheometer K setup and details of container ribs are shown in Figure 3.3.

a) b)

Figure 3.3 – Interface rheometer setup (ICAR K): a) overview, b) container ribs details

Three concrete rheometers were utilized in this study to measure rheological properties of investigated concrete mixtures. Two ICAR rheometers (ICAR K and ICAR M) as discussed in the previous section, and ConTec Viscometer 5 (Contec). Details of each of the used rheometers are discussed in Section 2.3.4. Concrete rheology was measured before and after conducting interface rheology experiments using ICAR M and Contec rheometers, and prior to interface rheology measurements with ICAR K. Additionally, slump flow according to ASTM C1611 [105] was determined for each mixture.

Testing protocols for both rheometers and interface rheometers are shown in Figure 3.4. For interface rheology measurements, a higher initial rotational velocity of 0.60 rps was selected to simulate as closely as possible the velocity of concrete in a pipeline during pumping. 0.60 rps is still relatively low compared to the real velocity that can be detected in the pumping circuit, however, it is the highest possible value of rotational velocity that can be achieved by the ICAR device.

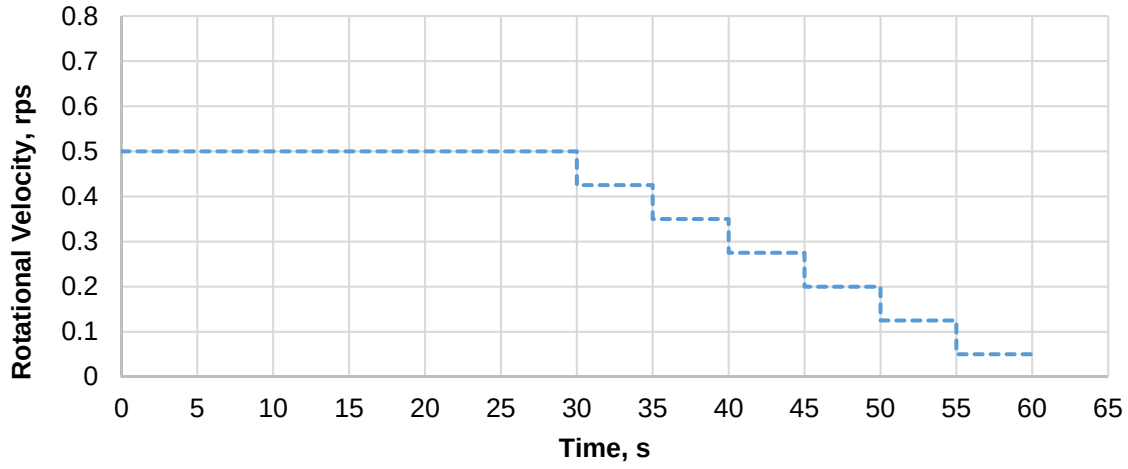

a)

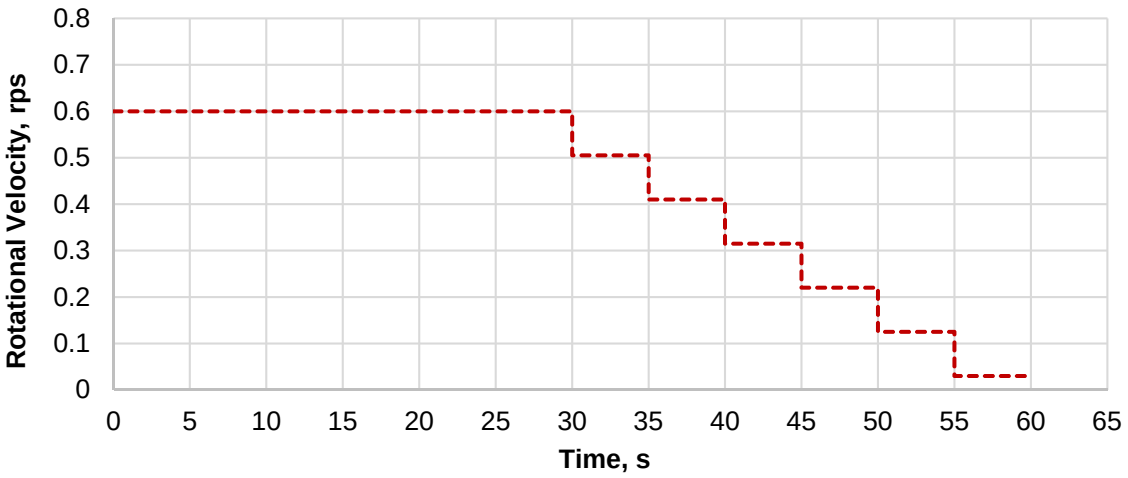

b)

Figure 3.4 – Test protocols: a) concrete rheology, b) lubrication layer interface rheology

3.3.2 Concrete Mixtures

Four concrete mixtures and one mortar were tested in this study. Each of the concrete mixtures was designed as representative of a different type of concrete: mixture A was developed as to represent a "sticky SCC", i.e. self-consolidating concrete mixture with relatively high plastic viscosity that is typically used in Europe, mixture B was designed as a "fluid SCC", i.e. self-consolidating mixture with lower plastic viscosity typically utilized on US construction sites, and mixture C was a "pumpable CVC", i.e. conventional concrete mixture with rheological properties that would allow for pumping of such mixture. Mixture D was a mortar mixture. Concretes B and C were further modified after conducting a whole round of testing (i.e. both rheology and interface rheology), therefore two mixtures were available for the B and C series (mixtures B1 and B2, and mixtures C1 and C2). All constituent materials were brought to laboratory temperature conditions (approximately 73°F/22.8°C) by being placed in the laboratory a day before the testing took place. Concrete was mixed in a standard drum mixer in general accordance with ASTM C192 [106], and batch volume for each mixture was 3.5 ft^3 (100 liters). Mixture proportions are shown in Table 3.2 (Mixtures A, B1 and B2) and Table 3.3 (Mixtures C1, C2 and D).

Table 3.2 – Mixture proportions (Mixtures A, B1 and B2)

Mixture ID:		A		B1		B2	
Materials				*lbs/yd³ (kg/m³)*			
Cement	ASTM C150 Type I	635	(377)	519	(308)	519	(308)
Fly Ash	ASTM C618 Class C	219	(130)	179	(106)	179	(106)
Slag Cement		22	(13)	19	(11)	19	(11)
Silica Fume		--	--	--	--	--	--
Total Cementitious Content		876	(520)	716	(425)	716	(425)
Water		280	(166)	302	(179)	302	(179)
w/cm		0.32		0.42		0.42	
Fine Aggregate	ASTM C33	1618	(960)	1439	(854)	1439	(854)
Coarse Aggregate	ASTM C33, 1/2"	1227	(728)	1509	(895)	1509	(895)
Chemical Admixtures				*fl. oz/yd³ (ml/m³)*			
HRWR	ASTM C494	64.6	(2500)	25.9	(1000)	25.9	(1000)

Table 3.3 – Mixture proportions (Mixtures C1, C2 and D)

Mixture ID:		C1		C2		D	
Materials				*lbs/yd³ (kg/m³)*			
Cement	ASTM C150 Type I	519	(308)	519	(308)	635	(377)
Fly Ash	ASTM C618 Class C	179	(106)	179	(106)	219	(130)
Slag Cement		19	(11)	19	(11)	22	(13)
Silica Fume		8	(5)	--	(5)	--	--
Total Cementitious Content		725	(430)	716	(430)	876	(520)
Water		297	(176)	297	(176)	297	(176)
w/cm		0.41		0.41		0.34	
Fine Aggregate	ASTM C33	1439	(854)	1439	(854)	1439	(854)
Coarse Aggregate	ASTM C33, 1/2"	1509	(895)	1509	(895)	--	--
Chemical Admixtures				*fl. oz/yd³ (ml/m³)*			
HRWR	ASTM C494	51.7	(2000)	51.7	(2000)	51.7	(2000)

3.3.3 Correction Procedure

Each concrete mixture was subjected to a procedure to determine the effect of the bottom portion of the inner cylinder on interface rheology measurements. This procedure was originally proposed by Macosko [43] for general rheometry, and later utilized by Feys [66] for concrete mixtures. The basic principle and underlying assumptions behind this correction procedure is that the registered torque at each rotational velocity level is directly related to the height of the

cylinder that is immersed in the fluid during the test. Different values of torque are expected for each individual filling heights, and it is proposed that the filling height-torque relationship is linear. Hence, this relationship can be extrapolated to the zero-filling height. Finally, by plotting obtained values of torque at "zero-filling height" with respect to measured rotational velocity, as indicated in Figure 3.5, one can obtain a torque correction value for each rotational velocity.

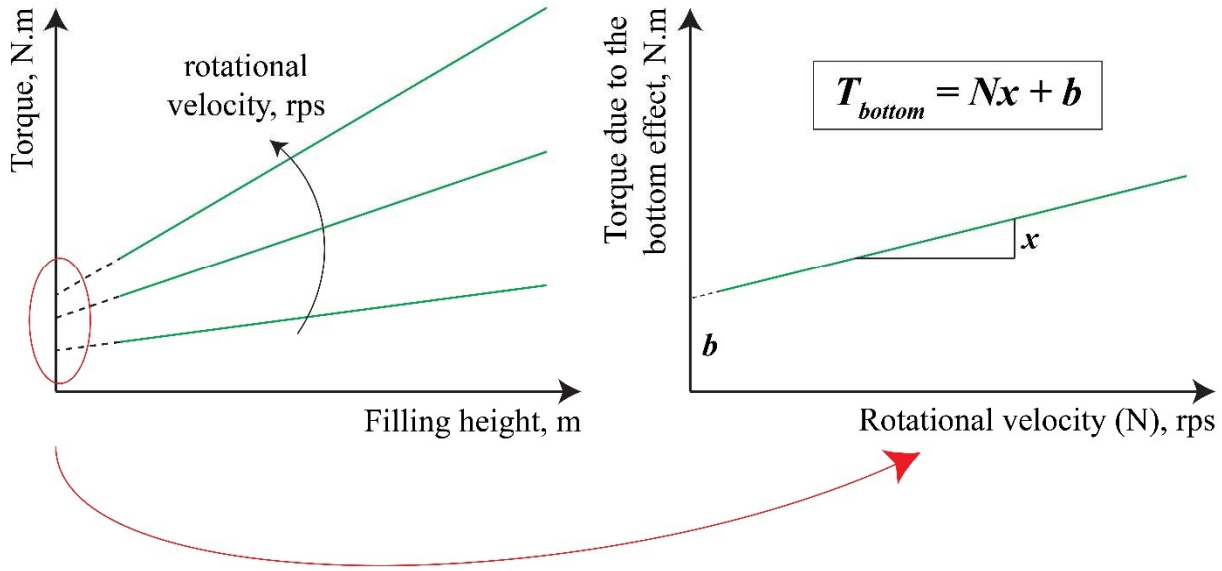

Figure 3.5 – Principle of the correction procedure

Each test was conducted incorporating several filling heights in the interface rheometer to evaluate the secondary flow effect of the bottom of the rotary cylinder. Four filling heights were typically used: (1) only the bottom part of the cylinder immersed in concrete, (2) approximately one third of the cylinder height immersed in concrete, (3) approximately two thirds of the cylinder height immersed in concrete, and (4) cylinder fully immersed in concrete.

The following steps were followed for the testing procedure:

1. Fill the container with concrete to achieve the specific filling height.
2. Insert interface rheometer head into the container.
3. Pre-shear concrete at a constant rotational velocity of 0.6 rps for 30 seconds.
4. Apply a decreasing set of seven rotational velocities, starting from 0.6 rps to and ending at 0.030 rps. Hold each velocity constant for at least 5 seconds.
5. Gently remove the interface rheometer head from the container and record value of the filling height, as shown in Figure 3.6.
6. Remove all material from the cylinder and clean it.
7. Manually remix concrete in the container to homogenize.
8. Repeat steps 1-7 for the next filling height.

Figure 3.6 – Filling height measurement

The above-described correction procedure was identical to the procedure used by Feys [66] with one exception. Step 6 (cleaning the cylinder after each test cycle) was added to the procedure as it was proposed that some inaccuracies associated with the correction procedure could stem from the fact that lubrication layer is not fully recreated for each filling height. In

order to address this issue, the cylinder was cleaned for each filling height, and therefore the lubrication layer was fully generated during each cycle of the test. Since concrete present in the container was reused multiple times, it was always manually remixed in order to homogenize it and to remove any remnants of the lubrication layer from the previous testing cycle.

3.4 Results and Discussion

3.4.1 Rheology

Measured rheological properties and initial workability results are shown in Table 3.4 for all tested mixtures. It is apparent from the results that the rheological properties of all mixtures significantly evolved with time, and that "stiffening" occurred in all cases.

Table 3.4 – Rheology, slump flow

Mixture ID	**A**		**B1**		**B2**		**C1**		**C2**		**D**	
Measurement	*A*	*B*	*A*	*B*	*A*	*B*	*A*	*B*	*A*	*B*	*A*	*B*
						Contec						
Yield Stress, Pa	143	497	336	575	36	68	290	452	136		416	599
Plastic Viscosity, Pa.s	64	65	24	25	18	24	18	11	8		9	11
						ICAR M						
Yield Stress, Pa	265	815	727	1,347	63	212	585	979	296		597	968
Plastic Viscosity, Pa.s	100	80	19	16	21	25	12	12	6		6	4
						ICAR K						
Yield Stress, Pa	190		527		58		583		294		602	
Plastic Viscosity, Pa.s	117		22		24		16		11		8	
						Measured right after mixing						
Slump flow, in. (mm)	18.00	(457)	13.75	(350)	13.75	(350)	22.75	(580)	22.75	(580)	19.75	(500)

Based on the current literature [11], [41], [107], it was expected that rheological properties obtained by the two different types of rheometers (Contec and ICAR) would be different, which was confirmed. The relationship between measured rheological properties by Contec and ICAR rheometers is shown in Figure 3.7a and Figure 3.7b for yield stress and plastic viscosity, respectively. The results shown that for both Bingham parameters, results obtained from ICAR rheometers were substantially higher than values that were measured by the Contec device. However, there exists a relationship between rheological parameters measured by both devices that can if needed be used to correct measurements for the other device. However, the relationship seen in our program was vastly different from that one reported by Khatib [11]. In our study, ICAR rheometers always produced higher values of Bingham parameters as slopes of the ICAR-Contec curves for both yield stress and plastic viscosity were greater than 1 (1.82 and 1.51 for yield stress measured by ICAR M and ICAR K, respectively, and 1.53 and 1.97 for plastic viscosity measured by ICAR M and ICAR K, respectively). On the other hand, Khatib reported that plastic viscosity measured by Contec rheometer was approximately 1.9 times higher than plastic viscosity as measured by ICAR rheometer, and yield stress measured by the same devices was essentially identical (for concretes with yield stress less than 100 Pa and plastic viscosity lower than 100 Pa.s) or slightly lower following exponential relationship when measured by Contec (for concretes with yield stress greater than 100 Pa and plastic viscosity greater than 100 Pa.s). Hence, it is evident that not only the model or brand of rheometer (Contec or ICAR) but also the particular device influences the determination of concrete rheological properties.

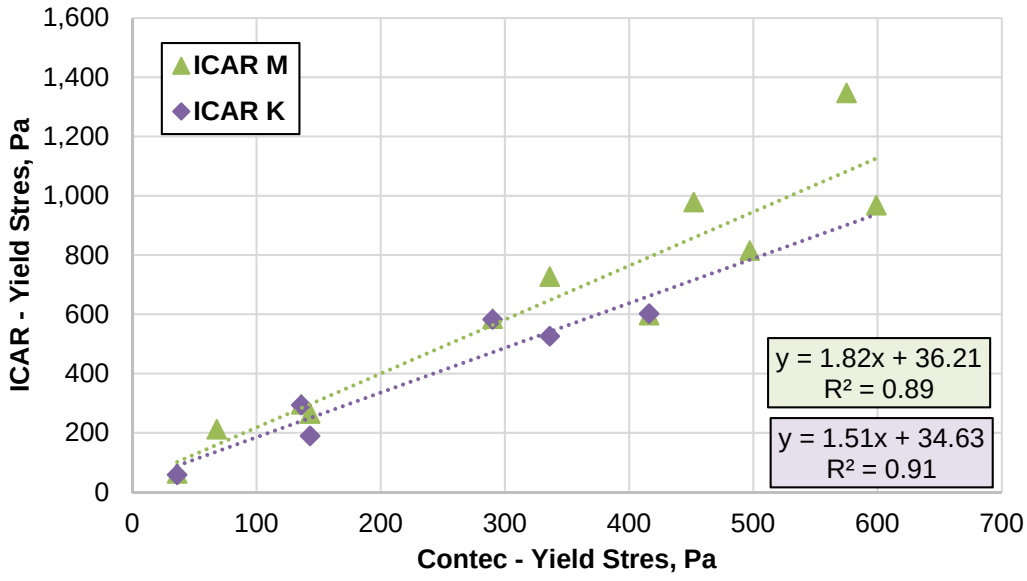

a)

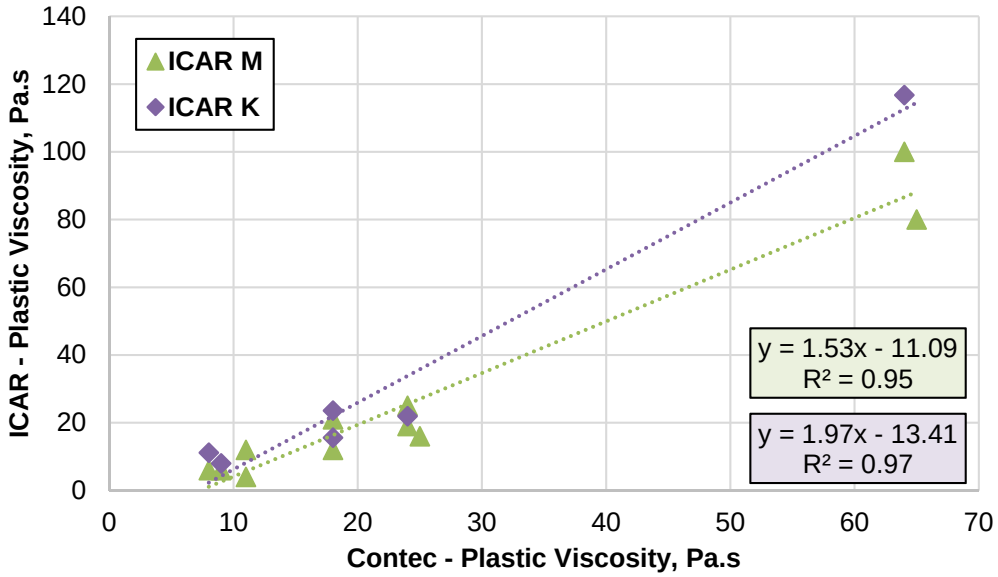

b)

Figure 3.7 – Relationship between measured rheological properties using Contec and ICAR rheometers: a) yield stress, b) plastic viscosity

This is confirmed by examining results produced by both ICAR rheometers, as shown in Figure 3.8a and Figure 3.8b for yield stress and plastic viscosity, respectively. Although identical models of the ICAR rheometer and the same test protocol were used to measure rheological properties of investigated concretes, slightly different results were obtained. As in the case of the

Contec-ICAR relationship, the results revealed that a strong linear relationship exists between Bingham parameters determined by both ICAR devices. The observed difference between rheological parameters determined via ICAR and Contec can be likely attributed to the different geometry of said rheometers. ICAR utilizes vane-based geometry with the rotating inner cylinder (or vane) and stationary outer cylinder, with the torque and velocity sensors connected to the rotating cylinder. On the other hand, Contec's inner cylinder is stationary, although it is also vane-like, and the outer cylinder rotates during the measurement to create the shear effect. The torque sensor is connected to the inner, stationary cylinder. Therefore, with the current state of concrete rheometry and known differences in results produced among different devices, it is reasonable to expect variability in produced results.

For two identical ICAR devices, the differences in results are likely caused by the torque sensor performance, as discussed in Section 3.4.2, as other variables that come to play in rheological measurements (test protocol, rheometer geometry, etc.) are the same for both devices. However, the overall differences in measured parameters were less pronounced for the ICAR rheometers. On average, 11% and 32% difference was observed in ICAR M and ICAR K measurements of yield stress and plastic viscosity, whereas an average difference of 107% and 26% was observed between ICAR M and Contec measurements of yield stress and plastic viscosity, respectively.

Nevertheless, results obtained from various rheometers are still valid and valuable. Although the current state of concrete rheology might not allow for determination of the "true" Bingham parameters of concrete mixtures, rheometers are typically used in comparative investigations where performance and properties of various concrete mixtures are evaluated. To

this extent, the uncertainty of rheological measurements with various devices does not affect applicability of concrete rheometers, as long as results from different devices are not combined.

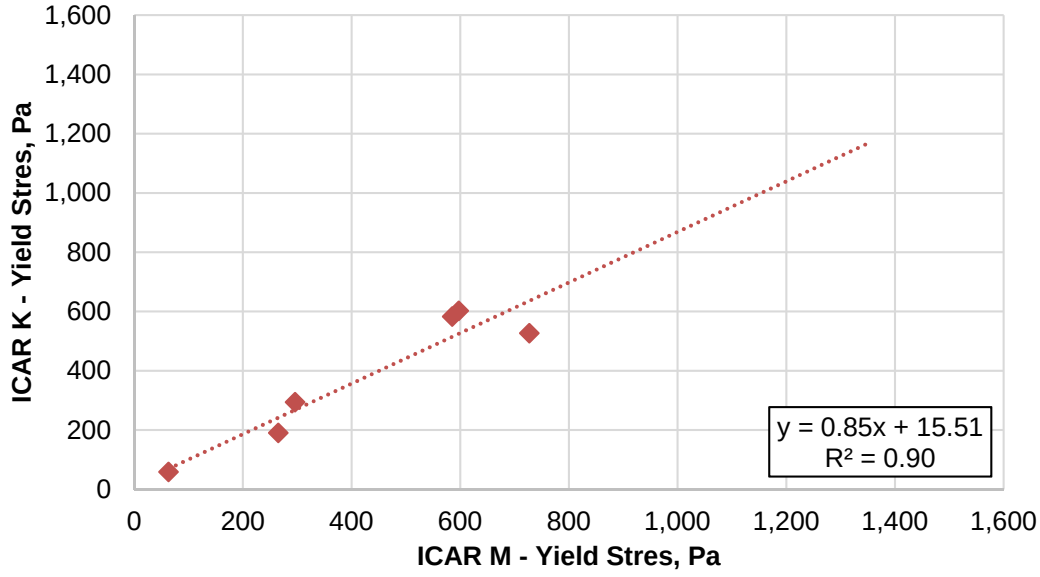

a)

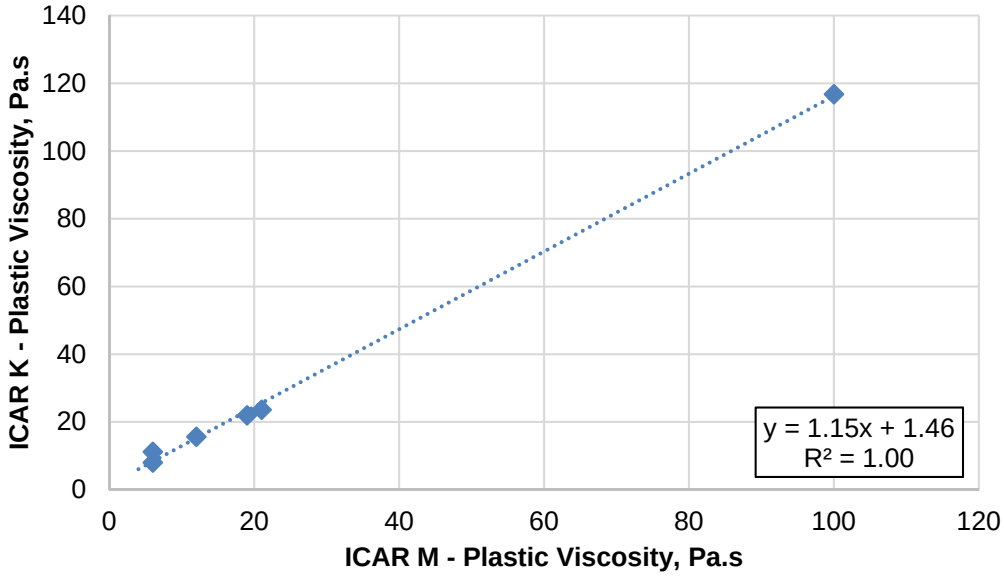

b)

Figure 3.8 – Relationship between measured rheological properties using ICAR M and ICAR K rheometers: a) yield stress, b) plastic viscosity

3.4.2 Zero-Torque Measurements

The first generation of ICAR rheometers is known to have issues with the torque sensor, in particular with its calibration to zero value before proceeding with rheological measurements. With this in mind, measurements with an empty container were performed to evaluate accuracy of the torque sensor, and to manually reset the torque sensor to zero value before proceeding with measurements on concrete mixtures. Results of these measurements for ICAR K are shown in Figure 3.9 and Figure 3.10 for zero-torque measurements with the standard ICAR vane, and Figure 3.11 with interface rheometer head. It is apparent from the results that using the "Zero Torque" button implemented in the ICAR software does not result in a complete zeroing of the torque sensors as mostly negative torque values were measured when no fluid was placed in the container (and therefore only air is sheared and thus torque should be zero). For ICAR K, registered negative torque values decreased for lower rotational velocities. Zero-torque measurements were performed prior to commencement of testing for each mixture. The results show that for the initial two mixtures (mixtures A and B1), the registered torque values were lower than values measured for the remainder of the testing. This is likely due to varying temperature of the sensor; the ICAR K was stored in a parked vehicle outside the research facility the night prior to the testing program, with temperatures below freezing point that night. Initially, it was noted that the device was cold on the surface, therefore it is reasonable to expect that temperature of the torque sensor was also lower at the beginning of the testing. This is further validated by zero-torque measurements obtained from ICAR M, as shown in Figure 3.12, that was stored in the laboratory before testing. Obtained zero-torque values of ICAR M are relatively consistent throughout the whole measurement set, and not as dependent on imposed

rotational velocity as zero-torque values of ICAR K. Additionally, zero-torque values were significantly lower for ICAR K then for ICAR M.

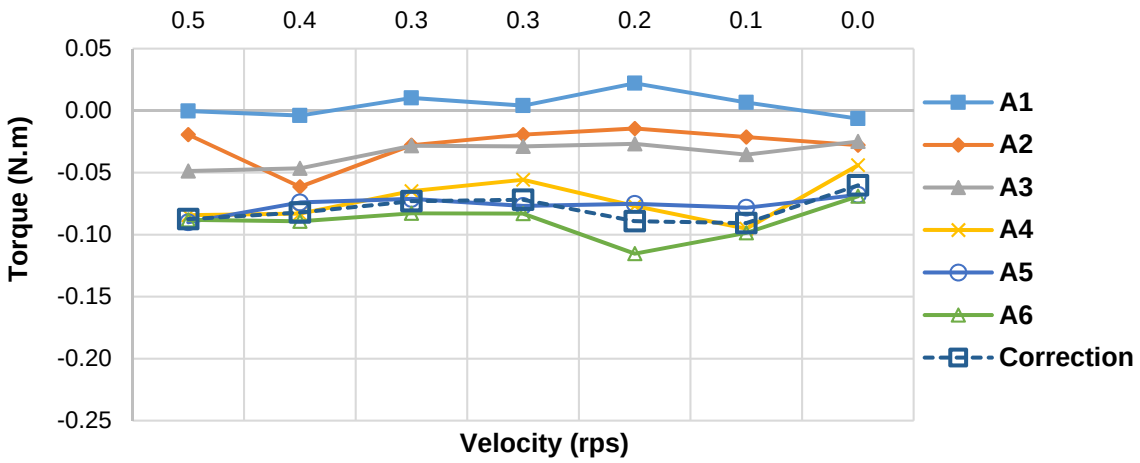

a)

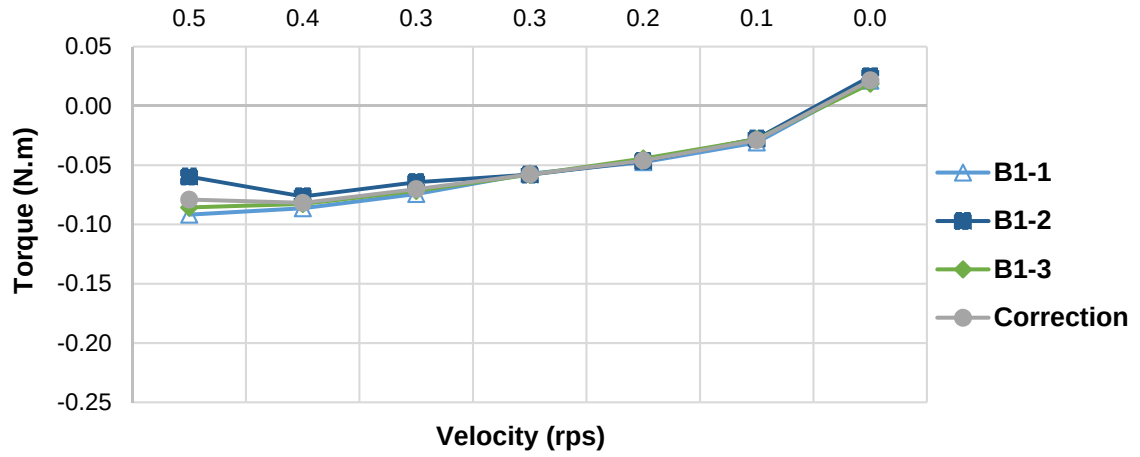

b)

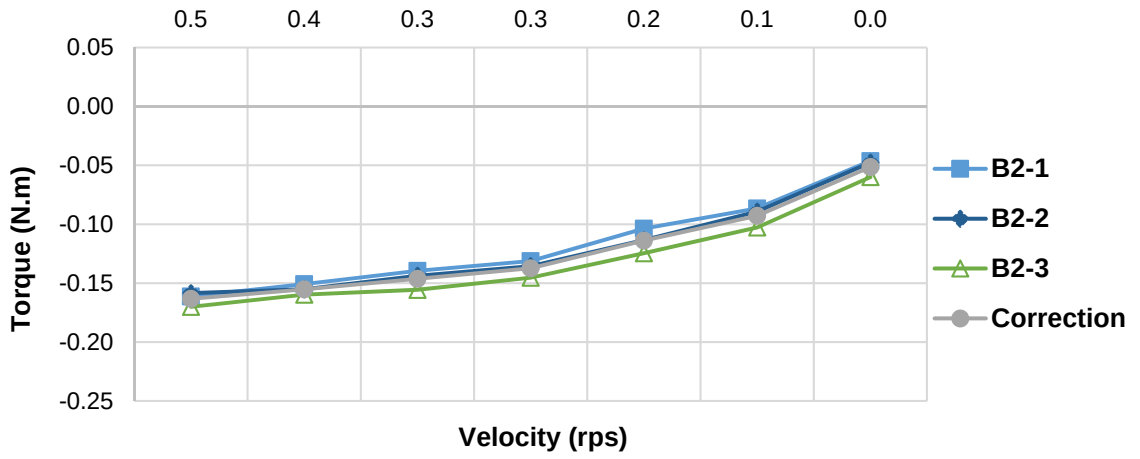

c)

Figure 3.9 – Zero-torque measurements, ICAR K, vane: a) Mixture A, b) Mixture B1, c) Mixture B2

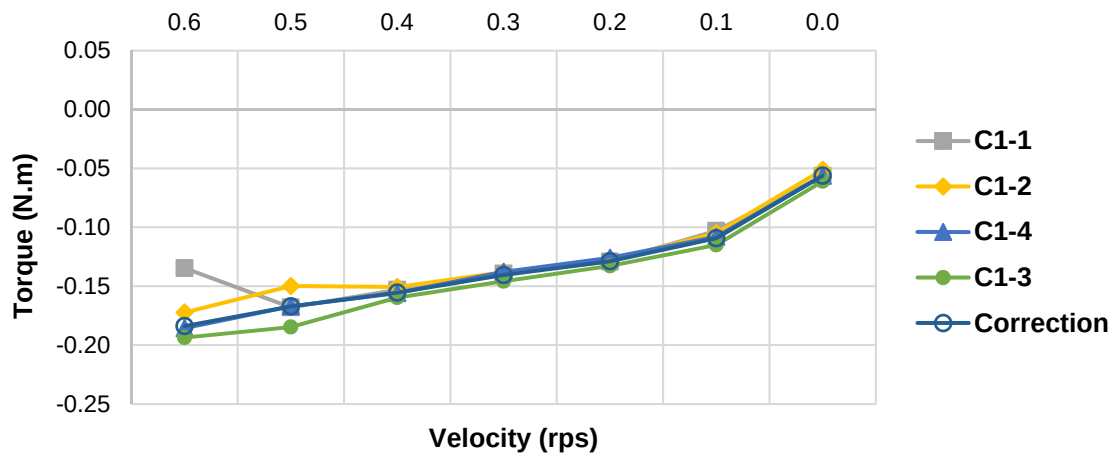

a)

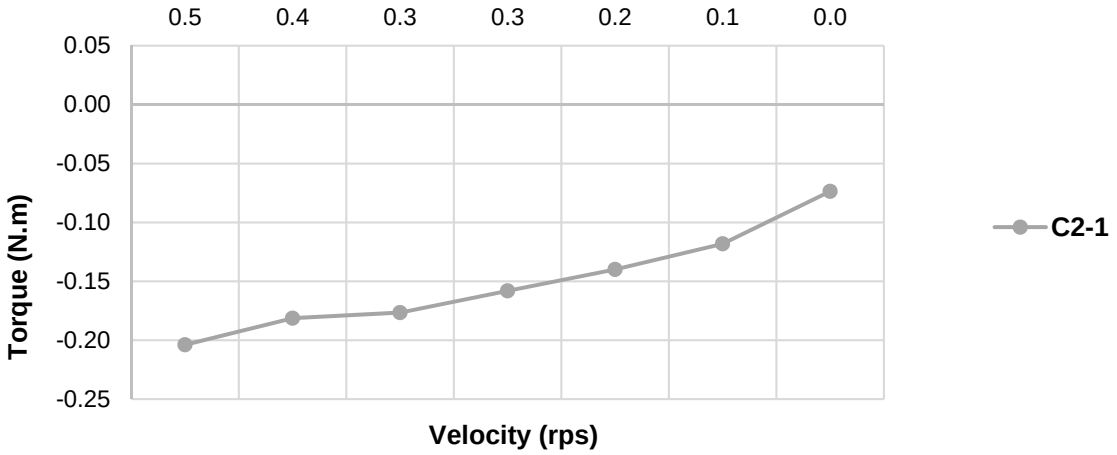

b)

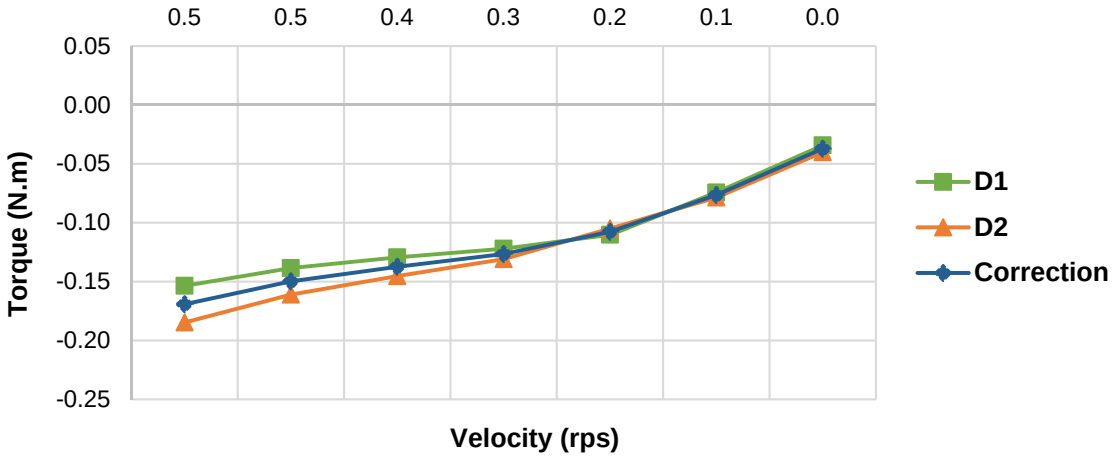

c)

Figure 3.10 – Zero-torque measurements, ICAR K, vane: a) Mixture C1, b) Mixture C2, c) Mixture D

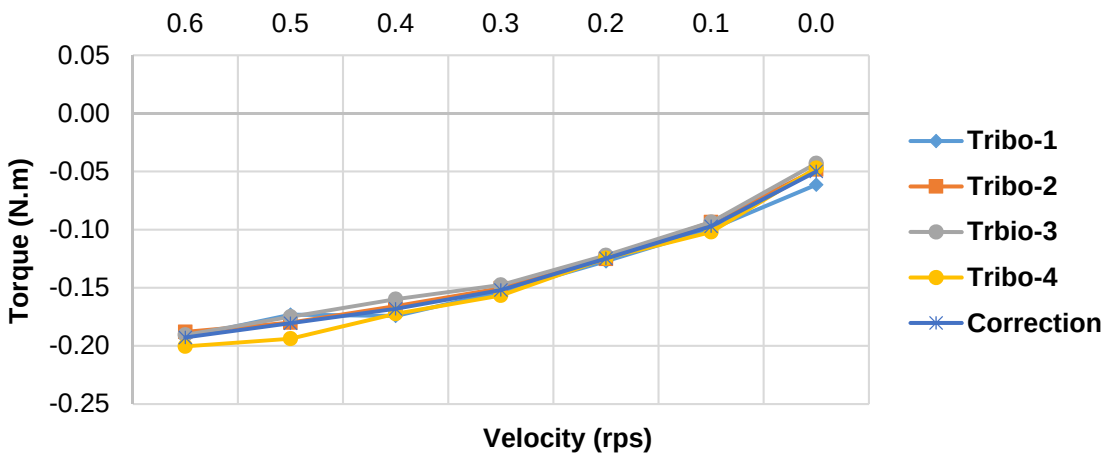

Figure 3.11 – Zero-torque measurements, ICAR K, interface rheometer head

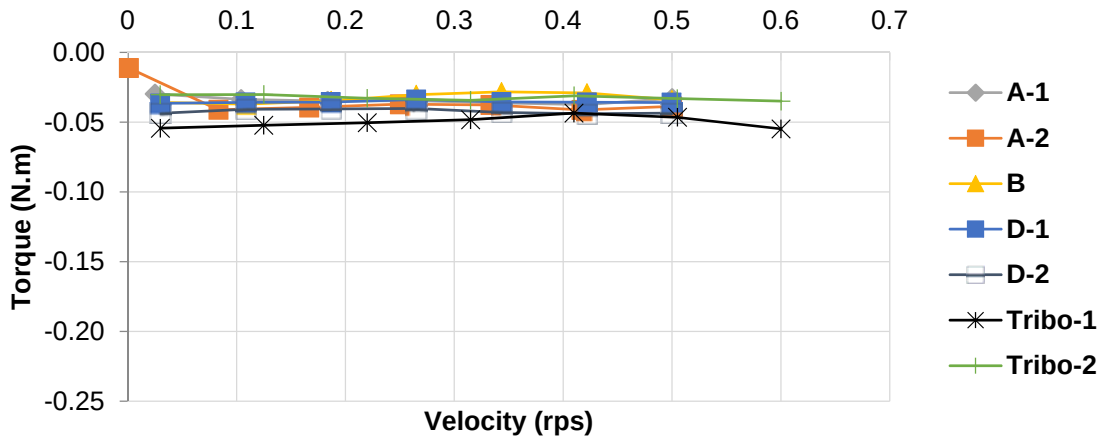

Figure 3.12 – Zero-torque measurements, ICAR M

Based on the measured zero-torque values, the following adjustments to the registered torque values obtained from individual tests (both rheology and interface rheology measurements) were made: (1) for ICAR M, since the zero-torque measurements showed a consistent trend thought the testing campaign, an average correction value based on measured zero-torque results was subtracted from the registered torque during data analysis, and (2) for ICAR K, a unique torque correction value was determined based on the zero-torque

measurements results for each series of mixtures, and also subtracted from the registered torque values during data manipulation phase of this study.

3.4.3 Correction Procedure

Results of the correction procedure, i.e. the filling height-torque and rotational velocity-torque curves, are shown in Figure 3.13 through Figure 3.32 for combination of all interface rheometers (interface rheometer K and M) and concrete/mortar mixtures (mixtures A, B1, B2, C1, C2 and D). For all mixtures except mixture C2, the correction procedure was performed with all three interface rheometer designs (interface rheometers K and M with the cone-shaped cylinder, and interface rheometer K with the flat-bottom cylinder); for mixture C2, only cone-shaped cylinders were used. For mixture D (mortar), measurements were carried out twice in a short sequence. For interface rheometer K, in the case of all mixtures but mixture A, measurements with the cone-shaped cylinder were performed first, followed by measurements with the flat-bottom cylinder. In all cases during the data analysis stage, results obtained for the smallest rotational velocity of 0.030 rps had to be removed from the data set as values obtained were apparently incorrect. This was due to the fact that at this very slow rotational speed and in combination with low filling height, the overall torque magnitude recorder by the ICAR device was very low (values were less than 1% of the maximum capacity of the load cell), therefore, the sensor was not sensitive enough to capture the resultant torque with a good accuracy.

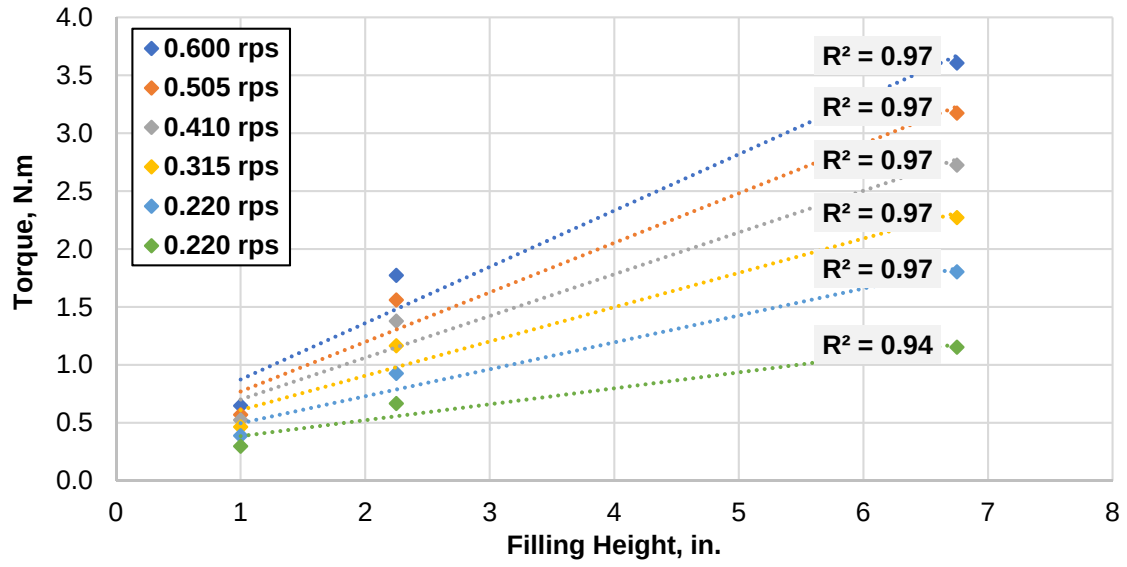

a)

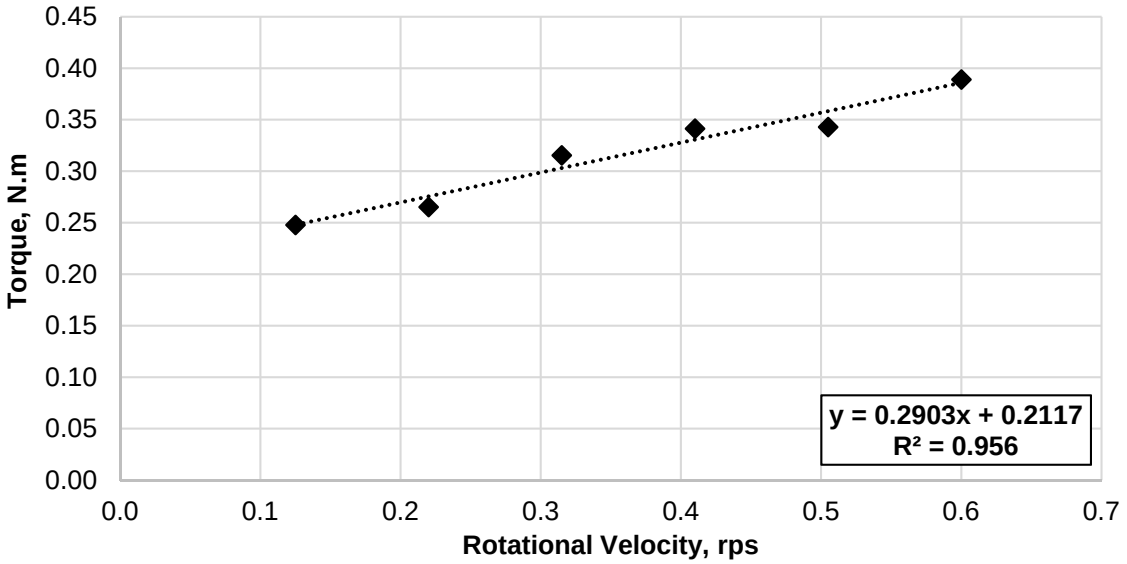

b)

Figure 3.13 – Correction procedure results, Mixture A, ICAR K – Cone: a) filling height-torque relationship, b) rotational velocity-torque relationship

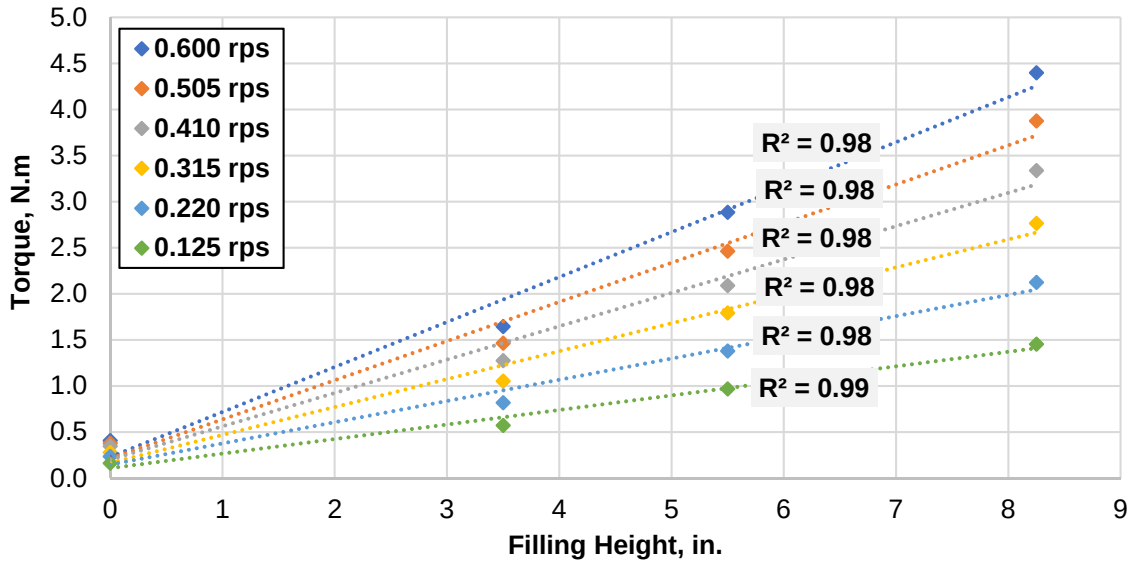

a)

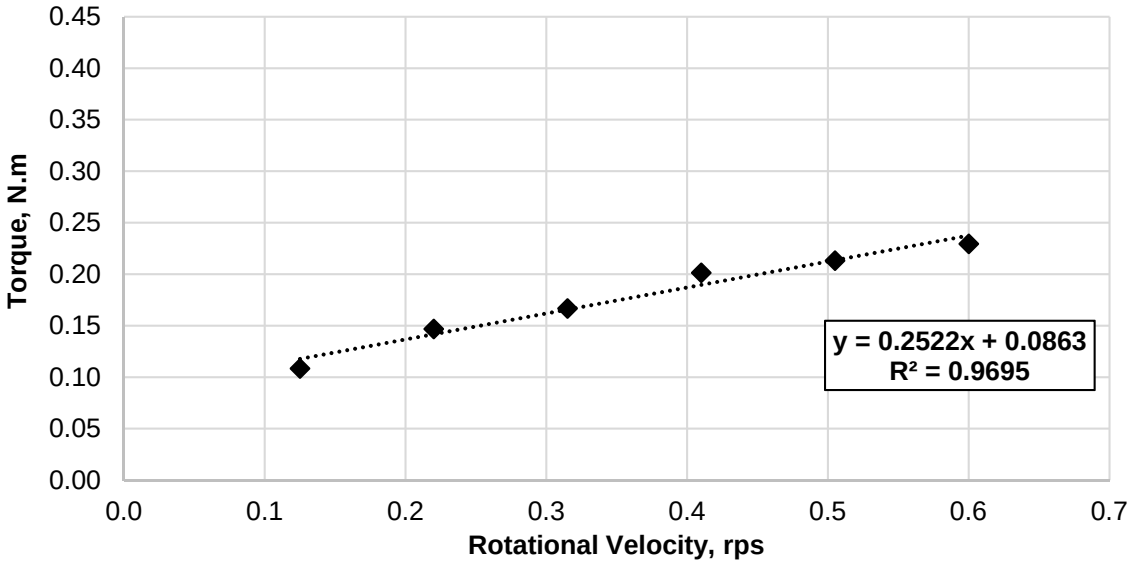

b)

Figure 3.14 – Correction procedure results, Mixture A, ICAR K – Flat: a) filling height-torque relationship, b) rotational velocity-torque relationship

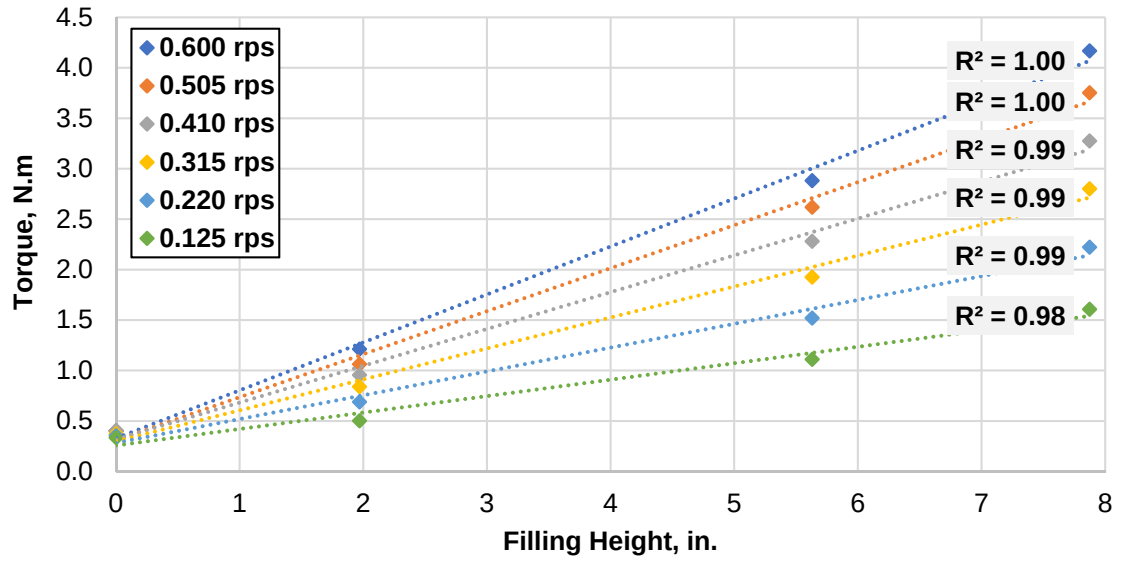

a)

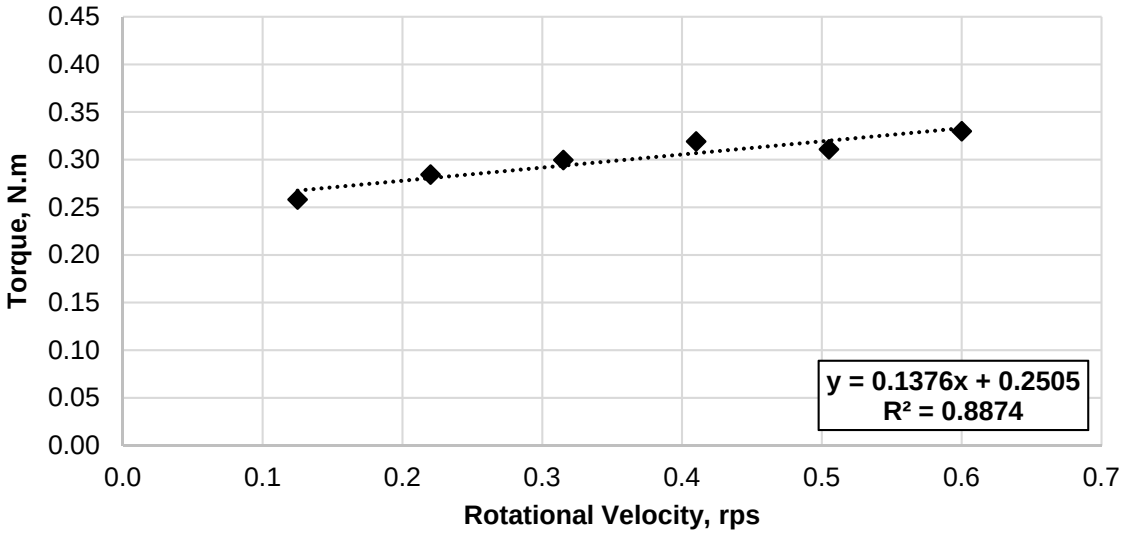

b)

Figure 3.15 – Correction procedure results, Mixture A, ICAR M – Cone: a) filling height-torque relationship, b) rotational velocity-torque relationship

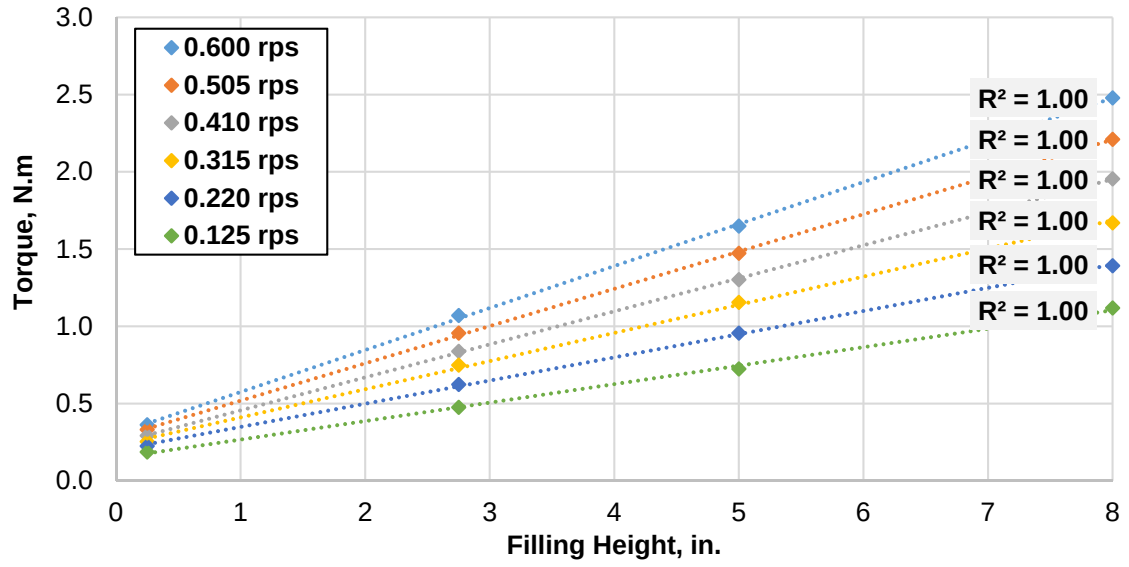

a)

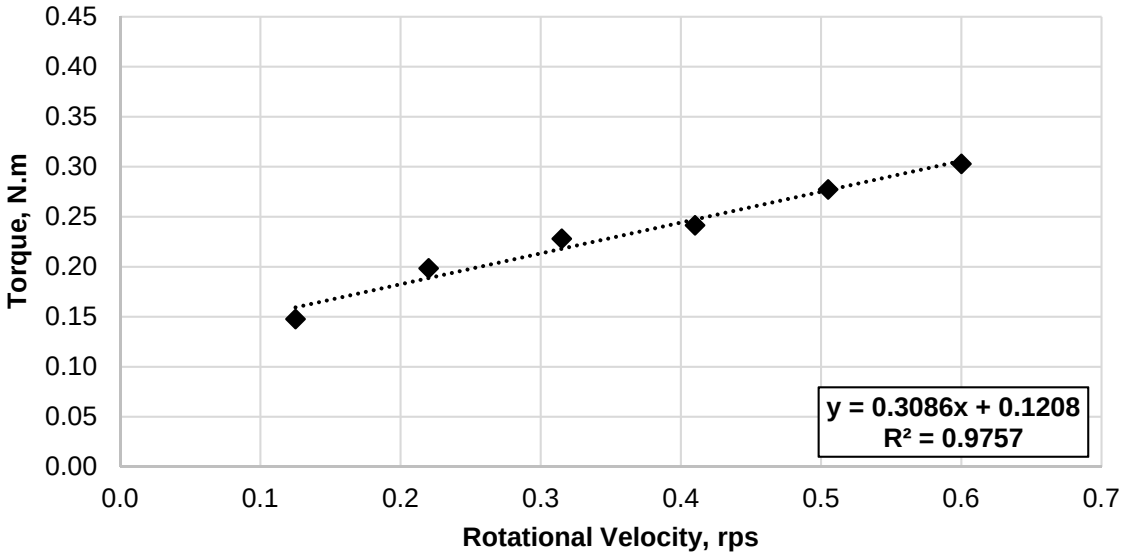

b)

Figure 3.16 – Correction procedure results, Mixture B1, ICAR K – Cone: a) filling height-torque relationship, b) rotational velocity-torque relationship

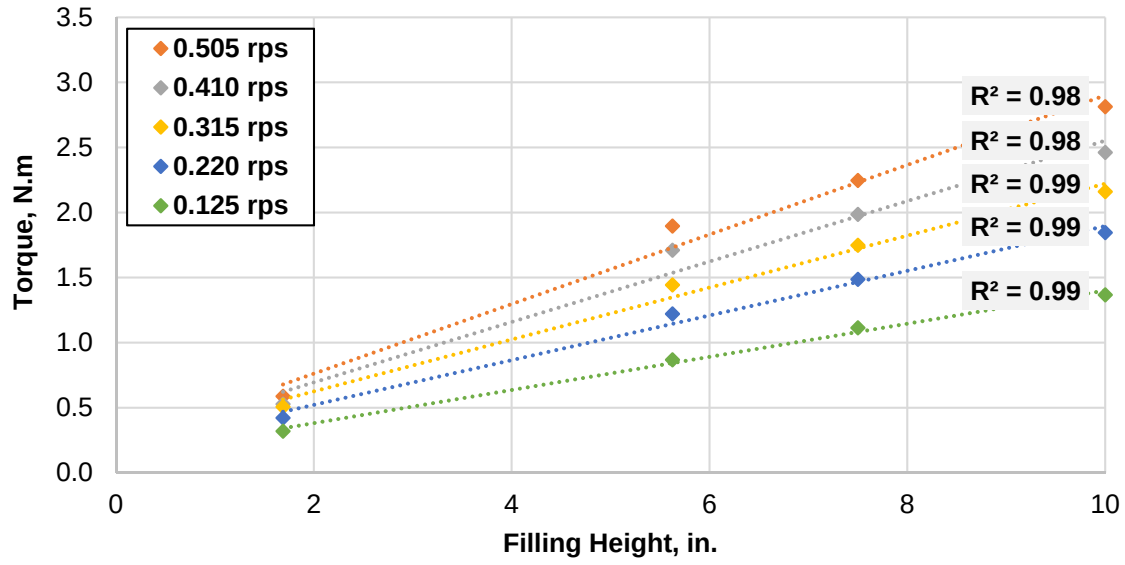

a)

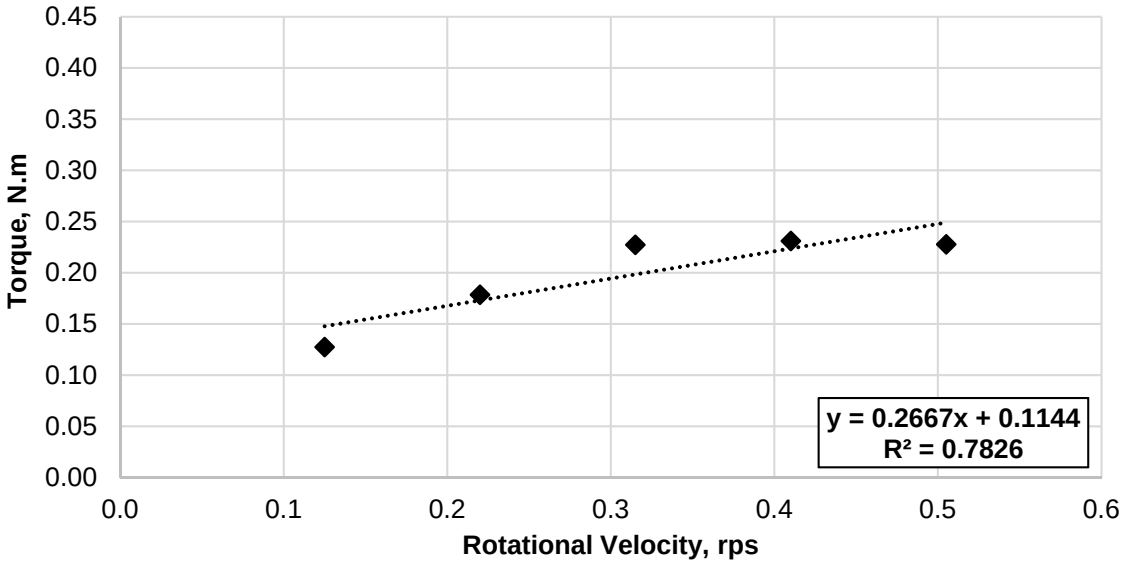

b)

Figure 3.17 – Correction procedure results, Mixture B1, ICAR K – Flat: a) filling height-torque relationship, b) rotational velocity-torque relationship

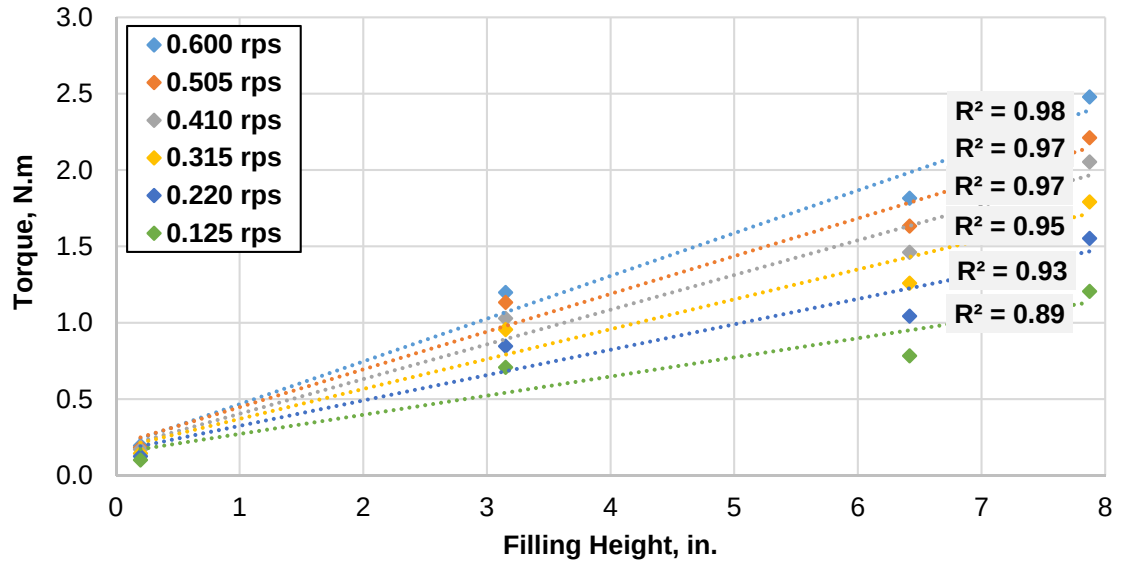

a)

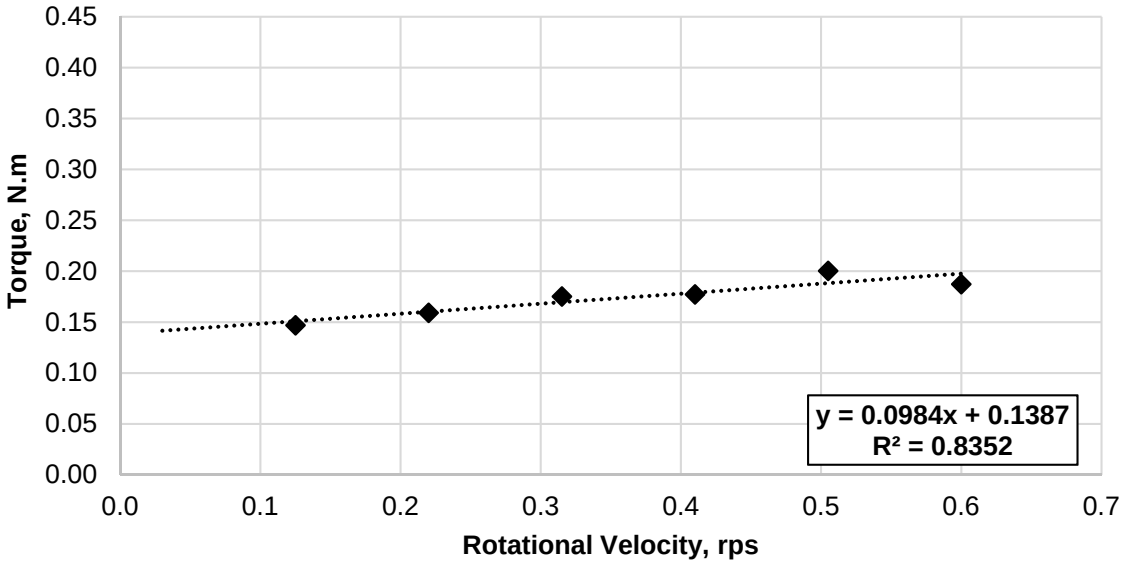

b)

Figure 3.18 – Correction procedure results, Mixture B1, ICAR M – Cone: a) filling height-torque relationship, b) rotational velocity-torque relationship

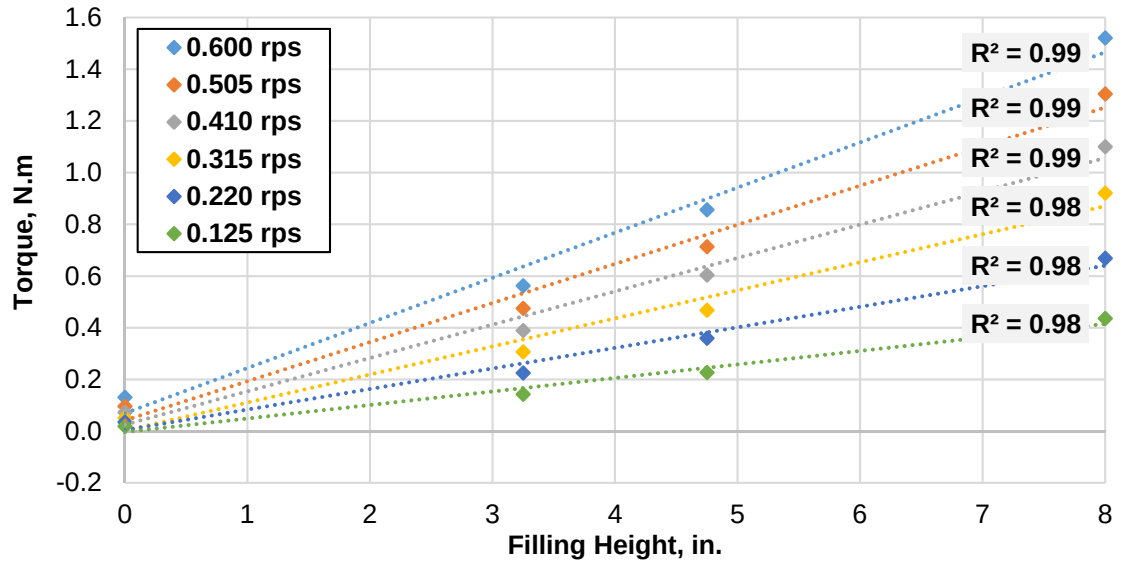

a)

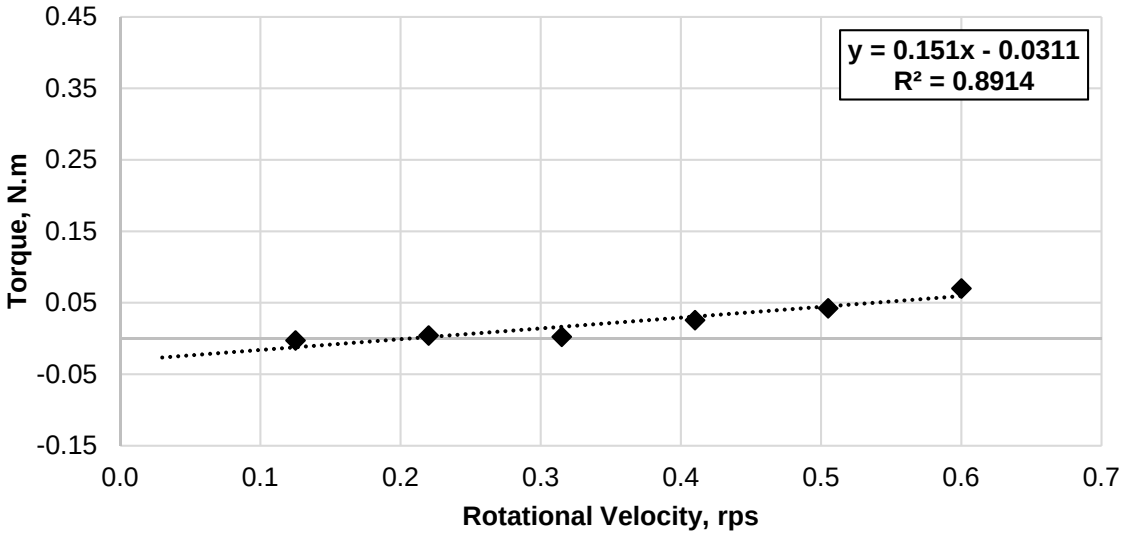

b)

Figure 3.19 – Correction procedure results, Mixture B2, ICAR K – Cone: a) filling height-torque relationship, b) rotational velocity-torque relationship

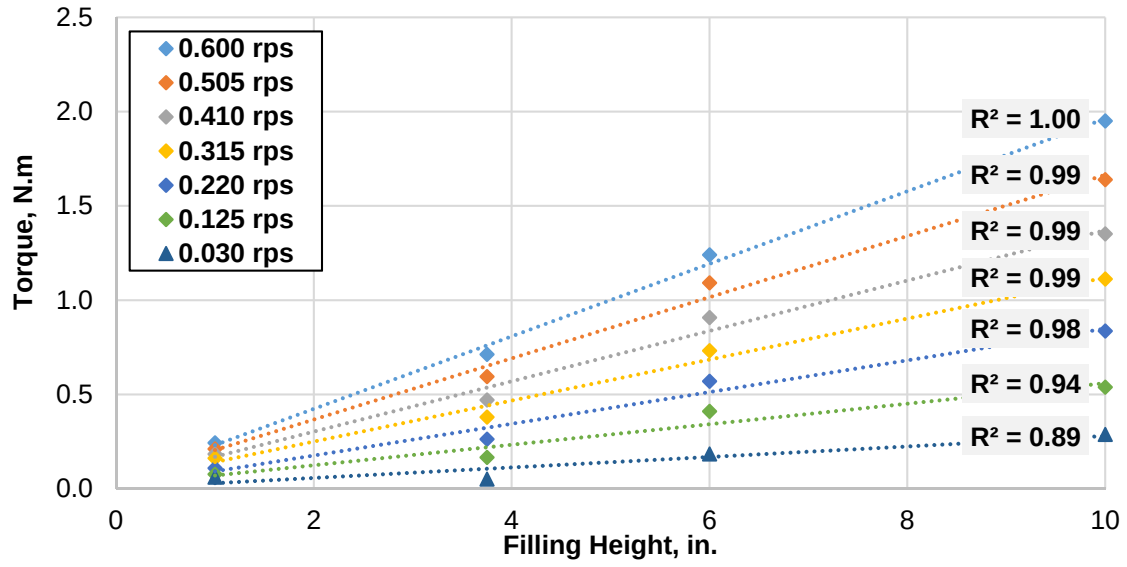

a)

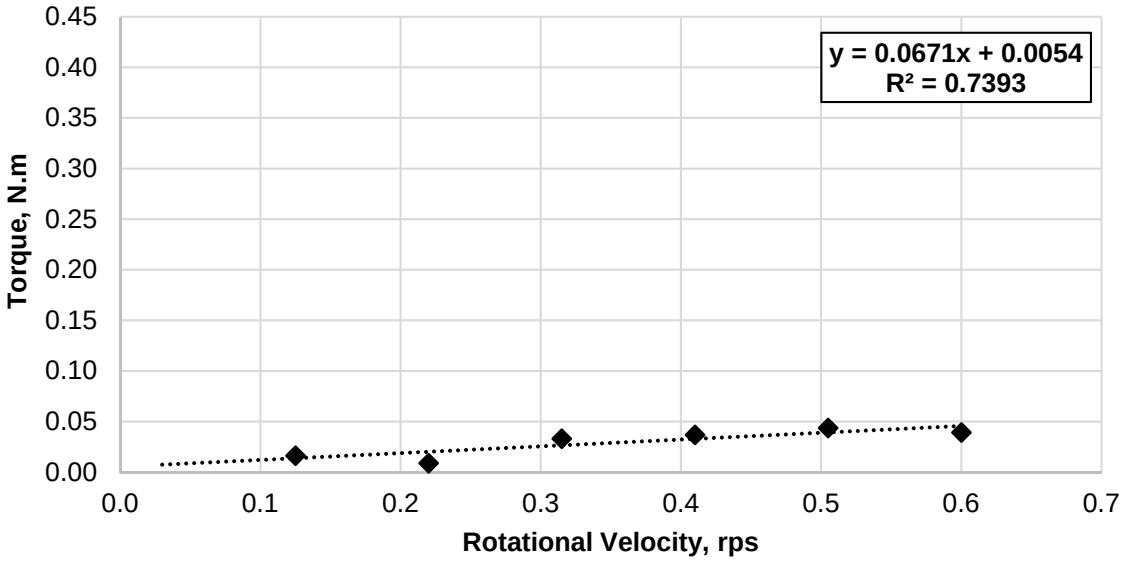

b)

Figure 3.20 – Correction procedure results, Mixture B2, ICAR K – Flat: a) filling height-torque relationship, b) rotational velocity-torque relationship

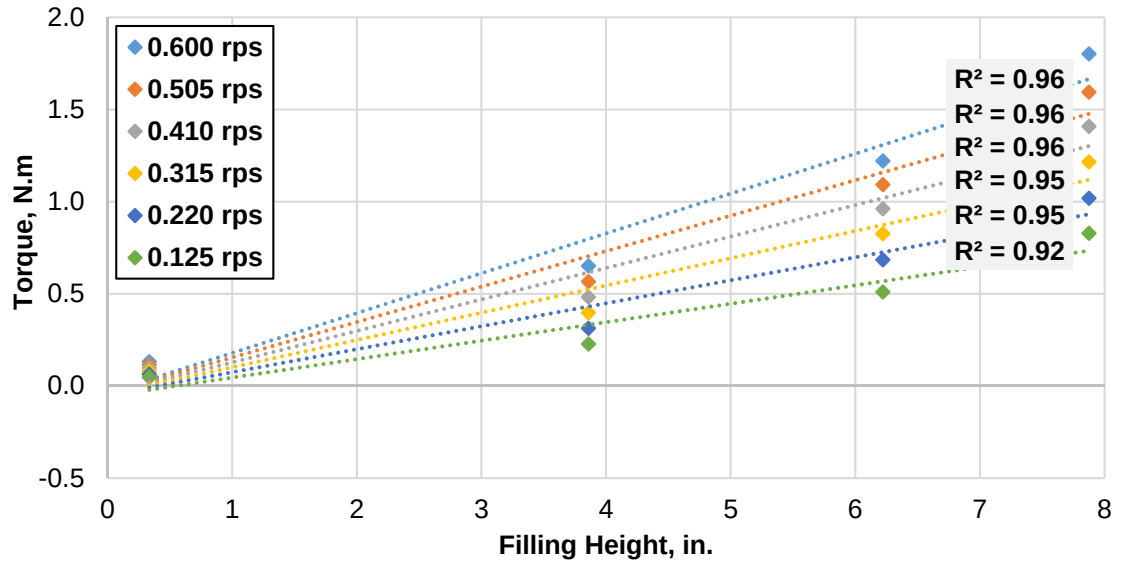

a)

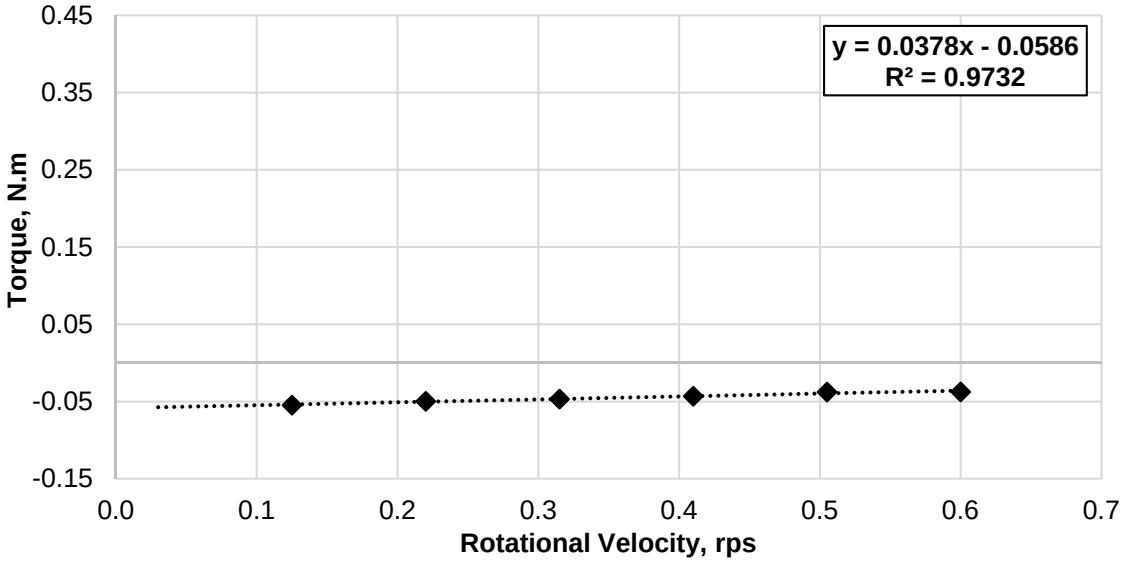

b)

Figure 3.21 – Correction procedure results, Mixture B2, ICAR M – Cone: a) filling height-torque relationship, b) rotational velocity-torque relationship

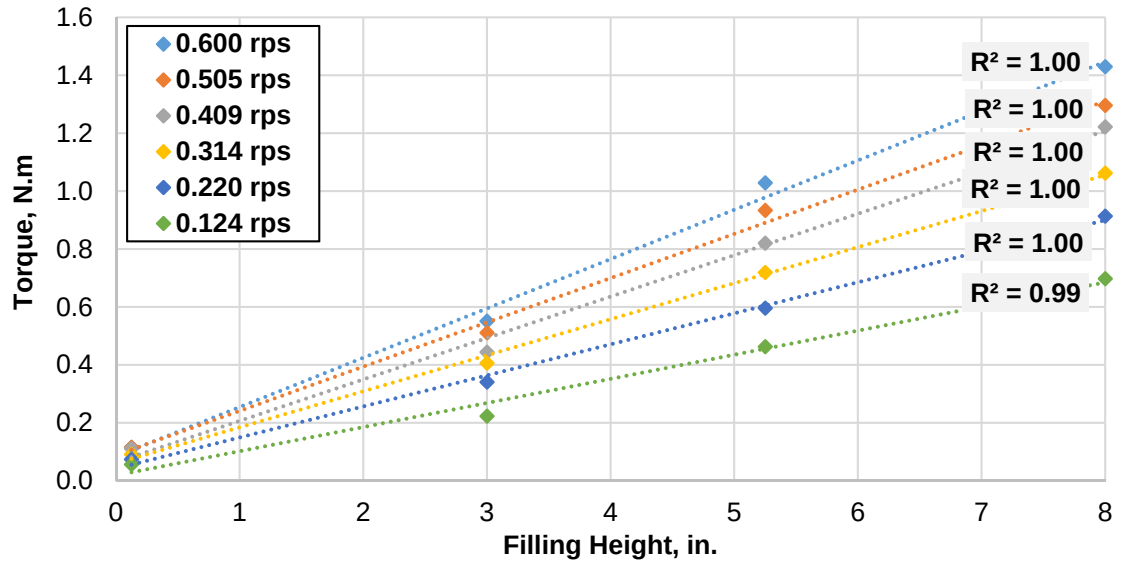

a)

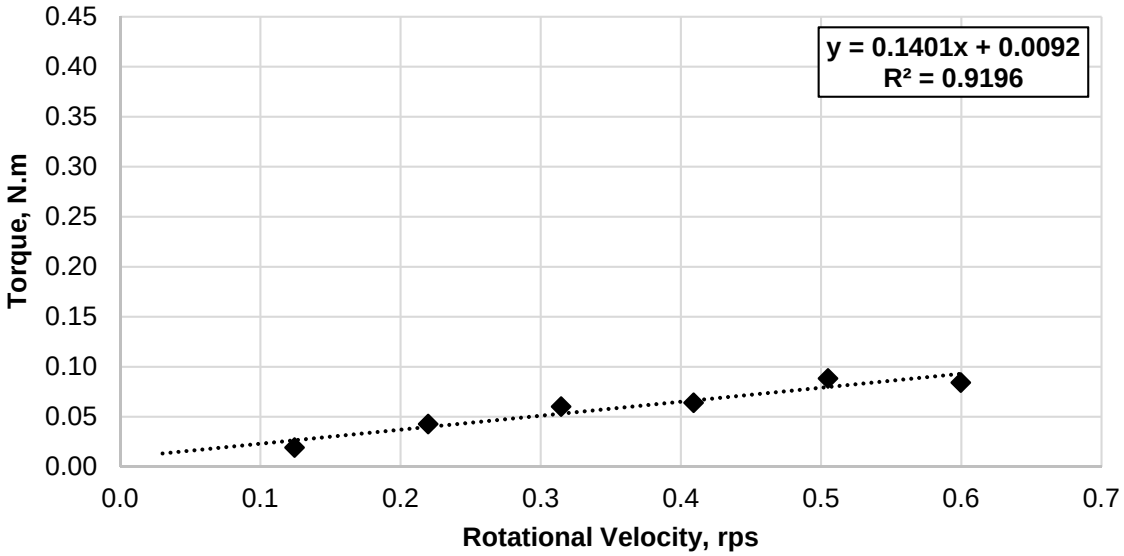

b)

Figure 3.22 – Correction procedure results, Mixture C1, ICAR K – Cone: a) filling height-torque relationship, b) rotational velocity-torque relationship

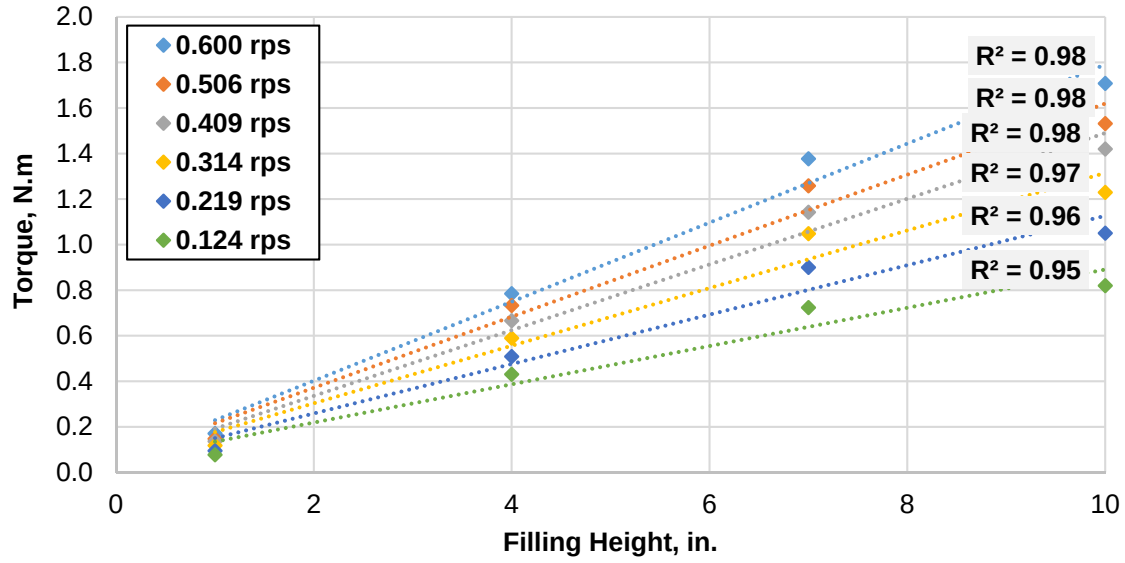

a)

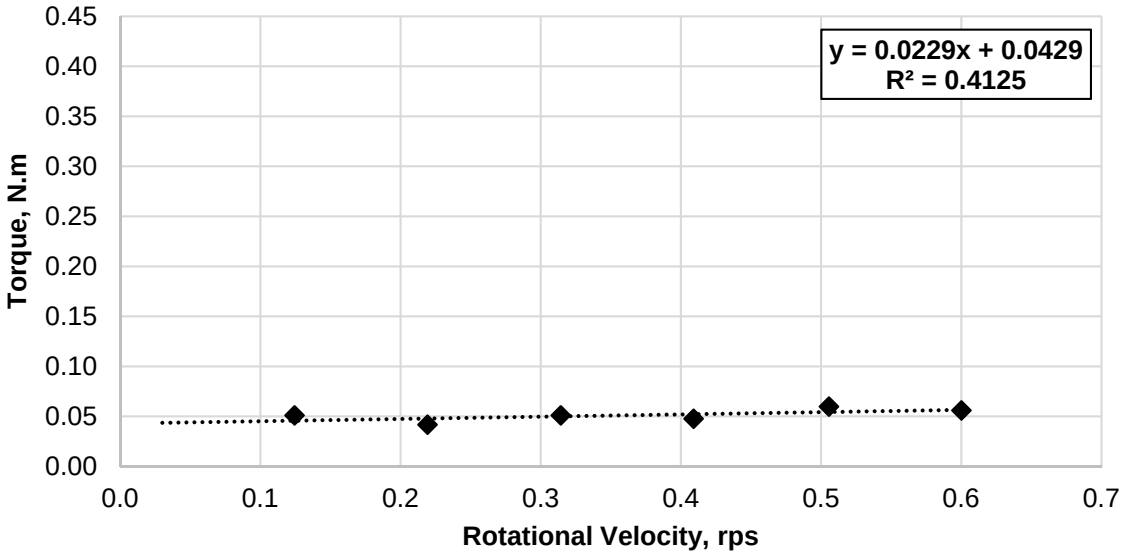

b)

Figure 3.23 – Correction procedure results, Mixture C1, ICAR K – Flat: a) filling height-torque relationship, b) rotational velocity-torque relationship

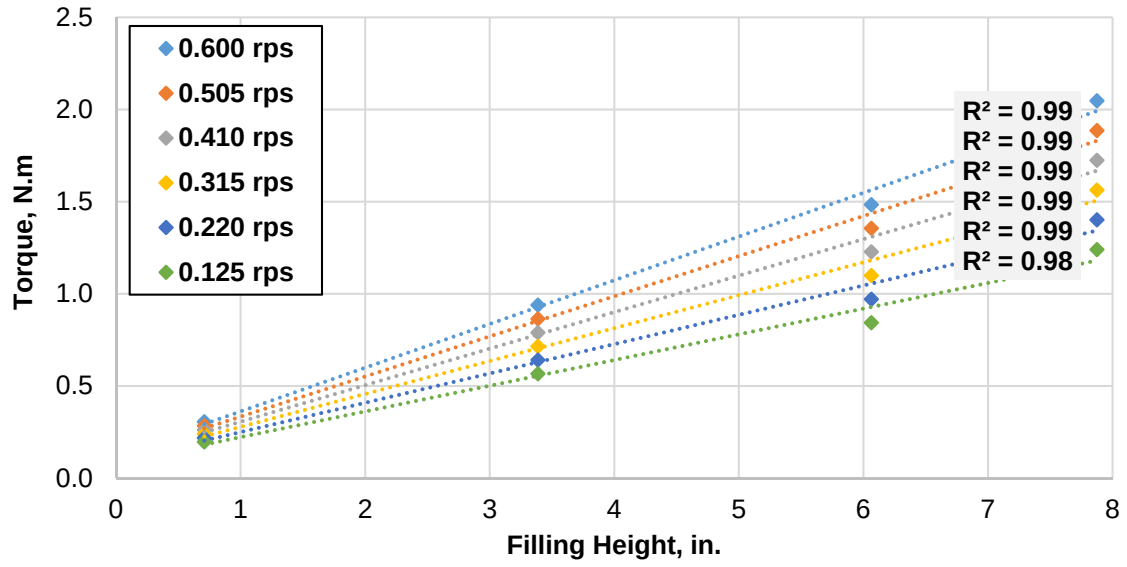

a)

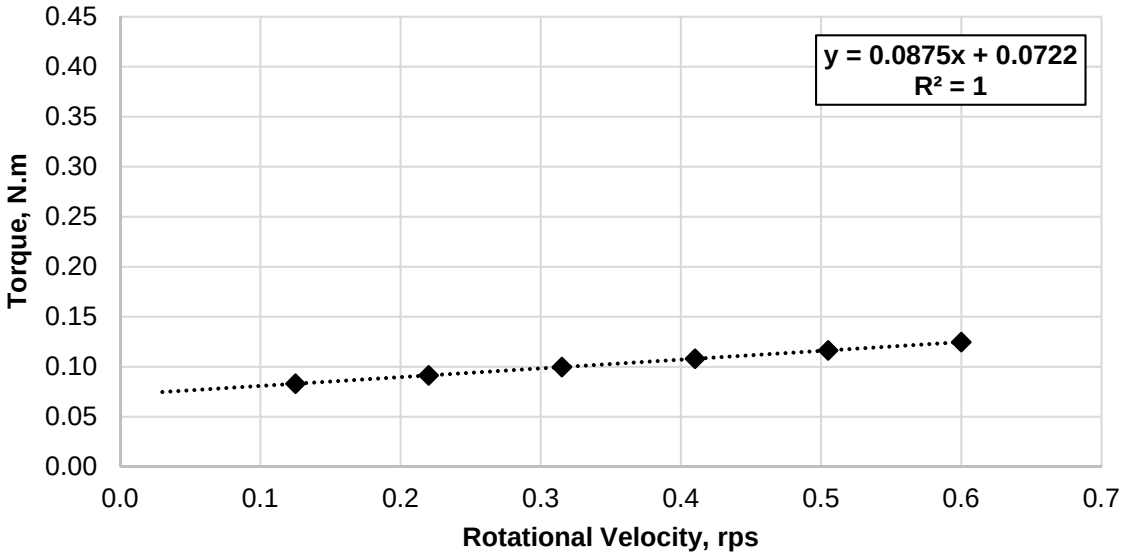

b)

Figure 3.24 – Correction procedure results, Mixture C1, ICAR M – Cone: a) filling height-torque relationship, b) rotational velocity-torque relationship

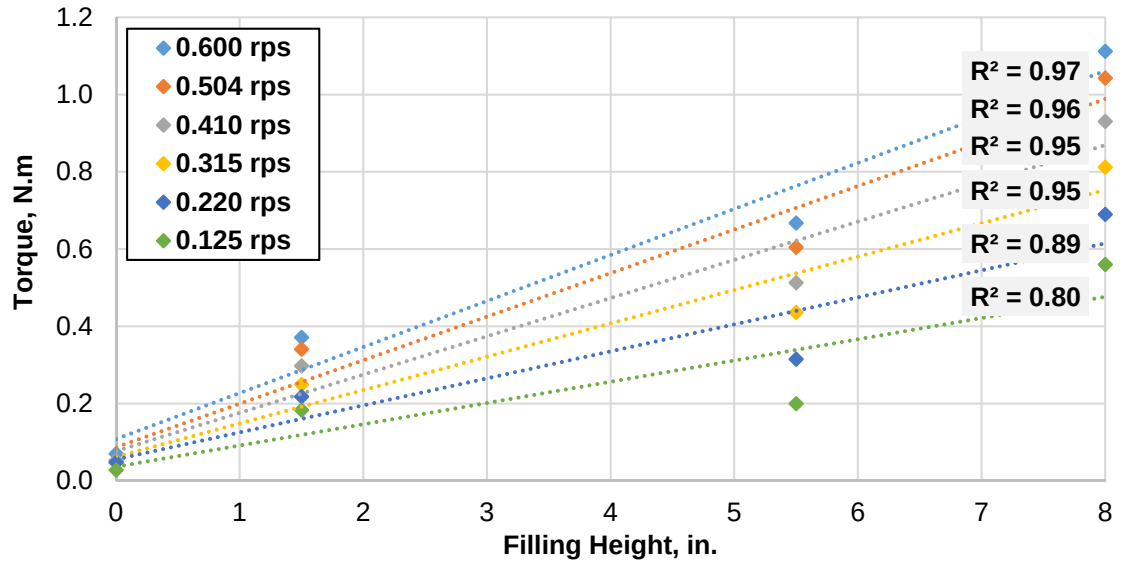

a)

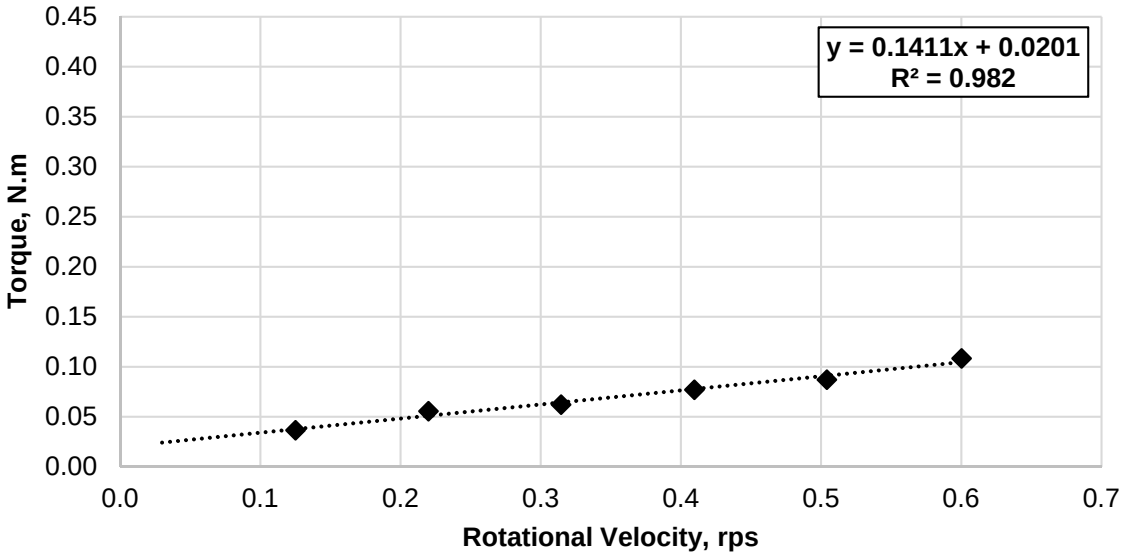

b)

Figure 3.25 – Correction procedure results, Mixture C2, ICAR K – Cone: a) filling height-torque relationship, b) rotational velocity-torque relationship

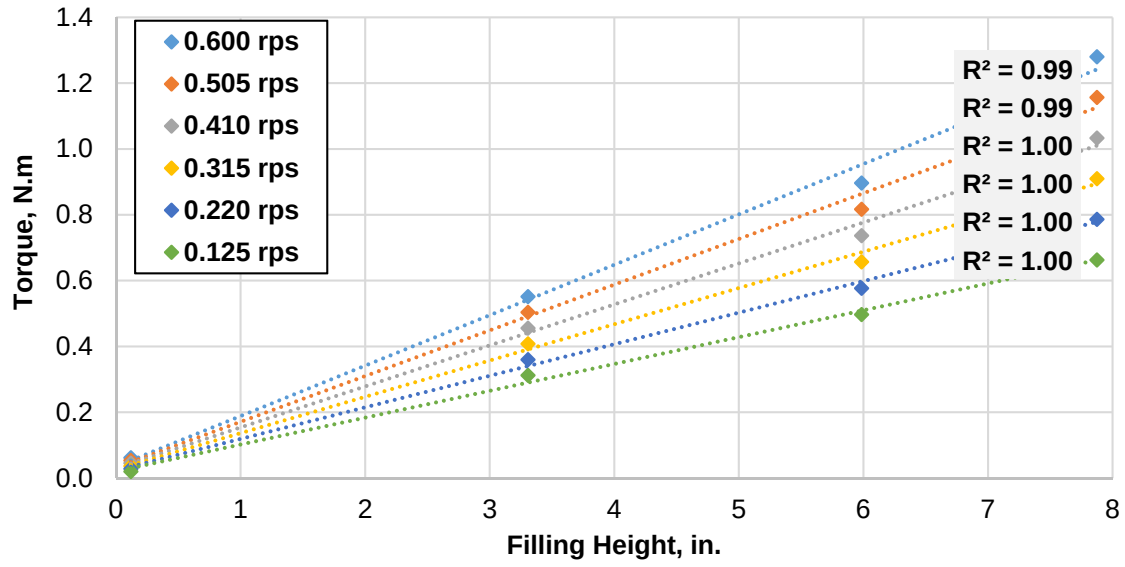

a)

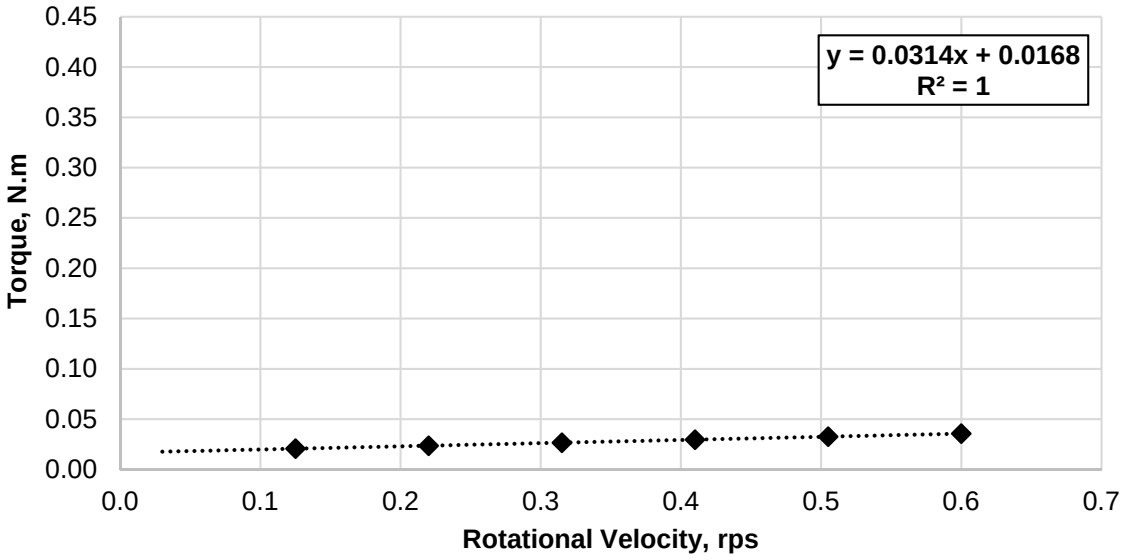

b)

Figure 3.26 – Correction procedure results, Mixture C2, ICAR M – Cone: a) filling height-torque relationship, b) rotational velocity-torque relationship

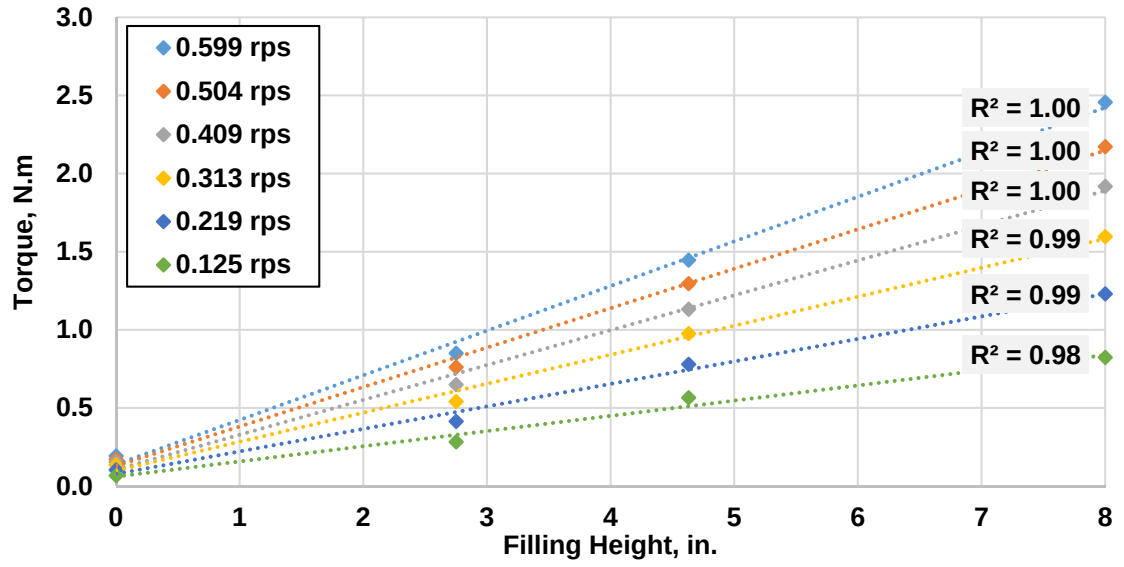

a)

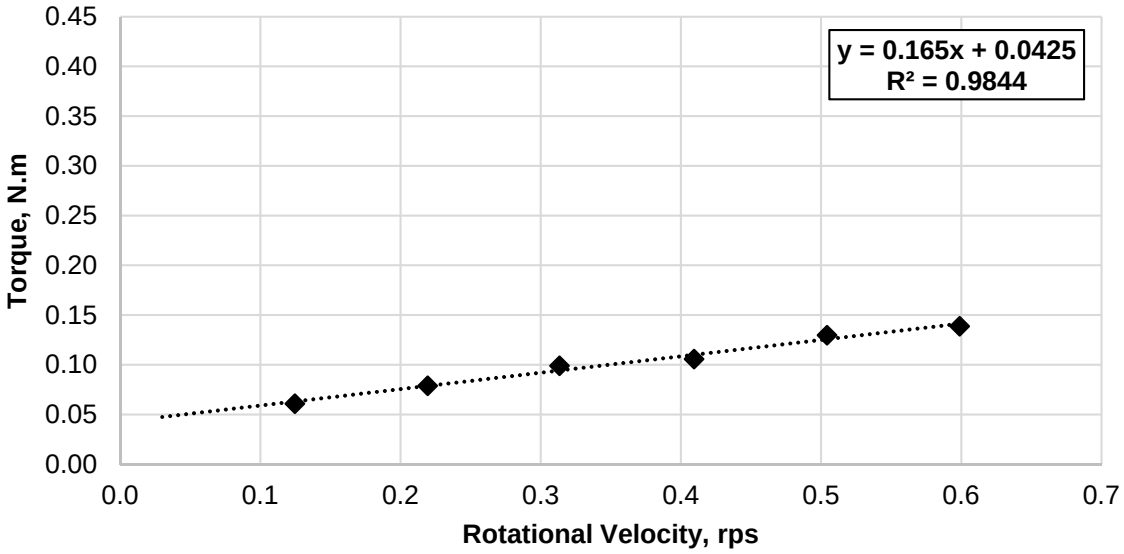

b)

Figure 3.27 – Correction procedure results, Mixture D, ICAR K – Cone – Measurement #1: a) filling height-torque relationship, b) rotational velocity-torque relationship

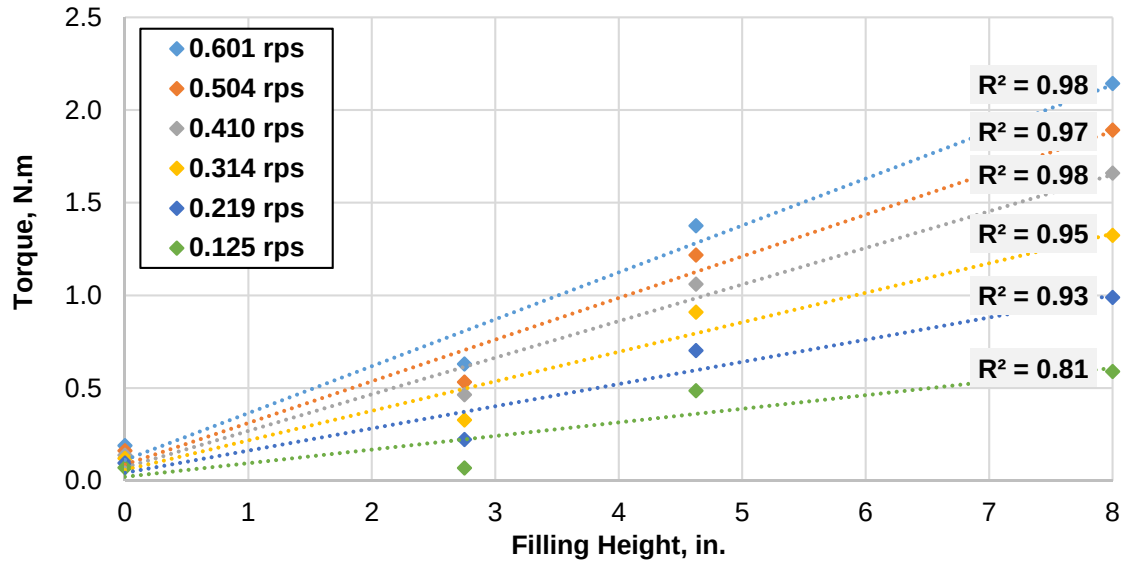

a)

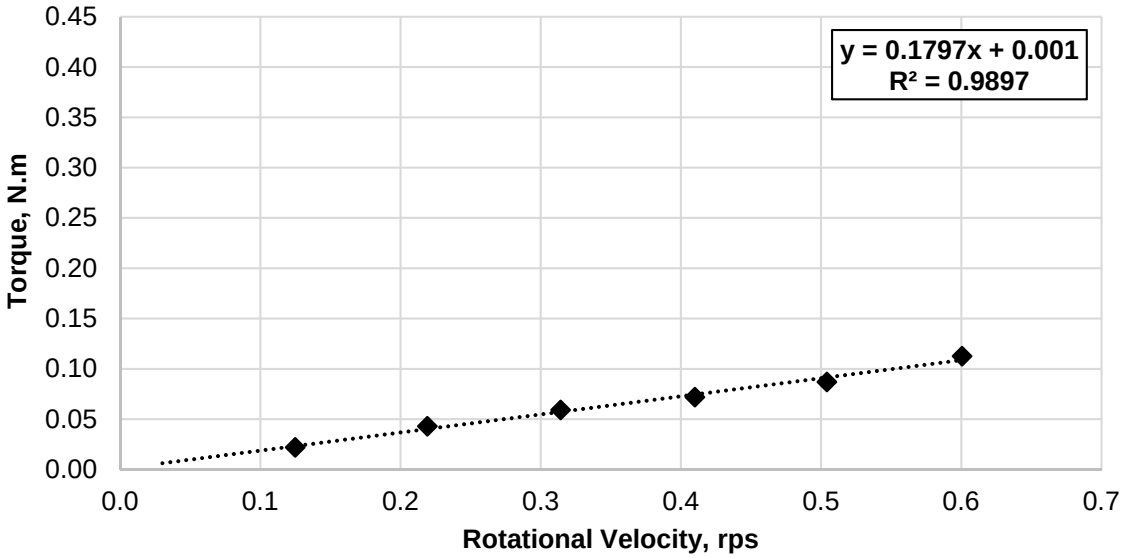

b)

Figure 3.28 – Correction procedure results, Mixture D, ICAR K – Cone – Measurement #2: a) filling height-torque relationship, b) rotational velocity-torque relationship

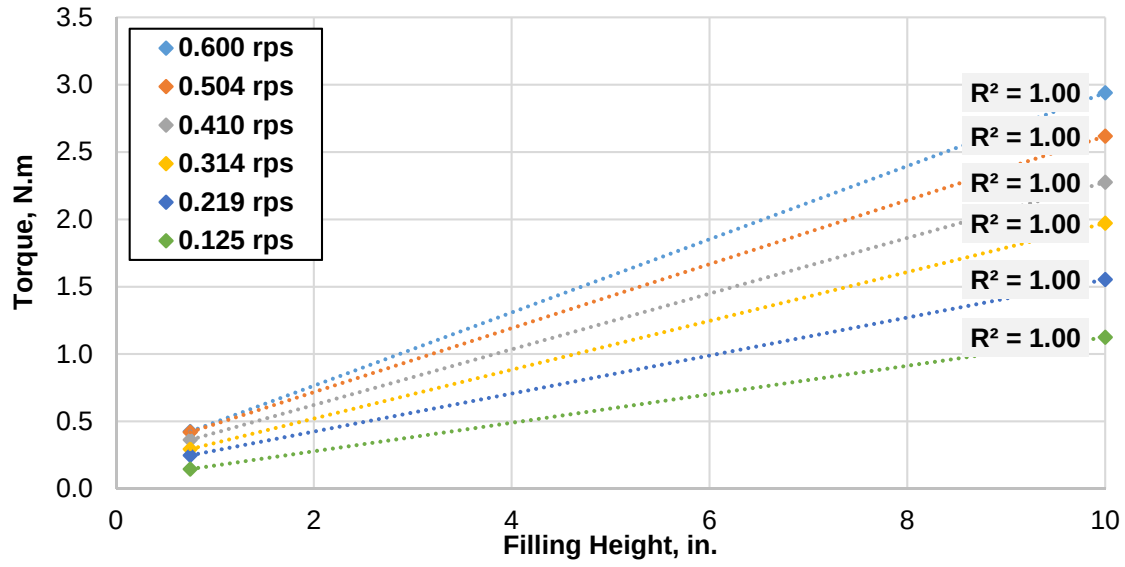

a)

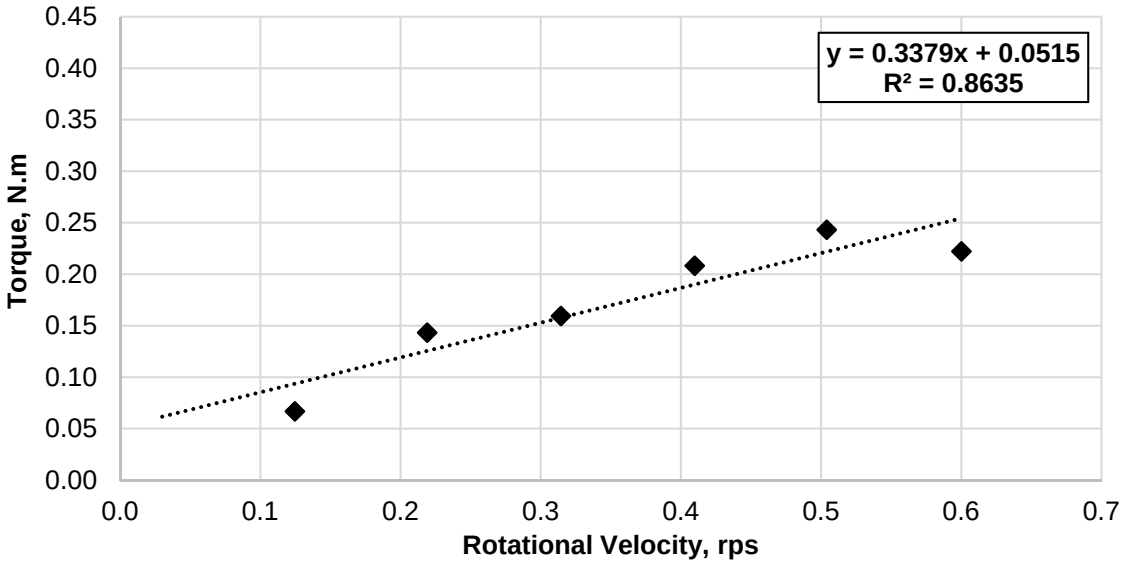

b)

Figure 3.29 – Correction procedure results, Mixture D, ICAR K – Flat – Measurement #1: a) filling height-torque relationship, b) rotational velocity-torque relationship

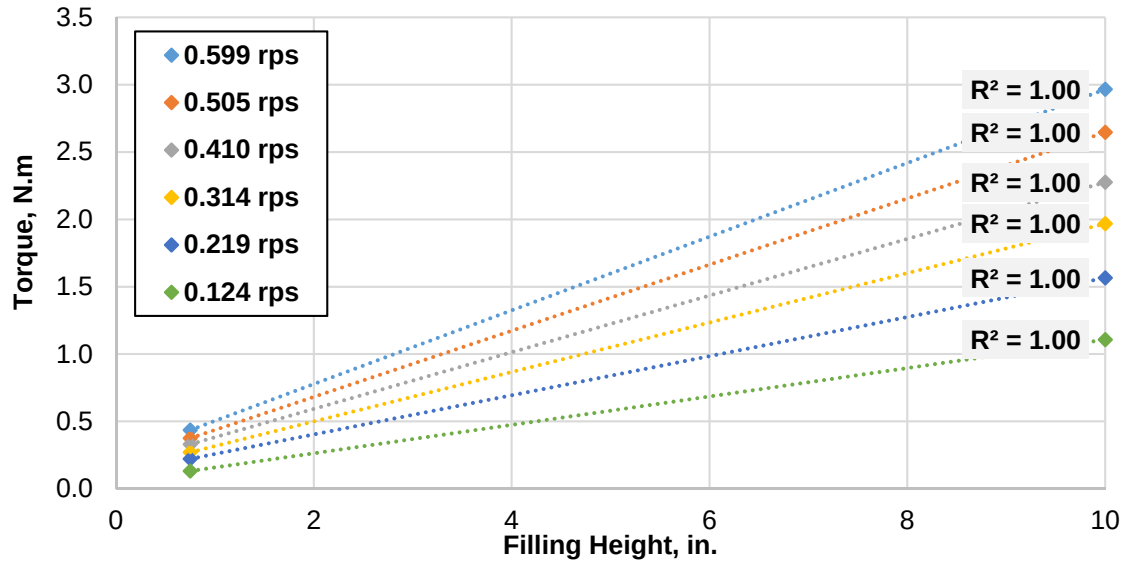

a)

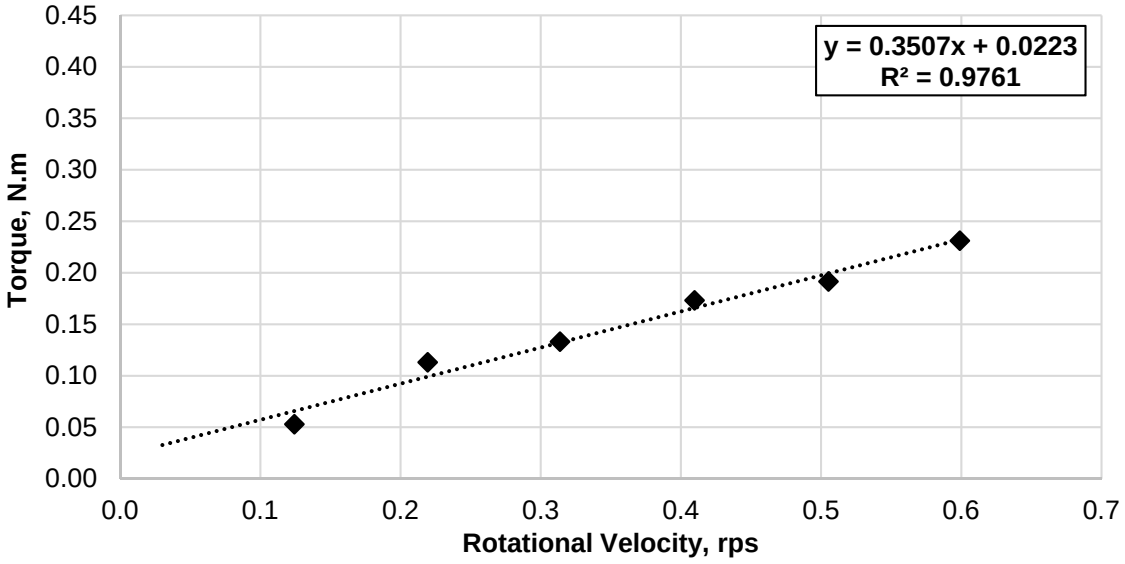

b)

Figure 3.30 – Correction procedure results, Mixture D, ICAR K – Flat – Measurement #2: a) filling height-torque relationship, b) rotational velocity-torque relationship

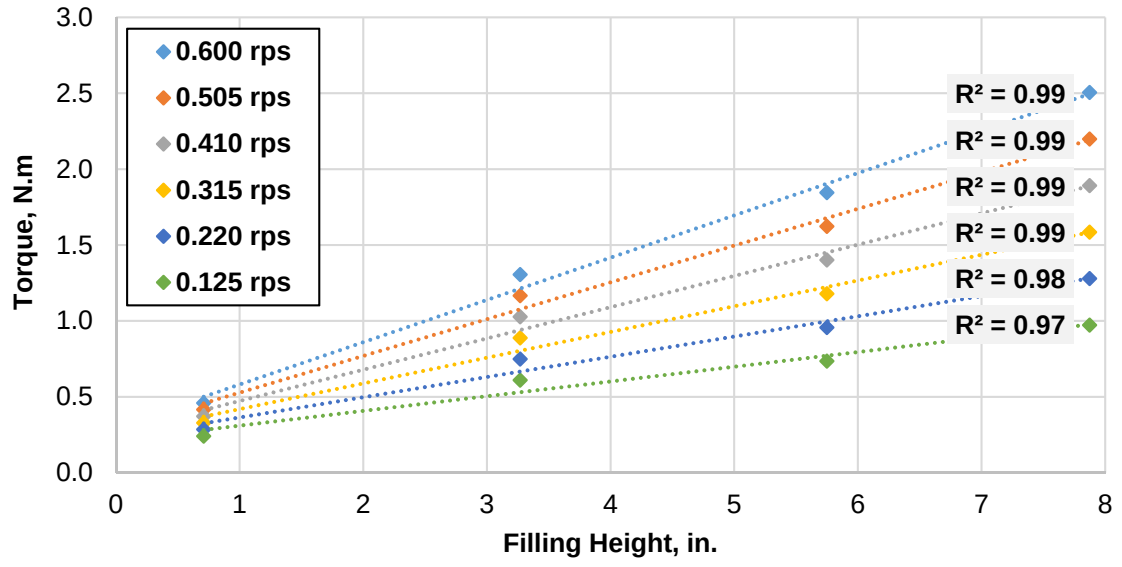

a)

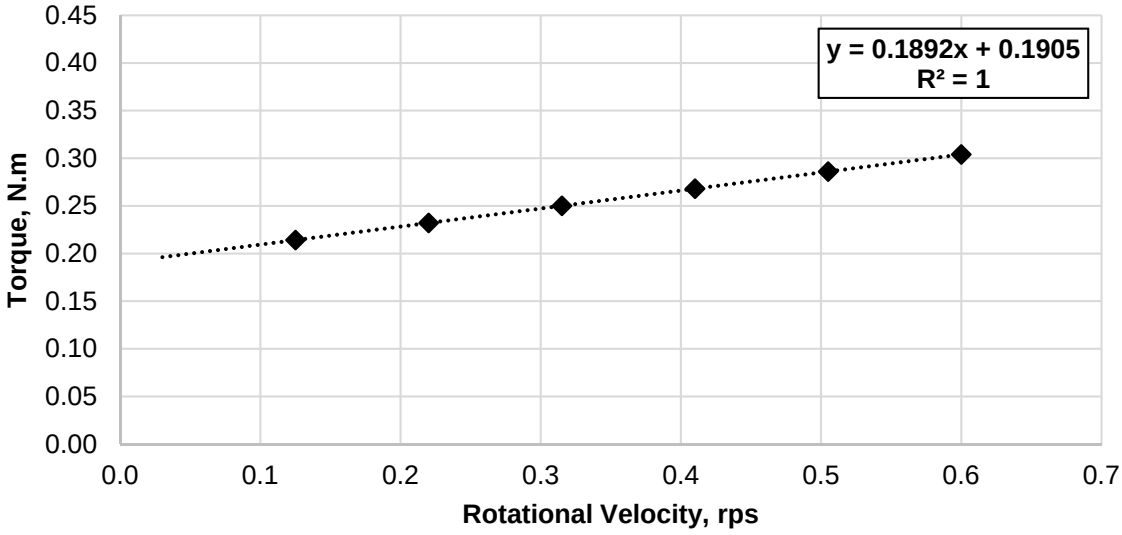

b)

Figure 3.31 – Correction procedure results, Mixture D, ICAR M – Cone – Measurement #1: a) filling height-torque relationship, b) rotational velocity-torque relationship

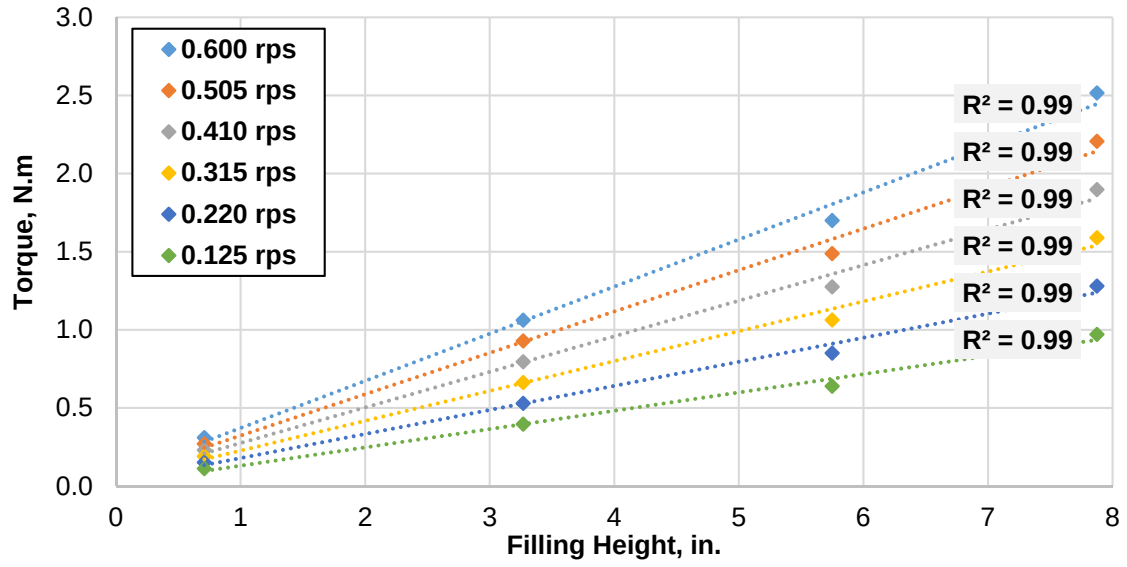

a)

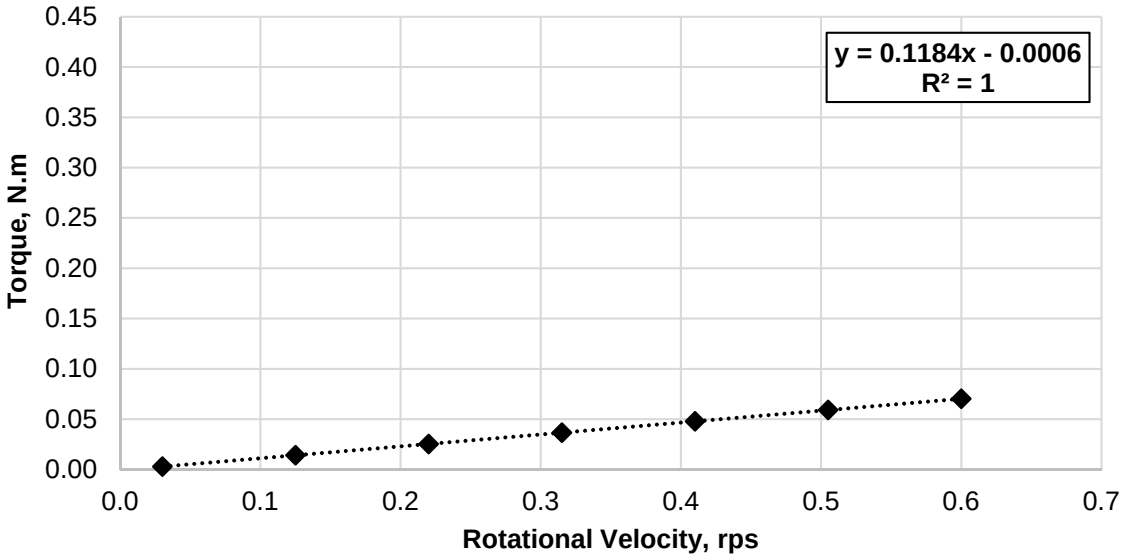

b)

Figure 3.32 – Correction procedure results, Mixture D, ICAR M – Cone – Measurement #2: a) filling height-torque relationship, b) rotational velocity-torque relationship

For mixture A, that was designed as a "sticky" SCC, i.e. mixture with a high value of plastic viscosity and low yield stress, a slightly non-linear behavior of the torque-filling height relationship (T-h) was observed for all interface rheometers and rotational velocities. This is

likely due to changing rheological properties of the mixture that occurred during the period at which the correction procedure was performed. This is, to some extent, unavoidable as even when only several filling heights are considered, the correction procedure takes approximately 10 minutes. For the case of this study, when 4 or 5 filling heights were implemented for each cylinder, the whole correction procedure took approximately 20 minutes to perform. In particular, for mixture A, the recorded changes in the rheological properties, especially in yield stress, were quite significant. Over the period of approximately 1 hour, yield stress of this mixture increased 2.5 times, as measured by the Contec rheometer, while viscosity of the mixture remained relatively constant at 64 Pa.s. Additionally, this was the very first tested mixture in this part of the study, therefore the correction procedure was performed in a slower manner compared to the rest of mixture set. Despite the presence of non-linearity in the torque-height relationship, the resulting torque-rotational velocity (T-N) curve showed a good linear correlation with R^2 values of 0.96, 0.97 and 0.89 for ICAR K with cone-shaped cylinder, ICAR K with flat-bottom cylinder, and ICAR M, respectively. The correction procedure results for Mixture A are shown in Table 3.5.

Table 3.5 – Correction procedure results, Mixture A

Interface Rheometer	Bottom Shape	T-N curve		Viscous Constant		
		Slope	Intercept	Initial	Corrected	Correction
		1/rps	*N.m*	*Pa.s/m*	*Pa.s/m*	
Interface Rheometer K	Cone	0.290	0.212	3,432	3,094	9.8%
	Flat	0.252	0.086	3,361	3,147	6.4%
Interface Rheometer M	Cone	0.138	0.250	3,258	3,107	4.6%

The results showed that the biggest effect of the bottom of the cylinder on the viscous constant measurement was recorded for interface rheometer K. The measurement with the cone-

shaped cylinder overestimated the viscous constant value by 9.8% when the bottom effect was not considered. The reduction of viscous constant after considering the bottom effect for interface rheometer K with flat-bottom cylinder and interface rheometer M was 6.4% and 4.6%, respectively. Coefficient of variation of interface rheology measurements between the interface rheometers was 3% and 1% for uncorrected and corrected values, respectively.

Results of the correction procedure for mixtures B1 and B2 are shown in Table 3.6 and Table 3.7, respectively. Mixture B1 was designed as an SCC mixture with lower plastic viscosity than mixture A. For interface rheometer K with cone-shaped cylinder, a linear T-h curve was obtained, resulting in a linear T-N relationship with R^2 value of 0.98. In the case of interface rheometer M, despite the fact that a non-linear behavior of the T-h diagram was observed, a T-N curve with R^2 of 0.84 was constructed. It appears that the non-linearity of the T-h curve can be contributed to non-steady rheological properties of tested mixture over the testing period, similarly to what was observed for mixture A. Although the plastic viscosity did not change significantly, approximately 70% increase in yield stress was observed for mixture B1, when comparing values measured before and after interface rheology testing. Although the recorded T-h diagram for interface rheometer K with the flat-bottom cylinder had better linearity than the same diagram obtained for interface rheometer M, the T-N curve showed significant non-linearity and the resultant R^2 was only 0.78.

Table 3.6 – Correction procedure results, Mixture B1

Interface Rheometer	Bottom Shape	T-N curve		Viscous Constant		
		Slope	Intercept	Initial	Corrected	Correction
		1/rps	N.m	Pa.s/m	Pa.s/m	
Interface Rheometer K	Cone	0.309	0.121	2,000	1,809	9.6%
	Flat	0.267	0.114	1,650	1,544	6.4%
Interface Rheometer M	Cone	0.098	0.139	1,598	1,547	3.2%

Table 3.7 – Correction procedure results, Mixture B2

Interface Rheometer	Bottom Shape	T-N curve		Viscous Constant		
		Slope	Intercept	Initial	Corrected	Correction
		1/rps	*N.m*	*Pa.s/m*	*Pa.s/m*	
Interface Rheometer K	Cone	0.151	-0.031	1,750	1,584	9.5%
	Flat	0.067	0.005	1,245	1,204	3.3%
Interface Rheometer M	Cone	0.038	-0.059	1,373	N/A	N/A

Mixture B2 was further modified from mixture B1 by an additional dose of high-range water reducer, hence the yield stress of this mixture significantly dropped (from 336 Pa to 68 Pa as measured by the Contec rheometer). For all three interface rheometers, the obtained results from the correction procedure were not ideal. For interface rheometer K with cone-shaped cylinder, a T-N relationship with R^2 of 0.89 was obtained, however, the lowest the rotational velocities deviated from the general trend set by measurements at higher velocities. Additionally, the intercept of this curve with the y-axis of the T-N graph (i.e. the cylinder bottom torque) was negative, suggesting that at very low velocities the effect of the bottom of the cylinder is negative. Similar observation was made for interface rheometer M; in this case, the whole T-N curve was below zero on the vertical axis. For interface rheometer K equipped with the flat-bottom cylinder, the point corresponding to the second lowest rotational velocity value (i.e.

0.220 rps) on the T-N curve was significantly lower than the rest of the data set, resulting in a relatively weak T-N correlation and R^2 value of 0.74. In addition to the above-discussed issue of changing rheological properties during the test period, it is likely that the registered torque values obtained for different filling heights were skewed by the very low yield stress of the B2 mixture. From the whole set of concrete mixtures investigated in this study, mixture B2 had the lowest yield stress value, which resulted in significantly lower torque values registered by the ICAR device, especially at low rotational velocities. As the ICAR rheometer was originally designed to evaluate rheology of concrete mixtures, the typical working range of the torque sensors is significantly higher than torque range encountered by the sensor during interface rheology measurements. Therefore, it is likely that distortion in the data and negative values obtained for this mixture were impacted by insufficient accuracy of the sensor at low torque values. Although the correction procedure delivered less than ideal results for this mixture, the viscous constant value was determined, and the corrected value obtained. For interface rheometer K and mixture B1, reduction by 9.6% and 6.4% was observed for the cone-shaped and flat-bottom cylinder, respectively. For mixture B2, 9.5% and 3.3% reduction in the viscous constant was recorded due to the correction procedure, for interface rheometer K and the cone-shaped and flat-bottom cylinders, respectively. With regards to interface rheometer M, the correction procedure was only evaluated for mixture B1 since the whole T-N correction curve was in negative quadrant for mixture B2. The corrected viscous constant value for mixture B1 was 3.2%, and similarly to mixture A, the bottom effect was lower for interface rheometer M compared to interface rheometer K when a similarly shaped cylinder was utilized. The coefficient of variation was 12% and 18% for the initial, uncorrected measurements for mixtures B1 and B2, respectively, and 9% considering values corrected for the cylinder bottom effect of mixture B1. The COV was not

evaluated for corrected results of mixture B2 since only two viscous constant values were available.

Mixtures C1 and C2 were developed as pumpable conventional mixtures. Results of the correction procedure are shown in Table 3.8 and Table 3.9 for mixtures C1 and C2, respectively.

Table 3.8 – Correction procedure results, Mixture C1

Interface Rheometer	Bottom Shape	T-N curve		Viscous Constant		
		Slope	Intercept	Initial	Corrected	Correction
		1/rps	*N.m*	*Pa.s/m*	*Pa.s/m*	
Interface Rheometer K	Cone	0.140	0.009	921	834	9.4%
	Flat	0.023	0.043	948	939	1.0%
Interface Rheometer M	Cone	0.088	0.072	882	836	5.1%

Table 3.9 – Correction procedure results, Mixture C2

Interface Rheometer	Bottom Shape	T-N curve		Viscous Constant		
		Slope	Intercept	Initial	Corrected	Correction
		1/rps	*N.m*	*Pa.s/m*	*Pa.s/m*	
Interface Rheometer K	Cone	0.141	0.020	730	643	11.9%
	Flat	N/A	N/A	N/A	N/A	N/A
Interface Rheometer M	Cone	0.031	0.017	674	658	2.4%

The correction procedure was successful for both mixtures C1 and C2 using cone-shaped interface rheometers, and the results were questionable for measurements with the flat-bottom cylinder. For mixture C2, the correction procedure using interface rheometer K with the flat-bottom cylinder was not performed due to time constraints during the testing. For mixture C1, T-N curves for interface rheometers with cone-shaped cylinders yielded R^2 coefficient of 0.92 and 1.00 for interface rheometer K and interface rheometer M, respectively. For interface rheometer K with the flat-bottom cylinder, the R^2 value of the T-N curve was relatively low with a value of 0.41, however, data points showed a uniform distribution along the trendline, therefore the

resulting correction equation was deemed usable. Similar to previous mixtures, the bottom effect of interface rheometer K with cone-shaped cylinder had the biggest effect on viscous constant value, the corrected value was reduced by 9.4% while for interface rheometer M, the reduction was only 5.1%. For the flat-bottom cylinder, the correction due to the cylinder bottom effect was only 1.0%. For mixture C2, the correction T-N curve had R^2 values of 0.98 and 1.0 for interface rheometer K (with cone-shaped cylinder) and interface rheometer M, respectively. The effect of the bottom of the cylinder on viscous constant correction was again more significant for interface rheometer K as the corrected value decreased by 11.9% for interface rheometer K while the correction reduction observed for interface rheometer M was only 2.4%.

The coefficient of variation for initial interface rheology measurements was 0.04 and 0.06 for mixture C1 and C2, respectively. For the corrected viscous constant, the coefficient of variation for all three interface rheometers became 0.07 and 0.02 for mixture C1 and C2, respectively.

Finally, results of the correction procedure measurements for mixture D (i.e. mortar) are shown in Table 3.10 and in Table 3.11. For this mixture, measurements were performed twice; for each filling height, the measurement was repeated right after the initial test was conducted.

Table 3.10 – Correction procedure results, Mixture D – first measurement

Interface Rheometer	Bottom Shape	T-N curve		Viscous Constant		
		Slope	Intercept	Initial	Corrected	Correction
		1/rps	*N.m*	*Pa.s/m*	*Pa.s/m*	
Interface Rheometer K	Cone	0.165	0.042	2,100	1,998	4.9%
	Flat	0.351	0.022	1,547	1,407	9.1%
Interface Rheometer M	Cone	0.189	0.190	1,673	1,575	5.9%

Table 3.11 – Correction procedure results, Mixture D – repeated measurement

Interface Rheometer	Bottom Shape	T-N curve		Viscous Constant		
		Slope	Intercept	Initial	Corrected	Correction
		1/rps	*N.m*	*Pa.s/m*	*Pa.s/m*	
Interface Rheometer K	Cone	0.180	0.001	2,001	1,890	5.5%
	Flat	0.338	0.052	1,514	1,378	9.0%
Interface Rheometer M	Cone	0.118	-0.001	1,688	1,626	3.7%

For interface rheometer M and interface rheometer K with the cone-shaped cylinder, very linear T-N curves were obtained. For interface rheometer M, curves for both the first and the repeated measurement resulted in R^2 value of 1.00, and for interface rheometer K with the cone-shaped cylinder, obtained R^2 values were 0.98 and 0.99 for the first and the repeated measurement, respectively. The T-N curve was slightly non-linear for measurements performed using interface rheometer K with the flat-bottom cylinder, resulting in T-N curves with R^2 value of 0.86 and 0.97 for the first and the second measurement, respectively. There were no significant differences between the first and the second measurements for interface rheometer K; for both cylinder types (cone-shaped bottom and flat-bottom) the effect of the bottom on interface rheology measurements was more pronounced for the flat-bottom cylinder with correction of 9.1% and 9.0% of the initial viscous constant value for the first and the repeated

measurement, respectively. The viscous constant value somewhat increased (by 5% and 2% for the cone-shaped and flat-bottom cylinder, respectively) between the first and the repeated measurement. This was not the case for interface rheometer M, where a decrease in the viscous constant value by 0.9% and 3.2% was observed for the initial and corrected value, respectively. For the first measurement, the effect of the bottom of the cylinder on the final value of viscous constant was 5.9%, which was more than what was observed for the cone-shape cylinder when interface rheometer K used. This was the only instance in the whole testing program when the interface rheometer M cylinder bottom had greater effect on the resultant values of viscous constant measurements than what was the effect of interface rheometer K when the same mixture was measured. For the second measurement, the cylinder bottom effect was lowered to 3.7%. Overall, it appears that the results of the first and the second measurements were in a general agreement, however, the effect of changing rheological properties of the mixture was demonstrated by slightly different results that were observed between the two measurement sets. To recall, the repeated measurement was carried out right after the first measurement at given filling height was performed, therefore the lubrication layer was already formed on the inner cylinder. Since this mixture did not contain coarse aggregate, the formation process of the lubrication layer was not affected by the wall effect, i.e. presence of large coarse aggregate particles creating a void space along the cylinder wall where the lubrication layer can be formed, as discussed in Section 2.5. Hence, the shear-induced particle migration process is the primary mechanism driving formation of the lubrication layer. The results suggest that this process was to some extent ongoing during the second round of measurements as slightly different results for the lubrication layer were obtained. However, since the differences in the results of the first and second round of measurements are not significantly different, and part of the difference can be

certainly contributed to accuracy and sensitivity of the torque sensor, it was concluded that the used pre-shear period of 25 seconds was sufficient. Moreover, it would not be practical to extend the test over a longer time span, especially considering the significant effect of concrete stiffening on quality of the correction procedure that was observed throughout this experimental program.

The coefficient of variation of interface rheology measurements was somewhat higher for mixture D compared to the other investigate mixtures, with values of 0.18 and 0.16 for the first and the second measurements.

Overall, the proposed correction procedure was found to be suitable in evaluating the effect of the bottom of the interface rheometer cylinder on determination of viscous constant of the lubrication layer. The correction procedure was carried out 17 times utilizing a set of six concrete and one mortar mixtures. In 13 cases (76%), the correction procedure delivered satisfactory results, in 1 case (6%), a doubtful but still applicable result was produced, and in three cases (18%), the resultant T-N relationship was not accurate and applicable for the correction process. The effect of the bottom of the cylinder on reduction of the viscous constant after the correction procedure was applied is shown in Figure 3.33. On average and excluding data for the mortar mixture D, the correction procedure resulted in viscous constant reduction of 10.2%, 4.6% and 3.8% for interface rheometer K with cone-shape cylinder, interface rheometer K with flat-bottom cylinder and interface rheometer M, respectively. The effect of the cylinder bottom was relatively constant for cone-shaped interface rheometers, a standard deviation of 1.2% and 1.3% were recorded for interface rheometer K and interface rheometer M, respectively. For interface rheometer K with the flat-bottom cylinder, the standard deviation was 3.9%, however, only three data points were included in the data set due to lack of measurement for

mixture C2. Overall, cone-shaped interface rheometers appeared to deliver better consistency of interface rheology measurements and the correction procedure than the flat-bottom cylinder. This might be primarily due to the ease at which the mixture can be consolidated along the interface rheometer head in the container. For the cone-shaped cylinder, the overall shape of the cylinder bottom allows better compaction of the mixture due to its slope, whereas it is believed that for the flat-bottom cylinder, inadequate consolidation or even a presence of air pockets along the bottom of the cylinder can be possible, especially when mixtures with lower workability are tested.

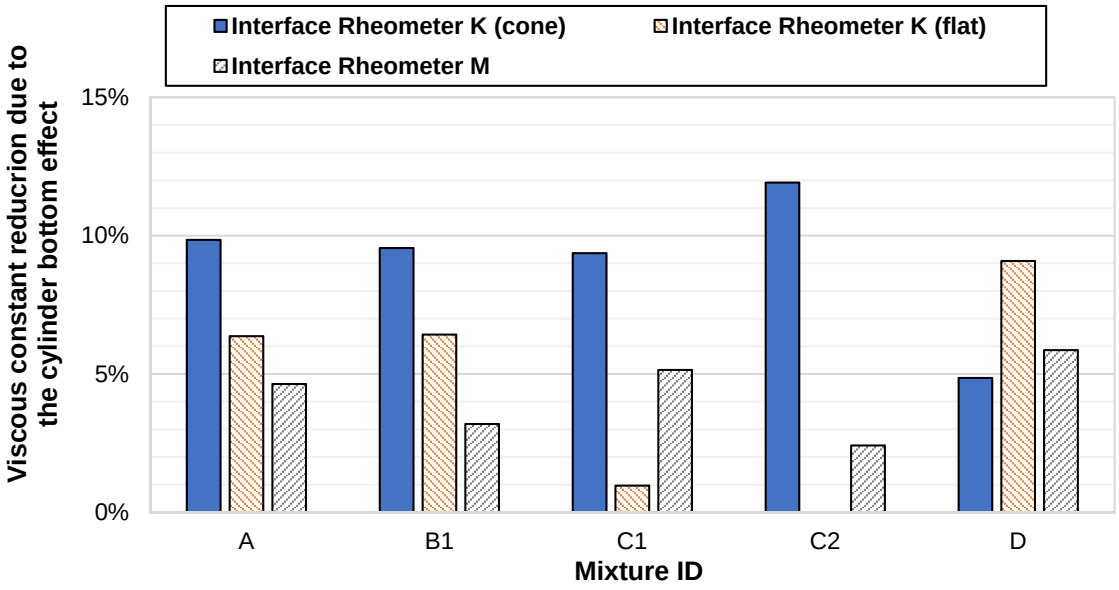

Figure 3.33 – Cylinder bottom effect for all interface rheometers and concrete/mortar mixtures

The main difference between the two cone-shaped interface rheometers was the angle and height of the conical portion of the cylinder. Interface rheometer M cone was 0.4 in. (10 mm) taller, resulting in a steeper angle between the horizontal plane of the cylinder compared to interface rheometer K cylinder, i.e. 44° compared to 39°. Based on data obtained in this study, it appears that the shape of the conical part can have significant effect on the overall contribution

of the bottom of the cylinder to the registered torque, as interface rheometer M had, on average, 62% lower effect on the final viscous constant value.

The slope of the T-N curve, i.e. a quantity that effectively represents the magnitude of the torque corresponding to the effect of the bottom of the cylinder, was compared to concrete Bingham parameters, i.e. yield stress and viscous constant, as shown in Figure 3.34. No correlation was observed for was found for the T-N curve slope-yield stress relationship. For plastic viscosity, no relationship was found for the flat-bottom cylinder, however, a weak correlation with R^2 values of 0.49 and 0.76 was observed for cone-shaped cylinders of interface rheometer K and M, respectively. Therefore, it appears that the overall magnitude of the corrective torque is to some extent dependent on plastic viscosity of the bulk concrete. However, further research is warranted to evaluate this hypothesis.

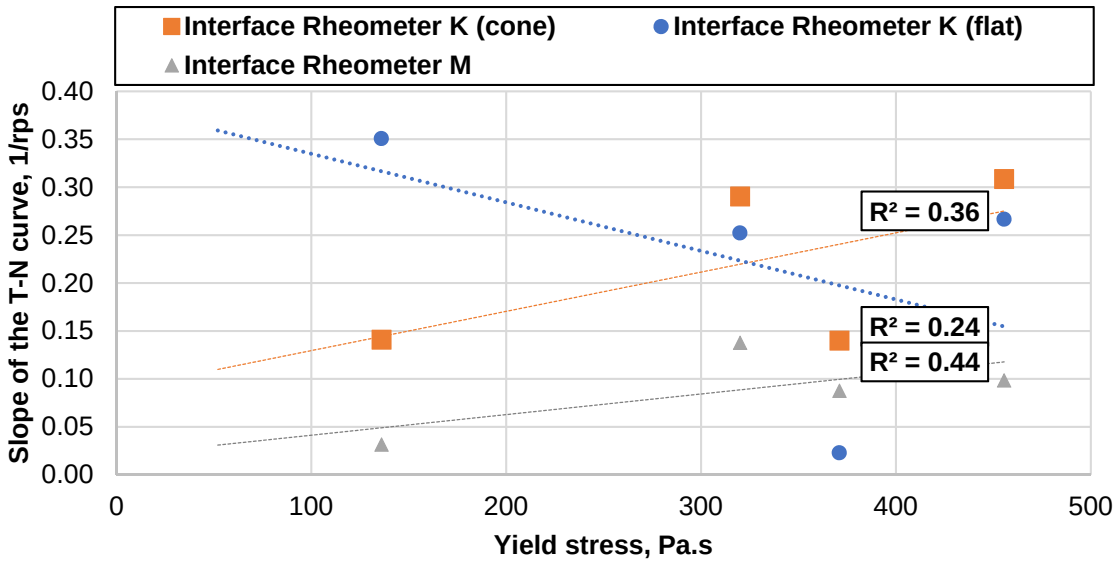

a)

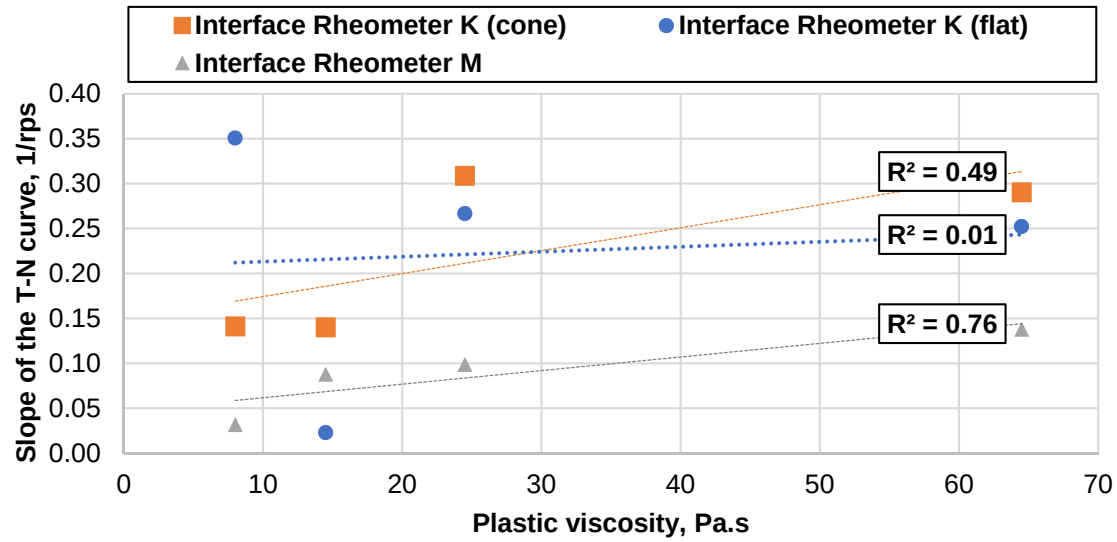

b)

Figure 3.34 – Slope of the T-N curve vs a) yield stress, b) plastic viscosity

Limitations and shortcomings of the correction procedure were primarily contributed to the following issues:

a. Accuracy and sensitivity of the torque sensor

As interface rheometers used in this study were based on the ICAR rheometer, which is a device that was originally designed for concrete rheological measurements, the torque sensor had to registered significantly lower values compared to its original intended use. The fact that the sheared lubrication layer does not generate large values of torque on the shaft of the inner cylinder is given by its intrinsic properties and cannot be avoided. To some extent, torque sensor accuracy and sensitivity issue can be mitigated by using higher rotational velocities and limiting minimum filling heights used during the correction procedure. Additionally, cylinders with greater dimensions (both diameter and height) could be used, however, the practicality of the interface rheology measurements could be compromised by increasing the radius of the cylinder. Therefore, it is essential that the torque sensor accuracy is considered when interface rheology testing data are analyzed.

b. Changing concrete rheological properties during interface rheology measurements

A non-linearity of the T-h curve was observed in many instances, and in the case of mixture B2, resulting in unsatisfactory T-N relationship. It was contributed to constantly changing rheological properties of concrete mixtures over the time span during which the correction procedure was performed. Unfortunately, this behavior cannot be fully avoided as the hydration process of cement-based materials is ongoing and cannot be interrupted. However, the stiffening effect on the correction procedure

can be limited by reducing the overall time that is required to perform it. This can be achieved by reducing the number of filling heights that are evaluated and/or by reducing the total number of rotational velocities implemented during the test procedure. However, before implementing these measures, their effect on the overall accuracy of the correction procedure must be evaluated.

c. Filling height measurements

Incorrect filling height measurements can significantly influence the linearity of the T-h curve. When measuring the filling height, in several instances, different heights were recorded around the cylinder perimeter, and subsequently, average values had to be used. Thus, in order to achieve a successful correction procedure, it is important to carefully evaluate each filling height. For purposes of this test campaign, an ordinary tape measure was used. However, it is advised to use more accurate measurement techniques to improve the overall accuracy of the method.

3.5 Conclusions

In this chapter, a testing program designed to improve and further evaluate a correction procedure to assess the effect of the bottom of the interface rheometer cylinder on characterization of rheological parameters of the lubrication layer was described. Seven mixtures, three rheometers and three interface rheometers were utilized to carry out the testing program. Based on the obtained data, the following conclusions are made:

- The proposed correction procedure was found to be a feasible way to determine the 3D flow effect caused by bottom of the interface rheometer cylinder during interface rheology characterization of the lubrication layer. The overall accuracy of the method was satisfactory, however, in several instances, the correction procedure delivered results (i.e. negative values

of torque corresponding to the cylinder bottom contribution to the measurements) that did not agree with the physical sense of the method.

- The overall effect of the bottom of the cylinder on the values of viscous constant were relatively low, on average less than 10%.
- Limitations of the correction procedure were assessed, and it was concluded that stiffening of the concrete mixture during the correction procedure process, the accuracy and sensitivity of the torque sensor, and the accuracy of filling high measurements were the primary factors effecting precision of the correction method. Mitigation strategies to minimize these effects were proposed.
- No correlation between yield stress were found to affect the slope of the T-N curve, i.e. the magnitude of the torque attributed to the effect of the bottom of the cylinder. A weak correlation was found between the T-N curve slope and plastic viscosity for interface rheometers with cone-shaped cylinders, however, further experimental evaluation is warranted to confirm the hypothesis that the cylinder bottom effect is direct relationship with concrete plastic viscosity.
- The consistency of interface rheology measurements and the correction procedure was better for cone-shaped cylinders. The angle between the horizontal plane of the cylinder and height of the conical part of the cylinder were found to have an influence on the overall magnitude of the cylinder bottom effect.

Chapter 4 - Laboratory Study on How Concrete Mixture Proportions Influence Rheological Properties of the Concrete and the Lubrication Layer

4.1 Introduction

Concrete rheological properties (yield stress and plastic viscosity) and rheological properties of the lubrication layer (viscous constant and interface yield stress) strongly influence pumping performance of concrete mixtures, as discussed in Chapter 2 of this dissertation. To this extent, the knowledge of how particular mixture proportioning parameters can change these properties is essential for a successful pumping operation. However, in current construction practices, concrete rheology is rarely evaluated during the mixture development process, and almost never considered as a quality control tool in the field. Typically, simplified workability test methods, such as the slump or slump flow tests, are utilized to predict whether a concrete mixture will be pumpable or not. These methods, however, do not evaluate the full spectrum of concrete rheological properties and properties of the lubrication layer, and therefore can often lead to inaccurate pumpability predictions.

In this chapter, an extensive laboratory study evaluating the effect of various mixture constituents on concrete and the lubrication layer rheology is discussed. As part of this study, over 35 different concrete mixtures were evaluated. Considered mixture proportion variables included air void content, water-to-cement ratio (w/cm), cement paste volume, fly ash replacement ratio, fine-to-coarse aggregate ratio (FA/CA), aggregate shape, use of viscosity-modifying admixture, and use of nano-clay particles. All concrete mixtures were designed to represent typically used high-performance concrete (HPC) mixtures for concrete bridge decks in the state of Kansas. To evaluate effect of individual mixture characteristics, all mixtures were

prepared in a laboratory and concrete rheological properties and lubrication layer properties were determined using ICAR rheometer and an ICAR-based interface rheometer with cone-shaped cylinder, respectively. Additionally, the combined effect of individual concrete parameters on pumping pressure was evaluated implementing Kaplan's pumping prediction model.

4.2 Research Significance

The current state-of-the art literature significantly lacks information on rheological properties of conventional vibrated concrete (CVC) mixtures as most of the work in the field of concrete rheology was performed on SCC mixtures. Similarly, very little information is available regarding properties of the lubrication layer of CVC mixtures. Therefore, the performed experimental work described in this chapter was aimed to expand current knowledge-base by considering rheology of CVC mixtures. Furthermore, coupling obtained concrete and lubrication layer rheological data with Kaplan's pumping model provides useful information to the concrete community regarding pumping pressure demand of the HPC-class of concrete mixtures.

4.3 Experimental Methods

4.3.1 Materials

Locally sourced concrete materials were used in this experimental program. Two types of coarse aggregate were utilized in this study: (1) crushed granitic rock obtained from Mill Creek quarry, Mill Creek, OK with nominal aggregate size of ¾ in. (19.5 mm); and (2) siliceous pea gravel obtained from Midwest Concrete Materials, Manhattan, KS with nominal aggregate size of ½ in. (12.5 mm). Gradation curves are shown in Figure 4.1, and other properties pertinent to mixture proportioning are shown in Table 4.1.

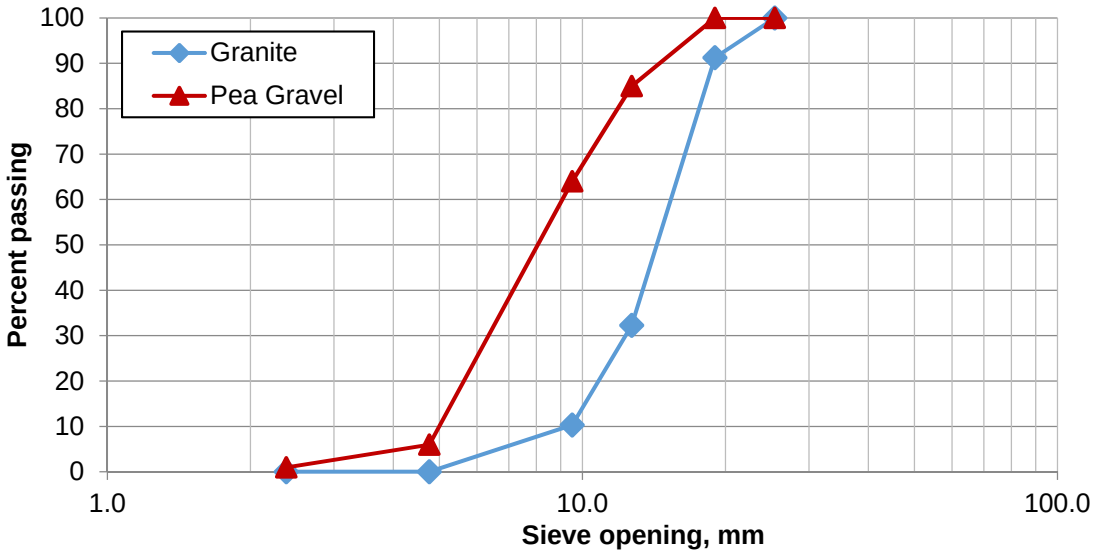

Figure 4.1 – Coarse aggregate gradation

Table 4.1 – Coarse aggregate properties

	Granite	Pea Gravel
Nominal aggregate size, in. (mm)	¾ (19. 5)	½ (12.5)
Specific gravity (SSD)	2.69	2.59
Absorption capacity, %	0.19	1.60

Natural siliceous fine aggregate conforming to the requirements of ASTM C33 was obtained from Midwest Concrete Materials, Manhattan, KS. Measured SSD specific gravity was 2.62, absorption capacity was 0.60% and fineness moduli was 3.0. Fine aggregate gradation is shown in Figure 4.2.

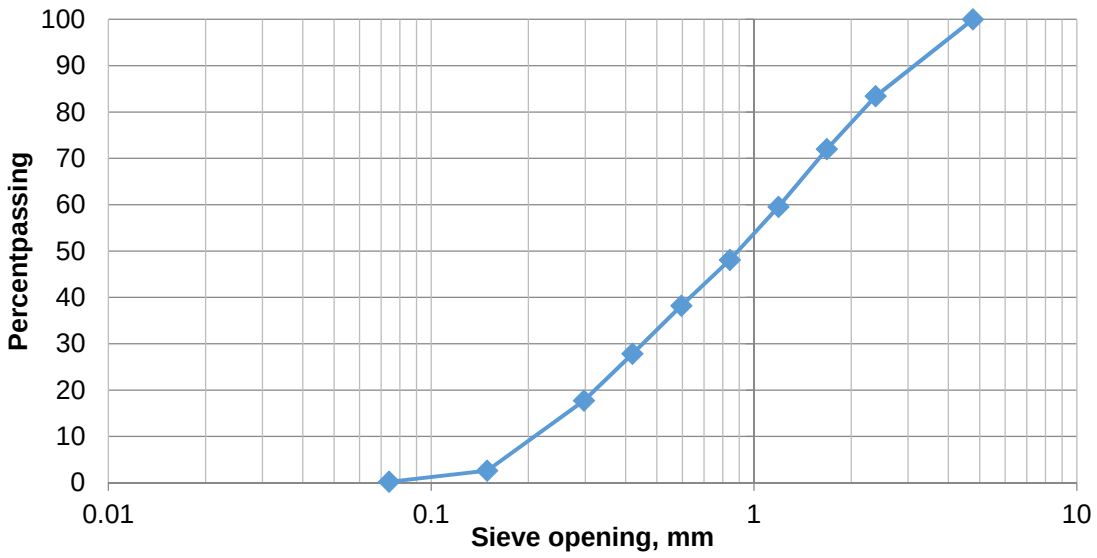

Figure 4.2 – Fine aggregate gradation

ASTM C150 Type I/II [108] portland cement manufactured by the Monarch Cement Company (MCC) in Humboldt, KS was utilized in this study. Cement properties obtained from a certified mill test report provided by MCC are shown in Table 4.2. Cement was obtained in 94-lbs (42.6 kg) bags, and upon receiving, the material was stored in sealed plastic barrels at room temperature.

Table 4.2 – Portland cement properties

Physical Properties		Chemical Properties	
325 Sieve passing, %	94.2	*Oxide Analysis*	
Blaine fineness, cm^2/g	3,660	SiO_2, %	21.33
Time of Setting - initial, hrs:min	2:35	Fe_2O_3, %	2.81
Time of Setting - final, hrs:min	3:55	Al_2O_3, %	4.46
Mortar Air Content, %	6.6	CaO, %	64.34
Autoclave Expansion, %	0.011	MgO, %	1.40
Compressive Strength - 1 day, psi	2,430	SO_3, %	2.76
Compressive Strength - 3 days, psi	4,010	*Calculated Compounds*	
Compressive Strength - 7 days, psi	5,180	C_3S, %	58.0
		C_2S, %	17.4
		C_3A, %	7.1
		C_4AF, %	8.5
		Others	
		Loss on ignition, %	1.37
		Insoluble residue, %	0.24
		Free lime, %	1.14
		Na2O, %	0.19
		K2O, %	0.51
		Equivalent alkalies, %	0.52

ASTM C618 class F fly ash [109] produced by Ash Grove Cement Company originating from the Chanute Power Plant, Chanute, KS, was also used in this laboratory study. Fly ash was obtained from a concrete producer located in Kansas City, KS and transported and stored at KSU facility in sealed plastic barrels.

Chemical admixtures used in this study included air-entertainer (AEA), water reducer (WR) and viscosity-modifying admixture (VMA). Euclid Eucon AEA-92S, conforming requirements of ASTM C260 [110], was used as an air-entraining admixture, and Euclid Plastol 6420, conforming requirements of ASTM C494 [111] for Type A and Type F admixtures, was used as water reducer. For mixtures investigating the effect of viscosity-modifying admixtures on concrete rheology, Sika Stabilizer-4R, conforming requirement of ASTM C494 for Type S admixtures, was utilized.

Lastly, clay particles were implemented in one mixture series investigated in this study. A hydrous magnesium aluminum-silicate product Acti-Gel® was obtained from Active Minerals, Inc. for use in this study. Detailed information about this product are available from [112].

4.3.2 Concrete Mixtures

Nine series of concrete mixtures were included in this study to investigate the influence of mixture constituents on concrete rheology and rheological properties of the lubrication layer. Each series of mixtures was developed with three different water-to-cement ratios (w/cm). The design plastic air void content was 6.5%, however, numerous mixtures were batched at different air content levels in order to evaluate the effect of the plastic air content on concrete and lubrication layer rheology. Additionally, it is not a trivial task to prepare such a large number of mixtures with consistent plastic air content level as the AEA dosage in not the only factor governing the amount of air that is stabilized during mixing. Therefore, in order to be able to compare mixtures with similar air contents, for certain series, mixtures with various values of plastic air content were prepared. Hence, during the data analysis stage described in this chapter, only mixtures with plastic air content deviating by no more than 1.5% from each other were directly compared. Mixture proportions and ID system developed for this study are shown in Table 4.3.

Table 4.3 – Mixture Proportions

Mixture ID	Cement	Fly Ash	Coarse Aggregate	Fine Aggregate	Water	w/cm
			lbs/yd³ (kg/m³)			-
C540-40	540 (320)	-- (--)	1,599 (949)	1,554 (922)	216 (128)	0.40
C540-43	540 (320)	-- (--)	1,577 (936)	1,557 (924)	232 (138)	0.43
C540-45	540 (320)	-- (--)	1,563 (927)	1,543 (915)	243 (144)	0.45
C520-40	520 (309)	-- (--)	1,618 (960)	1,572 (933)	208 (123)	0.40
C520-43	520 (309)	-- (--)	1,597 (947)	1,552 (921)	224 (133)	0.43
C520-45	520 (309)	-- (--)	1,583 (939)	1,538 (912)	234 (139)	0.45
C560-40	560 (332)	-- (--)	1,580 (937)	1,535 (911)	224 (133)	0.40
C560-43	560 (332)	-- (--)	1,557 (924)	1,513 (898)	241 (143)	0.43
C560-45	560 (332)	-- (--)	1,542 (915)	1,498 (889)	252 (150)	0.45
C540-40-R60	540 (320)	-- (--)	1,919 (1,138)	1,243 (737)	216 (128)	0.40
C540-43-R60	540 (320)	-- (--)	1,893 (1,123)	1,226 (727)	232 (138)	0.43
C540-45-R60	540 (320)	-- (--)	1,875 (1,112)	1,215 (721)	243 (144)	0.45
C540-40-R40	540 (320)	-- (--)	1,279 (759)	1,864 (1,106)	216 (128)	0.40
C540-43-R40	540 (320)	-- (--)	1,262 (749)	1,839 (1,091)	232 (138)	0.43
C540-45-R40	540 (320)	-- (--)	1,250 (742)	1,822 (1,081)	243 (144)	0.45
C540F25-40	405 (240)	135 (135)	1,587 (942)	1,542 (915)	216 (128)	0.40
C540F25-43	405 (240)	135 (135)	1,565 (928)	1,521 (902)	232 (138)	0.43
C540F25-45	405 (240)	135 (135)	1,550 (920)	1,507 (894)	243 (144)	0.45
C540-40-RR	540 (320)	-- (--)	1,537 (912)	1,554 (922)	216 (128)	0.40
C540-43-RR	540 (320)	-- (--)	1,516 (899)	1,533 (909)	232 (138)	0.43
C540-45-RR	540 (320)	-- (--)	1,502 (891)	1,518 (901)	243 (144)	0.45
C540-40-VMA	540 (320)	-- (--)	1,599 (949)	1,554 (922)	216 (128)	0.40
C540-43-VMA	540 (320)	-- (--)	1,577 (936)	1,557 (924)	232 (138)	0.43
C540-45-VMA	540 (320)	-- (--)	1,563 (927)	1,543 (915)	243 (144)	0.45
C540-40-NC	540 (320)	-- (--)	1,599 (949)	1,554 (922)	216 (128)	0.40
C540-43-NC	540 (320)	-- (--)	1,577 (936)	1,557 (924)	232 (138)	0.43
C540-45-NC	540 (320)	-- (--)	1,563 (927)	1,543 (915)	243 (144)	0.45

Chemical admixtures, except for the AEA, were kept at a constant dosage throughout the experimental program in order to avoid introducing additional variables in this study. The WR dosage was 12.5 fl. oz. per 100 lbs of cementitious materials (8.15 ml per kg of cementitious materials), thus, according to the manufacturer's guidelines it acted as a high-range water reducer. The amount of VMA added to the mixture was also based on manufacturer's recommendation, and its dosage was 4 fl. oz. per 100 lbs of cementitious materials (2.6 ml per kg of cementitious materials). The nanoclay particles addition was based on the total weight of

solids (i.e. cement and aggregate) as per manufacturer's specifications, and the addition rate was 0.0375% by weight of solids (aggregates and cementitious materials). Finally, the AEA was added as needed to achieve target plastic air void content, and the dosage ranged from 0.25 to 1.2 fl. oz. per 100 lbs of cementitious materials (0.16 to 0.78 ml per kg of cementitious materials).

All concrete mixtures prepared in this study were mixed in a Lancaster pan mixer at a constant mix volume of 1.9 ft^3 (53.8 l). The concrete materials laboratory where concrete was prepared and tested was maintained at 73°F(23°C)/50% RH. A standard mixing procedure (3 minutes mixing, 3 minutes rest, 2 minutes mixing), as specified by ASTM C192 [106] was followed. Constituent materials were kept stored in the laboratory prior to the mixing in order to stabilize them at room temperature (73°F/23°C). Samples of coarse and fine aggregates were taken 24 hours prior to the mixing, oven-dried and mixing water content was adjusted to accommodate for aggregate moisture.

4.3.3 Test Methods

Following fresh properties were evaluated: slump according to ASTM C143 [113], slump flow (when applicable) according to ASTM C1611 [105], plastic air content using the pressure method according to ASTM C231 [114], density according to ASTM C138 [115] and temperature according to ASTM C1064 [116].

In order to characterize concrete rheological properties and properties of the lubrication layer, an interface rheometer of a cone-shaped design, as discussed in Chapter 3, was utilized in this study, in conjunction with the ICAR rheometer. Test apparatus, rheological vane and rheometer cylinder are shown in Figure 4.3. The inner cylinder radius was 2.5 in. (63.5) mm and the outer cylinder radius was 6.3 in. (160.3 mm). A closely spaced series of vertical ribs was mounted on the container wall to prevent concrete slip along the outer cylinder wall.

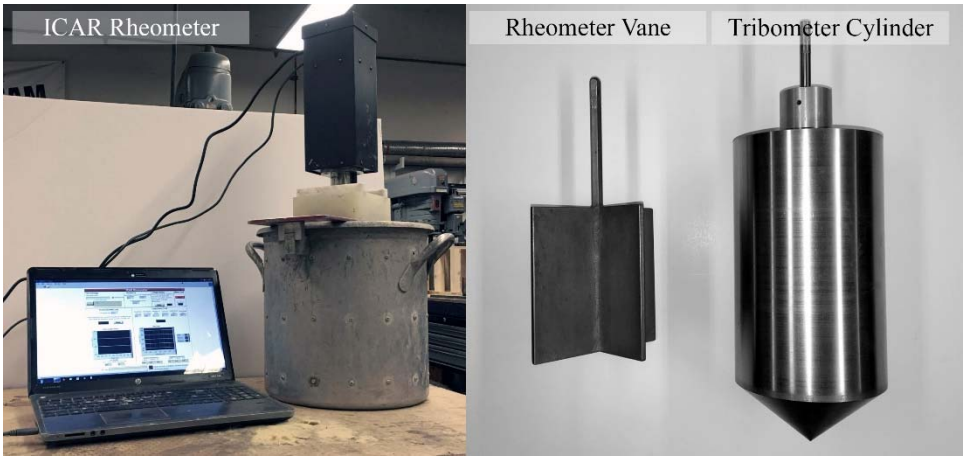

Figure 4.3 – Rheometer (left), rheometer vane and interface rheometer cylinder (right)

For rheological measurements, a 20-second pre-shear at 0.5 rps period was implemented to ensure that equilibrium in the material was reached (i.e. that thixotropy of the mixture was reversed) and a uniform torque signal is produced, followed by series of 7 decreasing rotational velocities with the lowest rotational velocity of 0.05 rps. Similarly, a 30-second pre-shear period at 0.6 rps, followed by 7 measurements at decreasing rotational velocities was utilized for the interface rheology measurements. A higher initial value of the interface rheometer cylinder rotational velocity was selected to approach as closely as possible velocities expected in a real pipeline. Although the highest value of rotational velocity that is possible to achieve with the ICAR rheometer was used, the linear velocity measured at the cylinder surface is still smaller than values that can be expected during standard pumping jobs. Test protocols for both types of measurements are summarized in Figure 4.4. For each tested mixture, slump/slump flow, plastic air content, unit weight and temperature were determined first, followed by rheological measurements of both the bulk concrete and the lubrication layer. To eliminate the effect of time-dependent changes in rheological properties of each mixture due to the hydration process as much as possible, concrete and lubrication layer rheological measurements were always

performed 20 minutes after water addition, and all measurements were completed within a 10-minute interval. Obtained data from the ICAR rheometer were corrected for the presence of the plug flow following a procedure discussed in Chapter 2. For interface rheology measurements, a data analysis is also described in Chapter 2. Since it was determined that the effect of the cylinder bottom for the particular cylinder geometry and configuration used in this experimental study was consistently approximately 10% (see discussion in Chapter 2), the correction procedure was not performed and all measured values of the viscous constant were corrected using the 10% correction factor. This approach was employed to allow for prompt completing of the testing and thus minimizing the effect of changing properties of the fresh mixture due to cement hydration.

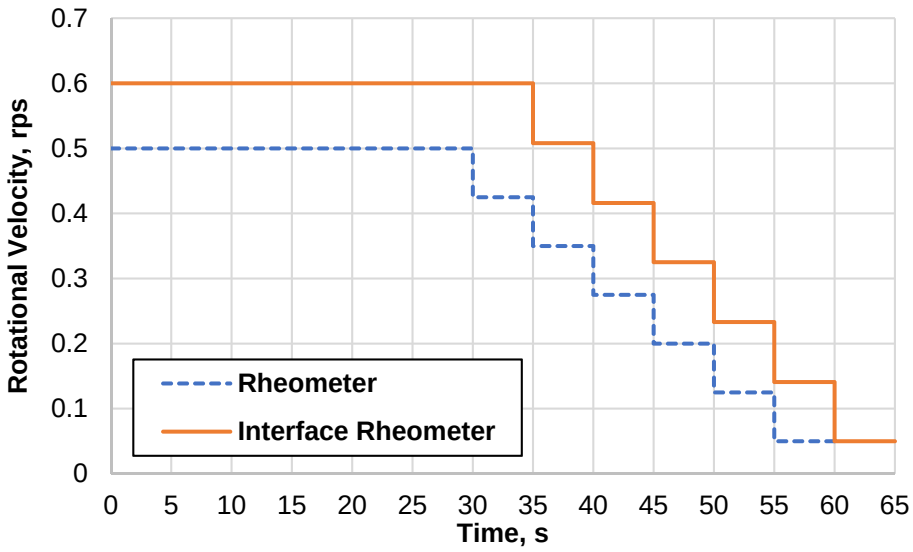

Figure 4.4 – Test protocols for rheological measurements

4.4 Results and Discussion

4.4.1 Fresh Concrete Properties

Fresh concrete properties for all mixtures are shown in Table 4.4. In the case of four mixtures, the slump test was not applicable, therefore the slump flow test was used instead. In terms of plastic air content, values ranging from 3.6% to 14.0% were measured. As expected, measured unit weights corresponded well to plastic air content values.

Table 4.4 – Fresh concrete properties

Mixture ID	Slump/Slump Flow, in. (mm)		Air Content, %	Unit Weight, lbs/ft³ (kg/m³)		Temperature, °F (°C)	
C540-40 A	0.50	(15)	3.6	138.6	(2,221)	75.5	(24.2)
C540-40 B	4.75	(120)	6.8	148.0	(2,371)	74.6	(23.7)
C540-40 C	6.25	(160)	11.5	138.6	(2,221)	72.4	(22.4)
C540-40 D	8.00	(205)	14.0	134.9	(2,161)	72.4	(22.4)
C540-43 A	3.00	(75)	5.7	145.8	(2,336)	74.3	(23.5)
C540-43 B	8.00	(205)	9.0	141.4	(2,266)	76.8	(24.9)
C540-43 C	7.25	(185)	10.0	140.1	(2,244)	74.3	(23.5)
C540-45 A	4.00	(100)	6.5	144.4	(2,312)	74.0	(23.3)
C540-45 B	8.50	(215)	8.3	142.0	(2,275)	73.7	(23.2)
C540-45 C	9.25	(235)	9.5	140.0	(2,242)	75.2	(24.0)
C520-40	4.50	(115)	6.8	147.6	(2,364)	76.7	(24.8)
C520-43 A	5.75	(145)	7.2	146.2	(2,342)	74.7	(23.7)
C520-43 B	7.25	(185)	9.0	142.0	(2,274)	75.8	(24.3)
C520-45	8.50	(215)	9.0	141.0	(2,258)	74.8	(23.8)
C560-40	8.00	(205)	8.0	142.2	(2,277)	74.7	(23.7)
C560-43	8.50	(215)	9.4	139.7	(2,238)	75.1	(23.9)
C560-45	18.75*	(475)	8.1	143.4	(2,297)	74.8	(23.8)
C540-40-R60 A	2.50	(65)	3.4	150.5	(2,411)	74.7	(23.7)
C540-40-R60 B	2.75	(70)	4.5	149.3	(2,392)	75.0	(23.9)
C540-43-R60	7.50	(190)	9.0	142.4	(2,281)	75.9	(24.4)
C540-45-R60	8.25	(210)	6.7	144.4	(2,312)	73.0	(22.8)
C540-43-R40	8.75	(220)	10.5	138.8	(2,223)	75.6	(24.2)
C540-45-R40	9.00	(230)	8.5	140.7	(2,253)	76.7	(24.8)
C540F25-40	8.50	(215)	9.2	137.4	(2,202)	74.7	(23.7)
C540F25-43	17.00*	(430)	8.5	141.5	(2,267)	74.6	(23.7)
C540F25-45	19.00*	(480)	8.0	146.6	(2,348)	74.7	(23.7)
C540-40-RR	6.00	(150)	8.0	141.0	(2,259)	75.7	(24.3)
C540-43-RR	7.25	(185)	7.5	137.5	(2,203)	75.8	(24.3)
C540-45-RR	16.00*	(405)	8.0	138.9	(2,225)	74.3	(23.5)
C540-40-VMA	1.50	(40)	6.1	147.2	(2,359)	74.1	(23.4)
C540-43-VMA	7.75	(195)	6.0	145.5	(2,330)	73.4	(23.0)
C540-45-VMA	6.50	(165)	5.4	144.9	(2,321)	73.3	(22.9)
C540-40-NC	3.50	(90)	6.0	--	--	73.8	(23.2)
C540-43-NC	4.75	(120)	5.1	149.2	(2,389)	73.2	(22.9)
C540-45-NC	8.50	(215)	9.6	140.7	(2,253)	72.5	(22.5)

* indicates slump flow

4.4.2 Mixture Proportions: Rheological and Interface Rheology Measurements

A variety of mixture parameters were considered and their effect on rheological properties of the lubrication layer as well as concrete rheological properties were investigated. A summary of all obtained results is shown in Table 4.5.

Table 4.5 – Bulk concrete rheological properties

Mixture ID	Air Content, %	Plastic Viscosity, Pa.s	Yield Stress, Pa	Viscous Constant, Pa.s/m	Interface Yield Stress, Pa
C540-40 A	3.6	44	1,686	1,815	157
C540-40 B	6.8	34	1,024	1,466	64
C540-40 C	11.5	19	490	1,384	34
C540-40 D	14.0	18	361	1,281	23
C540-43 A	5.7	36	656	1,245	68
C540-43 B	9.0	20	359	1,043	48
C540-43 C	10.0	15	299	906	31
C540-45 A	6.5	21	325	865	45
C540-45 B	8.3	19	279	636	39
C540-45 C	9.5	18	259	613	13
C520-40*	6.8	--	--	1,523	90
C520-43 A	7.2	30	567	1,229	77
C520-43 B	9.0	23	530	1,064	71
C520-45	9.0	22	420	931	53
C560-40	8.0	20	377	1,220	46
C560-43	9.4	13	349	973	43
C560-45	8.1	11	194	687	41
C540-40-R60 A**	3.4	--	--	--	--
C540-40-R60 B**	4.5	--	--	--	--
C540-43-R60	9.0	18	396	1,249	65
C540-45-R60	6.7	15	491	1,165	71
C540-43-R40	10.5	11	431	1,195	56
C540-45-R40	8.5	12	489	1,055	54
C540F25-40	9.2	14	482	1,130	28
C540F25-43	8.5	12	321	809	42
C540F25-45	8.0	10	126	477	38
C540-40-RR	8.0	23	594	1,642	94
C540-43-RR	7.5	14	323	1,063	85
C540-45-RR	8.0	8	222	882	67
C540-40-VMA	5.0	65	1,225	1,751	99
C540-43-VMA	6.0	33	405	1,018	104
C540-45-VMA	5.4	27	245	1,082	50
C540-40-NC	6.0	13	1,050	1,553	13
C540-43-NC	5.1	9	508	1,193	35
C540-45-NC	9.6	16	275	798	44

* rheological measurement identified as incorrect

** rheological measurement not performed due to mixture's stiffness

4.4.2.1 Air Void Content

The relationship between plastic air void content, viscous constant and interface yield stress is shown in Figure 4.5 and Figure 4.6, respectively. It is apparent that an increase in the air void content resulted in a reduction in both viscous constant and interface yield stress. In the case of viscous constant, the relationship appears to be linear for a wide range of air contents spanning from 3.6% to 14.0%. On average, a decrease in the value of the viscous constant of 1.5% (w/cm 0.40), 5.6% (w/cm 0.43) and 12.2% (w/cm 0.45) was observed. The results showed that with an increase in the water content, the reduction effect due to an increase in air content becomes more significant. When analyzing the data for the interface yield stress, a substantial increase was observed for very low plastic air content values, compared to the rate of increase observed in the 5.7%-14.0% range. Moreover, the effect of air content was more pronounced on the interface yield stress than on the plastic viscosity. The average drop in the interface yield stress value was 7%, 11% and 16% for w/cm of 0.40, 0.43 and 0.45, respectively.

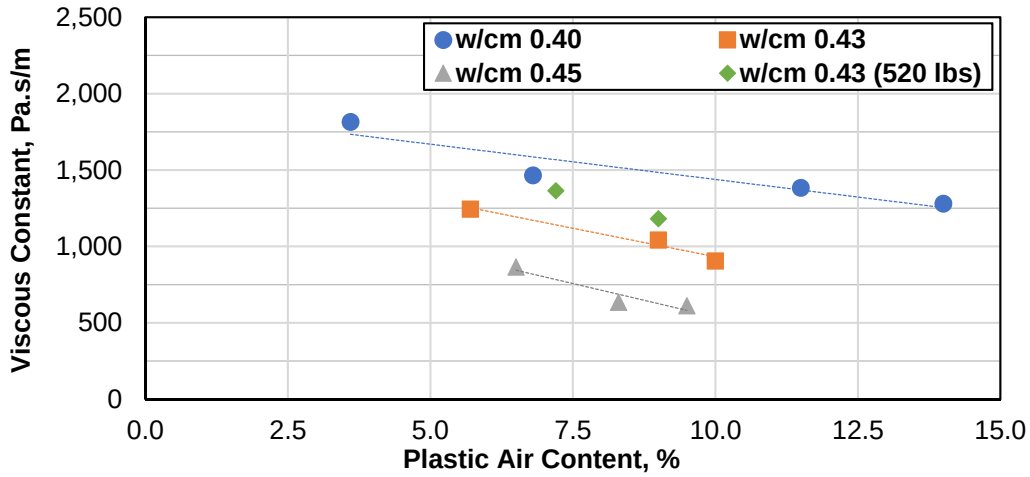

Figure 4.5 – Viscous constant vs air void content

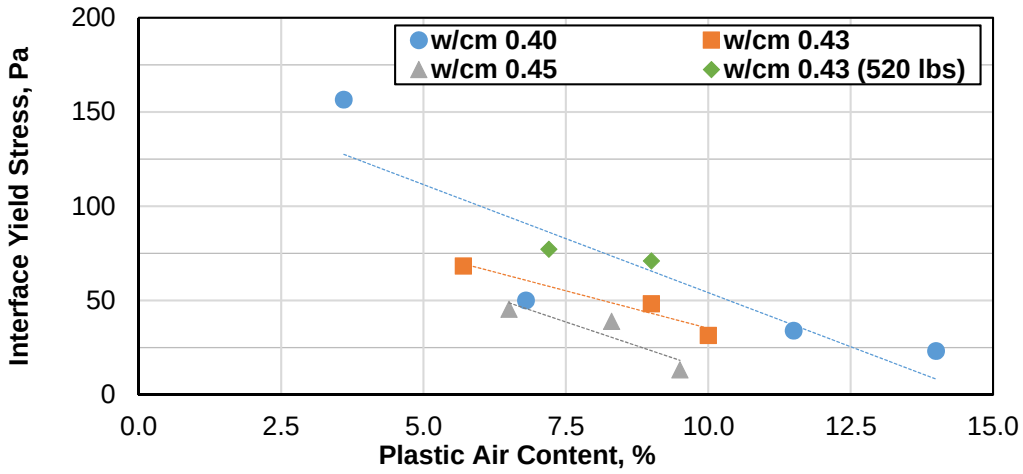

Figure 4.6 – Interface yield stress vs air void content

Changes in the lubrication layer properties generally corresponded well to changes in bulk concrete rheological properties due change in the air content (i.e. decrease in both plastic viscosity and yield stress when air content increases). It was reported that the air content has much more significant effect on plastic viscosity than on yield stress of concrete [117]. For concrete mixtures evaluated in this study, this was not the case; the results have shown very similar rates of decrease of plastic viscosity and yield stress per percent change in air content, as shown in Figure 4.7 and Figure 4.8, respectively. The yield stress was reduced on average by 10%, 13% and 7% for w/cm of 0.40, 0.43 and 0.45, respectively. The average measured plastic viscosity decrease per percent of air was in the similar range: 8%, 13% and 4% for w/cm of 0.40, 0.43 and 0.45, respectively. This discrepancy can be likely explained by exploring mixture proportions and materials used, particularly the type of air-entrainment agent used in this study as opposed to the air-entrainer used in the original Tattersall work in the 1980s and the overall size distribution of the air void system.

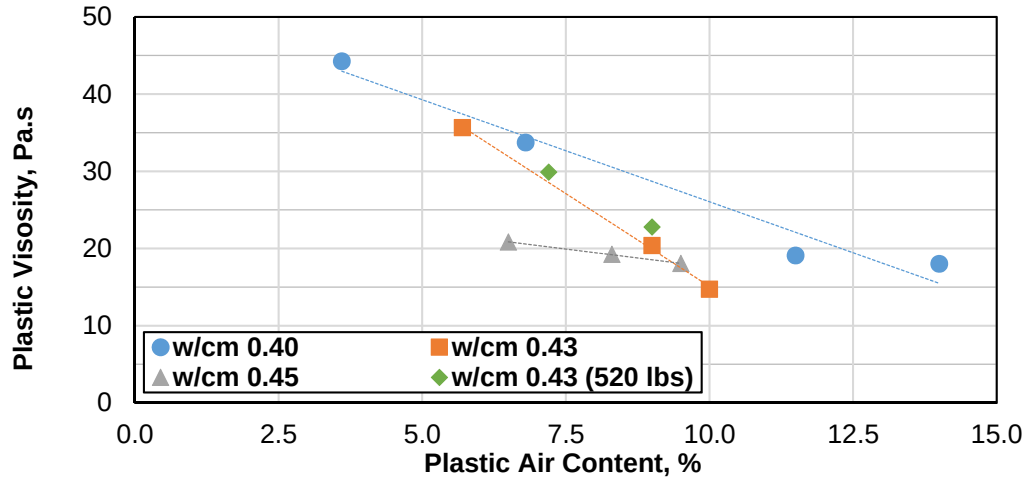

Figure 4.7 – Plastic viscosity vs plastic air content

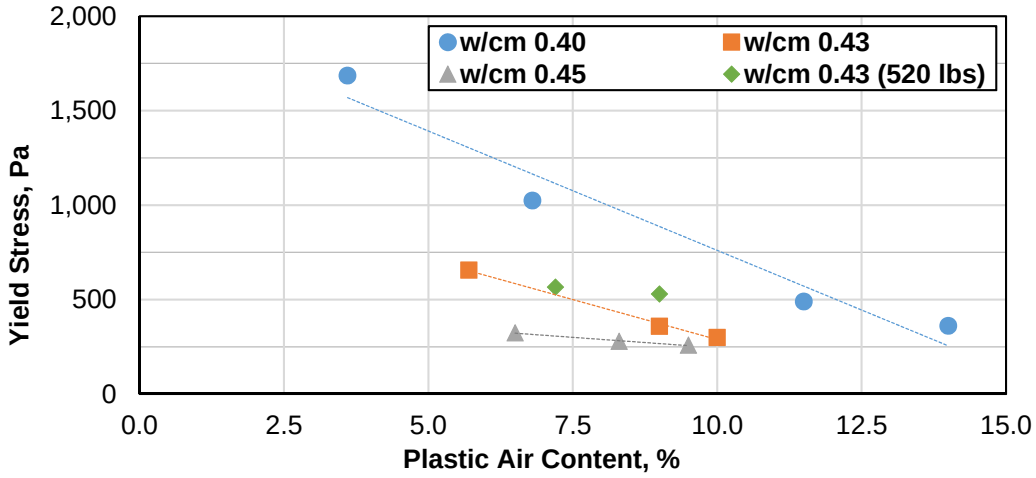

Figure 4.8 – Yield stress vs plastic air content

Two mechanisms, likely occurring simultaneously, are proposed that can explain the changes in the lubrication layer rheological properties related to the plastic air content:

(1) As the air content increases in the bulk concrete, or more precisely in cement paste, air bubbles act to reduce both yield stress and viscosity of the bulk concrete. Subsequently, lower yield stress and more importantly plastic viscosity allows for easier shear-induced migration of coarse and large fine aggregate particles throughout the cement paste, thereby it is reasonable to expect that the

lubrication layer of concrete with higher air content will contain less aggregate particles, or that finer aggregate particles will be contained in the layer, compared to the lubrication layer formed in a concrete mixture with a lower air content. This mechanism could possibly also influence the overall thickness of the lubrication layer as lower viscosity of concrete and an increased intensity of the shear-induced movement might lead to a thicker lubrication layer. However, this hypothesis needs to be verified once an accurate technique of lubrication thickness determination becomes available.

(2) Since the lubrication layer is primarily composed of cement paste (and some fine aggregate particles), an increase in the air void content means that the volume of air in the lubrication layer must increase as well. The final suspension that forms the lubrication layer (cement, water, fine aggregate particles and air bubbles) has therefore reduced its rheological properties due to increased amount of air in the layer. However, this hypothesis is valid assuming that the thickness of the layer does not significantly change with an increase in the air void content. If that is not the case, the whole problem becomes more complex as another variable (i.e. lubrication layer thickness) must be considered. Once again, until a reliable method that would allow for measurement of the lubrication layer thickness exists, it is nearly impossible to evaluate this assumption.

4.4.2.2 Cement Paste Volume and Fly Ash

Concrete mixtures with three cement contents, i.e. 520, 540 and 560 lbs/yd^3 (278, 268, and 258 kg/m^3), were fabricated to investigate the effect of the paste volume on rheological characteristics of the lubrication layer. The range of considered paste volumes (including air)

spanned from 28.9% to 33.6%. As shown in the previous discussion, rheological properties of bulk concrete as well as properties of the lubrication layer are dependent on concrete plastic air void content, hence, only mixtures with similar aid void contents were analyzed and are discussed thereafter. Measured values of viscous constant and interface yield stress with respect to the paste volume are shown in Figure 4.9 and Figure 4.10, respectively. As expected, an increase in the paste volume of the mixture resulted in a decrease in both viscous constant and interface yield stress as the overall resistance to flow of the mixture was lowered by the reduced concentration of aggregate particles. The paste content increase more significantly affected the interface yield stress than the viscous constant. The average decrease in the interface yield stress associated with a 1% increase in paste volume was 36% whereas the average reduction in the viscous constant of 9% was observed for the same change in the paste volume.

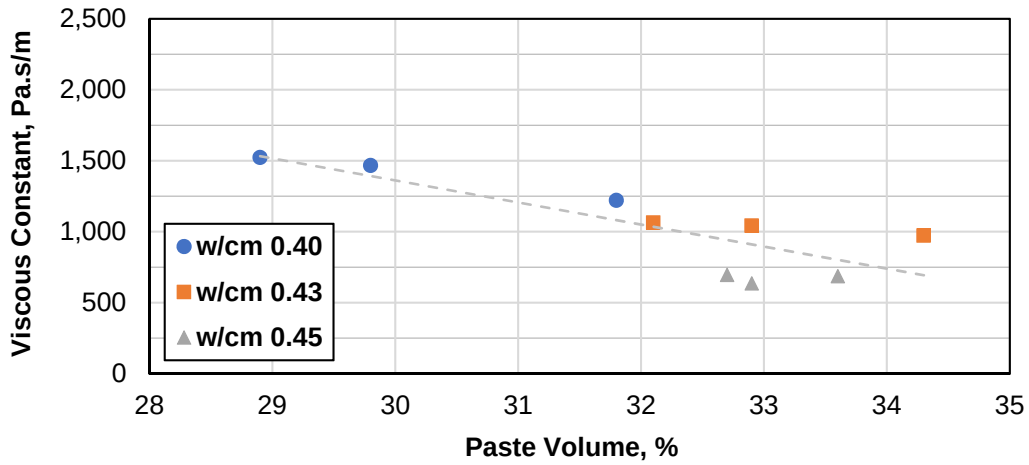

Figure 4.9 – Viscous constant vs paste volume

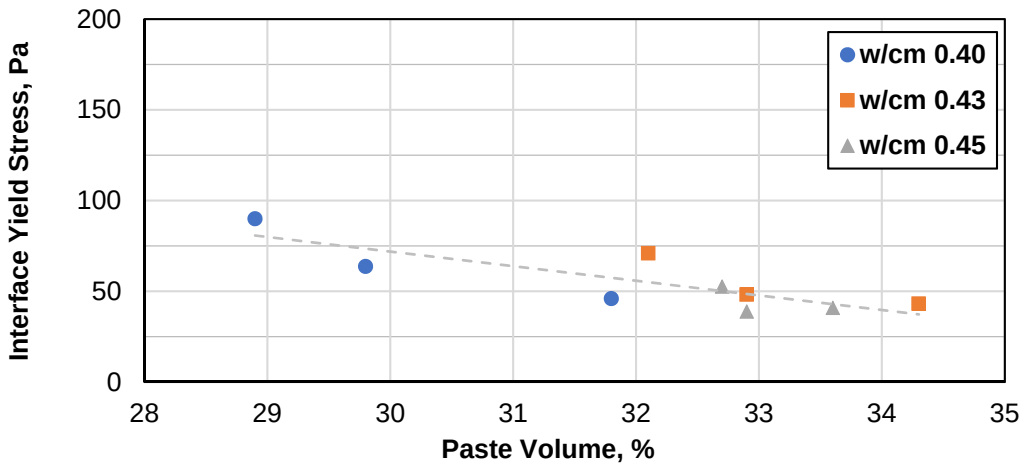

Figure 4.10 – Interface yield stress vs paste volume

It has been reported in the literature that an increase in the overall paste volume typically decreases both the yield stress and plastic viscosity of the bulk concrete [84], [118], however, most of the available data in the literature only considers SCC mixtures. The primary reason that can explain such changes in rheology of a concrete mixture is the fact that an increase in paste content leads to increased availability of the paste to coat aggregate particles, and subsequently reducing friction between individual particles and thereby reducing both yield stress and plastic viscosity. In our study, similar behavior was observed for conventional concrete. A reduction in both plastic viscosity and yield stress, as shown in Figure 4.11 and Figure 4.12, respectively, was recorded for all three w/cm values. On average, the reduction in plastic viscosity and yield stress was 38% and 57%, respectively, when the paste volume increased by 1%.

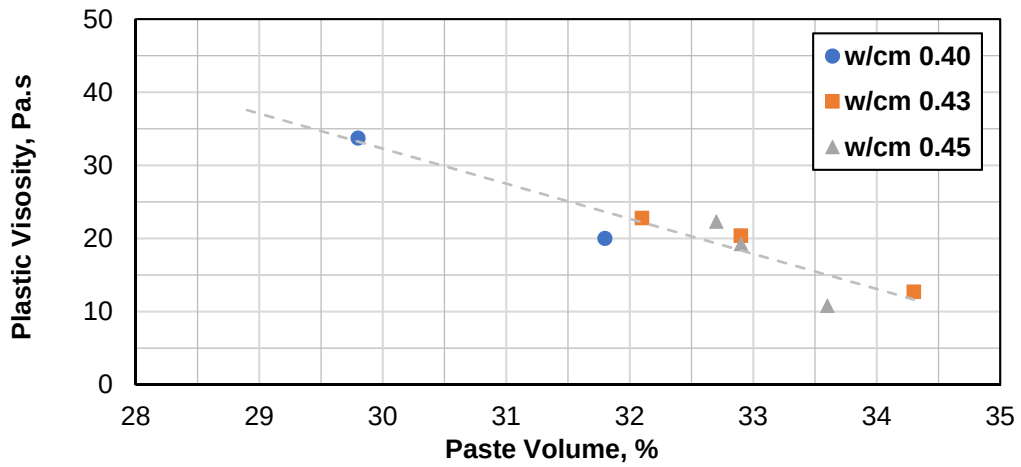

Figure 4.11 – Plastic viscosity vs paste volume

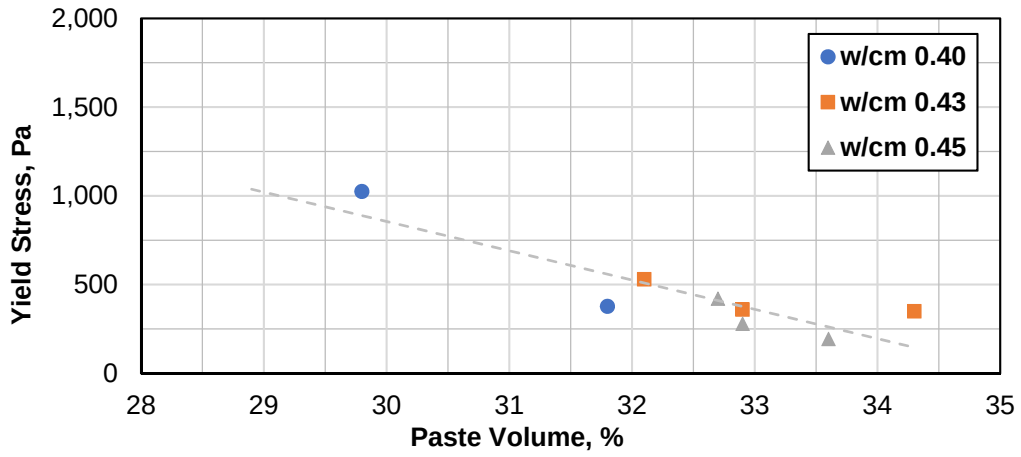

Figure 4.12 – Yield stress vs paste volume

When comparing recorded changes in both rheological properties of fresh concrete and properties of the lubrication layer, it is apparent that both trends are similar (i.e. decrease in all values with an increase in the paste content), however, the extent of the change is dissimilar for the analogous parameters.

It is also important to note both yield stress and plastic viscosity slightly increased for the same cement content change in case of the two mixtures with w/cm of 0.40 (C520-40 and C540-40 B). Both mixtures had identical plastic air void content of 6.5%, therefore the effect of air

voids on concrete rheological properties cannot explain this unexpected result. It is very likely that the C520-40 mixture was pushing the limits of the rheometer due to the mixture's relative stiffness and low workability (measured slump was only 1½ inches), and therefore results of concrete rheological measurements are likely incorrect because of the rheometer working range limitations. Therefore, this mixture was excluded from further analysis and discussion of concrete bulk rheological properties.

However, it is important to stress that the low workability of the bulk concrete and the subsequent impossibility of correct rheological characterization does not necessarily mean that the lubrication layer measurements are also incorrect, as the lubrication layer was properly formed and no indication in the data suggests that any issue exists with the results. This is primarily because only the cement paste, and a relatively small portion of fine aggregate particles contribute to the formation of the lubrication layer, thereby the measured rheological parameters of this layer are typically by an order of magnitude lower than the true rheological properties of the bulk concrete. Therefore, it is possible to characterize properties of the lubrication layer using interface rheometer even when rheological measurements on the bulk concrete cannot be performed due to its low workability.

A series of mixtures with 25% type F fly ash replacement (by weight) while maintaining the 540 lbs/yd^3 total cementitious content was also fabricated as part of this study.

Figure 4.13 shows change in viscous constant and interface yield stress, respectively, with the partial cement replacement by fly ash. As expected, for all three w/cm ratios, both lubrication layer rheological parameters decreased due to the geometry of the fly ash particles (round grains as opposed to flaky portland cement particles) and thus decreased resistance to flow. The magnitude of the change was driven by w/cm of a mixture series. For the 0.40 w/cm

series, both viscous constant and interface yield stress drop by 18% with the fly ash replacement, whereas for the 0.45 w/cm series, the interface yield stress change remained similar (16%) while the viscous constant was reduced by 45%. Somewhat similar behavior was recorded for changes in the bulk concrete rheological properties, as shown in Figure 4.14. As w/cm ratio increased, the overall magnitude of change increased too. For the two lower w/cm ratios (0.40 and 0.43), the plastic viscosity change was rather significant compared to the change in yield stress (25% and 41% vs 2% and 11%), however, for the 0.45 w/cm mixture series, yield stress change was slightly more pronounced (61% vs 41%). The results clearly showed, as in the previous case, that trends of change are alike for concrete rheological properties and rheological properties of the lubrication layer but the extent at which a property changes are dependent on other factors, such as water content.

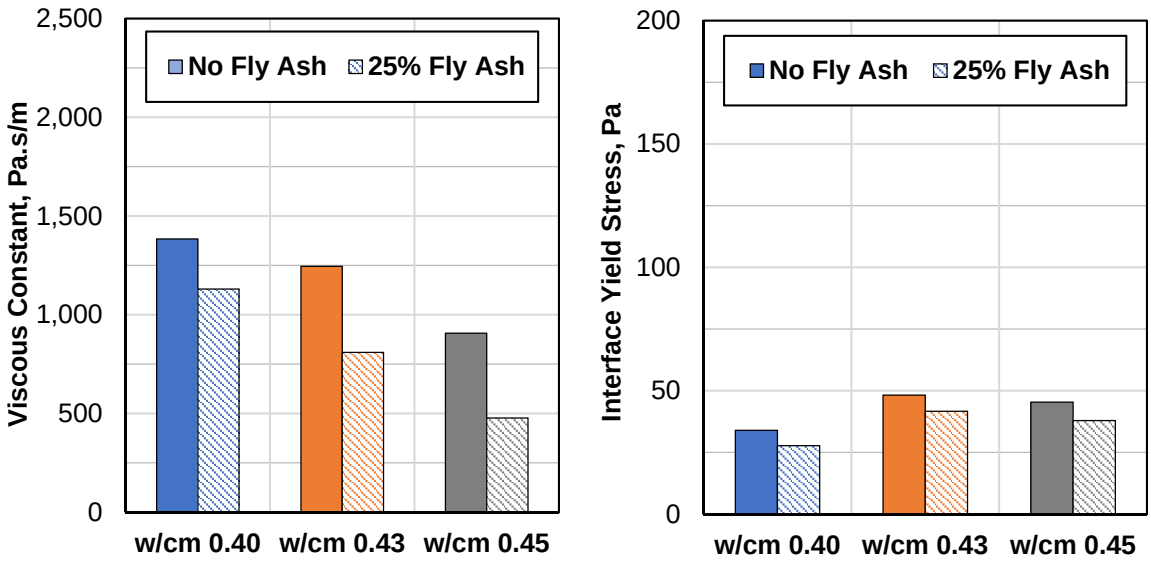

a) b)

Figure 4.13 – Viscous constant (a) and interface yield stress (b) vs 25% fly ash replacement rate

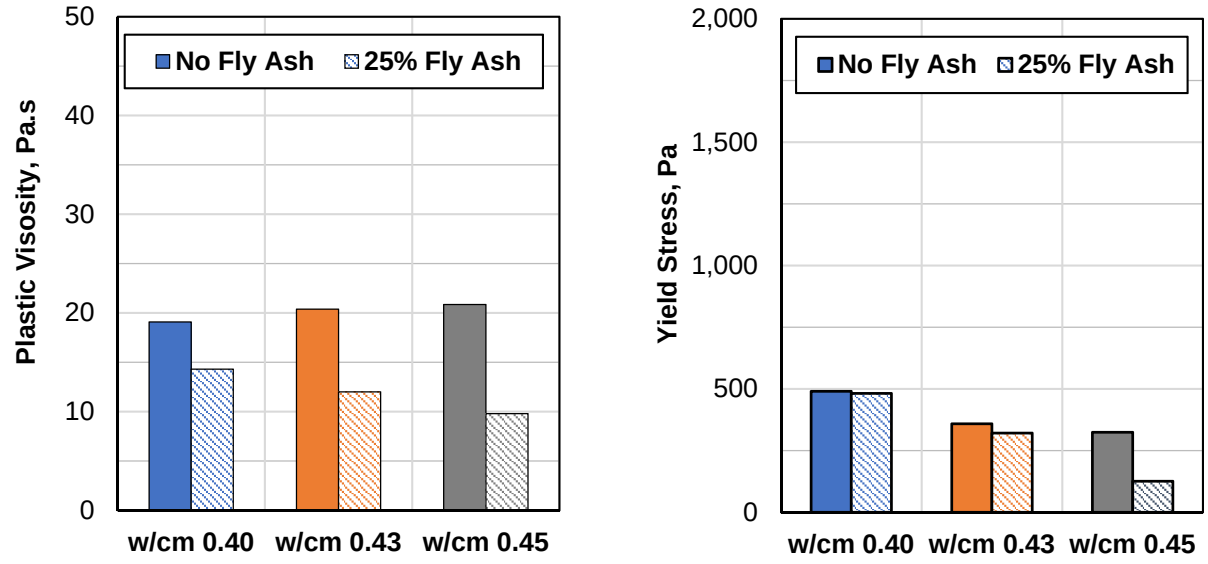

a) b)

Figure 4.14 – Plastic viscosity (a) and yield stress (b) vs 25% fly ash replacement rate

4.4.2.3 Water Content

Measured properties of the lubrication layer with respect to w/cm are shown in Figure 4.15 and Figure 4.16 for the viscous constant and the interface yield stress, respectively. Each

figure includes three sets of mixtures with different cement contents, i.e. 520, 540 and 560 lbs/yd³. To eliminate the influence of plastic air void content on the results, a linear interpolation was used to obtain results of C540-43 (540 lbs/yd³ of cement and w/cm of 0.43). The two other mixtures analyzed in this set, C540-40 and C540-45, had fresh air void content of 6.8% and 6.5%, respectively. Since the two air void content levels measured for the mixture C540-43A and C540-43B were 5.7% and 9.0%, a linear interpolation was found to be an appropriate technique to estimate rheological properties of the same mixture with an air void content of 6.8%.

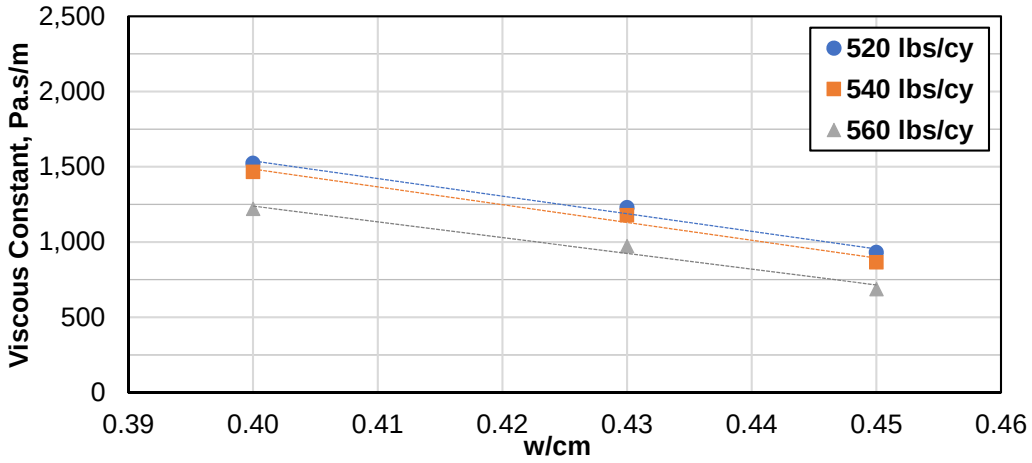

Figure 4.15 – Viscous constant vs water content

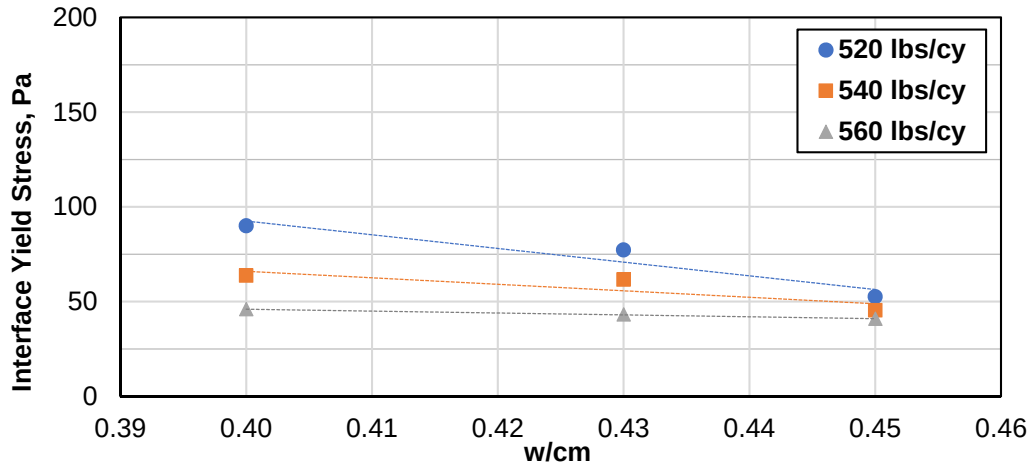

Figure 4.16 – Interface yield stress vs water content

A similar trend for the cement content was seen – the viscous constant reduction due to an increase in the w/cm was more significant than a decrease in the value of the interface yield stress. The viscous constant value decreased on average by 23% when w/cm increased by 0.01 whereas the interface yield stress only dropped on average by 13% for the same w/cm increase. However, significant differences in the change of lubrication layer properties were dependent on the total cement content. For instance, for the lowest considered cement content, i.e. 520 lbs/yd^3, the percentage change in both viscous constant and interface yield stress per 0.01 increase of w/cm was identical (21%). On the other hand, a 24% reduction in the viscous constant and only 6% reduction in the interface yield stress per 0.01 w/cm increase were recorded for the set of mixtures with cement content of 560 lbs/yd^3. These results suggest that while the general observed trends were the same (i.e. reduction of both viscous constant and the interface yield stress with an increase in mixture's water content), the particular behavior and magnitude of the change is likely dependent on other mixture characteristics such as total paste content.

In terms of measured rheological properties of the bulk mixture, a contradictory behavior was detected when comparing both yield stresses (i.e. concrete's yield stress and lubrication layer's interface yield stress) as well as both viscosity parameters (i.e. concrete's plastic viscosity and lubrication layer's viscous constant), as shown in Figure 4.17 and Figure 4.18. When the water content of the mixture was increased, a more significant change was observed in the value of the yield stress (33% reduction per 0.01 w/cm increase) when compared to measured changes in the plastic viscosity (23% decrease per 0.01 w/cm increase).

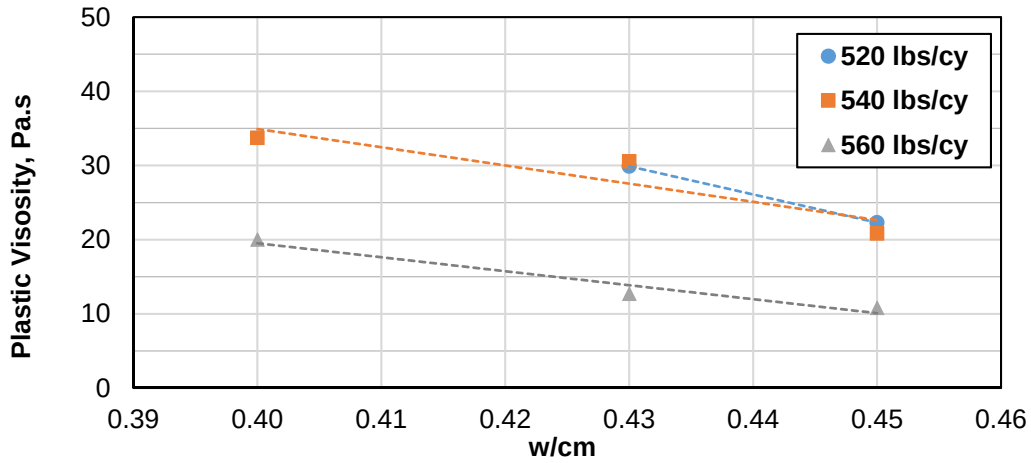

Figure 4.17 – Plastic viscosity vs water content

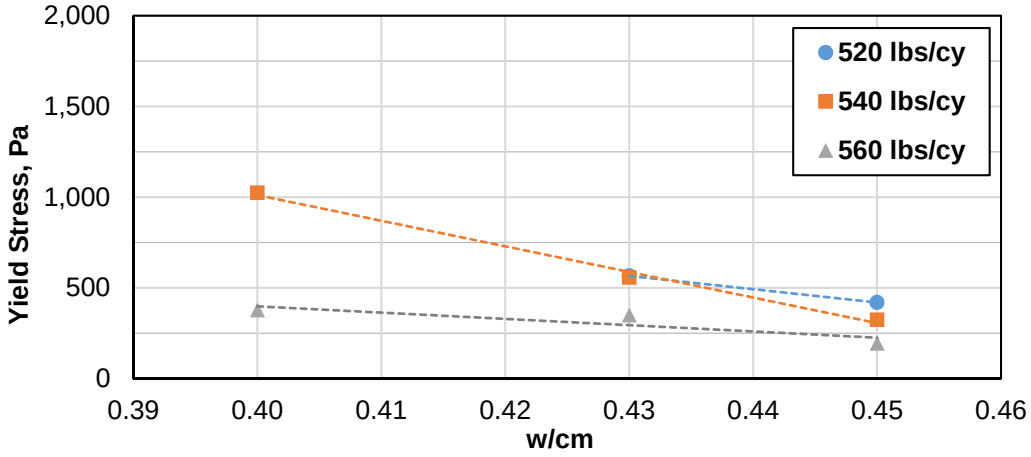

Figure 4.18 – Yield stress vs water content

4.4.2.4 Fine-to-Coarse Aggregate Ratio, Aggregate Shape

The effect of fine and coarse aggregate content on concrete rheological properties and lubrication layer characteristics was also investigated as part of the study. The effect of aggregate volume fraction, and specifically the fine-to-coarse aggregate (FA/CA) ratio, on rheological properties of concrete is more complicated than previously discussed mixture proportioning factors. In general, it is well established in the literature that an overall increase in aggregate content results in an increase in both yield stress and plastic viscosity [119], [120]. This is

because an increase in the total aggregate content results in a higher total solids concentration, which ultimately reduces the volume of space between solid particles filled with cement paste. Consequently, greater internal friction is present between aggregate particles and the overall resistance to flow is increased. For the FA/CA ratio, it has been shown that an optimum value at which both yield and/or plastic viscosity are minimized exists [117], [121]. However, this ideal ratio is dependent on specific mixture proportions as various values has been reported. Moreover, the value of FA/CA at which one of the rheological parameters of concrete is minimized is not necessarily identical for both yield stress and plastic viscosity.

The relationship between the FA/CA ratio, and viscous constant and interface yield stress are presented in Figure 4.19 and Figure 4.20, respectively. We examined three FA/CA ratios – 0.6, 0.5 and 0.4 as these are a typical representation of HPC mixtures. Additionally, mixtures with w/cm of 0.40 are not included in our analysis since their initial workability made it difficult to measure correctly their rheological properties. Results showed that rheological properties of the lubrication layer behave in a similar fashion as bulk concrete, i.e. that an optimal value of FA/CA exists where both viscous constant and the interface yield stress are minimized. In our study, the FA/CA value of 0.5 generated minimum values of both rheological parameters of the lubrication layer. Interestingly, the optimum value was identical for both evaluated parameters. Moreover, the magnitude of change with changing FA/CA was alike for the lubrication layer rheological parameters. When FA/CA changes from 0.4 to 0.5, both viscous constant and yield stress decreased by 16% and 31% for mixtures with w/cm of 0.43 and 0.45, respectively. Similarly, an increase of 15% and 22% (for w/cm of 0.43) in viscous constant, and 17% and 19% (for w/cm of 0.45) in yield stress was measured when FA/CA further increased from 0.5 to 0.6.

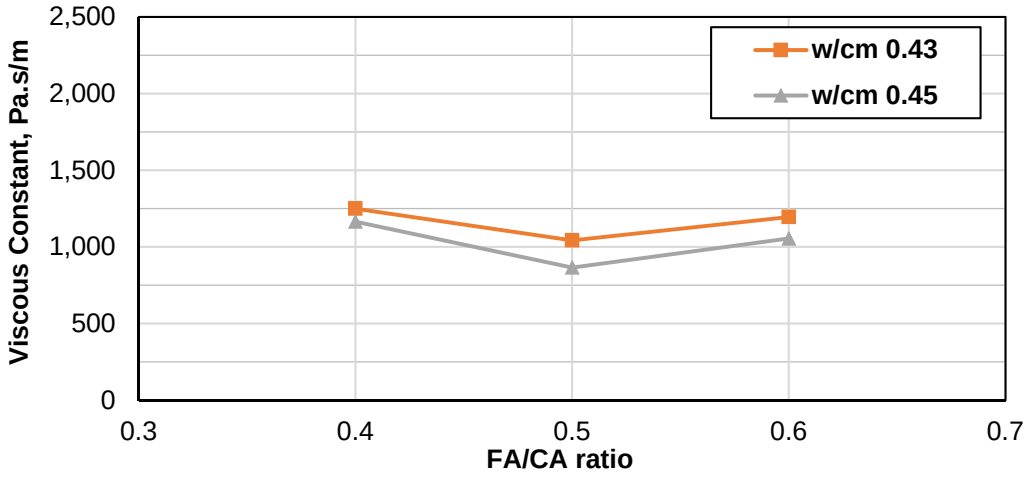

Figure 4.19 – Viscous constant vs FA/CA ratio

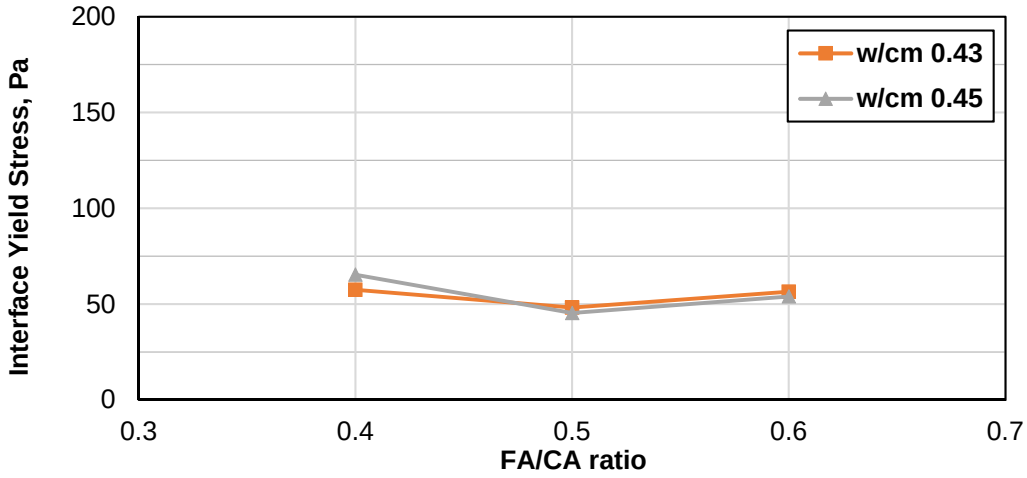

Figure 4.20 – Interface yield stress vs FA/CA ratio

On the contrary to previously discussed mixture parameters, the changes in rheological properties of bulk concrete did not correspond fully to changes in the properties of the lubrication layer when FA/CA ratio was altered, as shown in Figure 4.21 and Figure 4.22. Particularly, the maximum value of plastic viscosity, for both mixtures with w/cm of 0.43 and 0.45, was recorded at the FA/CA ratio value of 0.5, whereas the minimum value was measured at the FA/CA value of 0.6. On the other hand, the minimum yield stress value was measured for the FA/CA ratio of 0.5, similarly to viscous constant and interface yield stress. These results confirm

other researchers' findings that suggest that ideal FA/CA ratio at which concrete rheological properties are minimized is not necessarily the same for plastic viscosity and yield stress. Moreover, the dissimilar FA/CA value that resulted in the minimum value of viscous constant of the lubrication layer and plastic viscosity of bulk concrete (FA/CA of 0.6 vs 0.5) can be likely contributed to the formation mechanism of the lubrication layer. As mentioned previously, the lubrication layer is mostly formed by water and cement particles, and still-debated amount fine sand particles. With this respect, rheological properties of the lubrication layer are primarily affected by properties of the cement paste and factors that governs these properties (such as cement content, cement composition, water content, etc.). The contribution of other concrete constituents appears to be less significant, and its primarily driven by the ability of the cementitious system to form the lubrication layer. It is argued that coarse or fine aggregate do not play any role when it comes to rheological properties of the lubrication layer, it is rather suggested that, based on the results presented in this chapter, that contribution of these is less significant than the influence of the previously discussed concrete/cement paste constituents, especially when compared to the impact of the FA/CA ratio on rheological properties of bulk concrete mixtures.

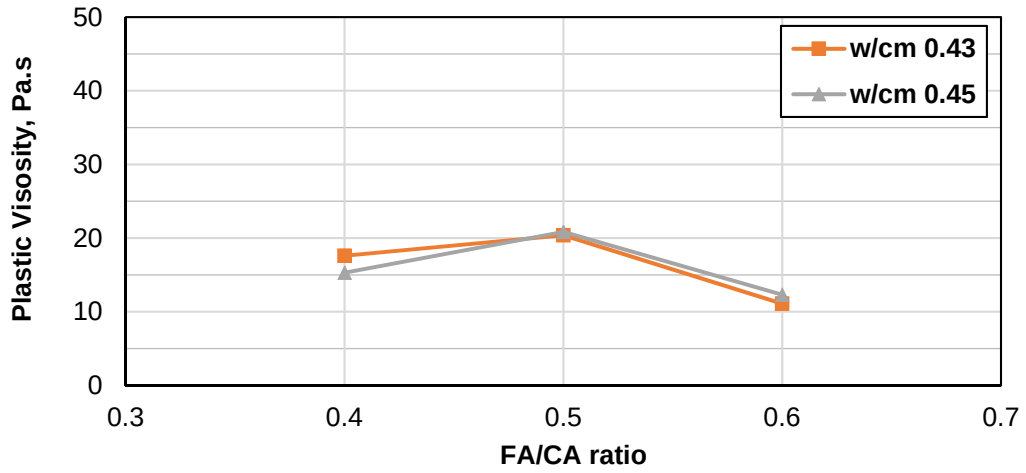

Figure 4.21 – Plastic viscosity vs FA/CA ratio

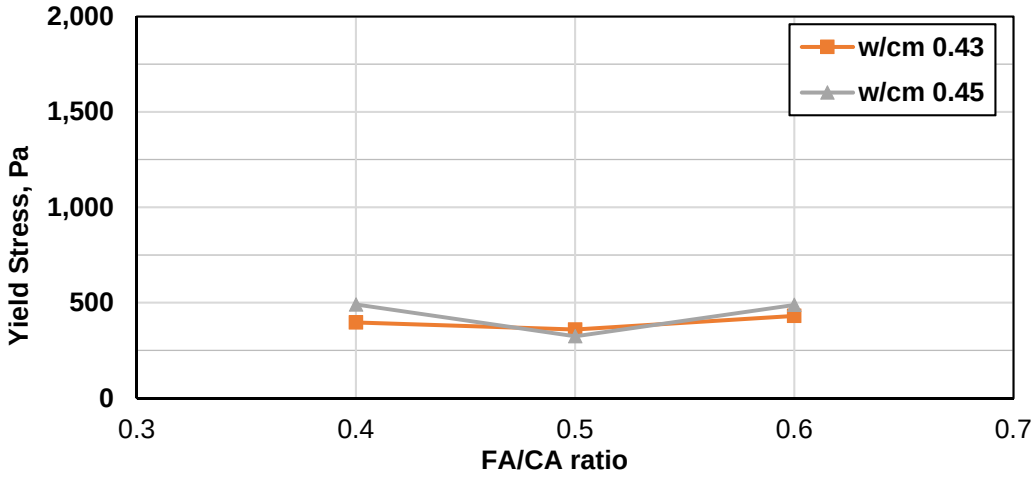

Figure 4.22 – Yield stress vs FA/CA ratio

Furthermore, coarse aggregate shape was also included among the variables that were investigated in this study. Two sets of mixtures with different aggregate shape, i.e. manufactured crushed aggregate and natural rounded aggregate, were tested. Each set included mixtures with three water contents (w/cm of 0.40, 0.43 and 0.45), and the total volume of coarse and fine aggregate was kept constant for the two corresponding mixtures. Measured rheological properties of the lubrication layer with respect to the aggregate shape are shown in Figure 4.23.

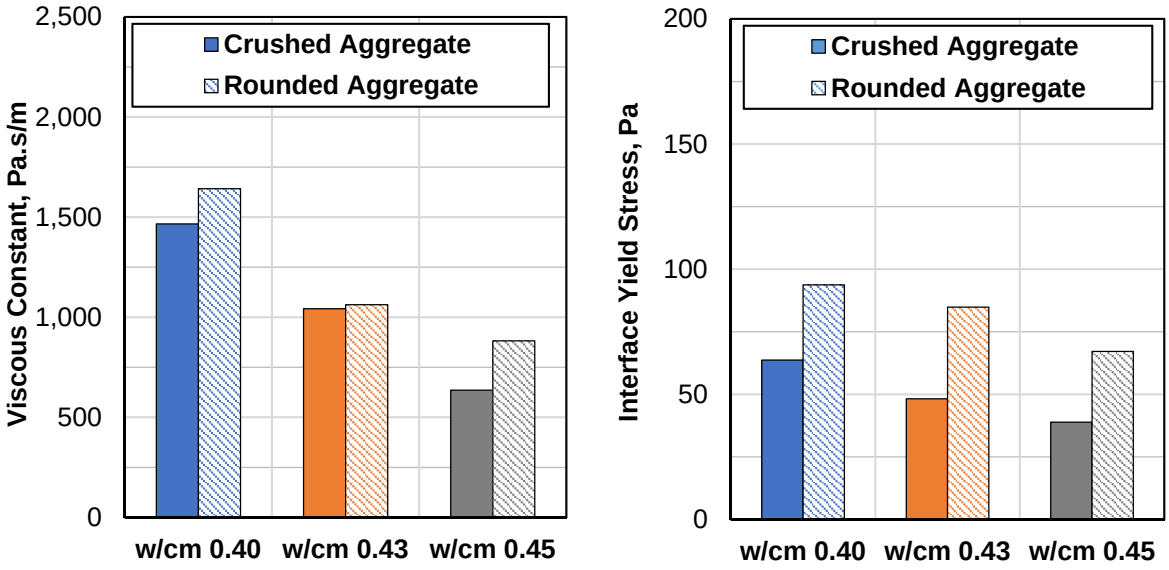

a) b)

Figure 4.23 – a) viscous constant, b) interface yield stress vs aggregate shape

Change in the aggregate shape had a different effect on the rheological properties of bulk concrete compared the rheological properties of the lubrication layer. As apparent from Figure 4.24, decrease in both yield stress and plastic viscosity of concrete were recorded when aggregate shape changed from crushed to rounded. This is in agreement with available literature [84]. However, both viscous constant and interface yield stress increased after the replacement of crushed coarse aggregate with rounded coarse aggregate. The overall increase in magnitude was dependent on w/cm ratio, however, in all cases, the interface yield stress increase was more significant (increase by 47%, 76% and 73% for w/cm of 0.40, 0.43 and 0.45, respectively) compared to the viscous constant increase (increase of 12%, 2% and 39% for w/cm of 0.40, 0.43 and 0.45, respectively). Since the cement paste properties were very similar for both mixture series, it is likely that the formation process of the lubrication layer is the key to the dissimilar behavior of lubrication layer properties and concrete rheological properties. When rounded aggregate is used, a smaller surface area of the aggregate fraction in the mixture requires less

cement paste to coat all aggregate particles. This directly translates into reduced concrete rheological properties as the flow resistance is decreased. One would expect that the values of the viscous constant and interface would decrease since the system allows for more cement paste to form the lubrication layer as it is not used to cover coarse aggregate particles. However, this was not the case in this scenario. It appears that the process of shear-induced particle migration was more limited in this system, eventually leading to a thinner lubrication layer, resulting in a reduction in both viscous constant and interface yield stress.

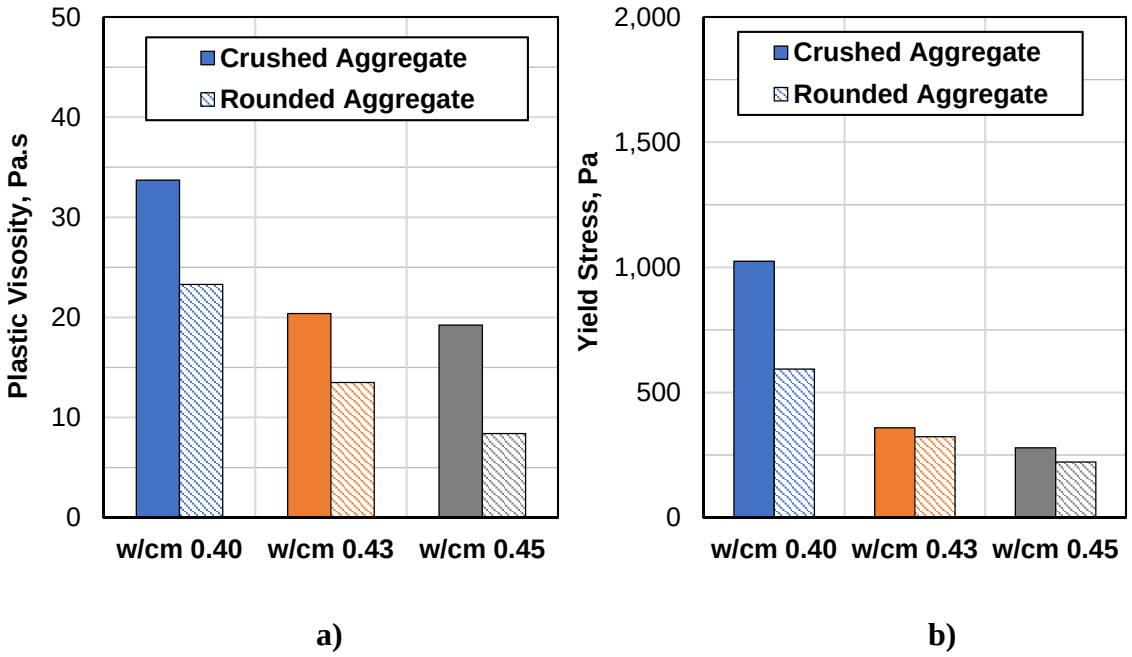

Figure 4.24 – a) plastic viscosity, b) yield stress vs aggregate shape

4.4.2.5 Viscosity-Modifying Admixture

Changes in lubrication layer properties connected to use of VMA are shown in Figure 4.25. Observed changes of viscous constant were not consistent across the set of investigated mixtures. For mixtures with w/cm of 0.40 and 0.45, an increase in viscous constant was observed with the use of VMA, whereas for the mixture series with w/cm of 0.43, a decrease in the value of the viscous constant was observed. For the interface yield stress, an increase was observed for

all three mixtures after addition of VMA. Moreover, the increase is more pronounced for mixtures with w/cm values of 0.40 and 0.43 as the interface yield stress value increased by more than 50%, compared to an increase by 10% for the mixture with w/cm of 0.45.

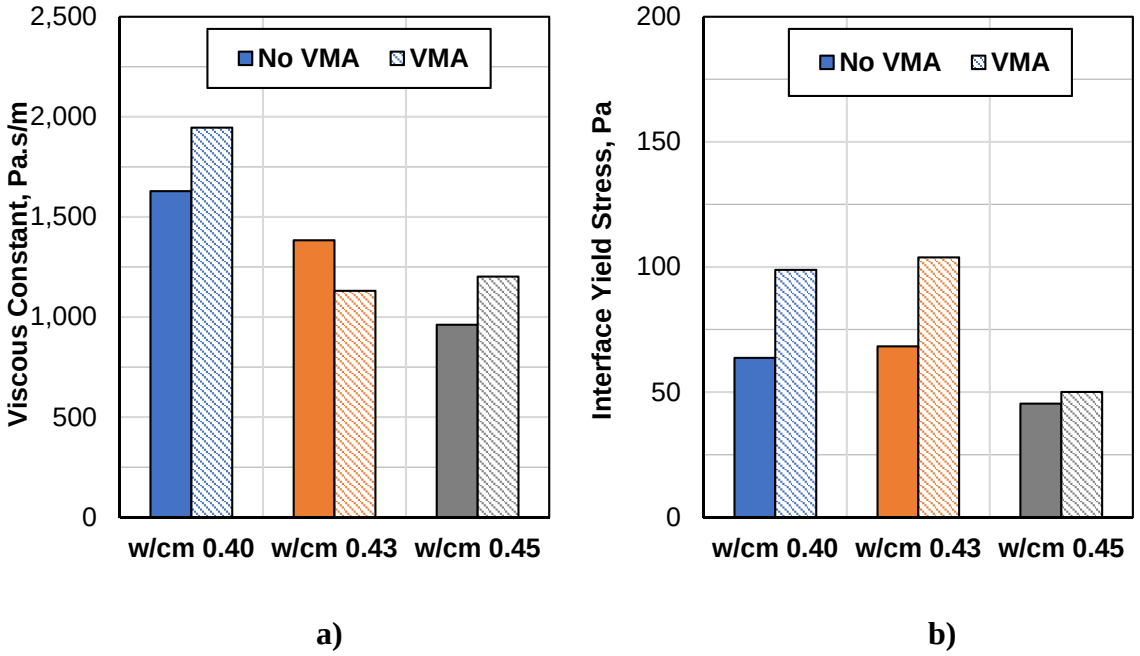

Figure 4.25 – a) viscous constant, b) interface yield stress vs VMA use

In terms of concrete rheological properties, as shown in Figure 4.26, non-consistent behavior was observed across the set of investigated mixtures. In the case of plastic viscosity, its value increased for mixtures with 0.40 and 0.45 w/cm while a reduction was observed for the mixture with w/cm of 0.43. This trend follows behavior of the viscous constant, as discussed above. Concrete yield stress increased by 20% for the mixture with w/cm of 0.40 and decreased by 38% and 24% for mixtures with w/cm of 0.43 and 0.45, respectively.

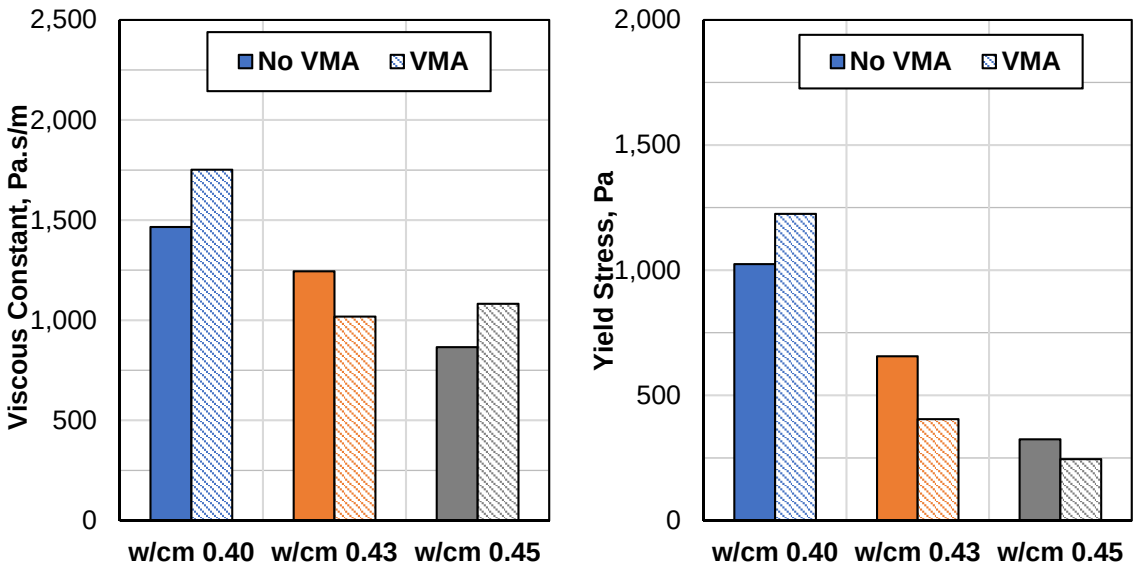

Figure 4.26 – a) plastic viscosity, b) yield stress vs VMA use

The results suggest that the functionality and effectiveness of the VMA is influenced by initial rheological properties of concrete mixtures. VMA is typically used only in SCC or highly-flowable mixtures to control segregation during placements by increasing viscosity, and subsequently cohesiveness of the mixture. It appears from our results that for less workable mixtures, i.e. mixtures with w/cm of 0.40 and 0.43 in this laboratory study, the influence of VMA on both rheological properties and properties of the lubrication layer might be altered. It is noteworthy that in terms of yield stresses, a different behavior was observed for bulk concrete (decrease in yield stress for all concretes but mixture with w/cm of 0.40) compared to interface yield stress (decrease in all cases). The results show that no general trend can be established for the relationship between concrete rheological properties and properties of the lubrication layer for mixtures containing VMAs, and therefore it is essential that effects of VMAs on these properties are carefully evaluated for each individual concrete mixture.

4.4.2.6 Clay Particles

The effect of nanoclay particles addition on properties of the lubrication layer is shown in Figure 4.27. Similarly to behavior observed for the use of VMA, nanoclay particles had shown different effects on concrete mixtures based on their w/cm. For mixtures with w/cm of 0.40 and 0.43, relatively small changes in the values of viscous constant were measured, albeit in the case of the 0.40 w/cm an increase in the viscous constant value of 6% was measured whereas a decrease of 4% was recorded for mixture with w/cm of 0.43. For the mixture with w/cm of 0.45, a much more significant change was recorded, i.e. 30% increase in the viscous constant. For the interface yield stress, similar behavior was again observed for mixtures with w/cm of 0.40 and 0.43 as the interface yield stress value decreased 80% and 50%, respectively. On the other hand, a very significant increase in the yield stress value was observed for the mixture with w/cm of 0.45.

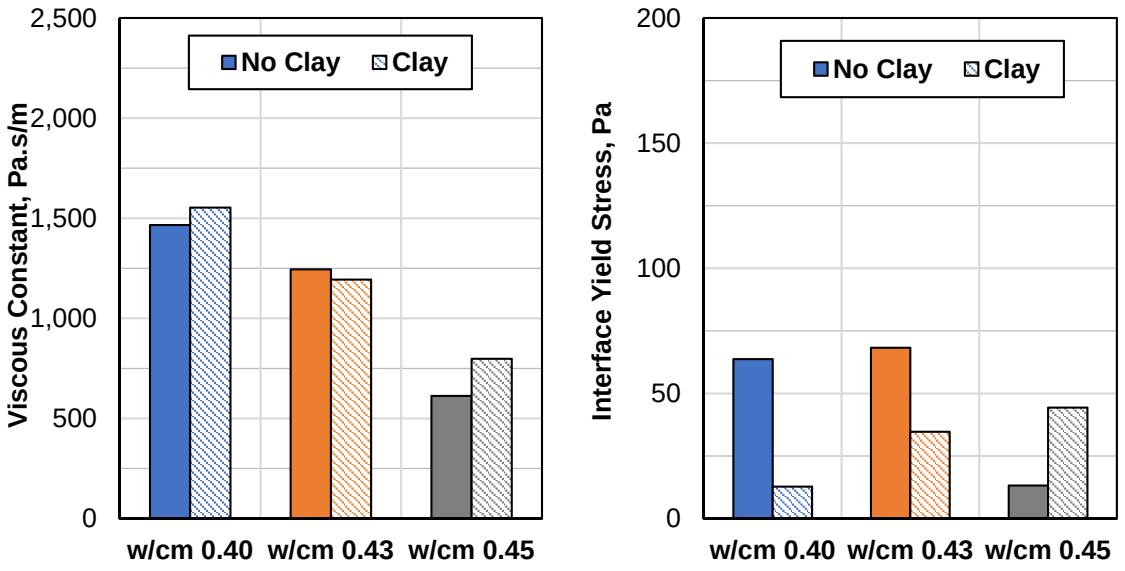

a) **b)**

Figure 4.27 – a) viscous constant, b) interface yield stress vs clay particles use

The effect of the nanoclay particles on concrete rheological properties is shown in Figure 4.28. In terms of plastic viscosity, a decrease in its value was observed for all three w/cm ratios, however, the effect was much more significant for mixtures with w/cm of 0.40 and 0.43. For the yield stress, almost no change was recorded for mixtures with w/cm of 0.40 and 0.45 (3% and 6% increase, respectively) while a decrease by 25% was observed for the mixture with w/cm of 0.43.

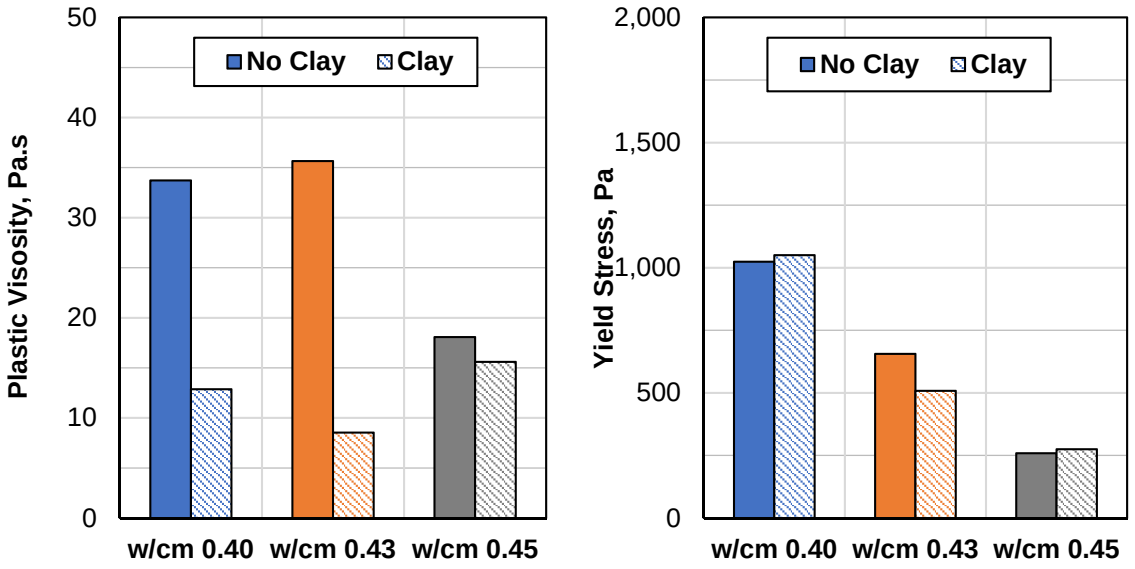

Figure 4.28 – a) plastic viscosity, b) yield stress vs clay particles use

The result showed that the nanoclay particles can significantly alter both concrete rheological properties, especially the plastic viscosity, and properties of the lubrication layer, especially the interface yield stress. The significant decrease in plastic viscosity after addition of the clay particles in the mixture could be problematic in terms of concrete stability under pressure and its segregation resistance, and could also lead to a reduction in required pumping pressure. Since no particular trend of change was observed for both lubrication layer properties

and concrete rheological properties, it is apparent that each individual concrete mixture must be tested in order to evaluate effects of nanoclay particles on its performance.

4.4.3 Pressure Analysis

In order to evaluate the effect of discussed mixture modifications on mixture's pumping performance, a comparative analysis using Kaplan's pumping model [65] was performed. The primary reasons for this analysis is to provide a comprehensive evaluation of investigated mixture modifications with respect to all rheological properties that can influence pumpability. As discussed previously, Kaplan's model allows estimation of pumping pressure based on concrete rheological properties and properties of the lubrication layer. Hence, it enables concrete practitioners to directly apply rheological measurements (of both bulk concrete and lubrication layer) into the decision-making process during concrete mixture design and development phase of the project.

Kaplan's model captures two different flow regimes that are governed by two different equations, as discussed in Section 2.4.3. When all shearing is done by the lubrication layer and the bulk concrete is pushed through the pipeline as a plug (slip flow), only rheological properties of the lubrication layer are considered for the pressure loss calculation. When a portion of the concrete is sheared (shear flow), the model is expanded to also include rheological properties of the bulk concrete. For purposes of this analysis, the distinction between these two flow regimes was made based on the flow behavior in the interface rheometer. If only lubrication layer was sheared in the interface rheometer, slip flow was assumed and Eq. 2-30 used; if a portion of the bulk concrete was sheared, shear flow was assumed and Eq. 2-29 utilized. Experimentally measured values of concrete and lubrication layer rheological properties were used, in addition to the following assumptions: pipe length of 1 meter, 62.5 mm pipe radius, 114 mm pump piston

radius, 0.85 filling coefficient of the pump cylinder, and two flow rate values of (1) 50 m³/h (65 yd³/h) and (2) 12.5 m³/h (16 yd³/h). These assumptions are based on realistic characteristics of concrete pumping and pumping operations that are routinely used on construction sites. The two select flow rates were chosen as representatives of "slow" and "fast" pumping. Flow regimes and estimated pressures for each mixture and flow rate are shown in Table 4.6.

Table 4.6 – Estimated pumping pressures based on Kaplan's pumping model

Mixture ID	Flow Regime	Estimated Pressure, kPa	
		Q = 50 m³/m	Q = 12.5m³/m
C540-40 A	Slip Flow	82.3	24.3
C540-40 B	Slip Flow	64.5	17.7
C540-40 C	Slip Flow	60.0	15.8
C540-40 D	Slip Flow	55.3	14.4
C540-43 A	Slip Flow	55.2	15.4
C540-43 B	Slip Flow	46.0	12.6
C540-43 C	Slip Flow	39.6	10.7
C540-45 A	Slip Flow	38.3	10.7
C540-45 B	Slip Flow	28.3	8.0
C540-45 C	Shear Flow	21.2	7.0
C520-40	Slip Flow	--	--
C520-43 A	Slip Flow	54.8	15.6
C520-43 B	Slip Flow	47.6	13.6
C520-45	Slip Flow	31.3	9.1
C560-40	Slip Flow	53.5	14.5
C560-43	Slip Flow	42.8	11.7
C560-45	Shear Flow	19.5	8.6
C540-40-R60 A	Slip Flow	--	--
C540-40-R60 B	Slip Flow	--	--
C540-43-R60	Slip Flow	55.1	15.1
C540-45-R60	Slip Flow	51.7	14.5
C540-43-R40	Slip Flow	52.7	14.5
C540-45-R40	Slip Flow	46.7	13.0
C540F25-40	Slip Flow	49.1	12.9
C540F25-43	Slip Flow	35.8	10.0
C540F25-45	Shear Flow	14.6	6.3
C540-40-RR	Slip Flow	72.9	20.5
C540-43-RR	Slip Flow	48.0	14.0
C540-45-RR	Shear Flow	20.9	11.5

4.4.3.1 Air Void Content

Estimated pumping pressure with respect to mixtures air void content is shown in Figure 4.29 and Figure 4.30 for flow rate of 50 m^3/h and 12.5 m^3/h, respectively. On average, pumping pressure decreased by 9.5% per 1% increase in the plastic air void content for the flow rate of 50 m^3/h, however, small deviations from this value are apparent based on mixture's w/cm. For the lower flow rate value of 12.5 m^3/h, approximately 70% pressure reduction was calculated comparing to the 50 m^3/h flow rate. When comparing the effect of the air void content on pumping pressure, lower reduction factor per percentage unit of air is observed for the lower flow rate, i.e. 6.4% per 1% increase in the plastic air void content on average. For both flow rates, the pressure reduction increased with an increase in w/cm.

In general, increasing air void content appears to be an effective and relatively cheap way to reduce required pressure. However, it is typically not recommended to rely on the air void system when it comes to pumping performance. It has been shown that the air void content changes due to pumping and does not even remain the same during the pumping operation as the applied pressure and subsequent dissolution mechanism alter the air void system in the pipeline [64], [92]–[95], [122]. As shown in this study, a relationship exists between rheological properties, rheological properties of the lubrication layer and the fresh air void system. Therefore, the initial input values of Kaplan's model (or any other pumping model based on concrete rheological characterization) could be inaccurate if not adjusted for the air content. Additionally, it is likely that not only the total air void content but also other properties of the air void system, especially coarseness of the air bubbles and their spatial distribution, influence rheological properties of both bulk concrete and the lubrication layer. Since these properties cannot be readily tested in the field, it is not feasible to optimize mixture for pumping by altering

the air void system. It is rather recommend using the science of rheology to determine properties of investigated mixture at various air contents, and using conservative values (i.e. at lower air void contents) as input data for pumping models to obtain realistic pressure predictions.

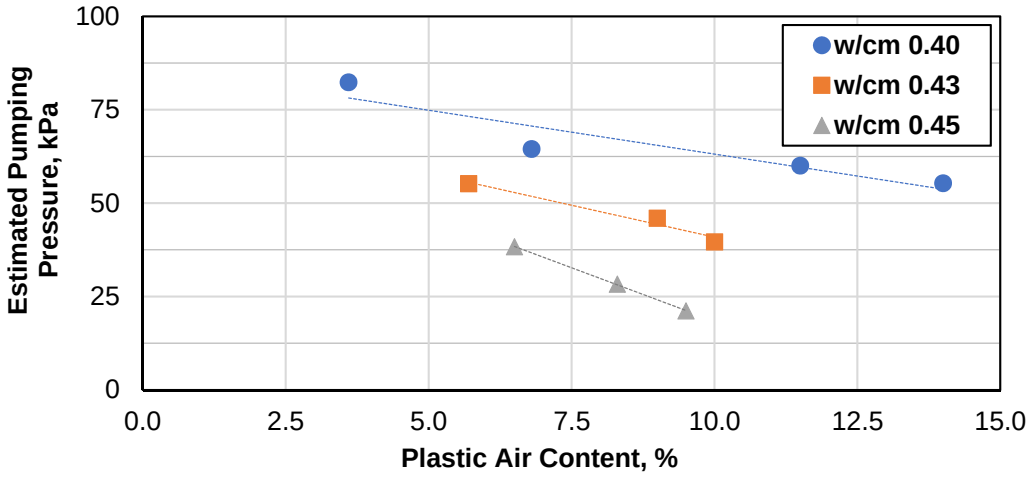

Figure 4.29 – Estimated pumping pressure vs air content, Q = 50.0 m³/h

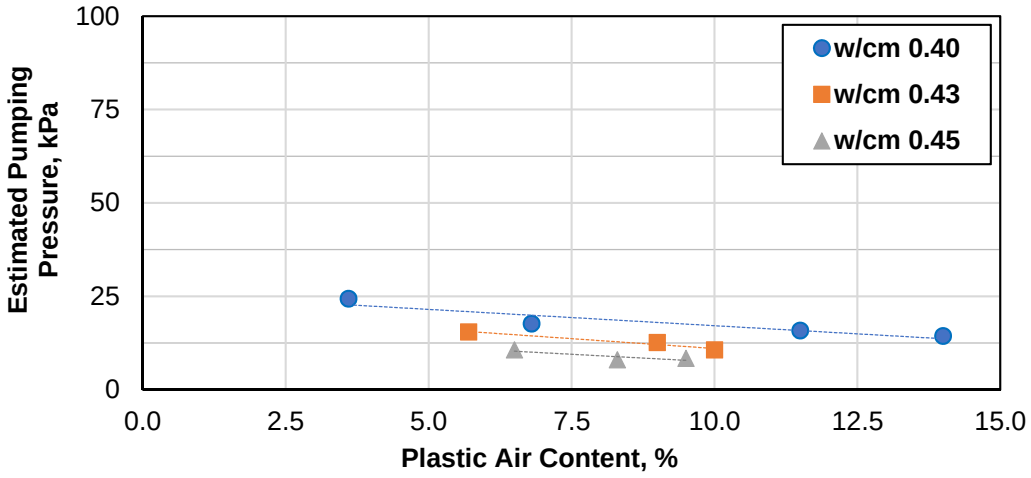

Figure 4.30 – Estimated pumping pressure vs air content, Q = 12.5 m³/h

4.4.3.2 Paste Content and Fly Ash

The relationship between estimated pumping pressure and paste content of investigated mixtures is shown in Figure 4.31 and Figure 4.32 for flow rate of 50 m³/h and 12.5 m³h, respectively. For the 50 m³/m flow rate, and despite missing a data point for the C520-40 mixture

(cement content of 520 lbs/yd³ and w/cm of 0.40) due to mixture stiffness, the greatest reduction of pumping pressure is estimated for the mixture with 0.45 w/cm, i.e. an average 45% pressure decrease when the paste content increased by 1%. On average, a pressure drop of 9% and 5% was estimated for the same paste content increase for mixtures with 0.43 and 0.45 w/cm, respectively. For the 12.5 m³/h flow rate, similar albeit less pronounced trends were observed. The 0.45 w/cm mixture series benefited the most from paste content increase, with an average pressure reduction of 34% associated with a 1% increase in the paste volume. An average decrease in pumping pressure by 9% and 7% due to 1% increase in the paste volume was estimated for mixtures with w/cm of 0.43 and 0.45, respectively.

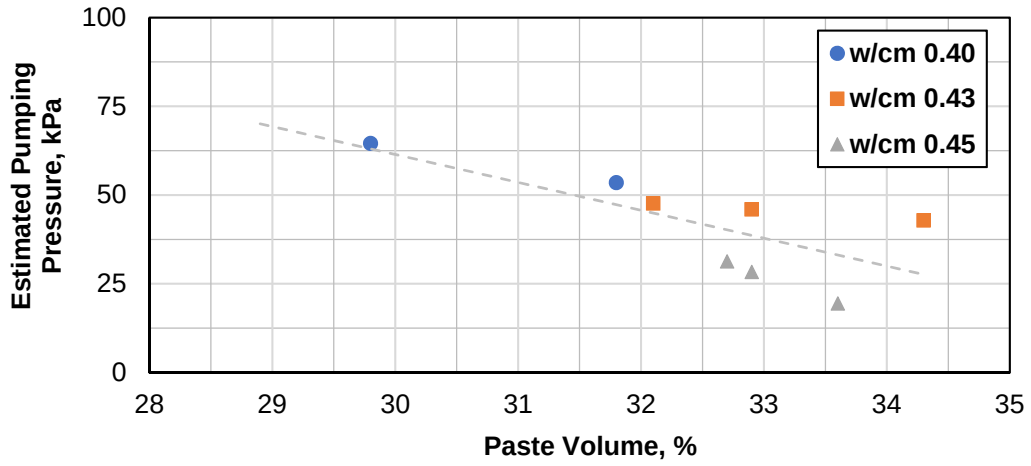

Figure 4.31 – Estimated pumping pressure vs paste volume, Q=50 m³/h

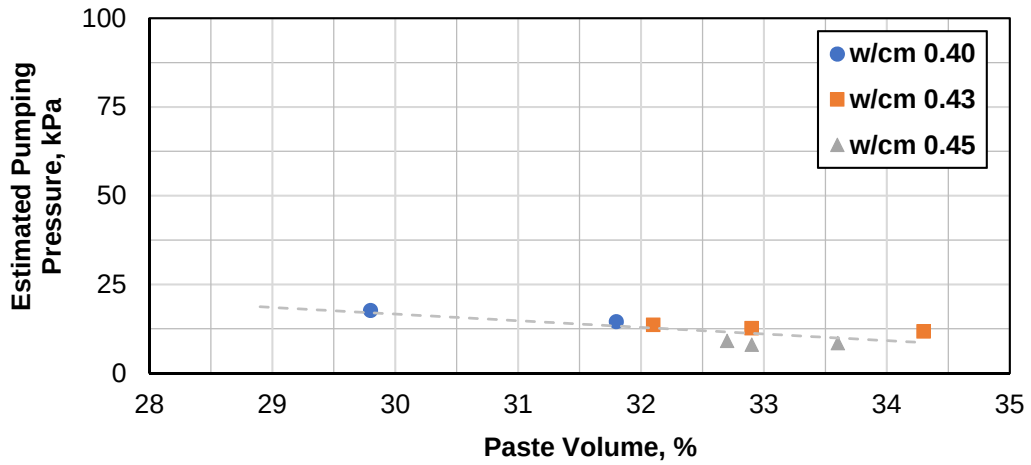

Figure 4.32 – Estimated pumping pressure vs paste volume, Q=12.5 m³/h

Similar to the effect of air void content, mixtures with higher w/cm showed more pronounced pressure drop when comparing values obtained for 50 m³/h and 12.5 m³/h flow rates. For the slower flow rate, mixtures with w/cm of 0.43 and 0.45 showed very similar pumping pressures.

The results show that even a relatively small increase in paste content can provide a significant reduction of pumping pressure, and can subsequently improve pumpability of the mixture. For comparison, when a 25% fly ash replacement rate (while keeping the total cementitious content at the 540 lbs/yd³ level) was used, the estimated pressure was reduced 18%, 34% and 64% for mixtures with 0.40, 0.43, 0.45 w/cm, respectively, for the flow rate of 50 m³/h. Similarly, for the flow rate of 12.5 m³/h, a pressure drop of 18%, 33% and 47% was estimated for mixtures with 0.40, 0.43, 0.45 w/cm, respectively. Results of pressure modeling for mixtures with fly ash are shown in Figure 4.33. These results show that when the decision is to be made regarding a mixture modification to optimize pumpability, the effectiveness of such modification is not universal and needs to be evaluated for every considered option. For instance, results presented in this study show that increasing cement content from 540 lbs/yd³ to 560 lbs/yd³ for a

mixture with 0.40 w/cm can result in 38% reduction in the pumping pressure while replacing 25% of portland cement with fly ash would decrease the pumping pressure by 18%, hence cement increase would be more effective. However, the same mixture modification for the 0.45 w/cm would yield 22% and 64% pressure reduction for cement increase and fly ash replacement, respectively. Therefore, for this particular mixture, fly ash replacement would be preferential measure for pumping pressure reduction.

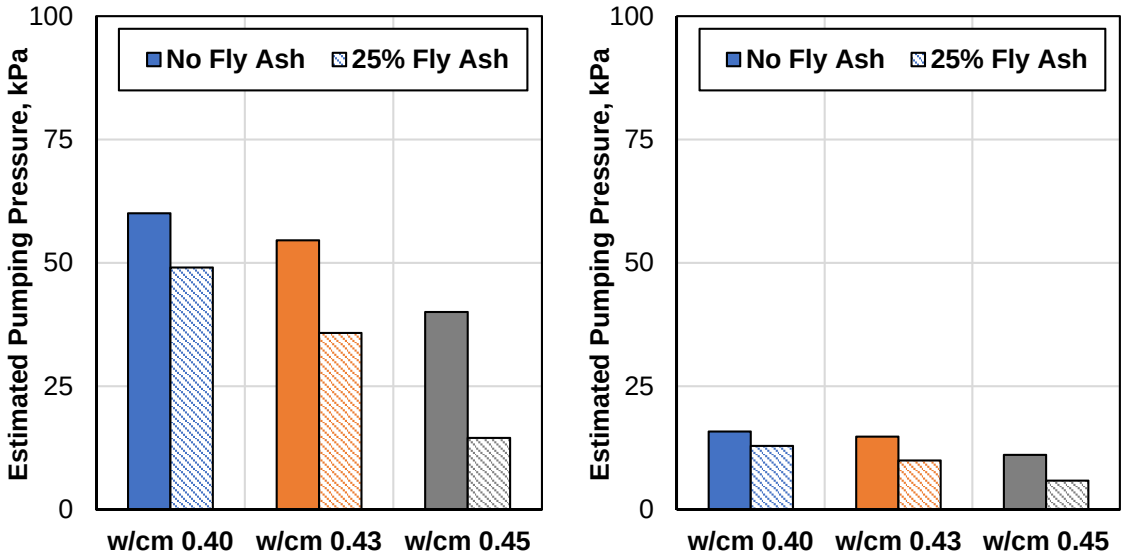

Figure 4.33 – Estimated pumping pressure vs 25% fly ash replacement rate: a) Q=50 m³/h, b) Q= 12.5 m³/h

4.4.3.3 Water Content

When w/cm was increased by 0.01, on average, the achieved decrease in estimated pumping pressure was 8%, for flow rates of 50 m³/h and 12.5 m³/h, as shown in Figure 4.34 and Figure 4.35, respectively. Therefore, water increase appears to be also an effective measure to reduce pumping pressures. However, increasing water content might cause worsening mixture performance in other key aspects, such as strength, volumetric stability or long-term durability. Additionally, if water content is increased significantly, static or dynamic segregation might

occur during the pumping operation, effectively negating any positive effect that water increase might have had on pumping pressure. Therefore, it is always important to consider other performance characteristics of a concrete mixture before increasing water content to optimize its pumpability.

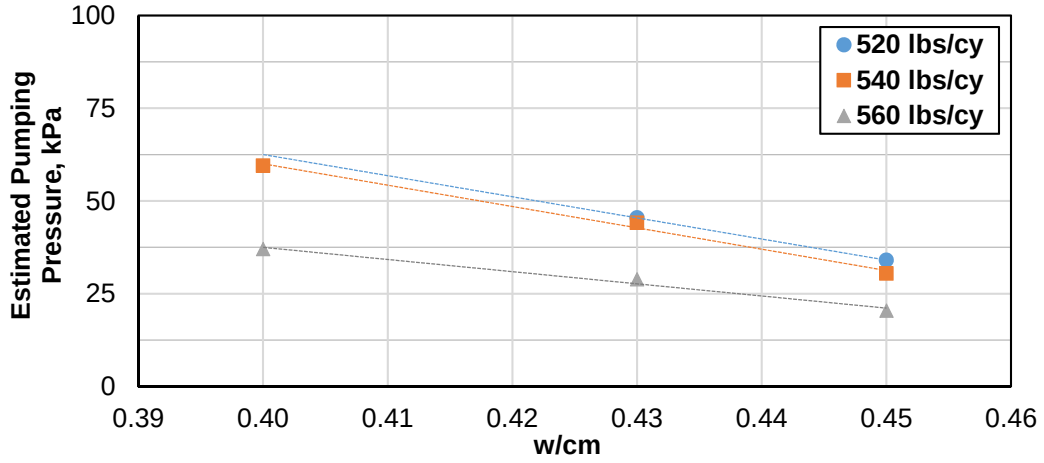

Figure 4.34 – Estimated pumping pressure vs water content, Q=50 m³/h

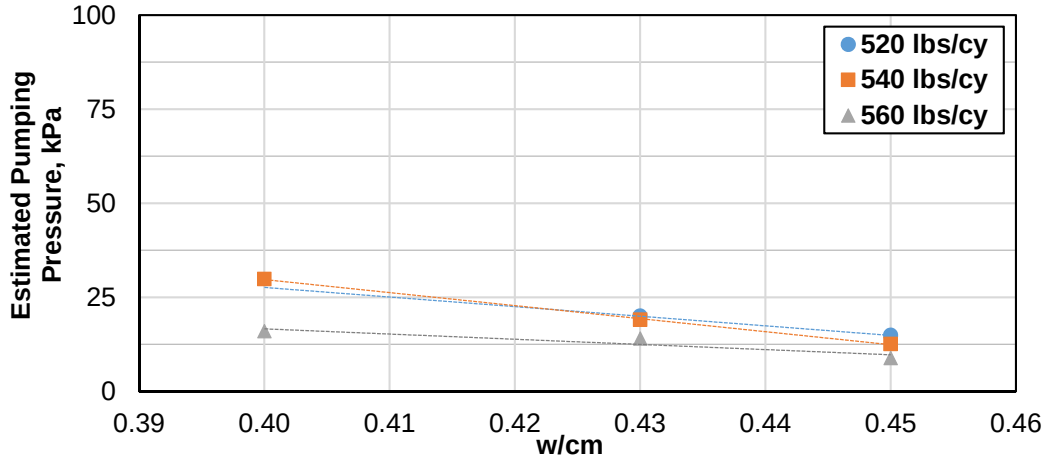

Figure 4.35 – Estimated pumping pressure vs water content, Q=12.5 m³/h

4.4.3.4 Fine-to-Corse Aggregate Ratio, Aggregate Shape

The effect of the FA/CA ratio on estimate pumping pressure is presented in Figure 4.36 and Figure 4.37. For the considered series of mixtures (w/cm 0.43 and 0.45) and the two flow

rates, the minimum pumping pressure occurred at the same FA/CA value of 0.50. For both flow rates, an average pressure increase of 16% and 24% was calculated when the FA/CA ratio changed to 0.4 or 0.6, respectively. Additionally, pumping of concrete at the slower flow rate of 12.5 m³/h would result in reduction of required pumping pressure by 72% when compared to the faster flow rate of 50 m³/h.

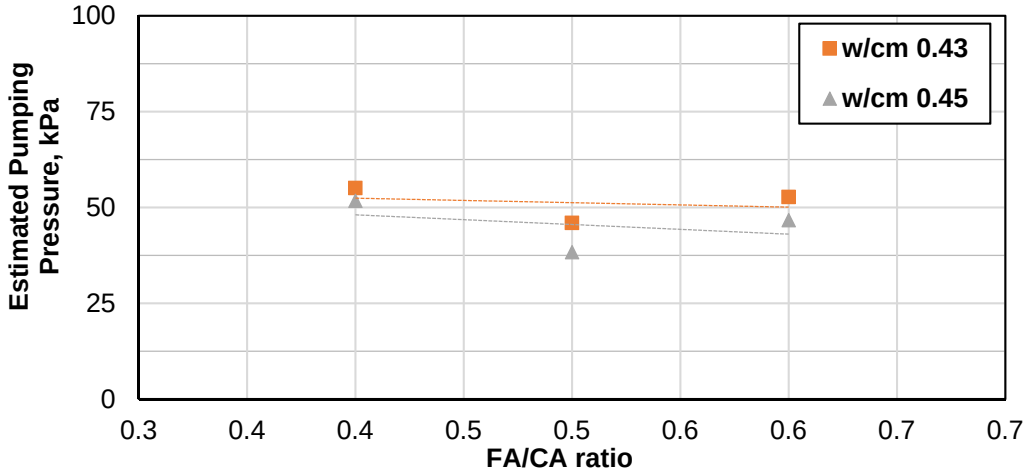

Figure 4.36 – Estimated pumping pressure vs FA/CA ratio, Q=50 m³/h

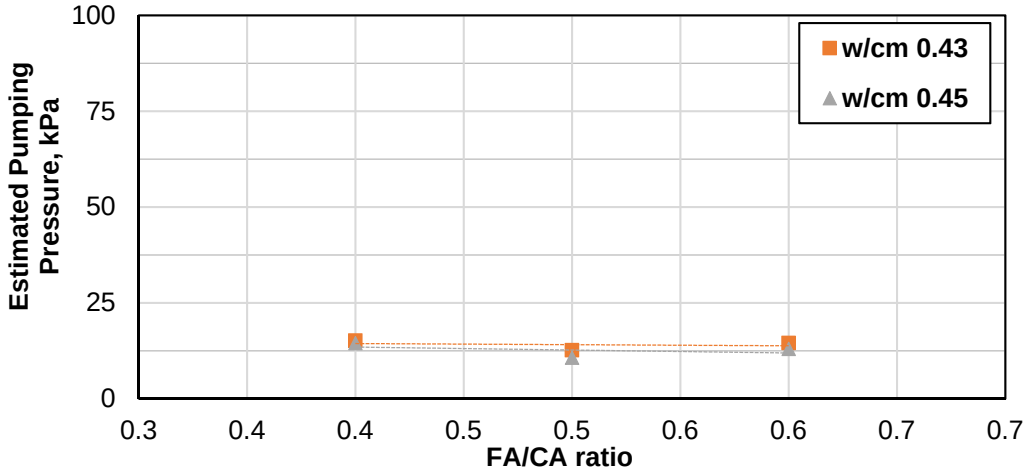

Figure 4.37 – Estimated pumping pressure vs FA/CA ratio, Q=12.5 m³/h

Presented results demonstrate that the effectiveness of mixture modification to optimize pumping performance is dependent on mixture proportions and that both concrete rheological

properties and rheological properties of the lubrication layer must be considered when such modifications are evaluated.

The importance of concrete rheology is clearly shown by results obtained for the series of mixtures with crushed and rounded aggregates, as illustrated in Figure 4.38. Despite the fact that both viscous constant and interface yield stress increased when crushed aggregate was replaced by rounded particles, for the flow rate of 0.50 m^3/h the estimated pumping pressure was reduced by 25% for the mixture with w/cm of 0.45. In this case, the concrete in the pipeline was determined to be sheared as the yield stress of the mixture was relatively low, and the increase in nominal values of rheological properties of the lubrication layer was overcome by significant reduction in both yield stress and plastic viscosity. For the other two w/cm ratios in this mixture series, the pumping pressure was calculated to increase by 13% and 4% for w/cm of 0.40 and 0.43, respectively. For the slow flow rate of 12.5 m^3/h, pressure increase was estimated for all cases when rounded aggregate was replaced by crushed aggregated particles, even in the case of the mixture with w/cm of 0.45 when shear flow was considered. In this scenario, the reduction in plastic viscosity and yield stress did not have such significant effect on pressure development due to the slow pumping rate, and rheological properties of the lubrication layer governed the pressure development. The estimated increase in pressure for the flow rate of 12.5 m^3/h was 16%, 11% and 28% for mixtures with w/cm of 0.40, 0.43 and 0.45.

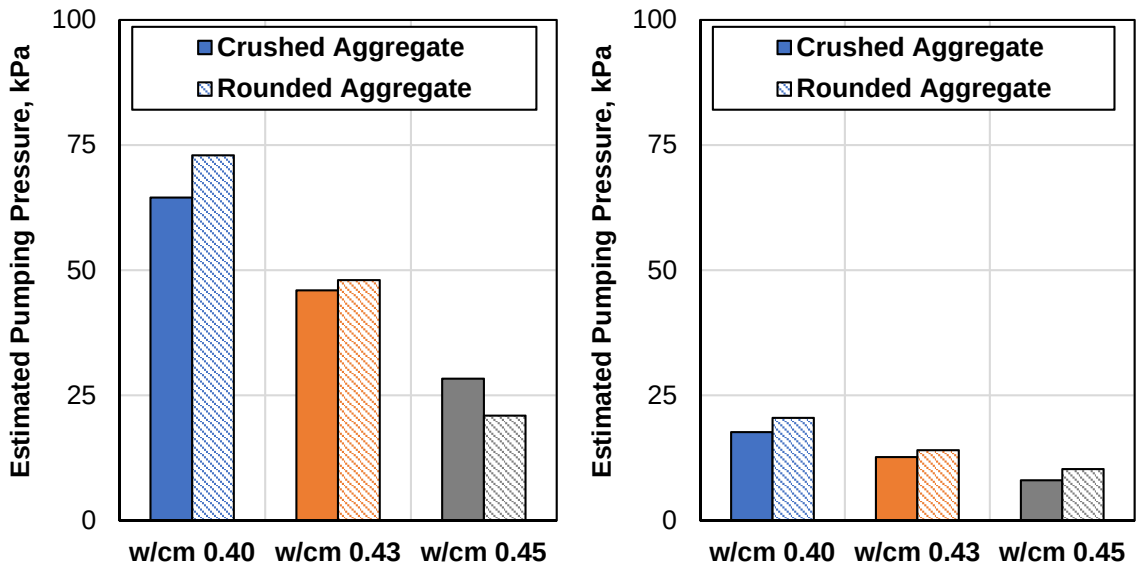

Figure 4.38 – Estimated pumping pressure vs aggregate shape: a) Q=50 m³/h, b) Q= 12.5 m³/h

4.4.3.5 Viscosity-Modifying Admixture

The effect of use of VMA on estimated pumping pressure is show in Figure 4.39. It is apparent that the influence of VMA on pumping pressure corresponded with effects of this admixture on viscosity-based parameters (i.e. plastic viscosity and viscous constant) of bulk concrete and the lubrication layer. For mixtures with w/cm of 0.40, an increase in pumping pressure was estimated for both flow rates, and a greater increase magnitude was observed for the higher flow rate value of 50 m³/m. This behavior closely followed the behavior of viscous constant as this property significantly increased for this series of mixtures. For concrete mixtures with w/cm of 0.43, a decrease in pumping pressure was calculated for both flow rates, and for the mixture with w/cm of 0.45, a decrease in pumping pressure after VMA addition was recorded for the flow rate of 50 m³/h, and essentially no change was shown for the flow rate of 12.5 m³/h. The calculated decrease in pumping pressure for the high pumping rate and w/cm of 0.50 can be once again contributed to the shear flow regime in the pipeline. Therefore, in addition to the fact that

both rheological properties of the lubrication layer and bulk concrete behave differently after using VMA for various w/cm ratios, it is apparent that estimated pumping pressure and the way it is influenced by the use of VMA is not only dependent on particular mixture proportions but also utilized pumping rate.

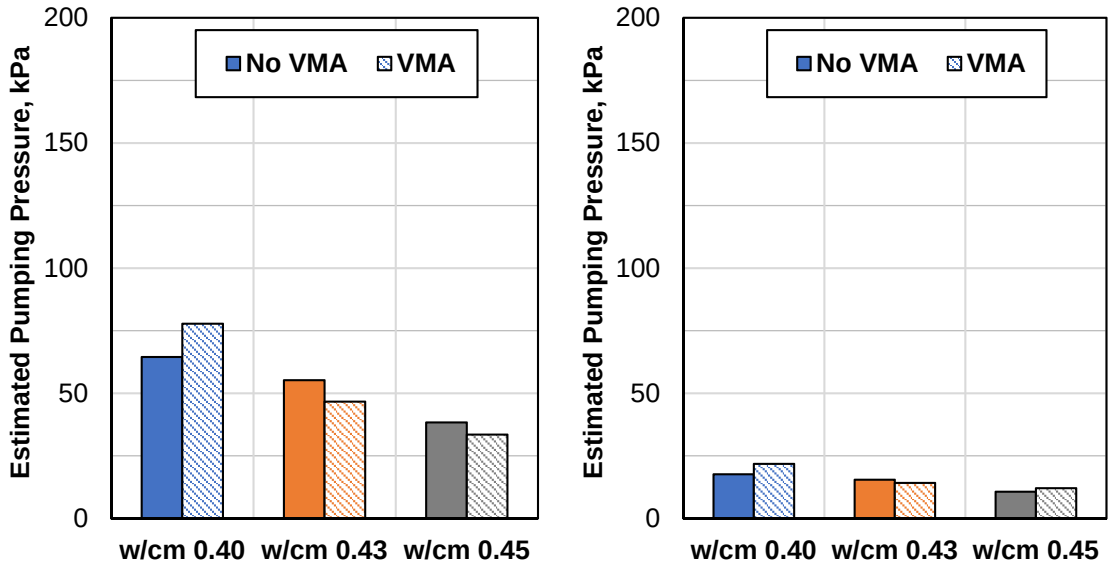

Figure 4.39 – Estimated pumping pressure vs use of VMA: a) Q=50 m³/h, b) Q= 12.5 m³/h

4.4.3.6 Clay Particles

Results of pumping pressure calculation for mixtures with added nanoclay particles are shown in Figure 4.40. Similarly to VMA, the required pumping pressure corresponded well to observed changes in rheological properties of bulk concrete and lubrication layer. The results showed that for the faster flow rate of 50 m³/h, almost no change in pumping pressure due to the clay particles was observed for concrete mixtures with w/cm of 0.40 and 0.43, and an increase was estimated for the mixture with 0.45 w/cm. The different trend for the 0.45 w/cm mixture is

caused by the shear flow regime that was expected for this mixture. However, for the slow pumping rate, a minimal change was estimated for all mixtures.

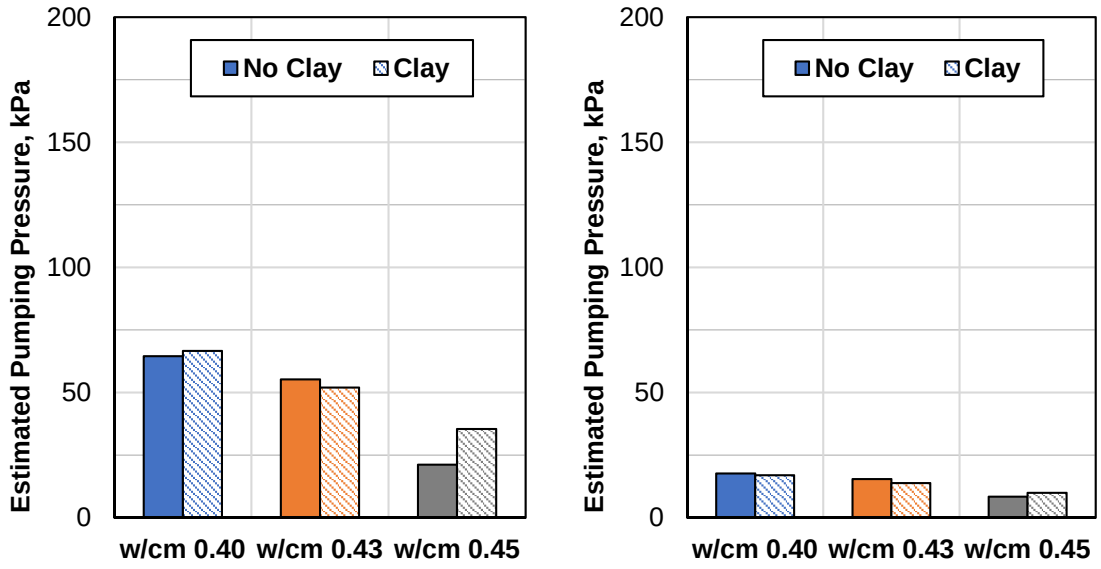

Figure 4.40 – Estimated pumping pressure vs use of clay particles: a) Q=50 m³/h, b) Q= 12.5 m³/h

4.5 Conclusions

In this chapter, the influence of mixture proportions on rheological properties of the lubrication layer (i.e. viscous constant and interface yield stress) was discussed. Additionally, an analysis reflecting all considered mixture modifications using Kaplan's pumping model was carried out to evaluate effects of concrete adjustments on estimated pumping pressure. The following conclusions are drawn:

- Interface rheometer originally designed to be used primarily for SCC mixtures can be successfully employed for lubrication layer characterization of conventional concrete mixtures.

- A strong influence of air void content on rheological properties as well as properties of the lubrication layer was observed. Since air void content of concrete mixtures is not constant in the field, and typically varies within the specified range for different concrete loads, it is important to consider the effect of this variation when one attempts to measure rheological properties of concrete mixtures, and especially when results are used for further analysis or modeling.
- In general, trends observed in rheological properties of the lubrication layer due to modifications of mixture proportions corresponded to changes that occurred in rheological properties of the whole mixture. This was true for all investigated mixture parameters (i.e. air void content, cement content, use of fly ash, water content, FA/CA ratio, use of VMA, and use of clay particles) except coarse aggregate shape.
- The overall magnitude of change in viscous constant and interface yield stress did not always correspond to the magnitude of change in the respective concrete rheological properties, i.e. plastic viscosity and yield stress. Presented results suggested that the rheological properties of the lubrication layer are not only influenced by the rheological changes of cement paste but also by the overall ability of the system to form the lubrication layer. It appears that changes in concrete constituents can result in changes in composition of the lubrication layer and its thickness. However, further research that would investigate true composition of the lubrication layer as well as an accurate technique for measuring lubrication layer thickness is needed.
- Measured rheological properties of the lubrication layer and concrete rheological properties can be utilized in pumping models to predict and evaluate adjustments in mixture proportions and their effect on concrete pumpability. In this work, Kaplan's pumping model was used to

evaluate various mixture modifications. It was found that changes in predicted pumping pressures ranging from 5% up to 65% can be achieved by adjusting one individual parameter of concrete mixture.

- It is not recommended to rely on increasing the air void content of fresh concrete to reduce the pumping pressure since the behavior of the air void system under pressure is not well understood. Therefore, it is not entirely clear as to what is the real effect of the air content on rheological properties of concrete during the pumping operation.

Chapter 5 - Full-Scale Pumping Experiment

5.1 Introduction

Concrete pumping has been studied extensively in the last two decades with the primary goals of determining the effect of pumping on concrete properties and understanding the factors that influence pumpability of concrete mixtures. To this extent, numerous testing campaigns implementing laboratory-based pumping circuits were carry out to allow researchers to control some of the variables associated with the concrete pumping process [13], [52], [65], [70]. Additionally, pumping trials are very often utilized as a tool to verify the pumpability of concrete mixtures, especially for larger projects when the costs associated with setting up these trials are outweighed by benefits of problem-free pumping, such as in the case of high-rise construction [123], [124].

Most of the research pumping trials that were carried out to-date included a horizontally-positioned pumping circuit with either 4 or 5 in.-diameter pipes (100 or 125 mm), some type of pressure monitoring system either based on direct measurements using pressure sensors or indirect pressure evaluation using strain gauges, flowmeters or other measures to assess concrete flow, and industry-grade concrete pump. The biggest challenge of these research pump trials is typically the magnitude of the operation. First, large volumes of concrete are needed for these experiments. This typically requires ready-mixed concrete to be used. Second, significant amount of labor force is needed to perform all tests associated with evaluating concrete during the fresh state, maintaining and servicing the instrumentation, and fabricating concrete specimens for further testing. Lastly, the cost associated with using a concrete pump with trained and certified personnel required to operate the machine is relatively high ($1,000 – $2,000 per day). Hence, only a very limited number of these trials are currently described in the literature.

This chapter describes a full-scale, controlled pumping experiment that was conducted. As opposed to setting up a trial pumping circuit, a concrete pump with a standard boom was used in this experimental work. The pumpline was instrumented with a pressure monitoring system at various locations along the pump boom. The primary goal of this testing was to collect more detailed data on concrete pumping performance in a controlled environment while utilizing standard pump configurations used on construction projects all over the world. Three mixtures designs, two concrete pump boom arrangements, and various concrete flow rates were investigated in this experiment.

5.2 Experimental Methods

5.2.1 Controlled Full-Scale Pumping Experiments

The full-scale pumping experiment was designed to effectively control some of the variables present during the pumping process, such as concrete flow rate, boom configuration, consistent sampling methods (sampling of in-place concrete as opposed to sampling concrete directly pumped in a bucket or a wheelbarrow, which is frequently done on construction sites), etc. Additionally, several sections of the pumping circuit were instrumented with strain gauges and calibrated for pressure to record real-time pumping pressures.

5.2.1.1 Pump and Concrete Sampling

Due to the limited volume of concrete that was available for this experiment, arrangements were made to pump as little concrete as needed for representative sampling. A Schwing 2023-5 S46 SX concrete pump with a 5 in.-diameter pipe (127-mm) was used. The total pipeline length was 151 ft (46 m), and the pump had approximately 79 in.-long (2000 mm-long) pistons with a diameter of approximately 9 in. (230 mm). Therefore, at least 1 yd^3 (760 liters) of concrete was always pumped before sampling, ensuring that the concrete resting in the pumping

line was completely replaced by new concrete pumped at particular target conditions (combination of the boom configuration and flow rate). The end of the pumping line was equipped with a standard rubber hose. Concrete was always discharged directly onto the ground.

Concrete samples were collected before and after pumping. Fresh mixture samples "before pumping" were sampled directly from the truck chute, and samples "after pumping" were obtained immediately after concrete was discharged from the pumpline.

Concrete was delivered from the adjacent ready-mix plant in three trucks. The total volume of concrete delivered for was 8, 4, and 8 cubic yards, respectively. For the first set of trials, sampling was done before the first pumping cycle, after three pumping cycles, and after the last pumping cycle. For the rest of the experiment, concrete was sampled before the first pumping cycle and after the last cycle. The pump was fully folded and cleaned with water after each truck was emptied in order to prevent mixing concretes with different properties in the pump system.

5.2.1.2 Flow Rate Measurements

The flow rate of concrete through the pipeline was estimated by recording the time required for at least five strokes of the pump. Knowing the volume of the pistons, this approach can be used to calculate the theoretical volume of concrete that was discharged with each stroke of the pump, and therefore to estimate the concrete's flow rate. This method of flow rate estimation might be slightly inaccurate, primarily for two reasons: (1) pump pistons are not always completely filled with fresh concrete, and (2) the discharge rate is not constant during the stroke of the piston [65]. However, this approach was deemed sufficiently accurate for the purpose of this work.

Concrete flow rate was determined by measuring time required for five strokes of the pump. Using the volume of each piston, the actual flow rate was computed according to Eq. 5-1:

$$Q = \frac{0.25\pi D_p^2 L_p}{5t} \quad \text{Eq. 5-1}$$

where Q is flow rate, D_p is piston diameter, L_p is length of the piston, and t is time required for five stokes of the pump.

5.2.1.3 Boom Configuration

For each pumping cycle, the boom configuration was registered. In general, two configurations were employed during this experiment: (1) "A" configuration with the boom divided into two approximately equal nearly vertical sections, and (2) "flat" configuration with the boom fully extended in the horizontal direction, as shown in Figure 5.1. These two configurations represent frequently used arrangements of concrete pumps on job sites, the "A" configuration being a situation when the pump and the point of placement are not in the same vertical levels (pump below/above a bridge deck, mat foundation placements, etc.), or when the pump is close to the location where the concrete needs to be placed; and the "flat" configuration representing situation when both the pump an the placement are at the same elevation height, but a relative distance away.

a) b)

Figure 5.1 – Boom configuration during the pumping experiment: a) "A", b) "flat"

5.2.1.4 Pressure Monitoring

A major goal of this study was to measure pumping pressure during standard concrete pumping operations, as the vast majority of scientific studies examined pumping pressures on horizontal laboratory pumping circuits. In order to monitor pumping pressures in the pipeline during the pumping operation, the pumping circuit was instrumented with strain gauges. Three locations along the pipeline were selected, as shown in Figure 5.2:

(1) at the end of the truck deck pipe – gauge A;

(2) second pipe segment of the boom first section – gauge B; and

(3) first pipe segment of the third boom section – gauge C.

Gauges A, B and C were located 15, 41.25 and 80.5 feet (4.5, 12.5 and 24.5 m) from the pump outlet, respectively.

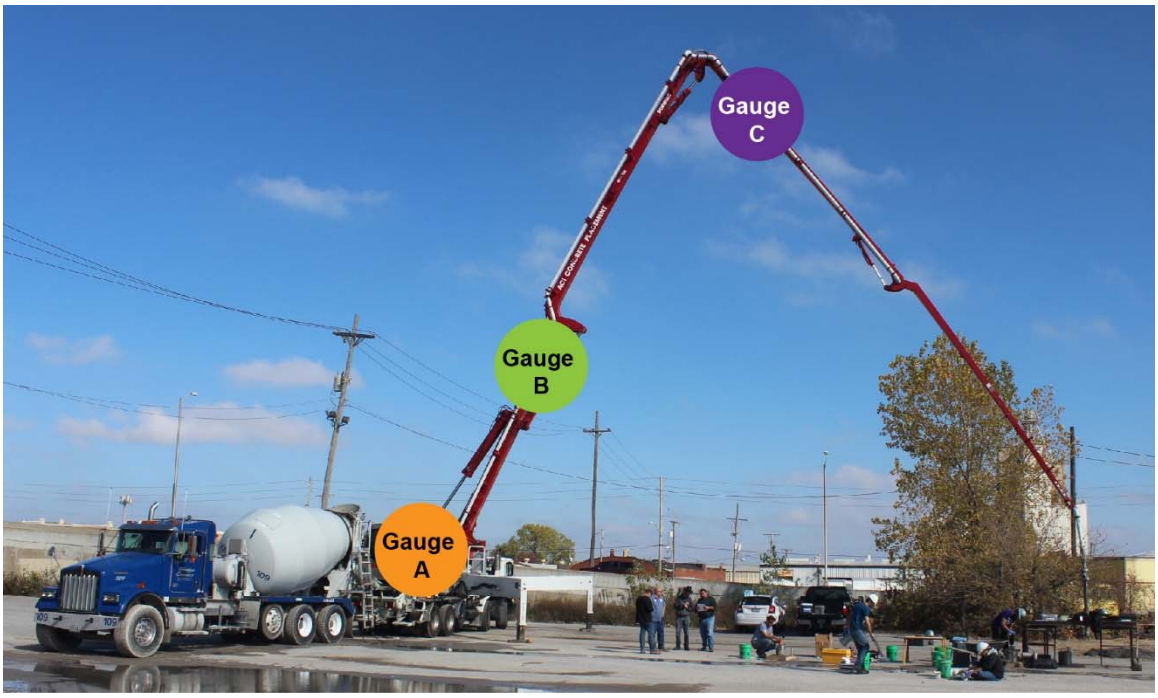

Figure 5.2 – Strain gauge locations

Vishay Micro-Measurements CEA-06-125UW-350 electric resistance strain gauges with gauge resistance of 350 ohms were mounted on the pipe surface perpendicular to longitudinal

axis of the pipe to measure hoop stresses generated by pressure inside the pipe. The M-Bond AE-10 system was used to mount gages on pipes. Gauges were mounted on mechanically and chemically cleaned surface and cured for 12 hours at a curing temperature of 125°F (52°C). Finally, gauges were covered with Micro-Measurements M-Coat W-1 protective coating. An example of a fully mounted and wired strain gauge is shown in Figure 5.3.

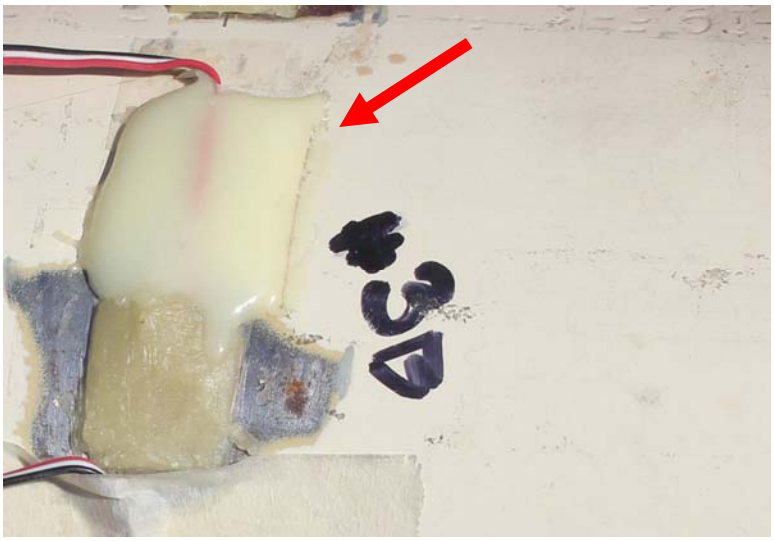

Figure 5.3 – Strain gauge with protective coating

Campbell Scientific CR800 and Accsense VersaLog Model BR data loggers were used to record data provided by strain gauges. A CR800 logger collected readings from gauge A and VersaLog data loggers were used to collect data from gauges B and C. Both devices operated at a sampling rate of 30 Hz (30 readings per second) in order to accurately capture the pressure development during each pump stroke. In order to complete the Wheatstone bridge required to detect voltage changes in strain gauges, Omega BCM-1 bridge completion modules were used. Two Anker Astro E7 batteries were used for each VersaLog data logger to provide an external power source required to achieve the sampling rate of 30 Hz. Figure 5.4 shows the data collection systems used.

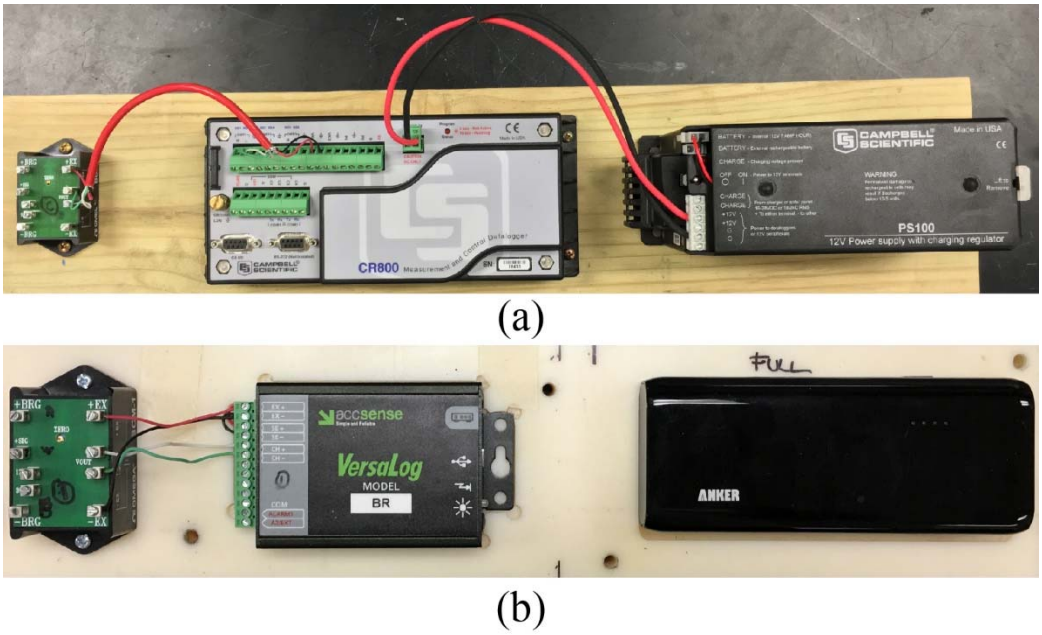

Figure 5.4 – Data acquisition system: a) Campbell Scientific CR800 system, b) VersaLog system with Anker Battery

In addition to strain gauges, two pipes were instrumented with Type T thermocouple wires embedded in high conductive thermal conduction epoxy (Omega 101) to account for temperature-induced strains during the pumping experiment. Temperature was sampled once per minute using an Omega OM-CP-IFC200 data logger. The complete data acquisition system used for gages B and C mounted on a pump pipe is shown in Figure 5.5.

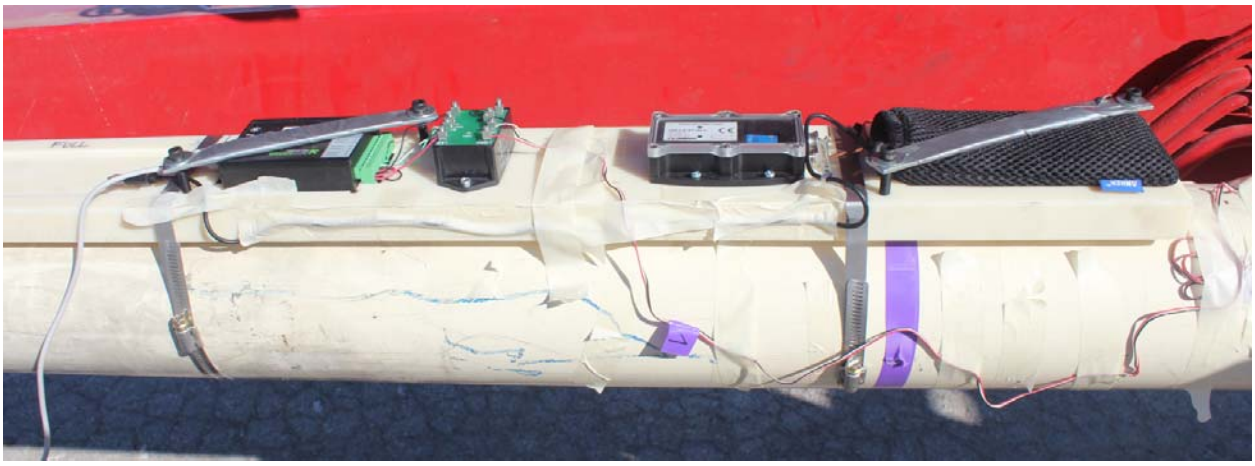

Figure 5.5 – Data acquisition system mounted on a boom pipe

The indirect approach of pressure monitoring utilized in this research study stemmed from reports of unsuccessful or troublesome use of pressure sensors for pumping pressure monitoring, primarily due to the granular nature of concrete that cause issues with a proper seal of the pressure sensor-concrete interface. Therefore, strain gauges were implemented in this research program. In an ideal system, registered values of strain obtained from gauges (in the hoop direction) could be immediately used to calculated pressure inside the pipe using the pressure vessel theory as shown in Eq. 5-2:

$$\epsilon = \frac{PD}{2tE} \qquad \text{Eq. 5-2}$$

Where P is internal pressure in the vessel (pipe), t is wall thickness of the pipe, D is pipe diameter and E is modulus of elasticity of the material. This equation is valid for a thin wall pressure vessel, i.e. a cylinder with wall thickness less than one twentieth of its radius. This equation can be applied for steel pump pipes used in this research program with diameter of 5 in. (127 mm) and wall thickness of .188 in (4.8 mm). However, this equation can become inaccurate if exact geometrical and material properties of the vessel are unknown, and when the registered strain values are imprecise due to misalignment of the strain gauge on the curved surface. Both of these conditions were present in the pumping experiment, therefore, all strain gauges were individually calibrated in a laboratory using known hydraulic pressure imposed by hand pump on the pipe. The calibration setup is shown in Figure 5.6.

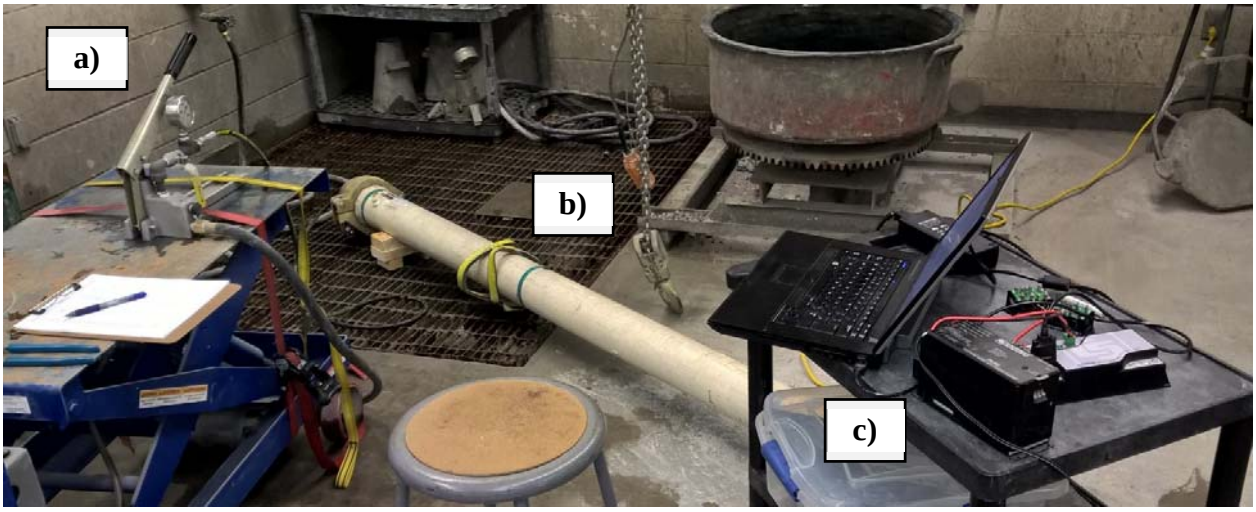

Figure 5.6 – Calibration setup: a) hydraulic pump, b) test pipe, c) data acquisition

The calibration procedure consisted of the following steps:

(1) strain of the gauge was recorded at the atmospheric pressure;

(2) the pipe was filled with water while aligned in a horizontal direction;

(3) pressure of 800 to 1000 psi was applied using a hand-pump and measured strain was recorded;

(4) pressure was released in 100 psi decrements and the corresponding strain for each step was recorded.

Using the measured data, calibration (pressure-strain) curves were obtained for each strain gauge. These relationships were utilized for data analysis of measured strain values obtained from the pumping experiment.

Additionally, pipes were placed in an outdoor environment in order to determine the effect of temperature on measured strains. Pipes were left outdoors in direct sunlight for a 12-hour temperature cycle, resulting in a temperature difference of approximately 30°F.

5.2.2 Concrete Mixtures

Three concrete mixtures developed based on routinely used high-performance concrete (HPC) mixtures for bridge decks in the State of Kansas were implemented in this study. These mixtures have been designed by others to minimize early-age volumetric changes, and subsequently reduce or completely eliminate early-age cracking. However, while these mixtures typically meet the early-age cracking performance requirements, according to Kansas Department of Transportation (KDOT) engineers, workability issues and pumpability problems were previously reported with these mixtures.

5.2.2.1 Concrete Materials

ASTM C150 Type I/II [108] portland cement manufactured by the Ash Grove Cement Company (AGC) plant in Chanute, KS was used in this study. Cement properties obtained from a certified mill test report provided by AGC are shown in Table 4.2.

Table 5.1 – Portland cement properties

Physical Properties		Chemical Properties	
325 Sieve passing, %	94.2	*Oxide Analysis*	
Blaine fineness, cm^2/g	3,660	SiO_2, %	21.33
Time of Setting - initial, hrs:min	2:35	Fe_2O_3, %	2.81
Time of Setting - final, hrs:min	3:55	Al_2O_3, %	4.46
Mortar Air Content, %	6.6	CaO, %	64.34
Autoclave Expansion, %	0.011	MgO, %	1.40
Compressive Strength - 1 day, psi	2,430	SO_3, %	2.76
Compressive Strength - 3 days, psi	4,010	*Calculated Compounds*	
Compressive Strength - 7 days, psi	5,180	C_3S, %	58.0
		C_2S, %	17.4
		C_3A, %	7.1
		C_4AF, %	8.5
		Others	
		Loss on ignition, %	1.37
		Insoluble residue, %	0.24
		Free lime, %	1.14
		Na2O, %	0.19
		K2O, %	0.51
		Equivalent alkalies, %	0.52

ASTM C618 [109] class F fly ash produced by Ash Grove Cement Company originating from the Chanute Power Plant, Chanute, KS, was also used in this study.

Limestone (Martin Marietta, Stamper Mine, Kansas City, MO) conforming to KDOT SCA-3 [125] requirements was used in this testing program. The nominal aggregate size was ¾ in. (19 mm). Siliceous natural sand (Pit #3, Holliday Sand & Gravel, Shawnee, KS) conforming to the requirements of ASTM C33 [126] was used as fine aggregate. The combined coarse and fine aggregate gradation met the KDOT MA-3 requirements for mixed aggregates for concrete. Specific gravity and absorption capacity of coarse aggregate was 2.64 and 1.7% respectively, and 2.62 and 0.3% for fine aggregate, respectively. Gradation curves of coarse and fine aggregate are shown in Figure 5.7 and the combined aggregate gradation is shown in Figure 5.8.

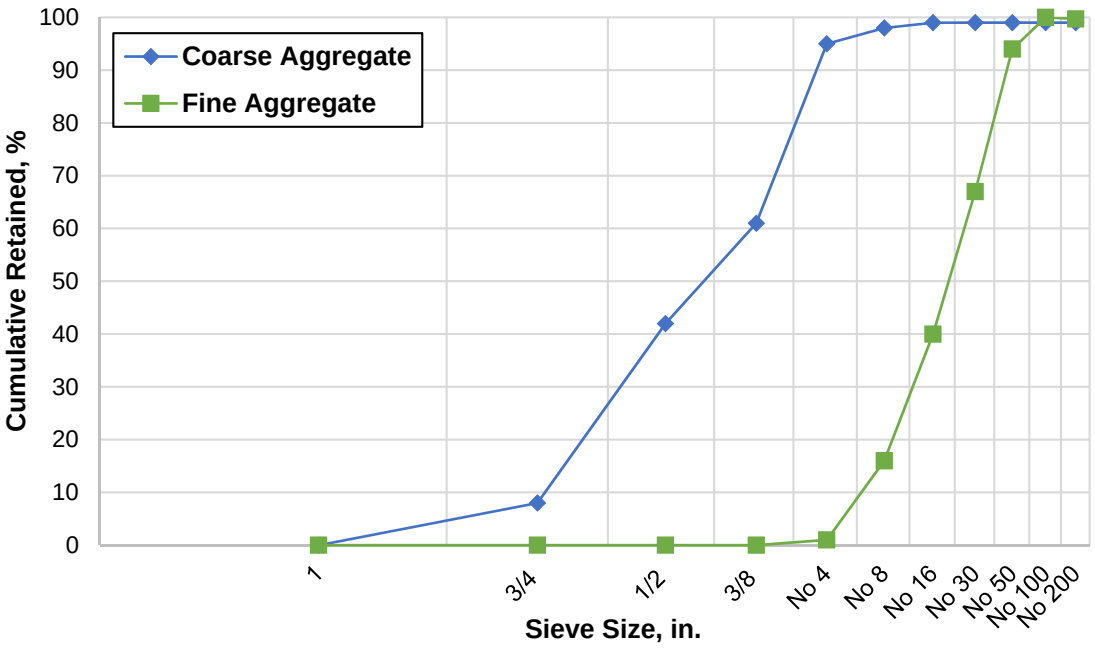

Figure 5.7 – Coarse and fine aggregate gradation

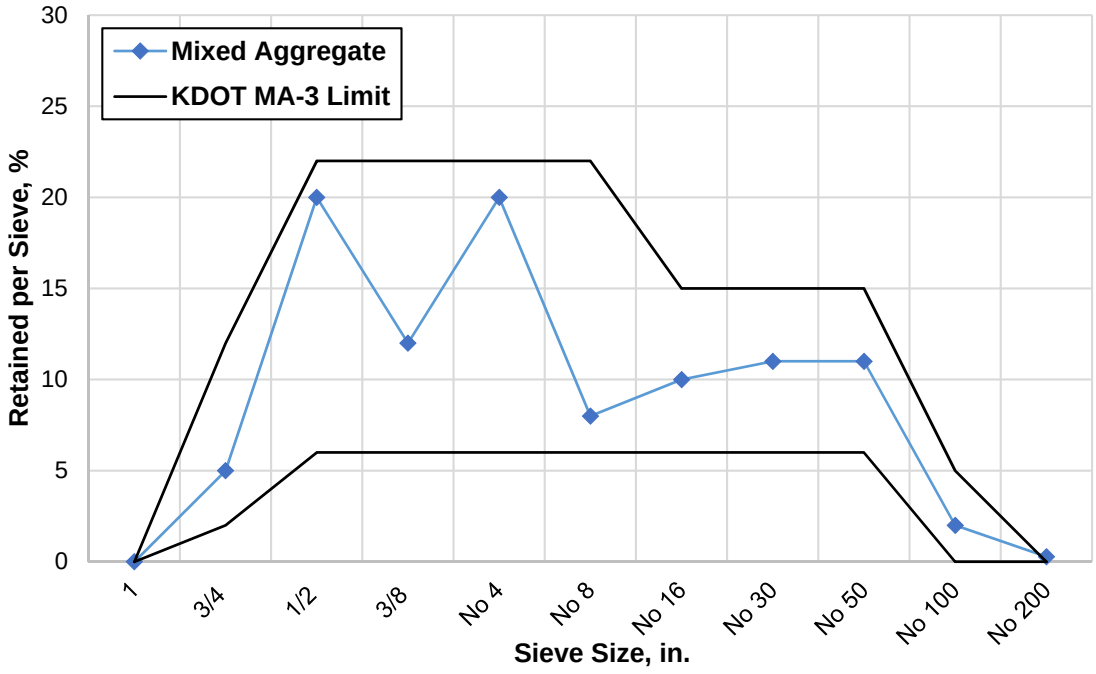

Figure 5.8 – Combined aggregate gradation

5.2.2.2 Mixture Proportions

The total cementitious content of investigated mixtures was 510 lbs/yd³ (303 kg/m³) with a water content of 219 lb/yd^3 (130 kg/m^3), therefore the resultant w/cm was 0.43. Mixtures 1 and 2 contained only portland cement whereas mixture 3 had 20% of cement by mass replaced by class F fly ash. The sand-to-total aggregate ratio was 0.40 for mixtures 1 and 3, and 0.50 for mixture 2; with nominal aggregate size of ¾ in. (19 mm). Air-entraining admixture (ASTM C260 [110], Euclid AEA-92S), high-range water reducing admixture (ASTM C494 [111] Type A & F, Euclid Plastol 6420), and hydration stabilizer (ASTM C494 Type B & D, Euclid Retarder 100) were used to achieve desired fresh concrete properties, i.e. 4 in. slump and 6.5% air content.

Mixture 1 was not initially pumpable; therefore 10.4 lbs/yd³ (6.2 kg/m³) of water was added to the truck, effectively increasing w/cm from 0.43 to 0.45. Mixture proportions are shown in Table 5.2.

Table 5.2 – Mixture proportions

	Mixture 1	Mixture 2	Mixture 3
Materials		*lbs/yd³ (kg/m³)*	
Portland Cement	510 (303)	510 (303)	408 (242)
Fly Ash	--	--	102 (61)
Coarse Aggregate	1886 (1119)	1570 (931)	1875 (1112)
Fine Aggregate	1257 (746)	1570 (931)	1250 (742)
Total Cementitious Content, kg / m³	510 (303)	510 (303)	510 (303)
Sand-to-Total Aggregate Ratio (by mass)	0.40	0.50	0.40
Design Air Content, %	6.5	6.5	6.5
Water	219/229 (130/136)	219 (130)	219 (130)
w/cm	0.43 / 0.45	0.43	0.43
Paste Content (by volume), %	22.6 / 23.2	22.6	23.0
Mortar Content (by volume), %	51.1 / 51.7	58.2	49.0
Admixtures		*fl oz/cwt (ml/m³)*	
Air-Entrainer	4.1 (158)	4.1 (158)	4.1 (158)
High-Range Water Reducer	35.7 (1381)	35.7 (1381)	35.7 (1381)
Hydration Stabilizer	15.3 (592)	15.3 (592)	15.3 (592)

5.2.3 Experimental Methods

5.2.3.1 Concrete in the Plastic State

Fresh concrete samples obtained before and after pumping were tested for slump [113], density [115], and temperature [116]. The plastic air void content was determined using the Super Air Meter device. Along the fresh concrete air void content, the SAM number was determined [127]. Additionally, rheological properties of concrete and properties of the lubrication layer were evaluated before and after pumping using the ICAR Rheometer, and

ICAR-based interface rheometer. Detailed discussion of these test methods is provided in Chapters 3 and 4 of this dissertation.

5.2.3.2 Hardened Concrete

In addition to evaluation of fresh concrete properties before and after pumping, specimens for hardened air void analysis were fabricated. Samples were cast into 29 in^3 (473 ml) paper molds shaped as trapezoidal prisms with dimensions of 2.25 by 3 in. (57 by 76 mm) at the bottom and 3.75 by 3 in. (95 by 76 mm). Upon fabrication, samples were stored on a testing site protected from a direct sunshine and rain.

Hardened air void specimens were analyzed in the laboratory using the flatbed scanner method incorporating image analysis techniques in accordance with ASMT C457 Procedure C [128]. All samples were cut into approximately 1 in.-thick (25 mm) slices, polished using a horizontal polishing table (ASW Diamond SW-1800), equipped with diamond nickel-plated disks (ASW Diamond NT-80, NT-100) and flexible resin processing disks (ASW Diamond PP360, PP600). Following the polishing process, sample surfaces were blackened using a black marker with a chisel tip (Sharpie® Magnum Permanent Marker), and air voids filled with barium sulfate powder to create a false-color image of each specimen. Subsequently, specimens were scanned at a resolution of 6400 dpi using an EPSON Perfection V600 Photo scanner. Finally, scanned images were analyzed utilizing a software tool previously developed by the author of this dissertation that allows for determination of the air void system parameters based on the scanned false-color image [129], [130]. This method of analysis allows for the determination of not only the basic parameters of the air void system as defined in ASTM C457, i.e. total air void content, spacing factor and specific surface, but also enables the user to assess other characteristics of the system such as air void size distribution and spatial arrangements.

5.3 Results and Discussion

5.3.1 Pressure Analysis

5.3.1.1 System Calibration

The strain-pressure relationship obtained for each strain gauge and a particular data acquisition system (each gauge was calibrated using the data acquisition system that would be later utilized during the pumping experiment) is shown in Figure 5.9.

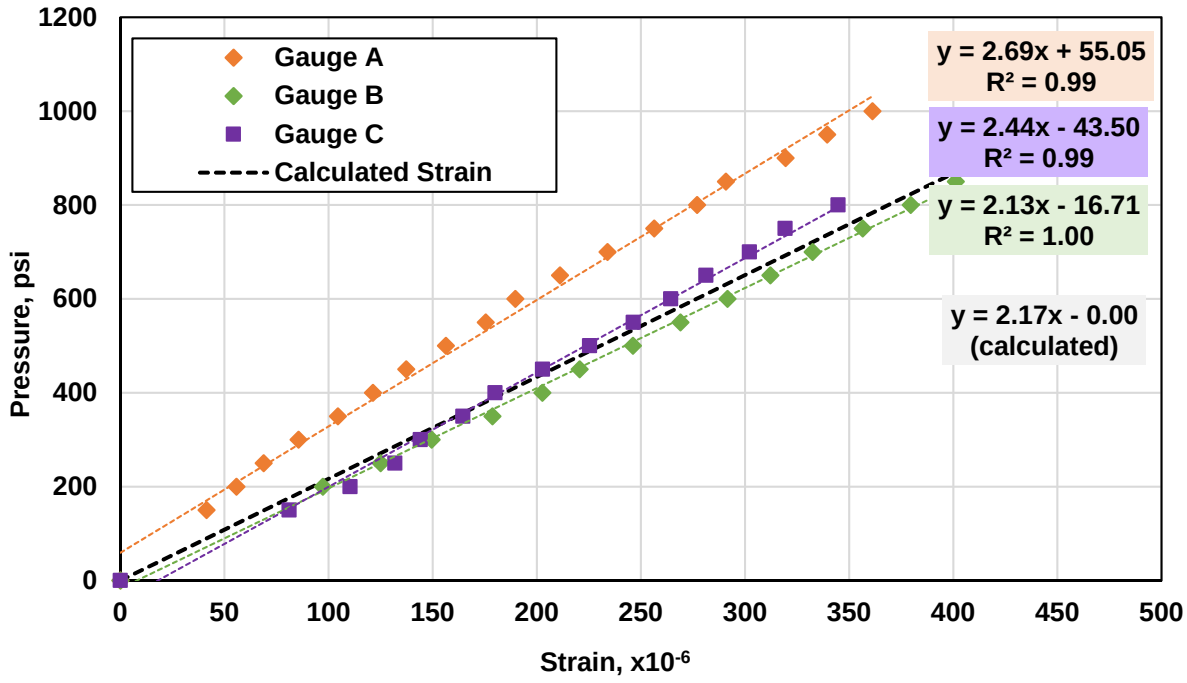

Figure 5.9 – Calibration curves

The calibration data clearly showed that laboratory-based evaluation of the pressure monitoring system was necessary for accurate assessment of pumping pressure. The highest deviation of the calibration curve from the ideal pressure-strain curve based on the hoop stress relationship for pressure vessels was obtained for Gauge A. In this case, the difference was approximately 50% for values of stain close to 100 με, and decreased to approximately 30% difference for values of strain in the 400 με area. For gauges B and C, it appears that the gauge

misalignment was smaller, resulting in deviation from the calculated system curve less than 10% for all strain values.

Additionally, steel pipes were instrumented with thermocouples and exposed to a day-night temperature cycle in order to account for temperature-induced strains during the measurements. However, it was found that the temperature changes created stresses that translated into strains of less than 30 με (with temperature swing of 35°F), therefore, the temperature-induced effects were not considered in further data analysis due to their very low effect on the final data. Moreover, the actual temperature data from the pumping experiment, as shown in Figure 5.10, shown that minimal temperature change was detected in the pipeline during the duration of the experiment, i.e. temperature-induced strains in the pipeline were negligible.

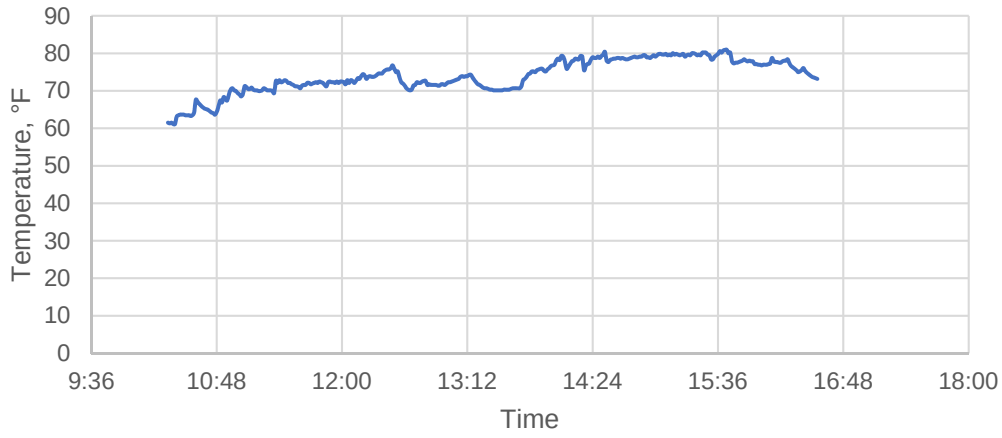

Figure 5.10 – Temperature of the pipe during the experiment

5.3.1.2 Pumping Pressures

The use of strain gauges as an indirect method of pressure monitoring during pumping operations was found to be a viable solution. Upon data reduction, pressure curves for each individual pumping test were produced, as shown Figure 5.11 through Figure 5.21. The time

stamp on the x-axis of these figures is an arbitrary number since data were collected continuously throughout the pumping campaign. Recorded data clearly showed that in most of the cases, properly calibrated strain gauges are capable of capturing pipe pressures during standard pumping operation.

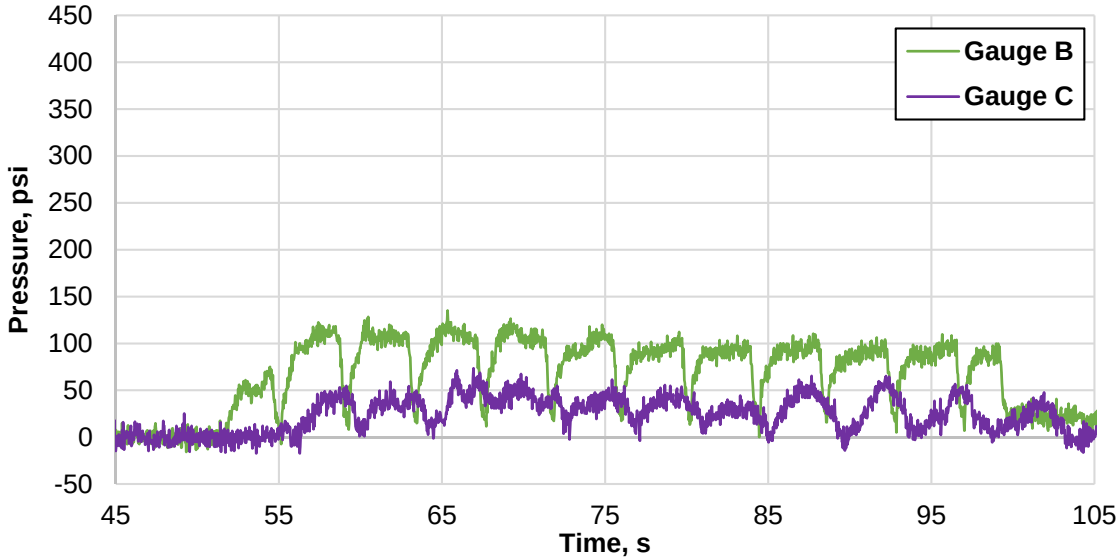

Figure 5.11 – Pumping pressures: Mixture 1, flat boom, Q = 97 yd³/h (21 l/s)

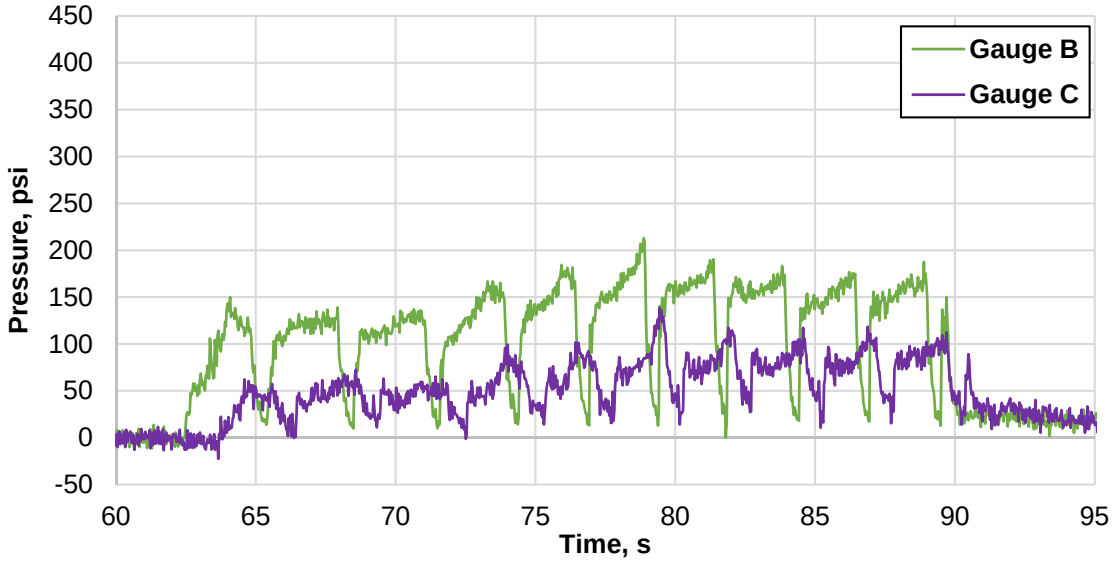

Figure 5.12 – Pumping pressures: Mixture 1, flat boom, Q = 152 yd³/h (32 l/s)

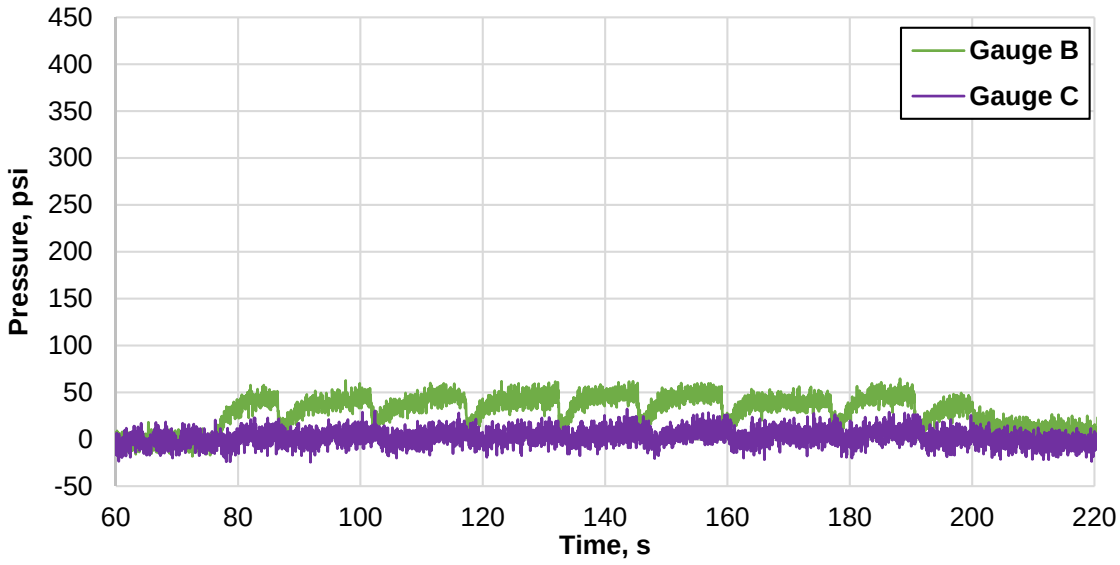

Figure 5.13 – Pumping pressures: Mixture 1, flat boom, Q = 26 yd³/h (6 l/s)

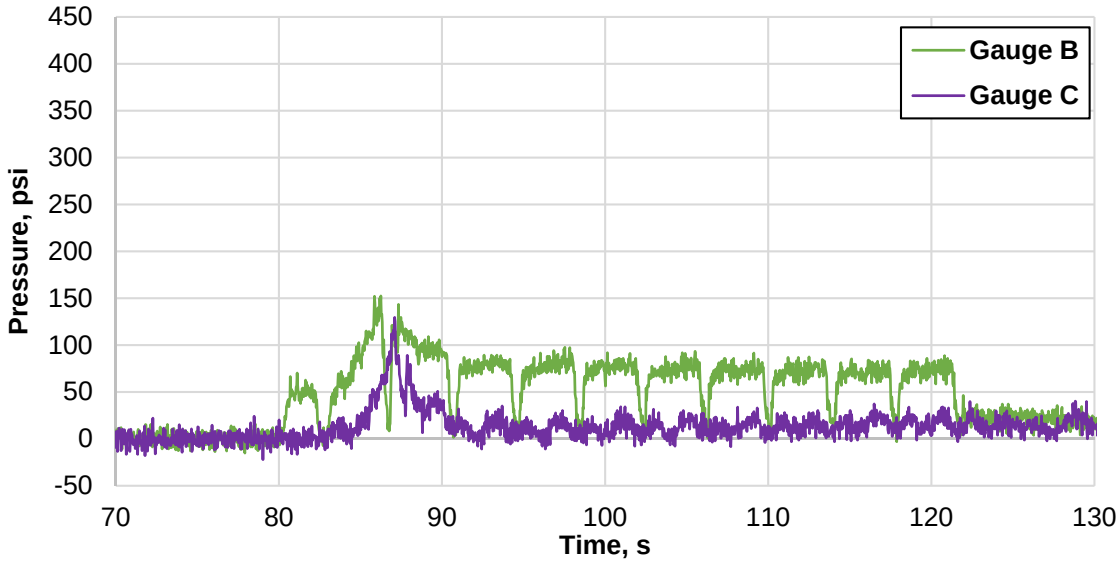

Figure 5.14 – Pumping pressures: Mixture 1, A boom, Q = 126 yd³/h (27 l/s)

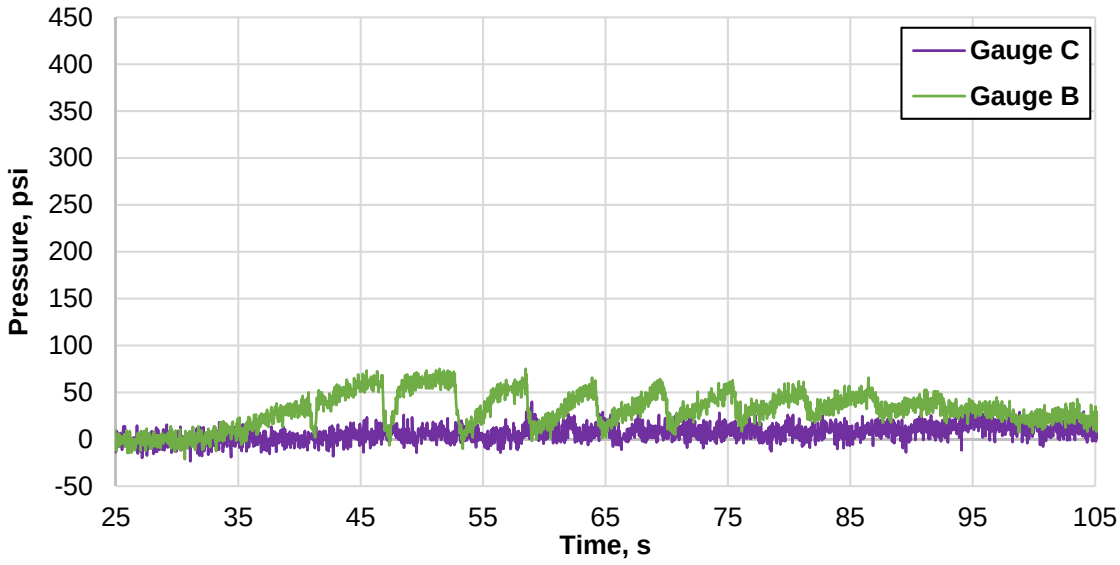

Figure 5.15 – Pumping pressures: Mixture 1, A boom, Q = 24 yd³/h (5 l/s)

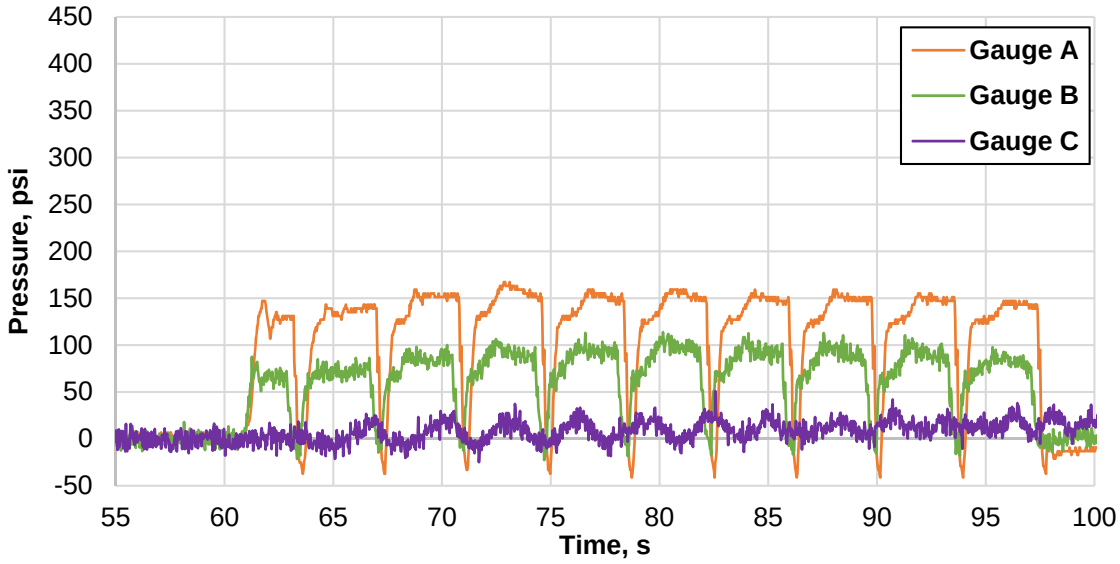

Figure 5.16 – Pumping pressures: Mixture 2, A boom, Q = 104 yd³/h (22 l/s)

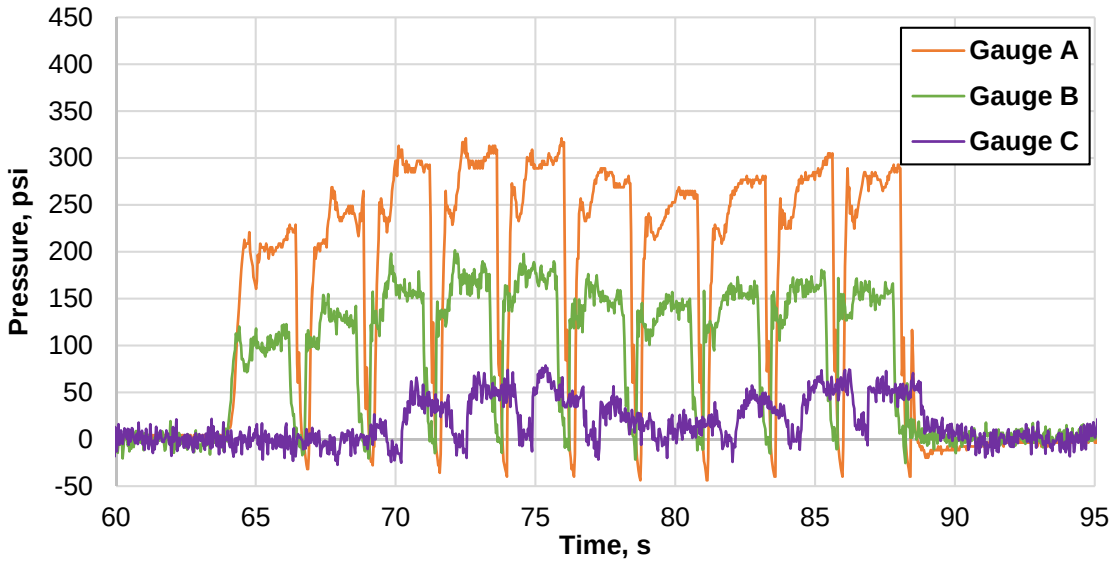

Figure 5.17 – Pumping pressures: Mixture 2, A boom, Q = 166 yd³/h (35 l/s)

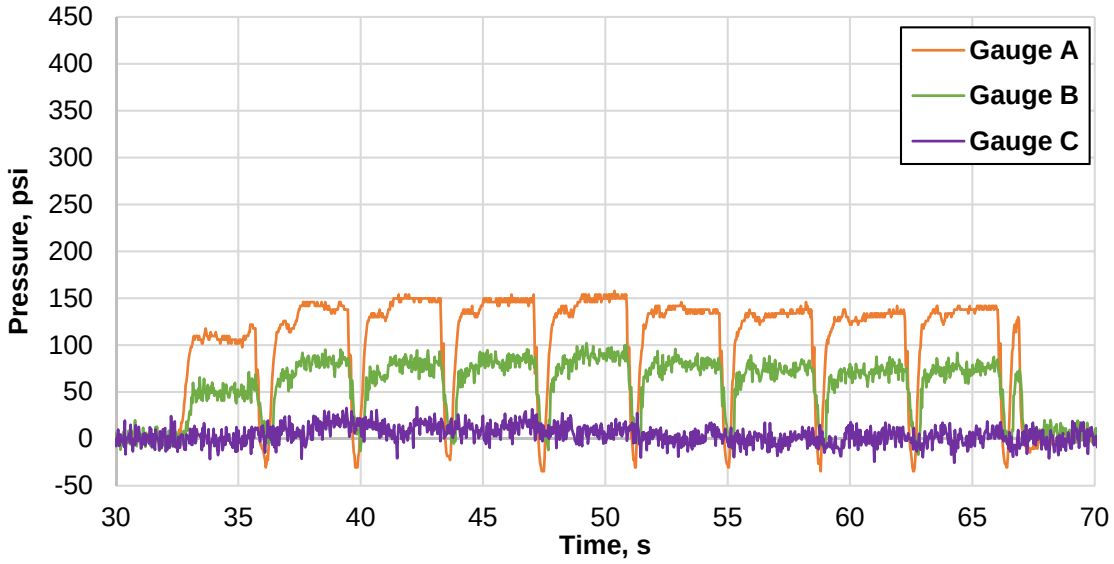

Figure 5.18 – Pumping pressures: Mixture 3, A boom, Q = 102 yd³/h (22 l/s)

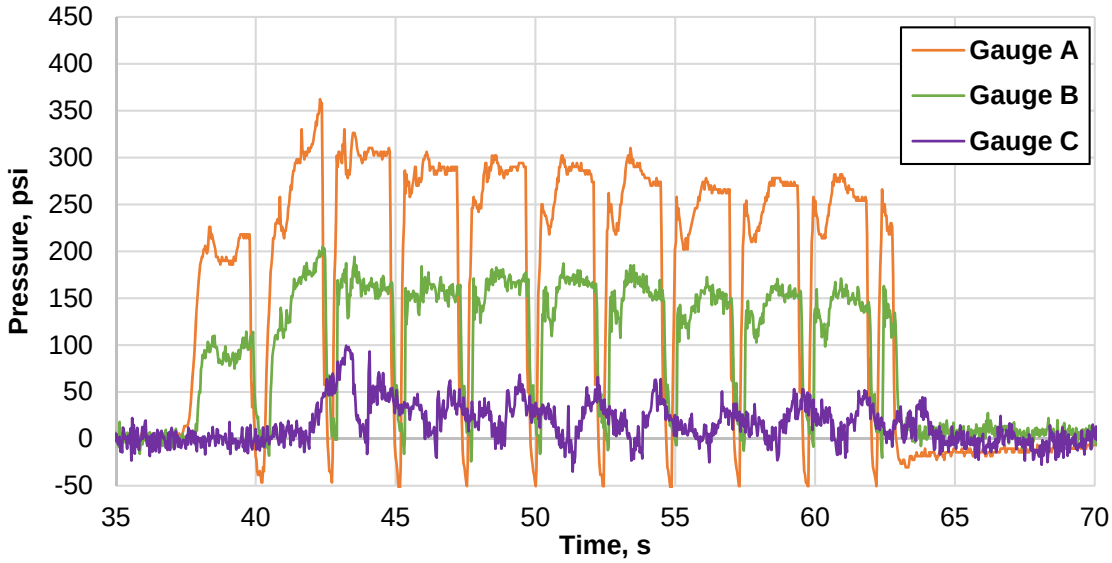

Figure 5.19 – Pumping pressures: Mixture 3, A boom, Q = 166 yd³/h (35 l/s)

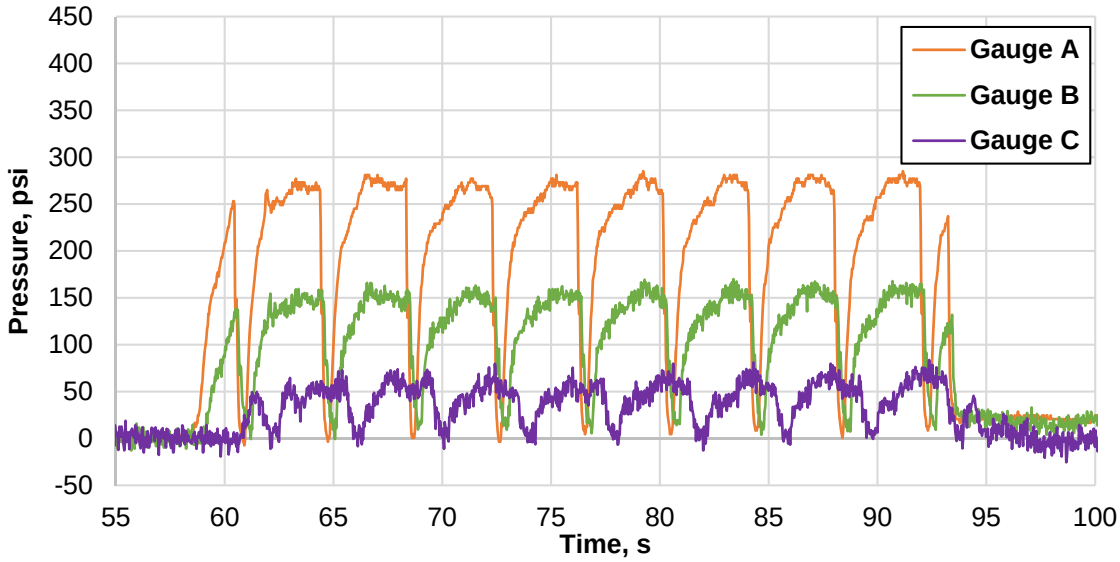

Figure 5.20 – Pumping pressures: Mixture 3, flat boom, Q = 99 yd³/h (21 l/s)

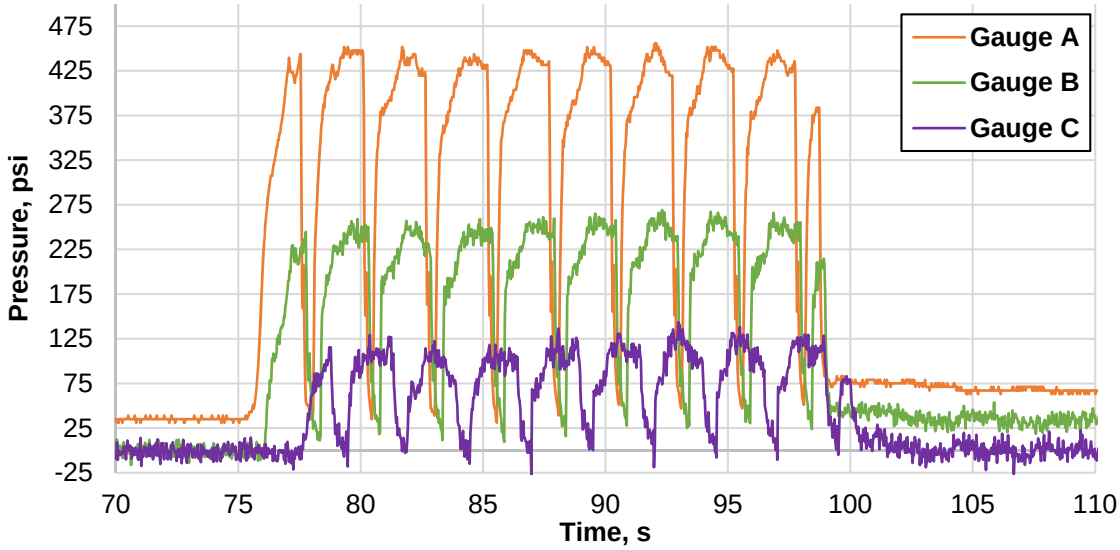

Figure 5.21 – Pumping pressures: Mixture 3, flat boom, Q = 158 yd³/h (34 l/s)

The collected data clearly showed that the pumping operation is not a continuous process with a constant value of pumping pressure throughout the pumping period, but rather a process characterized with distinct pressure pulses corresponding to strokes of pump pistons. The pulse-like shape of the pressure-time curve stems from the fact that two pistons that are working simultaneously are utilized in standard concrete pumps. The gaps between individual pulses are inevitable due to the action of the pump valve that is responsible for controlling concrete feed into the pumpline. Although the pump manufactures are developing valves that act swiftly to reduce the time at which no output from the pump is generated, it is not possible to smooth out the pressure-time curve entirely.

Three rather distinct shapes of individual peaks on the pressure-time curve were recorded, as shown in Figure 5.22, Figure 5.23, and Figure 5.24. The most common case was a curve with clearly defined pressure peaks, ramp up and ramp down segments corresponding to the filling and emptying period of the pump piston, and the action of the pump valve. Each of

these pressure peaks was identified for every pumping experiment by an iterative procedure during which the slope of the ramp up/down section of the pressure pulse was maximized. Therefore, the pressure plateau, highlighted red in Figure 5.22, was identified and further included in the data analysis. This shape of the pressure-time curve was observed for all measurements performed by gauges A and B.

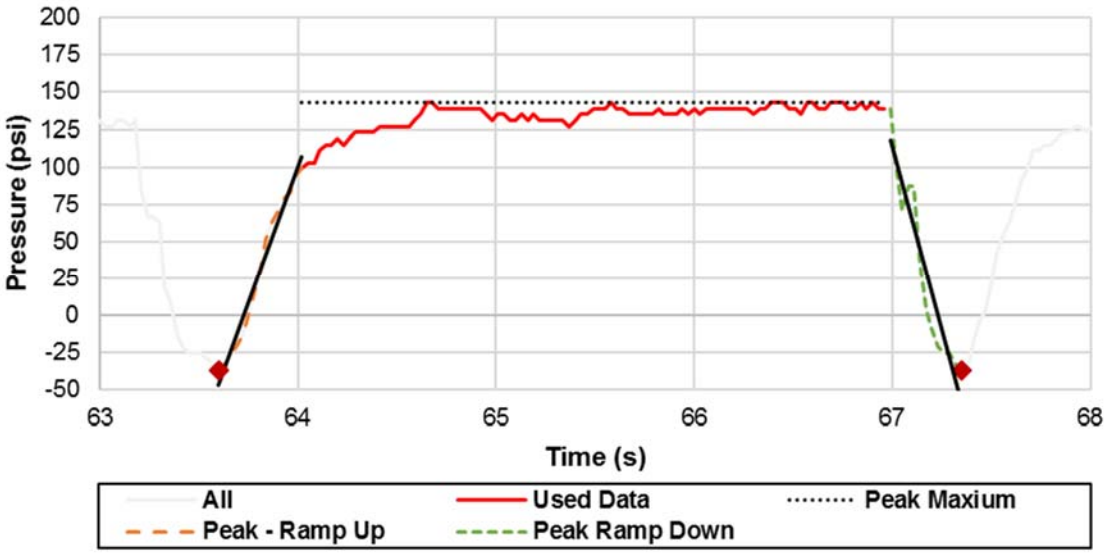

Figure 5.22 – Pumping pressure detail: Mixture 2, A boom, Q = 104 yd³/h (22 l/s), Gauge B

For several instances of measurements done by Gauge C, pressure-time curves shown in Figure 5.23 and Figure 5.24 were recorded. To recall, Gauge C was placed right after the peak elevation of the pumping circuit in the direction of pumping, i.e. it was expected that relatively low pumping pressure would be recorded at this location compared to gauge A and B. The first type of the pressure-time curve that was logged for Gauge C was characterized by distinguishable pressure pulses, however, the pressure plateau that was observed for data obtained from gauges A and B is missing. This is due to the fact that the gauge C was relatively far from the concrete pump, and significant pressure loss occurred before the pressure wave

reached the gauge location. The obtained data were visually examined, and individual peaks extracted for further analysis based on a visual assessment.

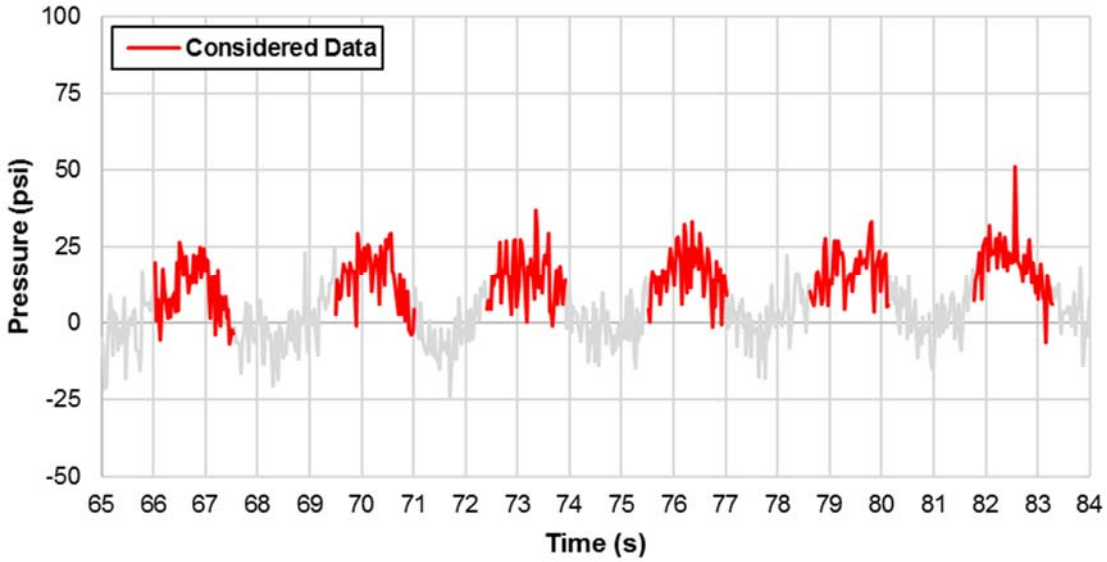

Figure 5.23 – Pumping pressure detail: Mixture 2, A boom, Q = 104 yd³/h (22 l/s), Gauge C

The third distinct shape of the pressure-time curve occurred only in three instances, and is shown in Figure 5.24. In this case, the pumping pressure was very low, rendering a pressure-time curve that did not show clearly distinguishable pressure pulses. However, it was possible to identify the pressure data by matching the time stamp of the Gauge C data with other gauges, therefore identifying the maximum pressure values for the data analysis.

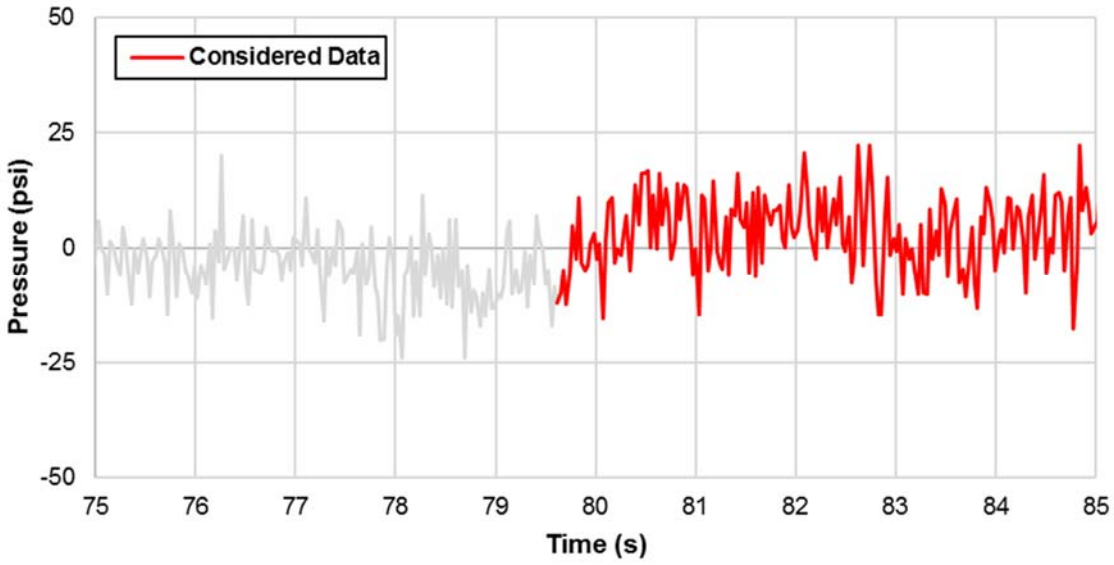

Figure 5.24 – Pumping pressures: Mixture 1, A boom, Q = 126 yd³/h (27 l/s), Gauge C

A summary of pressure data collected throughout the pumping experiments for gauges A and B is shown in Table 5.3. Due to a malfunction of the data acquisition system, data for Mixture 1 and Gauge A are not available. However, it was possible to extrapolate the pressure values at Gauge A location for Mixture 1 due to the linear nature of the pressure-distance relationship, as discussed further in this chapter. Nevertheless, the pumping pressures measured were not constant during each pumping cycle but varied with each stroke of the pump. The maximum variation of pumping pressures over the pumping period was recorded for Mixture 1, boom in the "A" configuration and flow rate of 126 yd³/h (26.8 l/s) with coefficient of variation of 17%. The lowest variation was for Mixture 3 with boom in the "flat" configuration and flow rate of 99 yd³/h (21 l/s) with coefficient of variation of of 0.9% of the average value. In general, the boom in "flat" position yielded a lower variability in maximum recorded pressure values with average standard deviation of 4% of the average while average standard deviation of 9% of the average was recorded for the "A" configuration.

Table 5.3 – Pressure data for gauges A and B

	Boom	Gauge	Maximum Pressure, psi											
			Peak 1	Peak 2	Peak 3	Peak 4	Peak 5	Peak 6	Peak 7	Peak 8	Peak 9	Peak 10	AVG*	SD*
Mixture 1	Flat	1	--	--	--	--	--	--	--	--	--	--	--	--
		2	122.5	128.2	135.1	126.3	119.8	112.3	108.0	110.4	106.2	109.6	117.8	9.0
		1	--	--	--	--	--	--	--	--	--	--	--	--
		2	139.0	137.1	166.8	184.3	212.9	190.4	183.2	176.7	187.4	--	175.3	21.9
		1	--	--	--	--	--	--	--	--	--	--	--	--
		2	57.6	62.5	59.9	61.8	61.8	59.9	56.1	64.4	--	--	60.5	2.4
	A	1	--	--	--	--	--	--	--	--	--	--	--	--
		2	143.2	89.1	97.5	91.8	93.3	91.4	87.2	85.3	88.8	--	96.4	16.0
		1	--	--	--	--	--	--	--	--	--	--	--	--
		2	75.1	75.1	65.6	64.0	62.9	61.7	65.6	--	--	--	67.1	4.8
Mixture 2	A	1	147.1	143.1	159.1	167.1	159.1	159.1	159.1	159.1	155.1	147.1	155.5	6.7
		2	87.5	86.3	100.0	106.5	113.0	113.7	112.6	113.0	110.3	97.7	104.0	9.6
		1	228.7	268.8	312.9	320.9	312.9	288.8	268.8	280.8	304.9	292.8	288.0	25.1
		2	122.7	154.7	198.1	201.5	197.7	176.0	157.0	172.9	180.6	171.8	173.3	21.8
Mixture 3	A	1	121.7	145.8	153.8	153.8	157.8	145.8	145.8	141.8	141.8	--	145.3	9.4
		2	95.1	94.3	95.5	101.9	95.9	89.0	87.5	91.7	--	--	93.9	4.0
		1	226.0	362.3	330.2	306.1	302.1	302.1	310.2	278.1	278.1	--	299.5	33.7
		2	204.9	194.2	183.9	182.8	187.0	185.1	172.5	170.6	171.0	--	183.5	10.1
	Flat	1	277.0	281.0	277.0	281.0	285.0	281.0	281.0	285.0	--	--	281.0	2.7
		2	159.3	165.8	163.1	162.3	169.2	169.9	167.3	167.7	--	--	165.6	3.3
		1	409.1	417.1	417.1	409.1	413.1	417.1	421.2	417.1	413.1	--	414.9	3.6
		2	258.9	257.0	258.9	261.1	265.0	269.2	267.3	266.1	--	--	262.9	4.0

* AVG: average, SD: standard deviation

Additionally, negative pressures exerted on concrete were observed in several instances, such as the case shown in Figure 5.25. The existence of a negative pressure during the pumping cycle suggests that a suction, or vacuum, is created for a small period of time when the pump piston retracts. The suction effect of the pump piston has been proposed as one of the possible factors contributing to the changes of the air void system due to pumping. Interestingly, significant negative pressures value (i.e. greater than 10 psi) were only observed when the boom was in the "A" configuration.

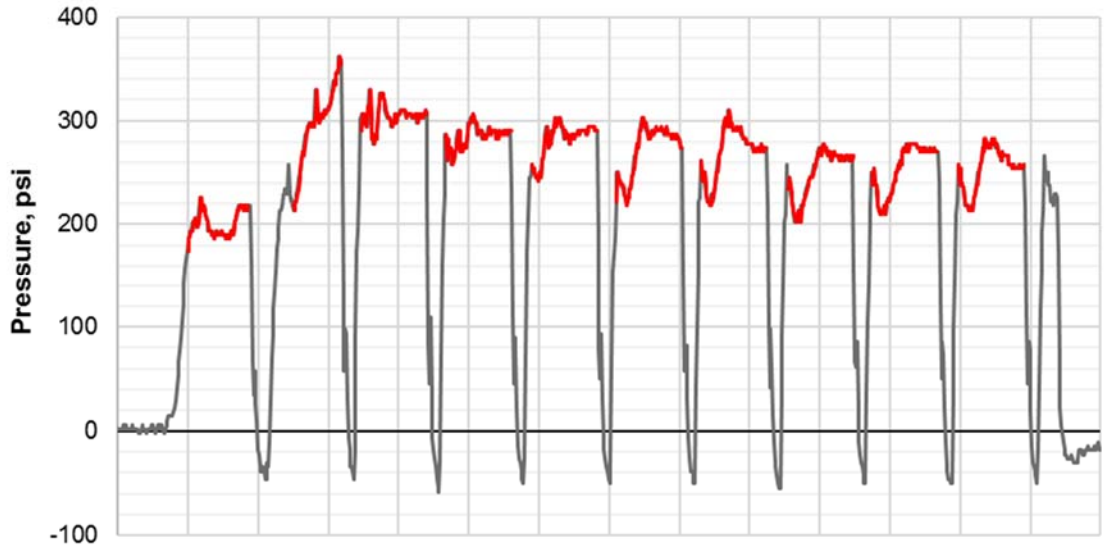

Figure 5.25 – Negative pumping pressures

Recorded pumping pressure as a function of the gauge location distance from the pump is shown in Figure 5.26 and Figure 5.27. To recall, gauges A, B and C were located at 15, 52 and 92 ft from the pump, respectively. As expected, it is apparent that the pumping pressure decreased linearly with the increasing distance from the pump. Due to a data logger malfunction, data for Gauge A when Mixture 1 was pumped were lost. However, the linear relationship between the gauge location and the distance from the hopper allowed for extrapolation of the missing Gauge A data.

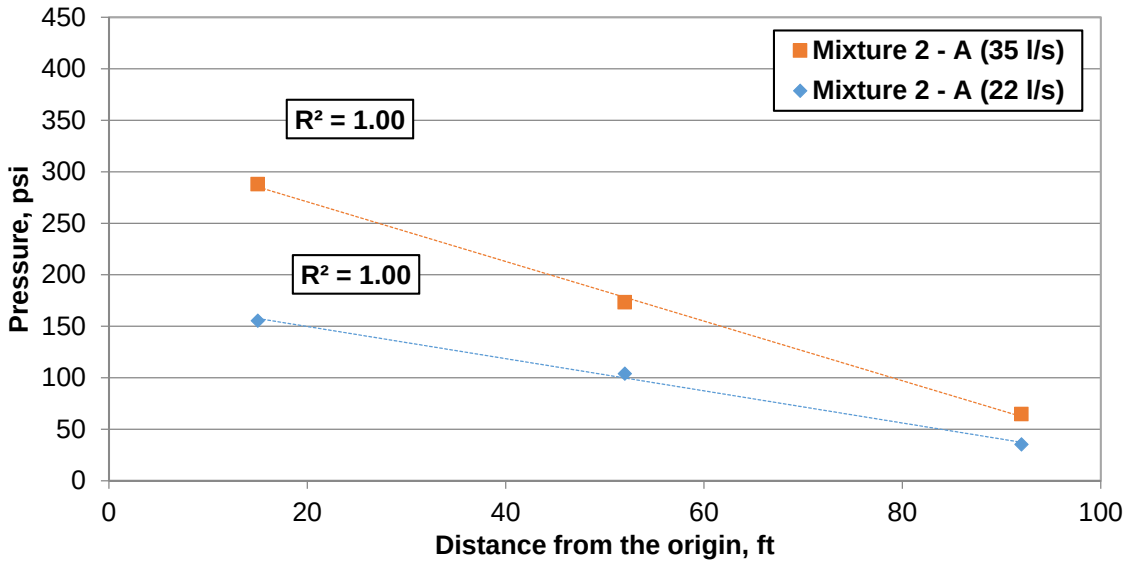

Figure 5.26 – Pumping pressure vs distance from the pump, mixture B

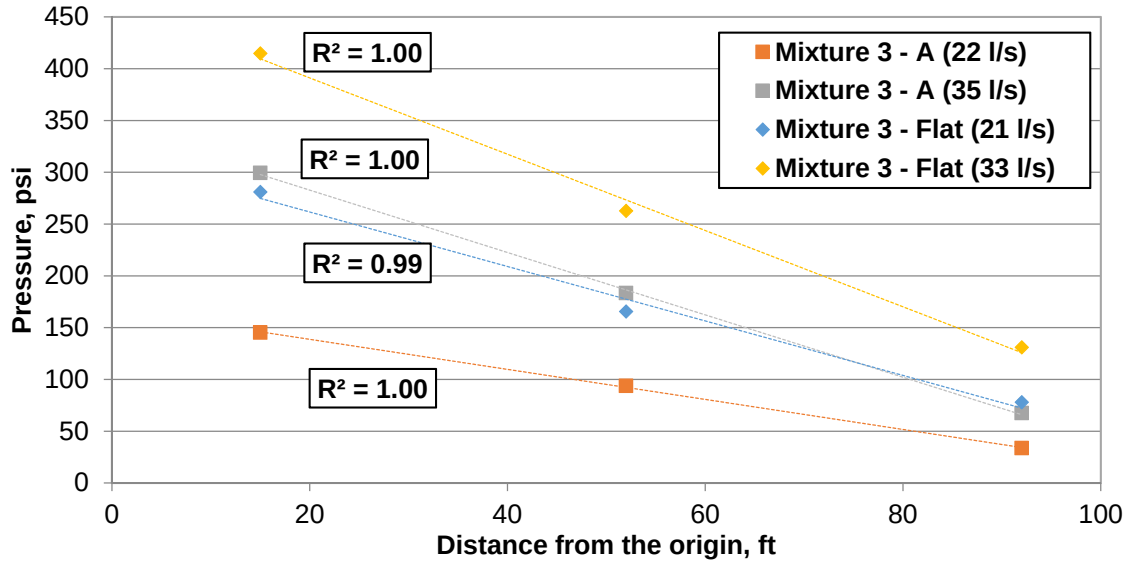

Figure 5.27 – Pumping pressure vs distance from the pump, mixture C

Maximum pumping pressures for each individual pumping test are shown in Table 5.4. The maximum pumping pressure recorded was 414.9 psi when Mixture 3 was pumped at the flow rate of 158 yd³/h (33 l/s), with the pump boom in a flat configuration.

Table 5.4 – Pumping pressures

Mixture	Boom	Pumping Pressure, psi			Flow Rate, yd³/h (l/s)
		Gauge A	Gauge B	Gauge C	
1	Flat	174.7	117.8	60.5	97 (21)
1		232.2	175.3	100.2	152 (32)
1	A	117.4	60.5	31.9	26 (6)
1		153.3	96.4	34.9	126 (27)
1		112.6	74.4	33.1	24 (5)
2	A	155.5	104.0	35.4	104 (22)
2		288.0	173.3	64.8	166 (35)
3	A	145.3	93.9	33.7	102 (22)
3		299.5	183.5	67.5	166 (35)
3	Flat	281.0	165.6	78.1	99 (21)
3		414.9	262.9	131.0	158 (33)

Measured pumping pressures and respective flow rates for all pumping tests conducted are presented Figure 5.28, Figure 5.29 and Figure 5.30 for mixtures 1, 2 and 3, respectively. In the case of Mixture 3, a direct comparison of pumping pressures between the flat and A boom configuration can be observed as flow rates for each couple of A and flat pumping tests were similar. However, there were significant differences between flow rates for Mixture 1, therefore an indirect comparison had to be made. As apparent from Figure 5.26 and Figure 5.27, there exists a linear correlation between the flow rate and the recorded pumping pressure valid for all three locations of strain gauges, which agrees with existing literature. Thus, a linear interpolation allows one to estimate the pumping pressure at a certain flow rate. The data shows that the required pumping pressure to achieve a particular flow rate value is higher when the boom is oriented in the flat configuration. This observation is somewhat contradictory to what one would expect as Bernoulli's law states that only the height difference between inlet and outlet plays a role on the pressure needed, regardless of the configuration of the pipeline. However, it has been

stated before that concrete can flow due to gravity in the decreasing part of a concrete pumpline. In that case, the values used in Bernoulli's equation must be reconsidered with only the first part of the pumpline. The inlet remains the same, but the outlet is now the highest point of the boom. In this case, the applied pressure must overcome gravity to pump the concrete up, but only half the length of the pipeline is filled, which reduces the total pressure. However, the registered pressure in point C, which is approximately at the highest point of the boom, still shows non-zero values, which means that the entire down-section may not empty under gravity, but the portion which empties must still be significant to cause the difference with the flat configuration. It is also important to point out that is it likely that not all concrete in the downward section of the boom can empty only due to gravity as friction between the concrete and pipe walls is present.

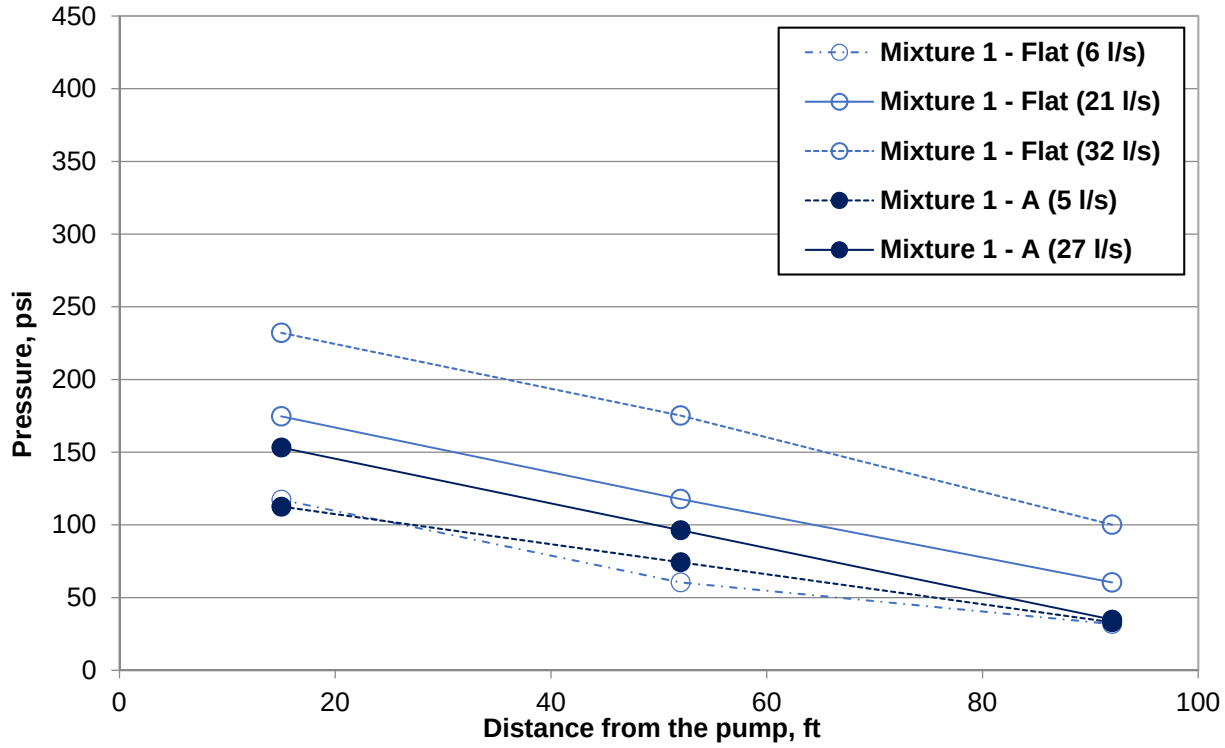

Figure 5.28 – Pumping pressure, Mixture A

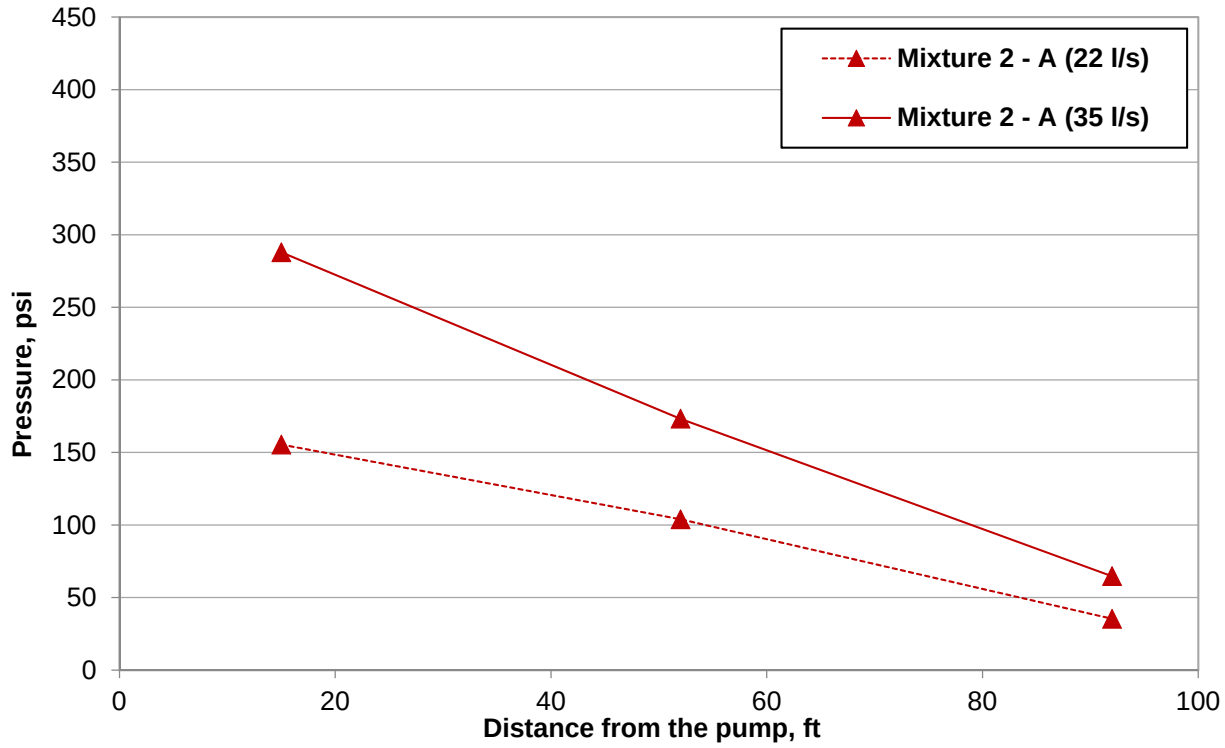

Figure 5.29 – Pumping pressure, Mixture B

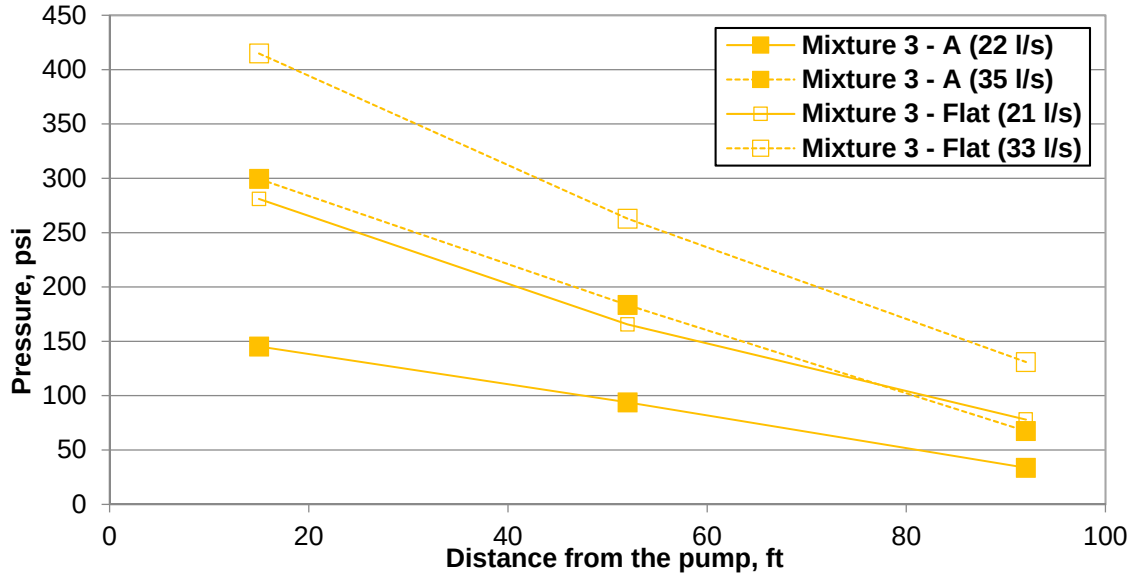

Figure 5.30 – Pumping pressure, Mixture C

5.3.2 Fresh Concrete Properties

The fresh concrete slump was measured before and after pumping, and obtained values are summarized in Table 5.5. The concrete sample "before pumping" was obtained periodically directly from the concrete truck, however, it was not feasible to sample the truck before every single pumping experiment. Therefore, the "before" values of slump are taken as averages of results measured from two consecutive samples obtained from the concrete truck prior to and following a particular pumping test.

Table 5.5 – Slump before and after pumping

Sample Source	Mixture	Boom Setup	Slump, in.	
			Before	After
Truck	Mixture 1	-	8.75	-
Pump		Flat	8.75	8.25
Pump		Flat	8.75	8.50
Pump		Flat	8.75	8.00
Truck		-	8.75	
Pump		A	8.25	5.25
Pump		A	8.25	6.50
Truck		-	7.50	-
Truck	Mixture 2	-	8.50	-
Pump		A	7.25	5.25
Pump		A	7.25	6.75
Truck		-	6.00	-
Truck	Mixture 3	-	7.25	
Pump		A	7.00	5.25
Pump		A	7.00	5.00
Pump		Flat	7.00	4.50
Pump		Flat	7.00	4.50
Truck		-	6.50	-

Comparison of measured slump values before and after pumping are shown in Figure 5.31. It is apparent that in all instances, slump decreased after pumping for all boom configurations. The slump reduction can be attributed to the decrease of free water in the mixture under pressure that decreases overall workability of the mixture. It is suggested that if aggregate moisture condition is not saturated surface-dry (SSD), or above SSD, mixing water can be forced

into aggregate pores under the pumping pressure and it is likely not released back into the mixture upon pressure relief, hence workability is reduced. During this pumping experiment, all fine aggregate was in above-SSD condition, however, the coarse aggregate was slightly below SSD, allowing approximately 1-2 gallons of water per cubic yard to be absorbed during the pumping operation. The mixing water is always compensated for aggregate moisture, however, the aggregate absorption process that is driven primarily by RH gradient is not rapid, and therefore it is likely that some porosity in the coarse aggregate is left unfilled before the mixture is pumped.

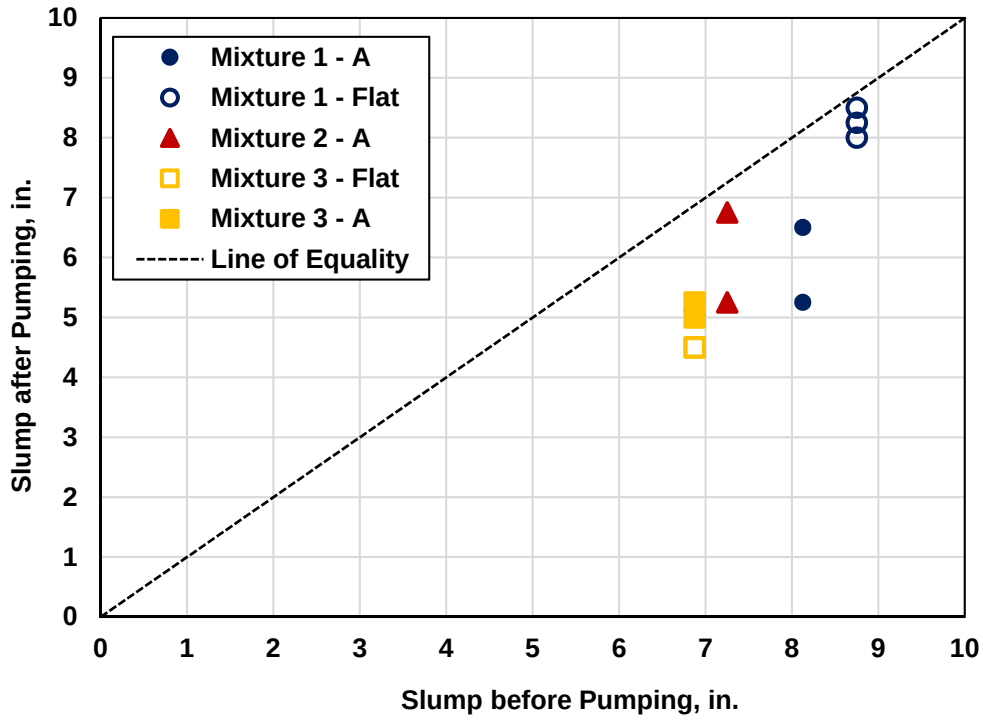

Figure 5.31 – Slump before and after pumping

The change in slump after pumping with respect to pumping pressure is shown in Figure 5.32. The results did not reveal any correlation between applied pumping pressure and change in the slump value. The amount of slump loss likely depends on the time from mixing, aggregate

moisture content before mixing, pumping pressure, and admixtures used. The change in concrete temperature before and after pumping is shown Figure 5.33. It is apparent from the data that very little or no change in temperature occurred during pumping. Although the changes in concrete temperature due to pumping were reported in the literature, in a majority of the cases the change occurred when concrete was pumped over very long distances (i.e. high-rise construction). From data obtained in this experiment, it appears that concrete temperature change is not a concern when a standard-size boom pump is used.

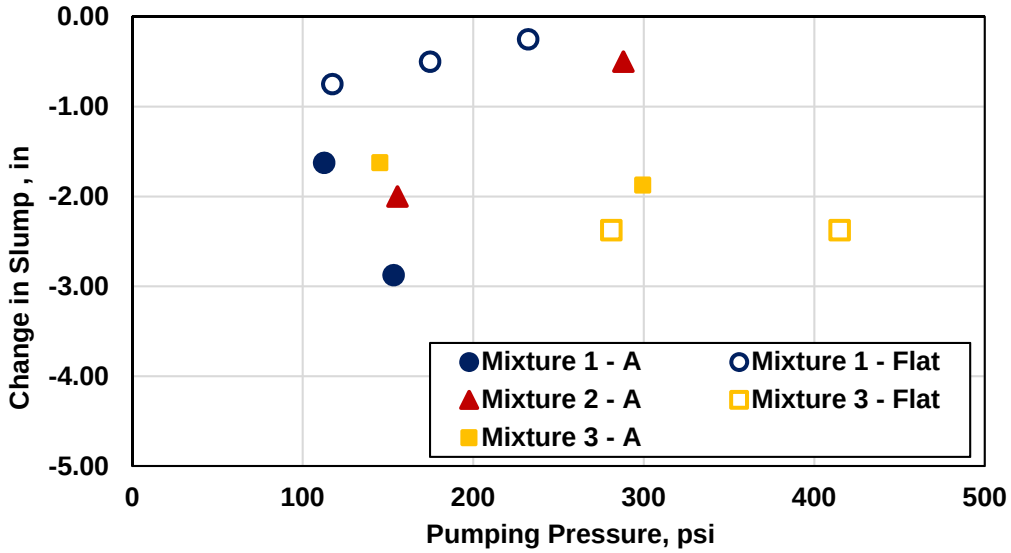

Figure 5.32 – Slump change vs pumping pressure

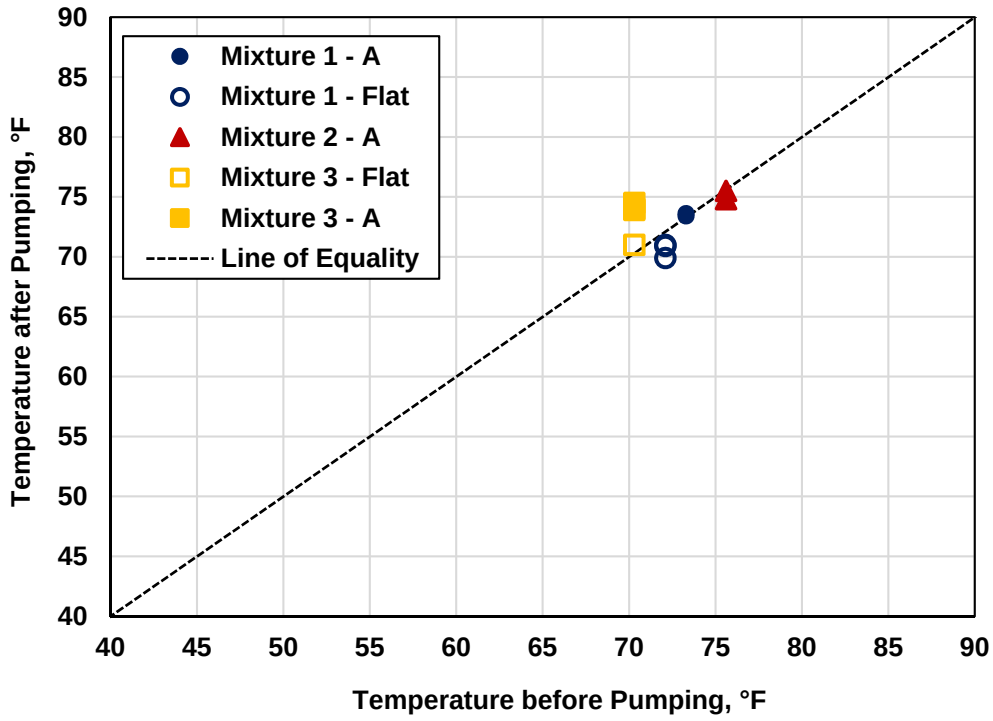

Figure 5.33 – Temperature before and after pumping

5.3.3 Air Void System

Air void content before and after pumping is shown Figure 5.34 and Figure 5.35 for measurements conducted in the plastic state and on hardened samples, respectively. Hardened air void content generally corresponded to the values of air void content measured in the plastic state, as shown in the Table 2. The results indicate that barely any change in the air content occurs after determining the fresh concrete air content. As this is typically determined within 5 to 10 min after the pumping operation, nearly all of the air re-appeared rapidly after the dissolution during the pumping process for the mixtures tested, which is logical due to the abundance of nucleation sites (aggregates, cement or SCM particles, or existing air bubbles).

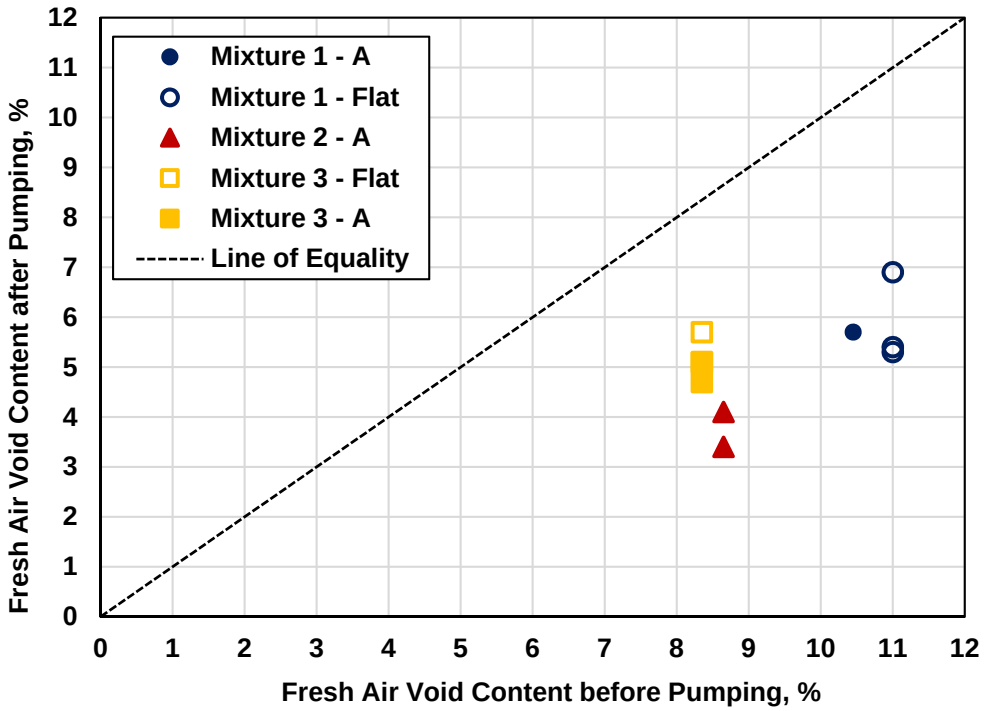

Figure 5.34 – Fresh air void content before and after pumping

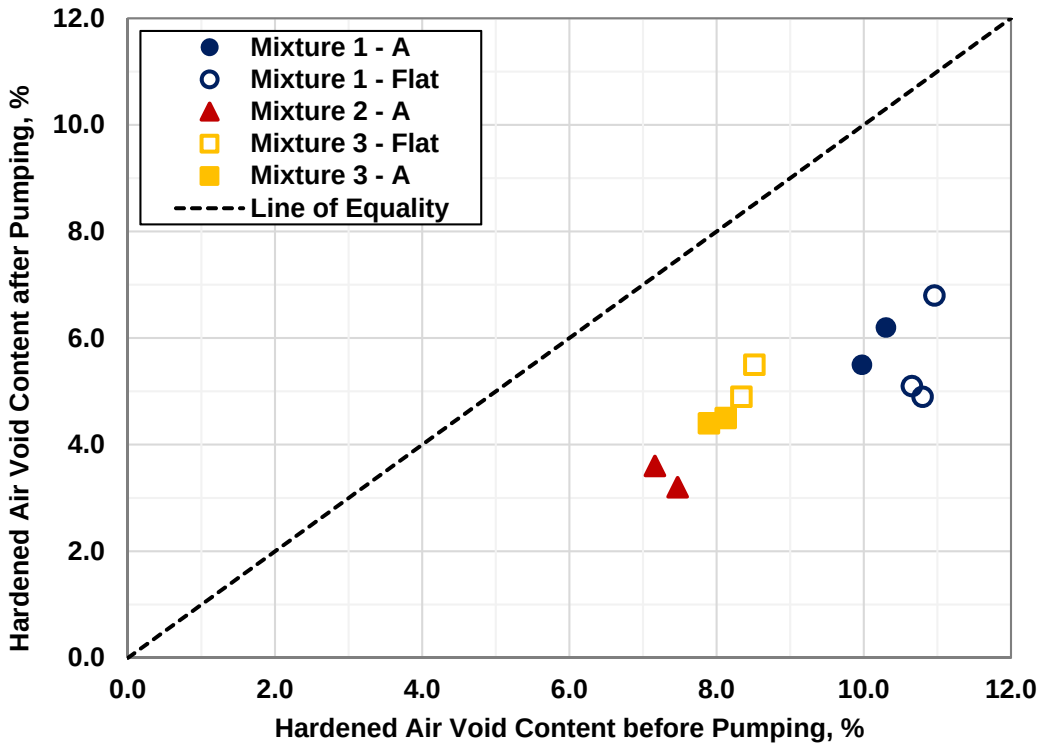

Figure 5.35 – Hardened air void content before and after pumping

To determine the influence of pumping on the air void system, samples taken after pumping must be compared to samples from the truck. However, the pumped and non-pumped samples were not characterized at the same time. For almost all mixtures, samples were taken from the truck before and after the pumping tests, and sometimes an intermediate sample was characterized too. This delivers a linear time-evolution of the measured properties before pumping, used as base-line to compare with the pumped samples. For instance, considering the first trial of Mixture 1, concrete was sampled and the hardened air void specimens fabricated at time zero, prior to three pumping tests with the boom in the flat configuration (5, 24 and 41 minutes after taking the initial concrete sample), followed by another sample taken 59 minutes after the initial sample was obtained. The hardened air void analysis showed that the initial air void content (at time zero) was 11.0%, and 10.5% for the second sample from the truck obtained

at 59 minutes. Thus, using linear interpolation, hardened air void content values of 10.96%, 10.80% and 10.65% were used as base values (before pumping) for the three pumping tests conducted at 5, 24, and 41 minutes, respectively.

Air loss occurred due to pumping for all pumping experiments. A slightly higher air loss of 4.8% on average was observed for mixture 1 compared to average air losses of 3.7% and 3.4% for mixtures 2 and 3, respectively. Furthermore, no significant difference in the amount of air lost between the "A" and "flat" boom configurations was identified. Similarly, no effect of measured pressure or flow rate (recall that concrete was pumped at flow rates ranging from 24 yd^3/h to 166 yd^3/h, i.e. 5.2 l/s to 35.3 l/s) was found to be correlated with the amount of air loss due to pumping.

The total air void content is not the sole important parameter of the air void system that determines its effectiveness in protecting concrete from freeze-thaw damage. The actual size-distribution and spatial uniformity of air voids in the paste matrix is equally important. Spacing factor is one of the metrics that can be used to characterize the air void system, and a spacing factor value of approximately 0.008 in. (0.200 mm) is generally accepted as a maximum value to ensure adequate freeze-thaw performance. Similarly, specific surface of the air void system provides an assessment of coarseness/fineness of the air void system with typical limit of 600 $in.^2/in.^3$ (24 mm^2/mm^3) for frost resistant concrete. Figure 5.36 and Figure 5.37 show the change in spacing factor and specific surface during the full-scale experiments, respectively. In all cases, the spacing factor significantly increased after pumping. For the specific surface, in all but two cases, an increase was also recorded, while in one case, the specific surface did not change after pumping.

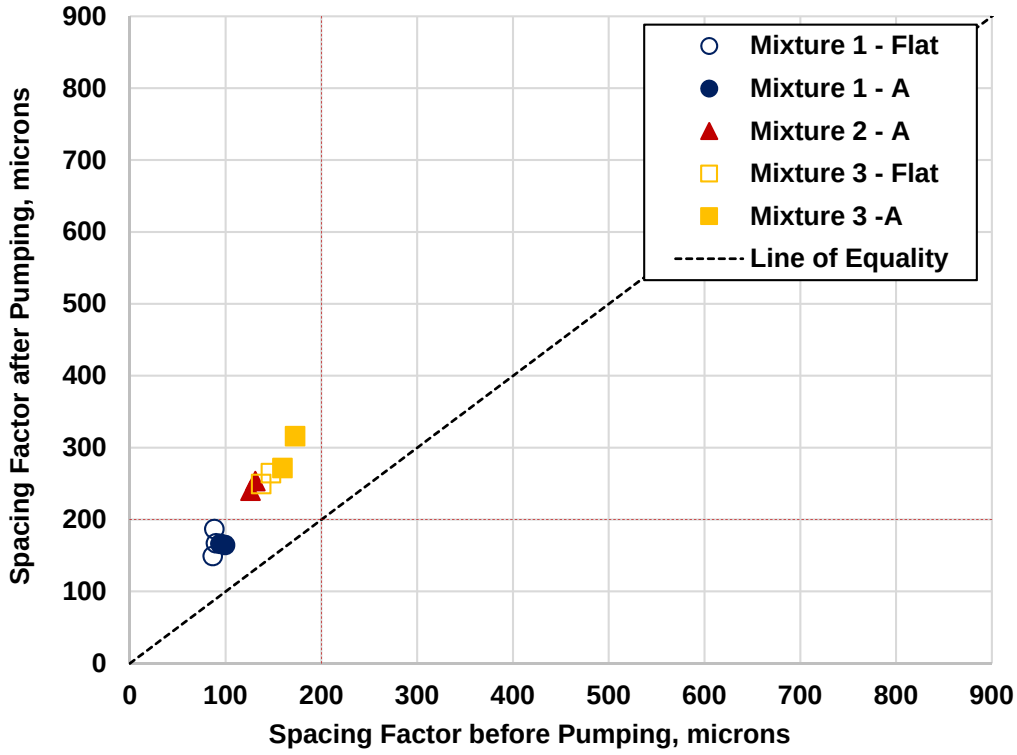

Figure 5.36 – Spacing factor before and after pumping

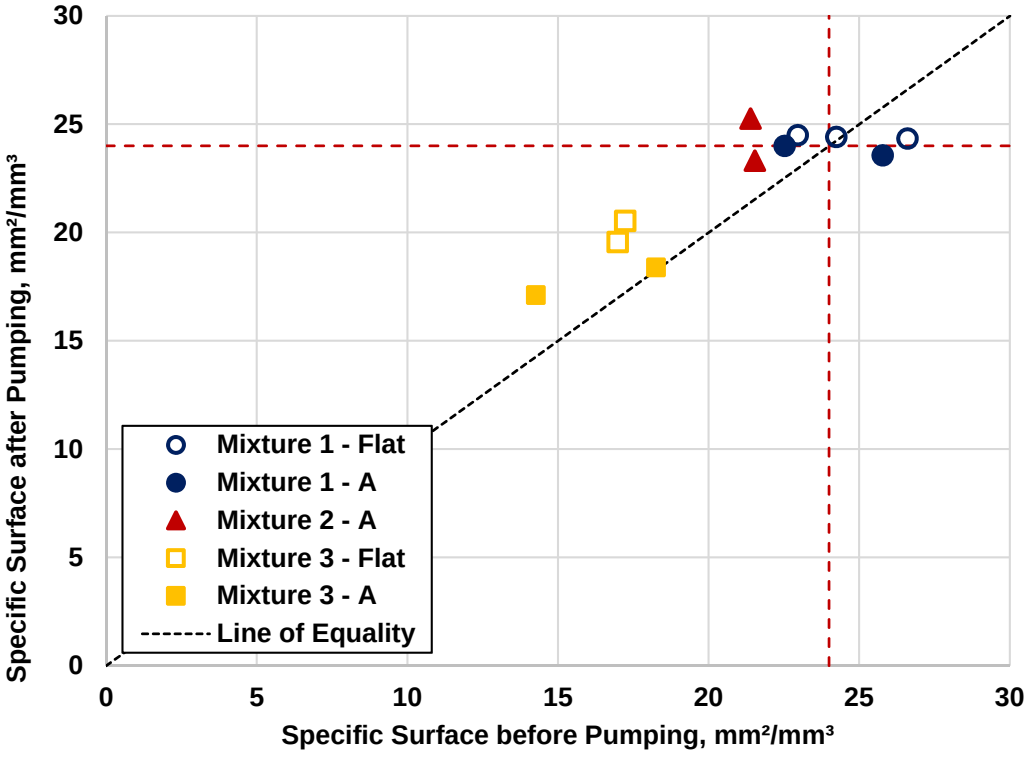

Figure 5.37 – Specific surface before and after pumping

Pumped concrete had an average increase in spacing factor of 98 micrometers. This growth of spacing factor resulted in 6 out of 11 samples exceeding the 200 to 230 micrometers limit of freeze-thaw durability. The biggest change in spacing factor was observed for Mixture 3, 121 micrometers on average, followed by Mixture 2 with an average increase of 106 micrometers, while the spacing factor after pumping of Mixture 1 increased by an average of 75 micrometers. To determine whether any direct relationship exists between pumping pressure and changes in the air void system, particularly the air void size distribution, maximum pumping pressure and corresponding changes of the spacing factor and specific surface are shown in Figure 5.38 and Figure 5.39, respectively.

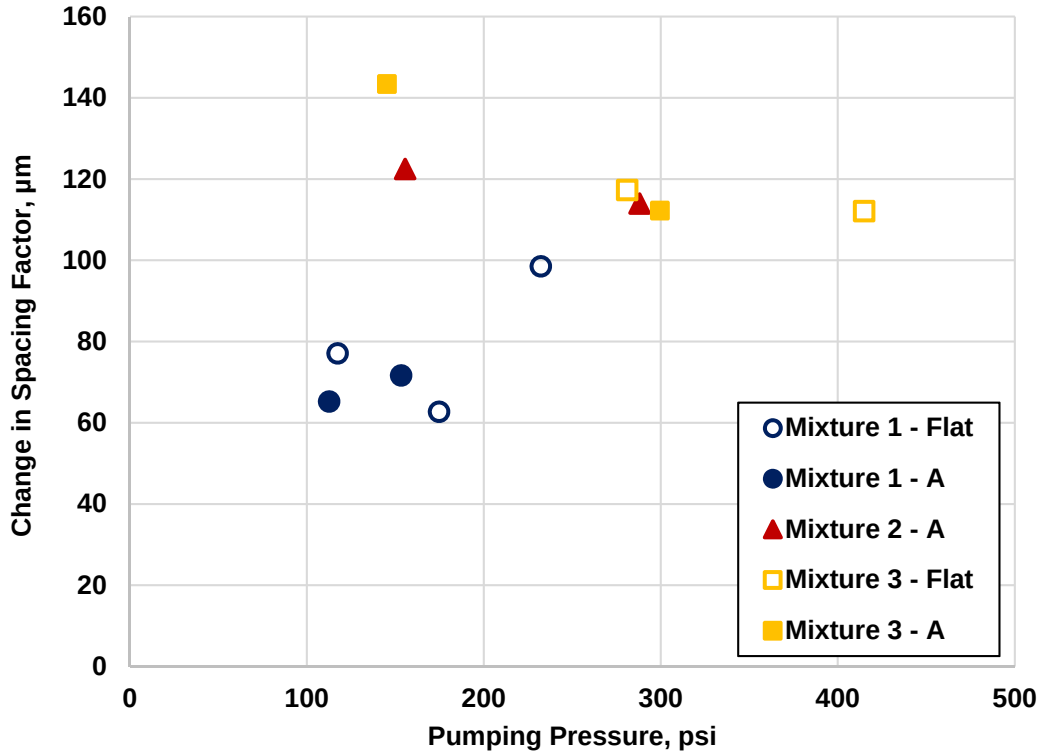

Figure 5.38 – Spacing factor vs pumping pressure

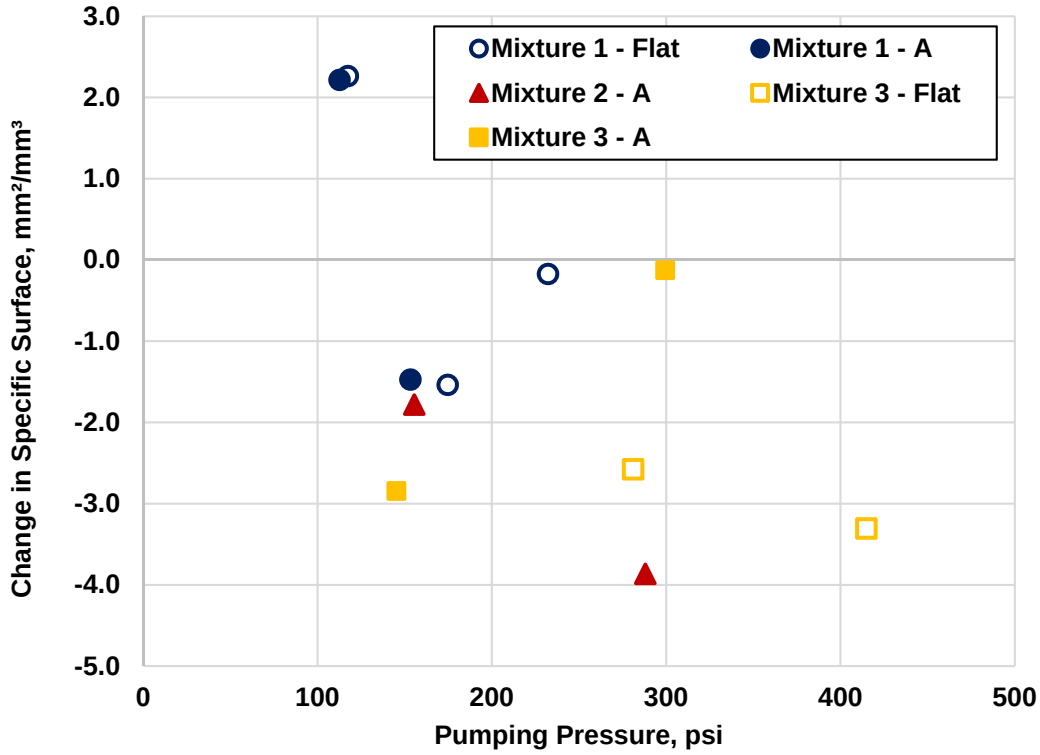

Figure 5.39 – Specific surface vs pumping pressure

It is apparent that neither the change in the spacing factor nor the change in the specific surfaces correlate well with the pumping pressure. Further exploration of the data obtained from the air void system analysis suggest that the increase in the spacing factor after pumping is primarily driven by the decrease in the total air void content of pumped concrete. To recall, Power's models utilized to calculate the spacing factor are approximations based on two parameters: (1) paste-to-air ratio, p/A and (2) specific surface, α, of the air void system [131]. For small values of p/A, the model is idealized by evenly distributing the cement paste around each air void (creating a so-called frosting around each air bubble), and the thickness of this layer is Power's spacing factor. For large values of p/A, a uniform air void is assumed. Each air void in this idealized system has a specific area equal to the bulk specific surface of the system (α). Air voids are then organized into a cubic lattice with such spacing so that that the lattice air

void content equals to the bulk air void content. Finally, the distance from the center of the lattice to the nearest air void surface is the spacing factor. Both models produce the same values when p/A is exactly 4.342. Therefore, the change in the spacing factor after pumping is directly related to the change of the overall air content of the system and the change in the air void size distribution represented by the value of the specific surface.

A cumulative size distribution of the air void system for all investigated mixtures is shown in Figure 5.40, Figure 5.41 and Figure 5.42 for Mixture 1, Mixture 2 and Mixture 3, respectively. Although there is one mixture for each set that shows a small shift in the distribution curve, the overall results clearly indicate the air void size distribution for mixtures before and after pumping does not change. Hence, the contribution of the specific surface parameter to the change in the value of spacing factor after pumping is much less significant than the contribution of the change in the total air void content.

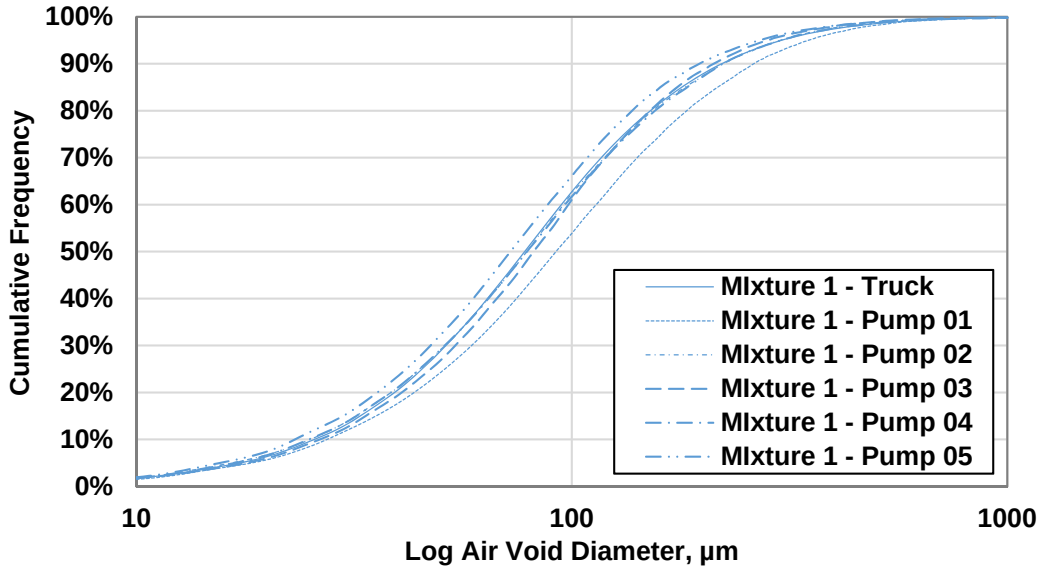

Figure 5.40 – Air void size distribution, Mixture 1

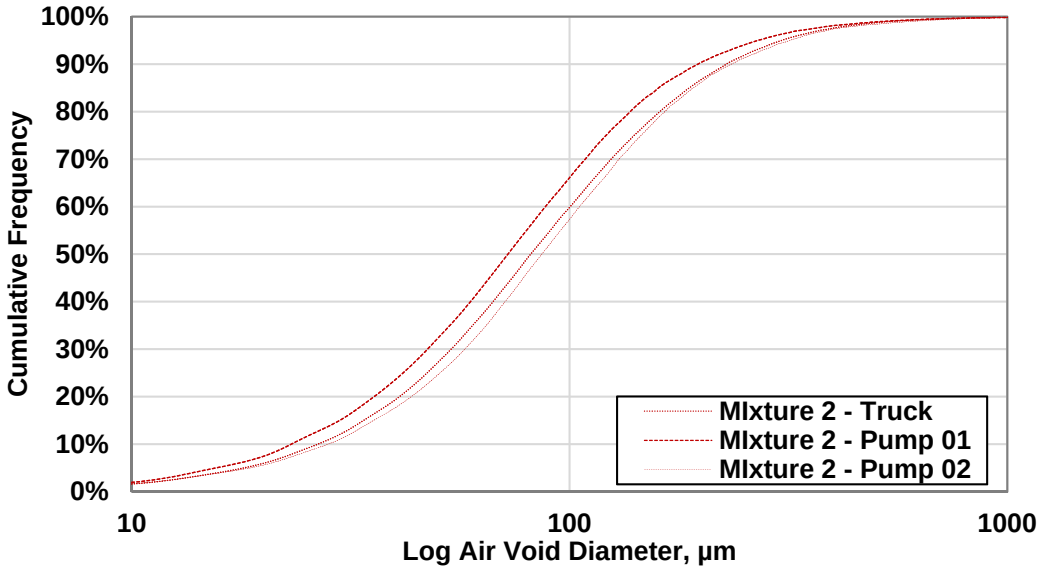

Figure 5.41 – Air void size distribution, Mixture 2

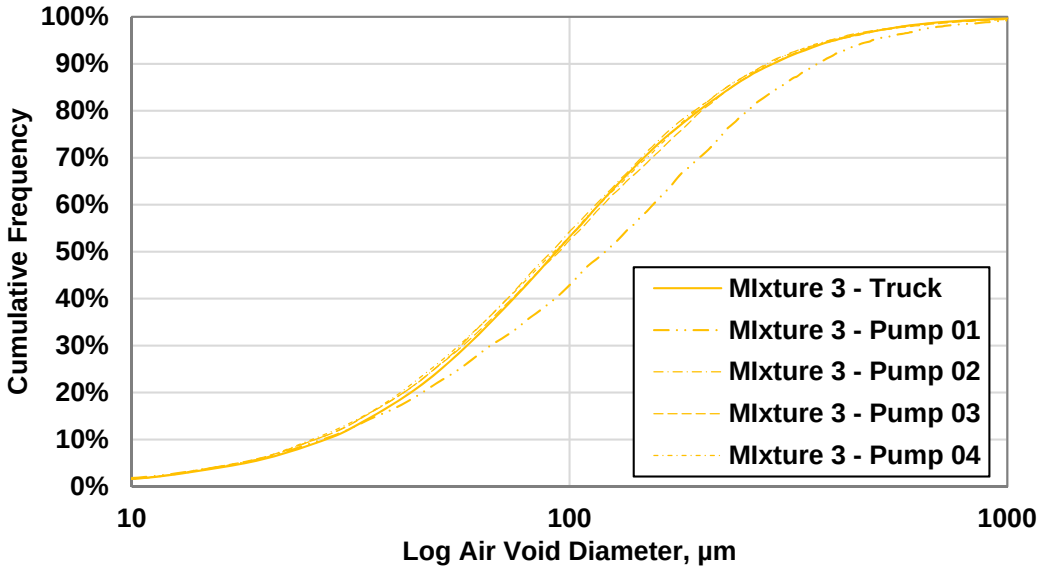

Figure 5.42 – Air void size distribution, Mixture 3

Moreover, it was previously suggested that air voids with diameters smaller than 50 micrometers are lost due to pumping [92]. Based on the data obtained from the hardened air void analysis, it is apparent that, at least in the case of the investigated conventional concretes, this is not always true as all the hardened air void specimens fabricated from pumped concrete

contained from 22% to 32% of air voids with diameter less than 50 μm. Additionally, no difference in the relative amount of air voids smaller than 50 μm was identified between pumped and non-pumped concrete.

Obtained data suggest that rather than being reliant on the investigated pumping characteristics (pumping pressure, boom configuration), observed changes in the air void system properties (total air void content, spacing factor) are dependent on the mixture-specific properties and proportions.

The results of the Super Air Meter (SAM) testing conducted before and after pumping are shown in Figure 5.43. The SAM test was always conducted in parallel with measuring the fresh air void content. The SAM test is proposed by the manufacturer of the device as a replacement of hardened air void analysis for quality control and assurance in the field. As per the manufacturer's recommendation, the SAM value of 0.20 should be used as an acceptance limit for freeze-thaw durability. A total of 16 SAM tests were performed; 6 SAM tests for concrete before pumping and 10 tests for pumped concrete. Out of the 6 tests performed on concrete before pumping, in all, the SAM number agreed with the hardened air void analysis, i.e. the spacing factor value was less than 200 μm and the SAM number was less than 0.20. However, for the pumped concrete, 2 out of the 10 tests (20% of the data set) generated a false-negative result (i.e. spacing factor less than 200 μm and SAM number larger greater than 0.20), 2 tests (20% of the data set) resulted in a false-positive (i.e. spacing factor greater than 200 μm and SAM number less than 0.20) result and only 6 tests (60% of the data set) showed an agreement between the SAM number and the hardened air void analysis. Therefore, if the SAM test was used as a quality tool in the field for pumped concrete, 40% of mixtures would be either accepted while exceeding the upper limit value of the spacing, or rejected while compliant with the

spacing factor limit. Based on the obtained data, it is apparent that further research and validation of this test method is needed before employing the SAM test as a quality control tool for pumped concrete.

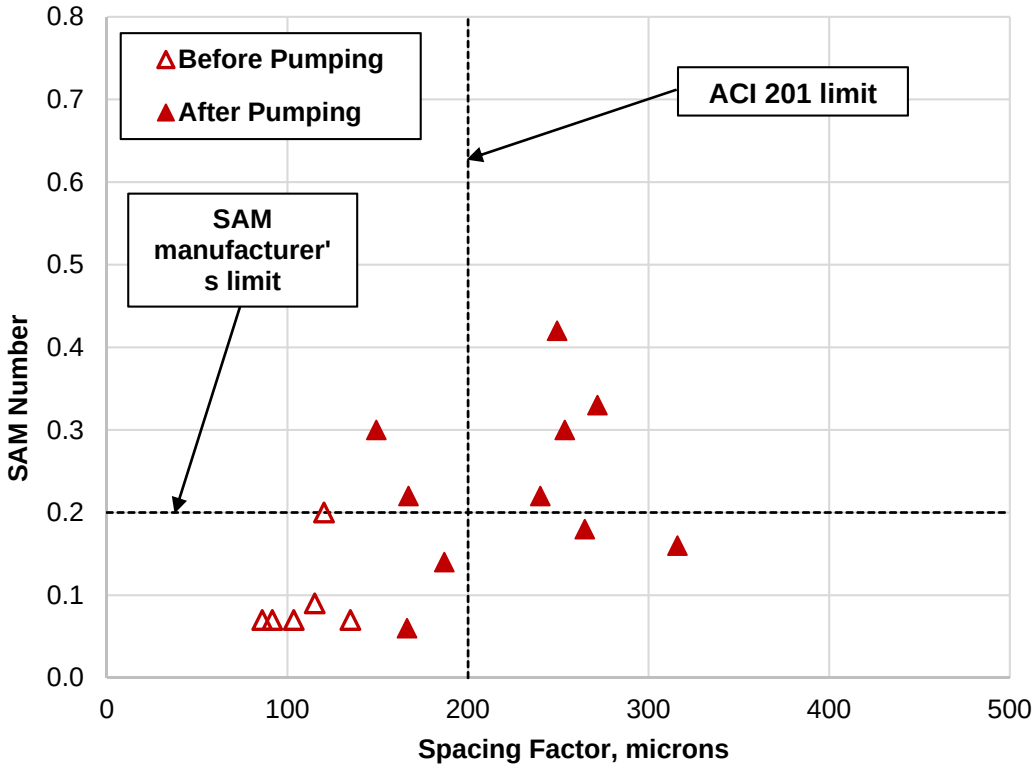

Figure 5.43 – SAM number before and after pumping

5.3.4 Rheology and Lubrication Layer Properties

Rheological properties (plastic viscosity and yield stress) and properties of the lubrication layer (viscous constant and interface yield stress) were measured before and after pumping. Figure 5.44 and Figure 5.45 show yield stress and plastic viscosity with respect to measured slump, respectively. It is apparent that a weak relationship (R^2 value of 0.54) exists between yield stress and slump, which is in general agreement with the existing literature. For the plastic-viscosity-slump, no relationship was found, as expected. The obtained data clearly show that the slump test is not capable of truly capturing rheological properties of concrete mixture, and

therefore if such characterization is required in the laboratory or in the field, this widely utilized test method must be replaced with a more advanced one that is capable of evaluating both concrete yield stress and plastic viscosity.

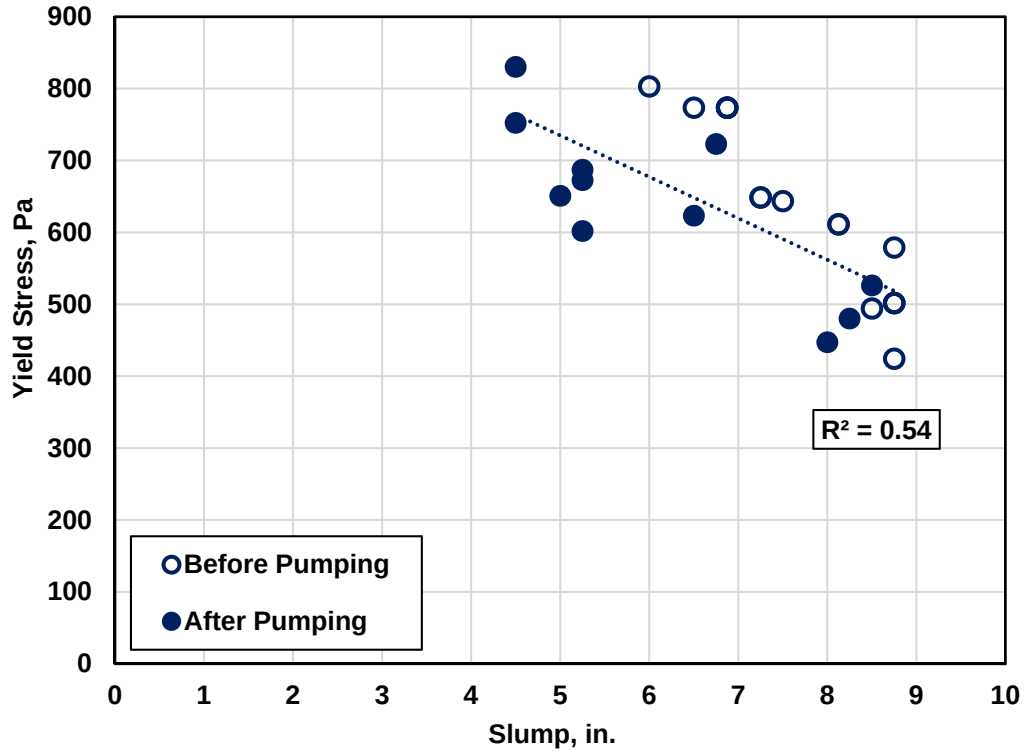

Figure 5.44 – Yield stress vs slump

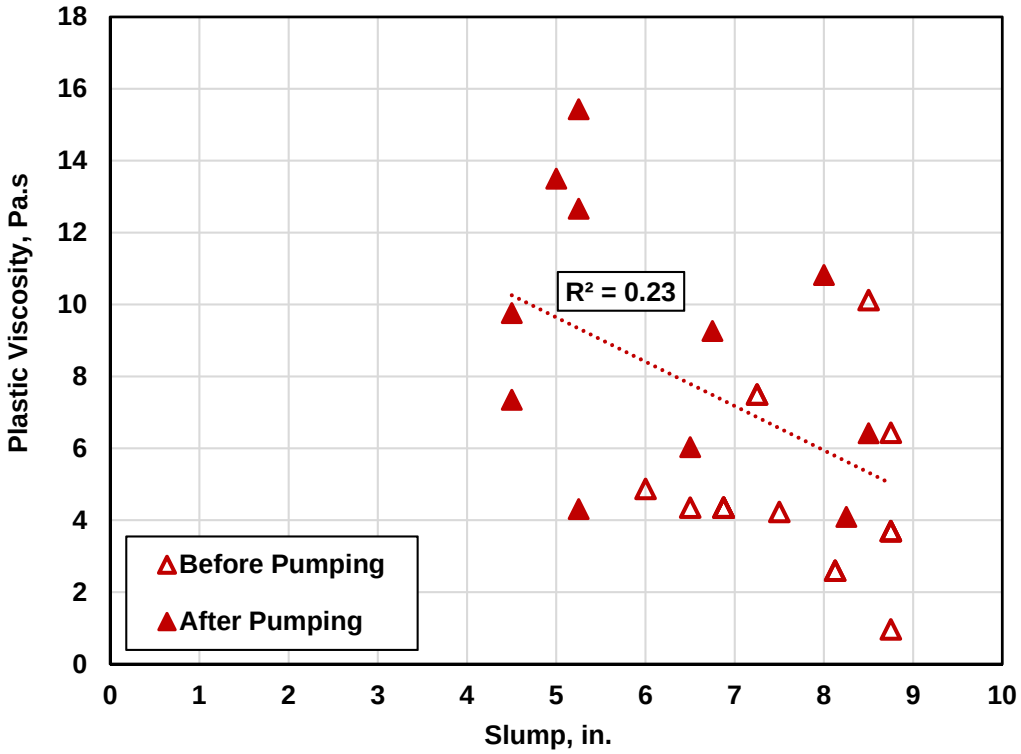

Figure 5.45 – Plastic viscosity vs slump

Figure 5.46 and Figure 5.47 show concrete rheological properties with respect to the corresponding properties of the lubrication layer, i.e. plastic viscosity with respect to viscous constant, and yield stress with respect to interface yield stress, respectively. The data showed that for the set of investigated mixtures, no relationship exists between plastic viscosity and the viscous constant. In fact, for the set of measured values after pumping, the viscous constant remained relatively consistent across the sample with values between 750 and 1000 Pa.s/m while the plastic viscosity ranged from 4 to 16 Pa.s. In terms of yield stress and interface yield stress, a very weak relationship with R^2 value of 0.35 was obtained for the whole set of data. When the data is divided into two groups – before and after pumping, one can calculate the R^2 of 0.86 for data points obtained for samples before pumping, while the R^2 for the samples after pumping drops to 0.17. This suggest that the changes in workability of pumped concrete, primarily due to

the free water migration into unsaturated aggregate voids, affect disproportionately affect rheological properties of concrete and properties of the lubrication layer.

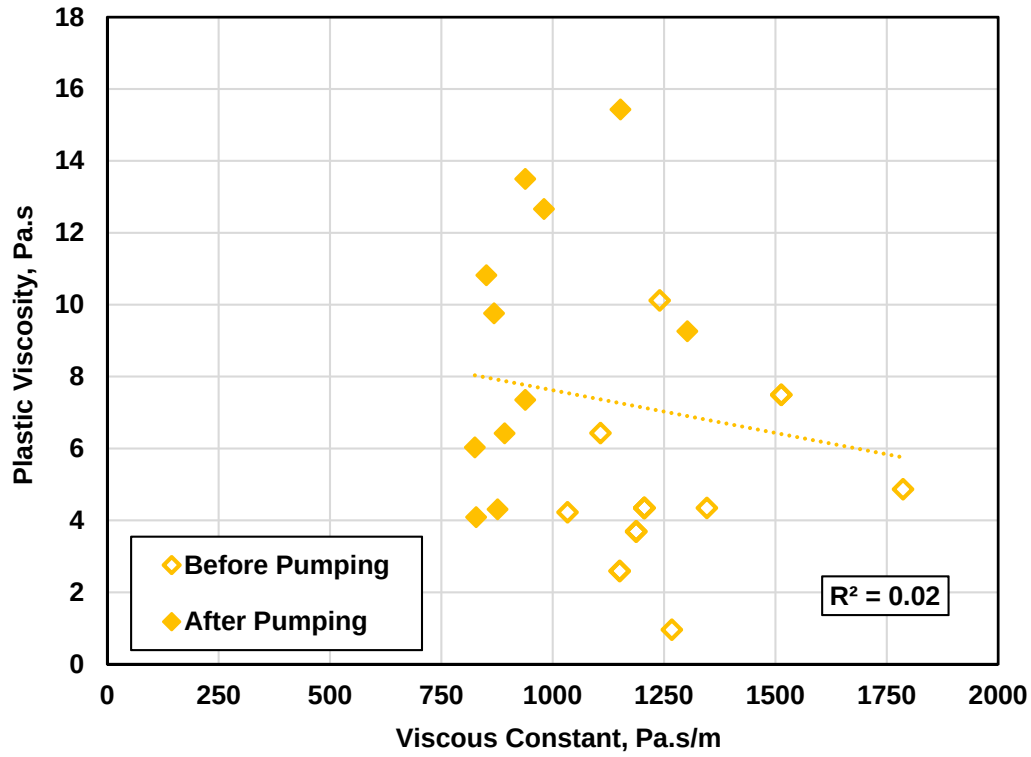

Figure 5.46 – Plastic viscosity vs viscous constant

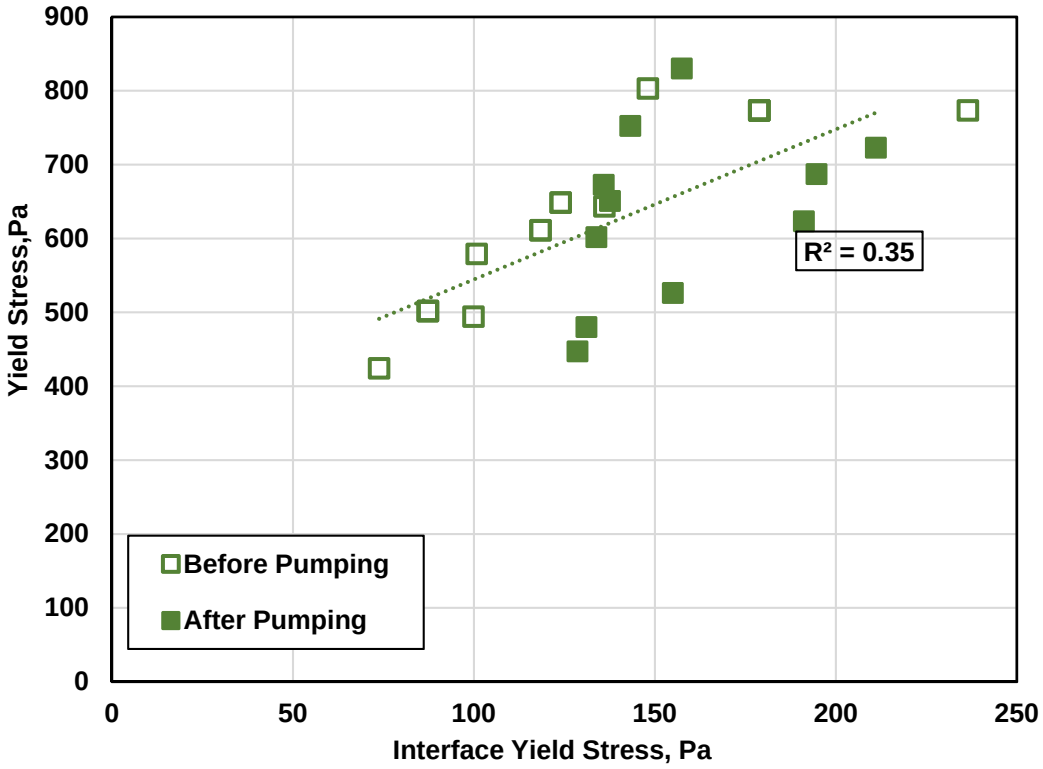

Figure 5.47 – Yield stress vs interface yield stress

Figure 5.48 and Figure 5.49 show values, both before and after pumping, of yield stress and plastic viscosity, respectively. In 6 out of 11 cases, yield stress slightly decreased after pumping, which does not correspond to the measured decrease in slump after pumping. However, in 5 instances, the measured value of yield stress after pumping was higher than the yield stress before pumping, which is in agreement with the observed decrease in slump after pumping. However, plastic viscosity of all concrete mixtures increased after pumping, i.e. concrete resistance to flow was increased for concrete mixtures after pumping. As discussed previously, a relatively weak relationship between the yield stress and measured slump values was obtained. Although it is generally accepted that there exists a strong relationship between slump and yield stress, it appears that the value of concrete viscosity has also some effect on results of the slump tests. Since slump was reduced after pumping for all concrete mixtures even

though the yield stress decreased in some instances, it appears that it was that the increase in plastic viscosity after pumping that contributed to the slump loss after pumping.

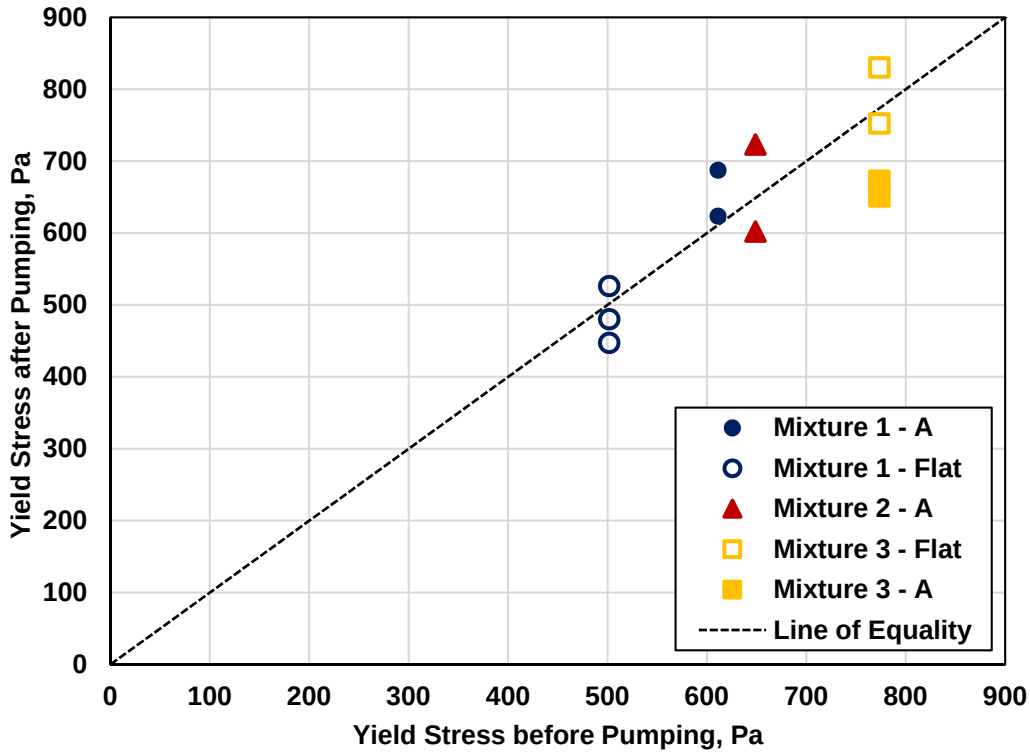

Figure 5.48 – Changes in yield stress due to pumping

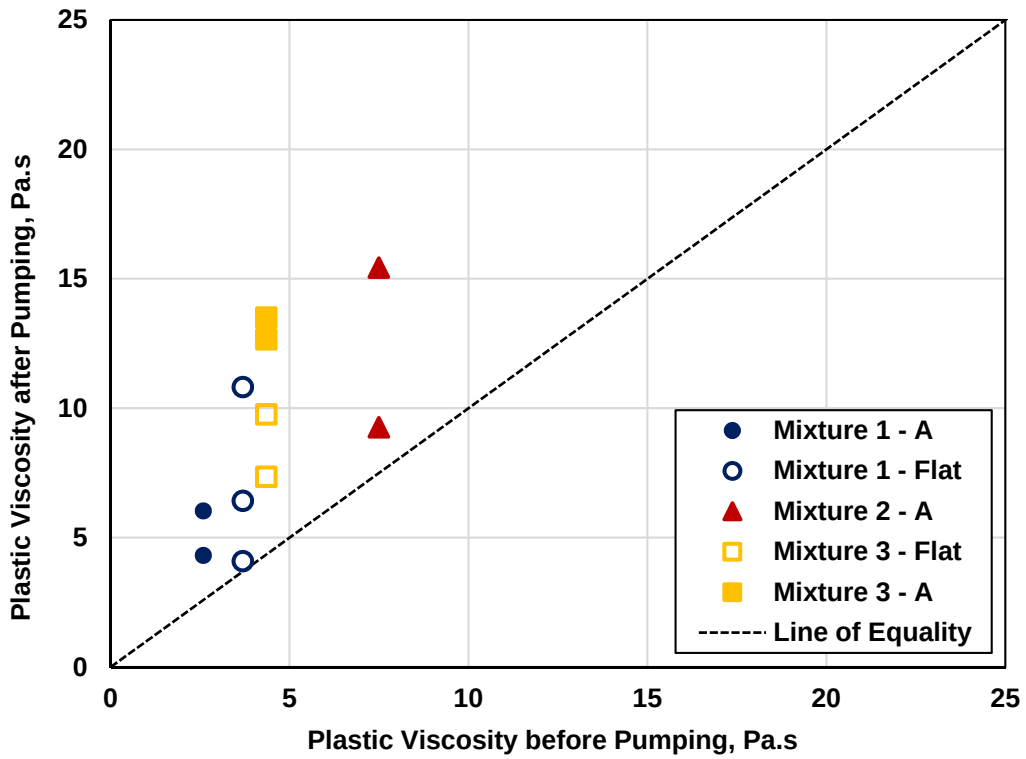

Figure 5.49 – Changes in plastic viscosity due to pumping

Changes in yield stress and plastic viscosity with respect to pumping pressures are shown in Figure 5.50 and Figure 5.51, respectively. It is apparent from the presented data that for the set of investigated mixtures, no relationship exists between pumping pressure and change in any of the elementary rheological properties.

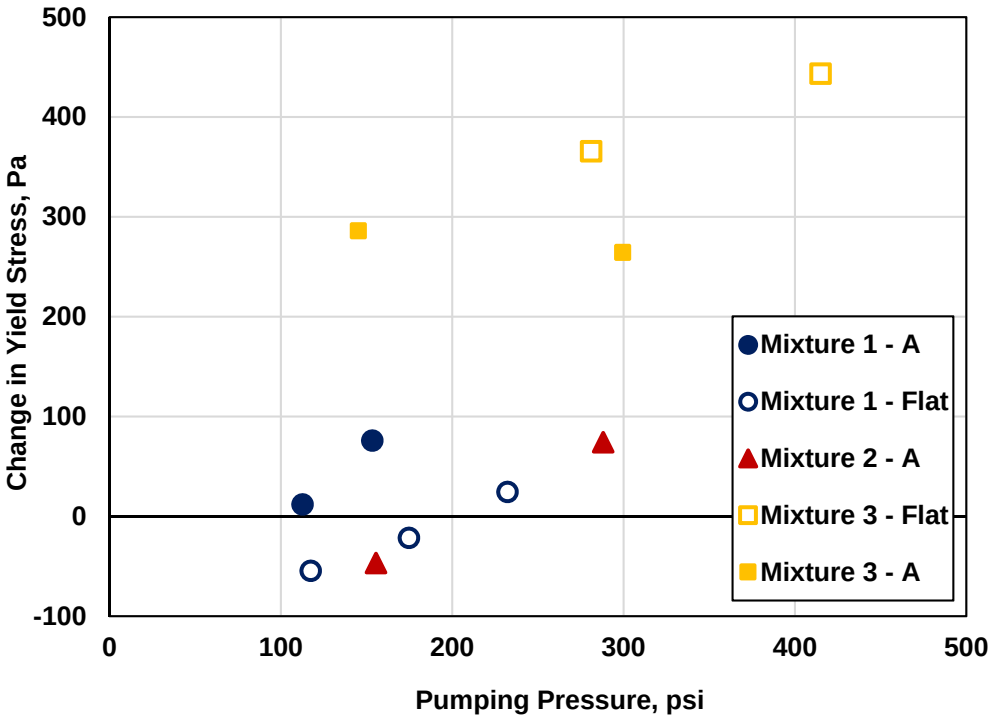

Figure 5.50 – Changes in yield stress vs pumping pressure

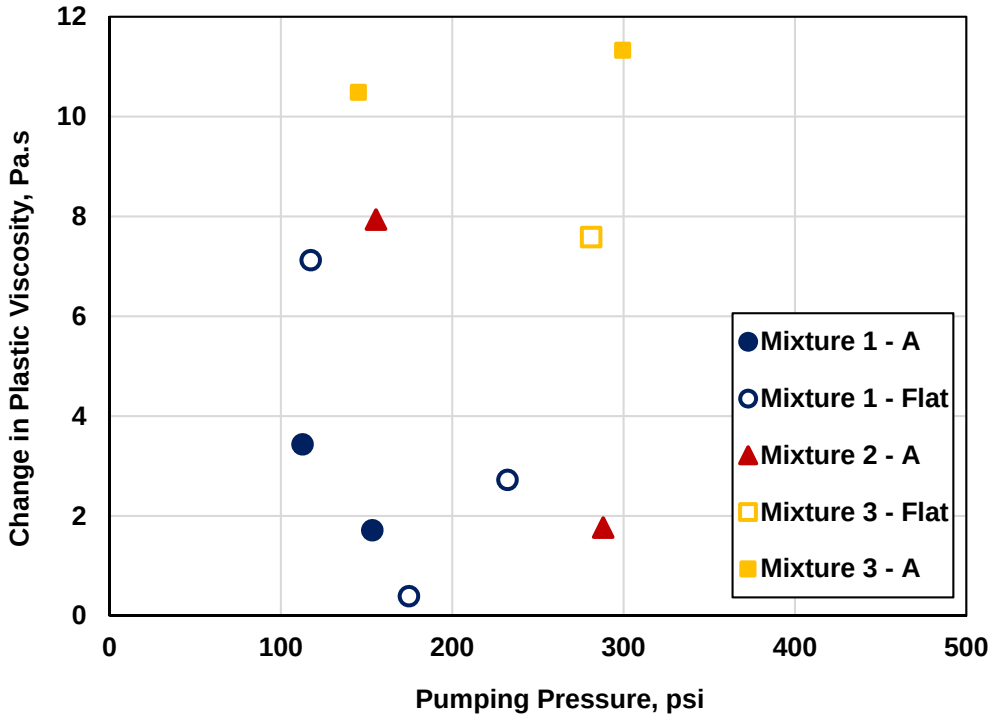

Figure 5.51 – Changes in plastic viscosity vs pumping pressure

5.4 Conclusions

In this chapter, a full-scale controlled pumping experiment was described. The pressure analysis, influence of pumping on concrete fresh properties, concrete rheology and air void system were discussed.

It was demonstrated that the use of stain gauges as an indirect method of monitoring pumping pressure is a viable option for standard job site concrete pumps. Furthermore, it has been shown that a linear relationship exists between pumping pressure and the flow rate of pumped concrete. Based on obtained pumping pressure values, it was determined that the pumping pressure for a constant flow rate of concrete will be higher when the pump boom is oriented in the "flat" configuration, i.e. with the boom in a full horizontal extension.

Pumping can significantly affect concrete fresh properties. During this testing program, decrease in slump, air content, increase in plastic viscosity, and both increase and decrease in yield stress was observed after pumping.

No relationship between the air loss and pumping pressure or flow rate was detected. Moreover, the results of the total air void measurements in both plastic and hardened state were in general agreement, proving that nearly all air dissolved during the pumping process reappears rapidly after the pressure is relieved.

The spacing factor increased after pumping. It was determined that the change in the spacing factor is primarily driven by the air loss, and that the air void system structure, in terms of air void size distribution, was not significantly affected by the pumping process. Moreover, significant amount of air voids with diameter less than 50 μm was detected in after-pumping hardened air void samples. Results of the experiment suggests that the changes induced in the air void system, such as total air loss (or gain) and spacing factor change, are not significantly

affected by the pumping process and its parameters (pumping pressure, flow rate, boom configuration) but are rather reliant on the characteristics of individual concrete mixture.

Lastly, the Super Air Meter was utilized to characterize the air void system of investigated mixtures. The results indicated that for significantly large number of tests, the SAM test produced either false-positive or false-negative results for pumped concrete. Therefore, further research is needed before this test method can be implanted as a field quality control tool for pumped concrete.

Chapter 6 - Concrete Pumping Evaluation – Field Investigation

6.1 Introduction and Research Significance

Concrete pumping is utilized on large number of construction sites across the United State and around the world on the daily basis. To this extent, understanding how pumping can change both fresh and hardened concrete properties is essential in order to achieve durable and as-designed performance of concrete infrastructure.

A field testing campaign was carried out to evaluate the effect of pumping on concrete properties in actual job site conditions. Particular focus was placed on comparing properties of concrete sampled from the mixing truck and at the point of placement. Many departments of transportation (DOT) in the country require concrete to be sampled at the point of placement for quality control/assurance purposes, including the Kansas Department of Transportation (KDOT). However, there are still many DOTs that routinely require sampling directly from the mixing truck chute, i.e. sampling of concrete that was not pumped and is not representative of the in-place concrete.

Six new bridge-deck construction projects located in Eastern Kansas were selected in cooperation with KDOT to be part of this project. During the summer construction season of 2015, each of the selected job sites was visited during the bridge deck placement to evaluate concrete fresh properties before and after pumping, including concrete rheology and properties of the lubrication layer. Additionally, samples for hardened air void analysis were fabricated and further analyzed in the laboratory. This field investigation allowed for evaluation of concrete pumping and its influence on concrete properties in field conditions, and compliments research effort described in Chapter 5 of this dissertation.

6.2 Experimental Methods

6.2.1 Project Sites

Five bridge construction sites (Bridge Nos. 169, 164, 184, 163 and 165) selected to be part of this study were located in Lawrence, KS. These sites were part of the K-10 South Lawrence Trafficway (SLT) project [132]. This highway project consists of a 6-mile-long four-lane highway that will serve as a connection completing a loop around the city of Lawrence, KS. The construction work included 24 new concrete bridges and the total worth of the construction contract was over $140 million. Five bridge deck placements of this project were visited in the summer of 2015; all of the jobsite visits occurred in the night and early in the morning as the construction schedule was designed to avoid concrete placement during hot summer days.

Additionally, a bridge deck construction site located on the Interstate Highway 70 (I-70) west of Kansas City, KS was included in this field investigation. This project site consisted of partial, two lane bridge deck replacement on an existing highway bridge. An overview of investigated project sites is shown in Table 6.1.

Table 6.1 – Field testing campaign project sites

Site ID	Project	Bridge	Mixture Design ID
Site 1	SLT	Bridge 10-23-10.71 (169) (mainline WB K-10 over Haskell Ave)	1PL1501A-F
Site 2	I-70	Bridge No. 70-105-4.37 (096) WB	1PMC082B
Site 3	SLT	Bridge 10-23-9.56 (164) (mainline K-10 over Naismith Creek WB)	1PL1501A
Site 4	SLT	Bridge 10-23-13.66 (184) (Ramp EB23-EB10 over K10)	1PL1501A
Site 5	SLT	Bridge 10-23-8.97 (163) (Louisiana St over K-10)	1PL1505A
Site 6	SLT	Bridge 10-23-9.57 (165) (mainline K-10 over Naismith Creek EB)	1PL1505A

6.2.2 Concrete Sampling and Testing

At each visited site, samples of fresh concrete were taken before and after pumping. Concrete samples taken before pumping were sampled directly as discharged from the concrete truck into the pump hopper. Concrete sampling was always performed when approximately one half of the concrete was discharged in order to obtain a representative sample of the concrete mixture.

Concrete samples taken after pumping were obtained once sampling from the truck was performed. Fresh concrete was always obtained after being placed in the formwork, and not from bucket or a wheelbarrow, which is commonly done on construction sites. This was done to ensure that the obtained sample was representative of in-place concrete. Since it took approximately 10 minutes to fully discharge one concrete truck during all of the placements, it was made sure that both fresh concrete samples, i.e. before and after pumping, were obtained from the same concrete truck. This was not always a trivial task since in many instances,

concrete pump was at a different elevation level than the bridge deck placement, however, a successful effort was made to coordinate the simultaneous sampling at two locations.

Concrete fresh properties, i.e. slump [113], air content [128], temperature [116] and density [115], were determined for all samples before and after pumping. Concrete rheological measurements and evaluation of the lubrication layer properties were also performed; following a procedure described in Chapter 3 of this dissertation. Additionally, the Super Air Meter was used to assess quality of the concrete air void system [127]. Since two sets of concrete samples were obtained at the same time, concrete sampled before pumping was always tested first. The concrete that was sampled after pumping was kept aside in buckets covered with lids to prevent moisture loss until testing of the first concrete sample was finished. Prior to testing of the second concrete sample, concrete was hand-remixed in the bucket. The overall duration of the fresh concrete testing was approximately 40 minutes. In addition to fresh concrete testing, specimens for hardened air void analysis were fabricated for concrete before and after pumping. These samples remained on the project site for at least 24 hours stored in coolers before being transported to K-State laboratory. The hardened void analysis was performed following a procedure outlined in Chapter 5 of this dissertation, and in general accordance with Method C of ASTM C457 [128].

6.2.3 Mixture Proportions, Pumping

As indicated in Table 6.2, an identical concrete mixture was utilized at all SLT project sites with one exception – on Site 1, concrete mixture was enhanced by PVA fibers. For all of the SLT project sites, the total cementitious content was 564 lbs/yd^3 (335 kg/m^3) with 25% portland cement replaced by slag cement, and w/cm of 0.41.

For the I-70 project site, a mixture with total cementitious content of 510 lbs/yd³ (303 kg/m³), 20% of class F fly ash and w/cm of 0.43 was utilized. Concrete mixture proportions for both sites are shown in Table 6.2.

Table 6.2 – Mixture proportions – field evaluation

Mixture ID:	**1PL1501A**	**1PMC082B**
Project Site:	**SLT**	**I-70**
Materials	*lbs/yd³ (kg/m³)*	
Portland Cement	423 (251)	405 (240)
Fly Ash	--	105 (62)
Slag	141 (84)	--
Coarse Aggregate	1875 (1112)	1718 (1019)
Fine Aggregate	1250 (742)	1389 (824)
Total Cementitious Content, kg / m³	564 (335)	510 (303)
Sand-to-Total Aggregate Ratio (by mass)	0.43	0.43
Design Air Content, %	6.5	6.5
Water	231 (137)	219 (130)
w/cm	0.41	0.43
Paste Content (by volume), %	24.6	23.4
Mortar Content (by volume), %	52.0	59.8
Admixtures	*fl oz/cwt (ml/m³)*	
Air-Entrainer	See Table 6.3	0.75 (158)
High-Range Water Reducer		7.45 (1381)
Hydration Stabilizer		0 (0)

Dosages of chemical admixtures for STL mixtures were adjusted by concrete producer on as-needed basis in order to achieve required fresh concrete properties based on the ambient temperature at the time of concrete placement. Dosages for each STL project site are shown in Table 6.3,

Table 6.3 – SLT admixture dosage

Bridge	169	164	184	163	163	165
Time	N/A	N/A	N/A	5:30-7:30 AM	After 7:30 AM	N/A
Admixture	**Dosage, oz/cwt (ml/m³)**					
Air-Entrainer	1.5 (227)	2.5 (374)	2.2 (334)	1.8 (267)	1.7 (259)	1.8 (275)
High-Range Water Reducer	8.9 (1337)	6.9 (1043)	6.9 (1043)	6.9 (1043)	7.6 (1150)	6.9 (1043)
Hydration Stabilizer	2.5 (377)	0.0 (0)	2.5 (377)	2.5 (377)	2.5 (377)	0.0 (0)

Pump configuration and overall arrangements of the construction site varied significantly throughout this research program. As all of these deck placements were of a relatively large scale requiring significant volumes of concrete to be placed, the whole bridge deck placement took approximately from 3 to 6 hours, based on the particular dimensions of the bridge deck. Two distinct placement configurations were observed during all of the placements: (1) concrete pump and the placement were at the same elevation, and (2) concrete pump was below the bridge. For the first case, the boom of the pump would be initially in the "A" position and as the placement progressed it would get extended into the "flat" configuration to reach the end of the bridge deck, or vice versa (i.e. starting in the "flat" position and retracted to the "A" configuration). Hence, the pumping variables were changing during the course of concrete sampling. For the second case, concrete boom was always in the "A" shape to overcome the elevation difference between the location of the pump (i.e. below the bridge) and the bridge deck. Moreover, two concrete pumps of the same type were always used for placements with the pump located below the bridge deck to compensate for the reduced working range of the boom due to the elevation difference. Concrete pump configuration for each visited job site is shown in Table 6.4.

Table 6.4 – Concrete pump configuration

Site ID	Project	Pump Location	Number of Pumps Used
Site 0	SLT	Below the bridge	2
Site 1	I-70	At the bridge deck elevation	1
Site 2	SLT	At the bridge deck elevation	1
Site 3	SLT	Below the bridge	2
Site 4	SLT	At the bridge deck elevation	1
Site 5	SLT	At the bridge deck elevation	1

6.3 Results and Discussion

Changes in slump before and after pumping are shown in Figure 6.1. Throughout the data set, both increase and reduction in slump after pumping was observed, in one case even for the same field site (Site 3). Out of the total 13 investigated concrete mixtures, in 5 instances, an increase in the slump after pumping was observed whereas the slump value decreased in 8 cases after pumping. The greatest recorded decrease in slump was 1.50 in. and the maximum slump increase after pumping was 2.75 in. Compared to the full-scale experiment discussed Chapter 5 of this dissertation, the workability change after pumping was less significant. According to the batch tickets provided at job sites, coarse and fine aggregate were in above-SSD condition for majority of the mixtures, which suggests that the water migration due applied pressure might have been eliminated, subsequently lowering the impact of pumping on in-place workability of investigate concrete mixtures.

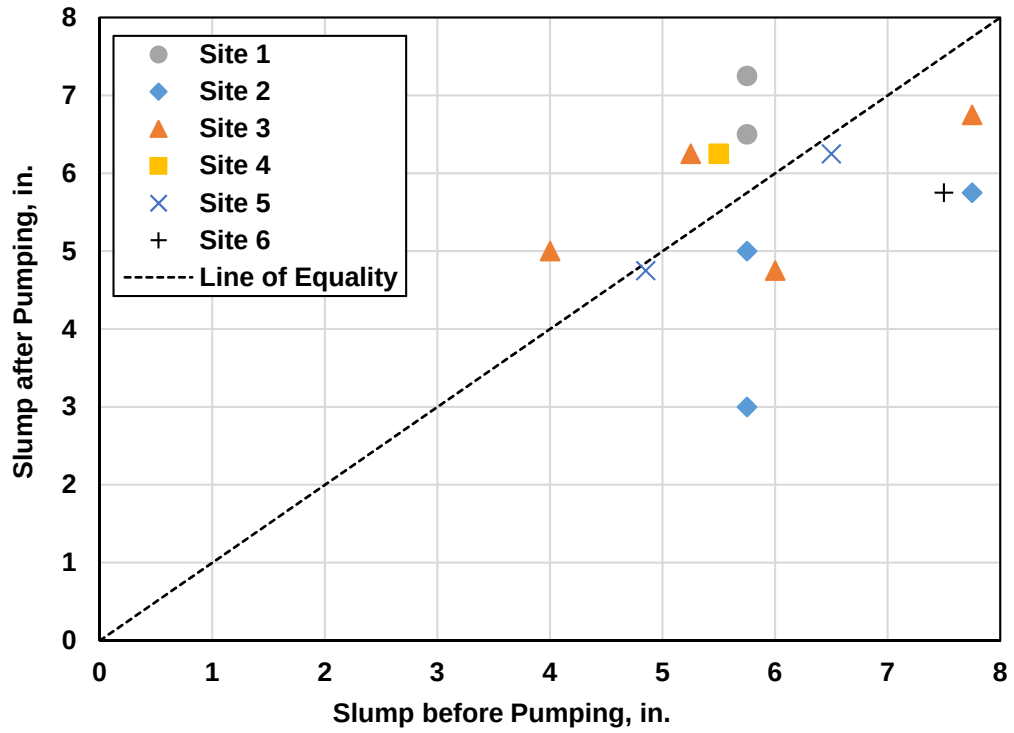

Figure 6.1 – Slump before and after pumping – field investigation

Measured values of temperature after pumping are shown in Figure 6.2. In all but one cases, temperature after pumping increased. On average, increase in concrete temperature after pumping was 3.3°F. However, the measured increase in concrete temperature cannot be solely attributed to pumping as the ambient temperature during the placements was ranging from 75°F to 85°. Hence, the temperature increase was likely due to a combination of pumping and the ambient environmental condition. An increase by 3°F is typically not an issue for standard-size placement, however, for mass concrete placements, even such a small increase in the initial concrete temperature at the point of placement can be a serious concern in terms of specified concrete temperature limits. Therefore, it is essential to carefully consider concrete placement technique and evaluate its effect on the mixture in terms of temperature changes for mass concrete structures.

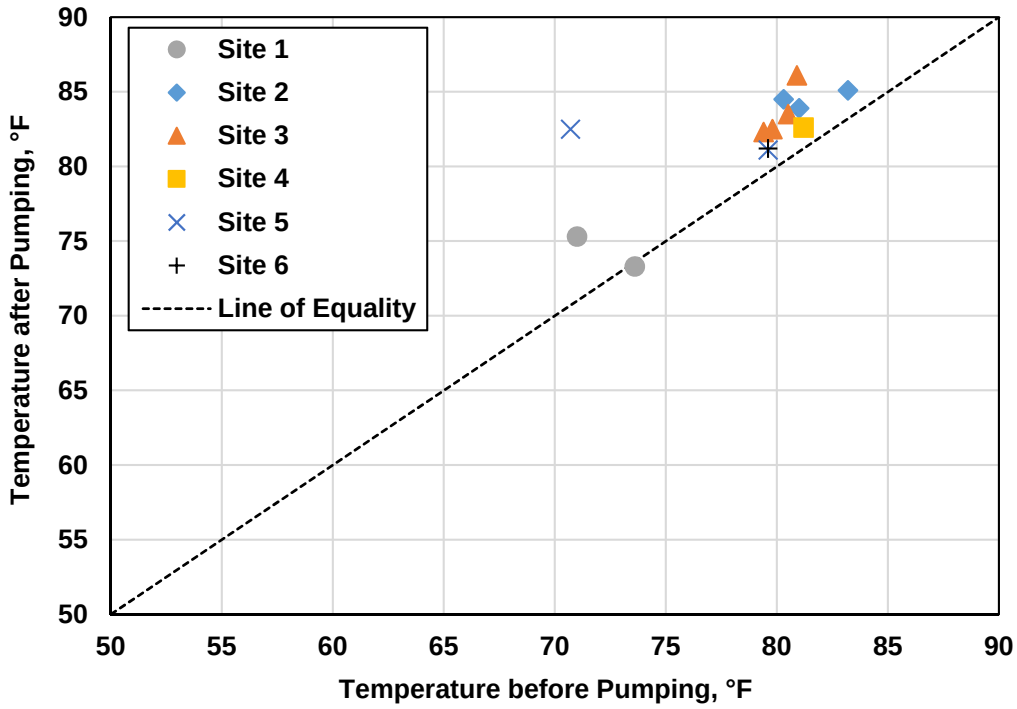

Figure 6.2 – Temperature before and after pumping – field investigation

Changes in concrete plastic air void content and unit weight before and after pumping are presented in Figure 6.3 and Figure 6.4, respectively. Figure 6.5 shows that the measured values of the plastic air void content and unit weight were in a good agreement. In all but two cases (11 out 13), an increase in the total air void content was observed after pumping. On average, 1.5% air gain was observed after pumping. Maximum recorded increase in the air void content value was 3.6% while the smallest recorded increase was 0.8%. The only instance when a decrease in the plastic concrete air void content was observed occurred on Site 2. The concrete mixture used on Site 2 utilized an air-entraining admixture (AEA) produced by a different manufacturer than the AEA that was used in mixtures evaluated on other field sites. Additionally, bridge deck placements on the SLT project (i.e. all field sites but Site 2) were generally greater in terms of their depth compared to the Site 2 placement, which was only 8.5 in.-thick. It is therefore hypothesized that the formwork geometrical conditions at all field sites except Site 2 allowed the

pumped mass of concrete interact with the fresh concrete that has been previously placed to the formwork. During the discharge, concrete with relatively high velocity (compared to the concrete at rest already placed in the formwork) creates flow conditions comparable to the conditions in a concrete mixer. This allows pumped concrete to be re-mixed while entrapping/entraining additional air, which likely helps to overcome the air loss that occurred in the pipeline. Additionally, plastic concrete present in the formwork can act as a cushion to absorb a portion of the kinetic energy of the discharged concrete, thereby reducing the effect of impact that is associated with air loss in pumped concrete. This hypothesis can be further expanded when comparing results obtained from the full-scale experiment described in Chapter 5 and data obtained through the field investigation. For both experimental and field sites, similar concrete pumps in terms of boom length and pipe size were used. Also, the field pump boom configuration varied between the "flat" and "A" setups, which was similar to the full-scale experiment. Moreover, similar concrete mixtures in terms of their proportion characteristics (total cementitious content, partial replacement of portland cement with supplementary cementitious materials, w/cm) were utilized in both the full-scale experiment and the field investigation. The only major difference between the field and experimental sites were the placement conditions. As opposed to discharging concrete directly onto the ground as done during the full-scale experiment (i.e. high impact force of pumped concrete when discharged and very little or no remixing action), pumped concrete was placed into a relatively deep formwork at all field sites but Site 2, which corresponds to at all field sites where air gain after pumping was recorded. Therefore, it appears that this hypothesis is valid, and although more experimental and analytical work is warranted to confirm this concept, it is apparent that the discharge conditions during concrete pumping play significant role in terms of changes in concrete properties.

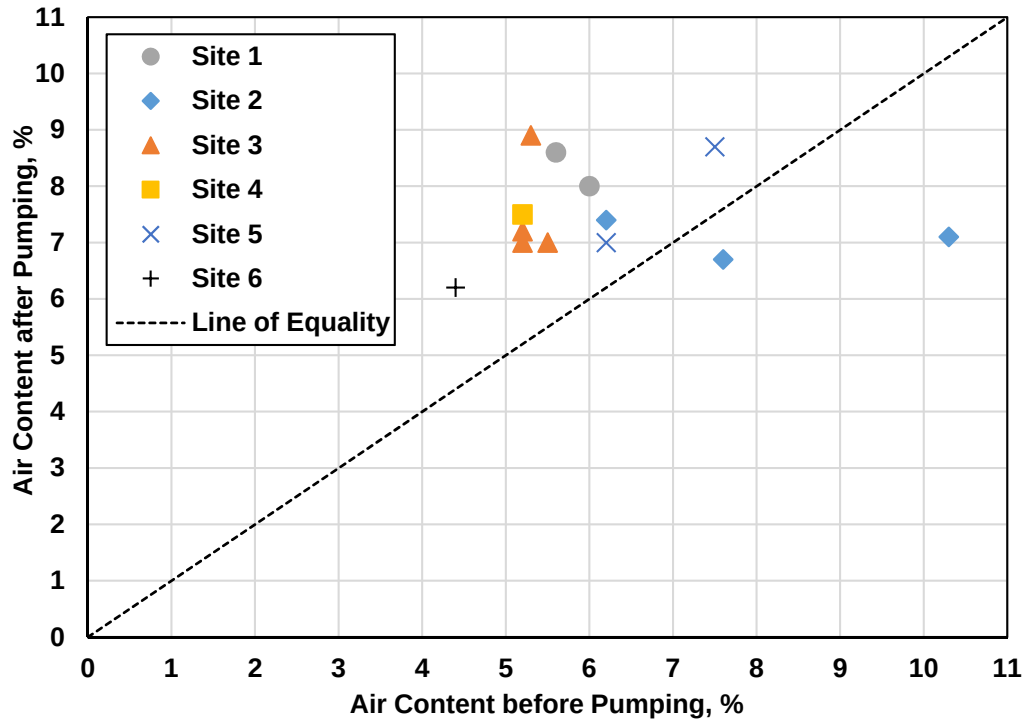

Figure 6.3 – Plastic air content before and after pumping – field investigation

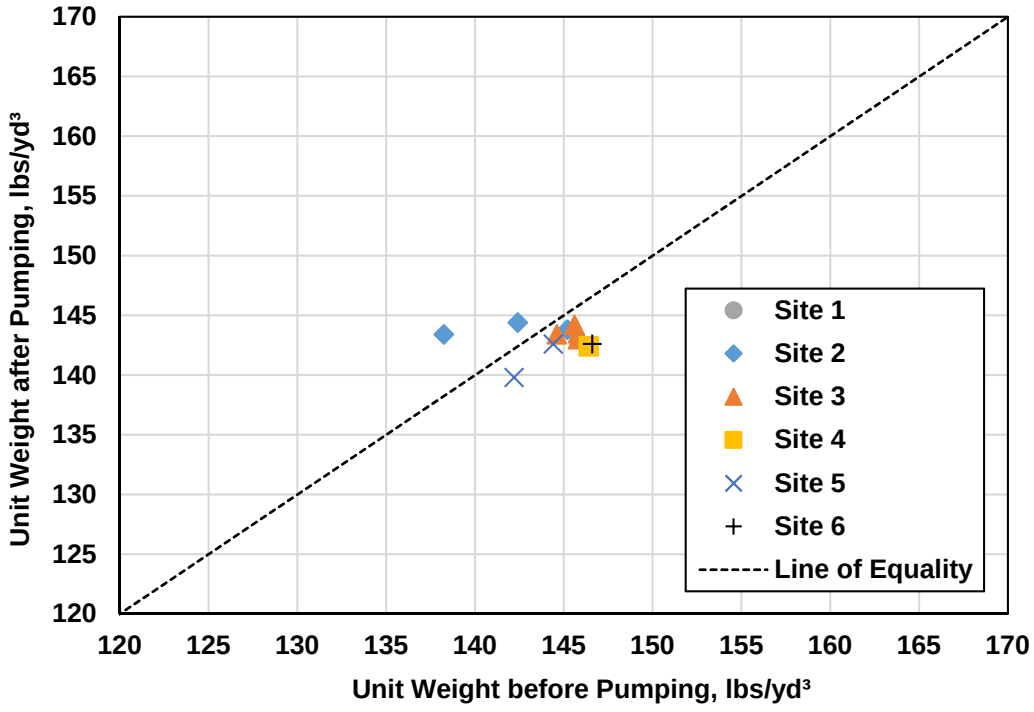

Figure 6.4 – Unit weight before and after pumping – field investigation

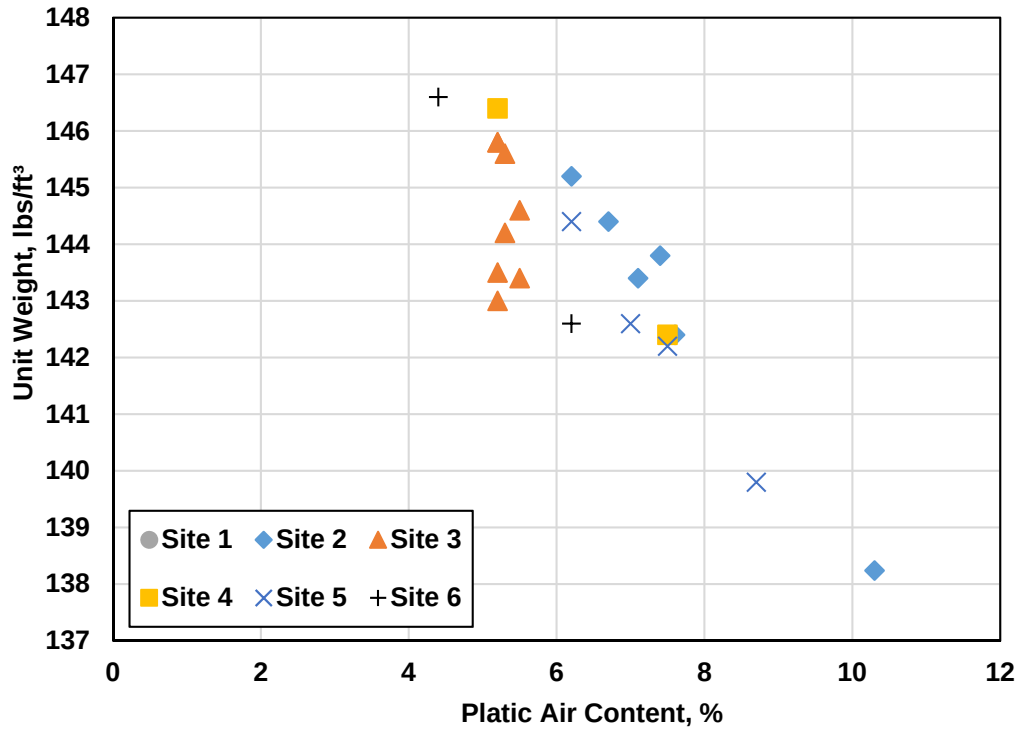

Figure 6.5 – Unit weight vs plastic air content – field investigation

Hardened air void content of concrete before and after pumping is shown in Figure 6.6. Measured values of hardened air void content corresponded well with the values of plastic air void content, similar behavior was observed during the full-scale pumping experiment. On average, the difference between the plastic air void content and the hardened air void content was only 0.8%.

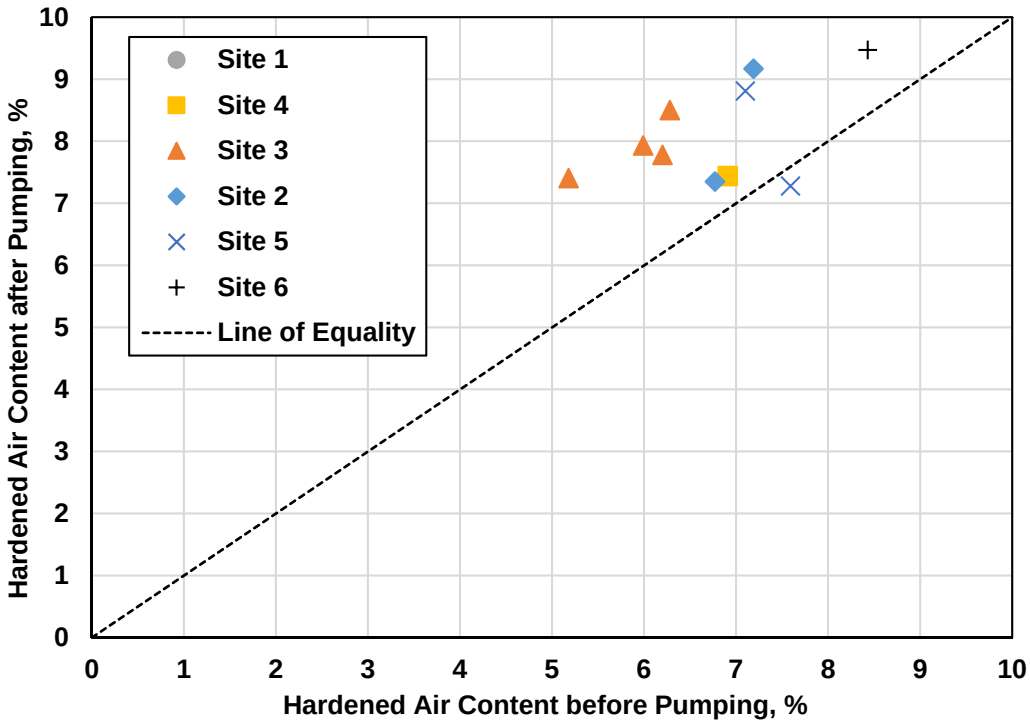

Figure 6.6 – Hardened air content before and after pumping – field investigation

Values of spacing factor for concrete before and after pumping are presented in Figure 6.7. Although an increase in the air void content was measured for all but one sample throughout the data set, an increase in the spacing factor was observed in four instances. Therefore, it is evident that for these four instances, the air void system after pumping was coarser than before pumping. It was not expected to observe the very variable behavior of the air void system after pumping in the field. Since all field mixtures were very similar, the same pumping equipment was used, and the pumping conditions were consistent throughout the project (except Site 2), one would expect that the spacing factor change would consistent throughout the field campaign. Based on previously discussed results, it appears that the discharge conditions in the formwork can play a significant role in terms of the air void system alteration after pumping. As concrete is discharged into the formwork, concrete remixing can occur, allowing for entrainment of

additional air voids in the system. This process can result in an increase the total air void content, as observed in all but one instances of the job site testing program. The increase in the air void content will be very likely accompanied by decrease in the spacing factor value due to greater total air void content translating into higher specific surface (assuming the air void size distribution has not changed significantly). However, if this secondary mixing phase is not present, or relatively large air voids are entrapped during the remixing process without entraining smaller air voids, a decrease in the specific surface of the air void system can be expected, thereby causing the spacing factor to increase after pumping.

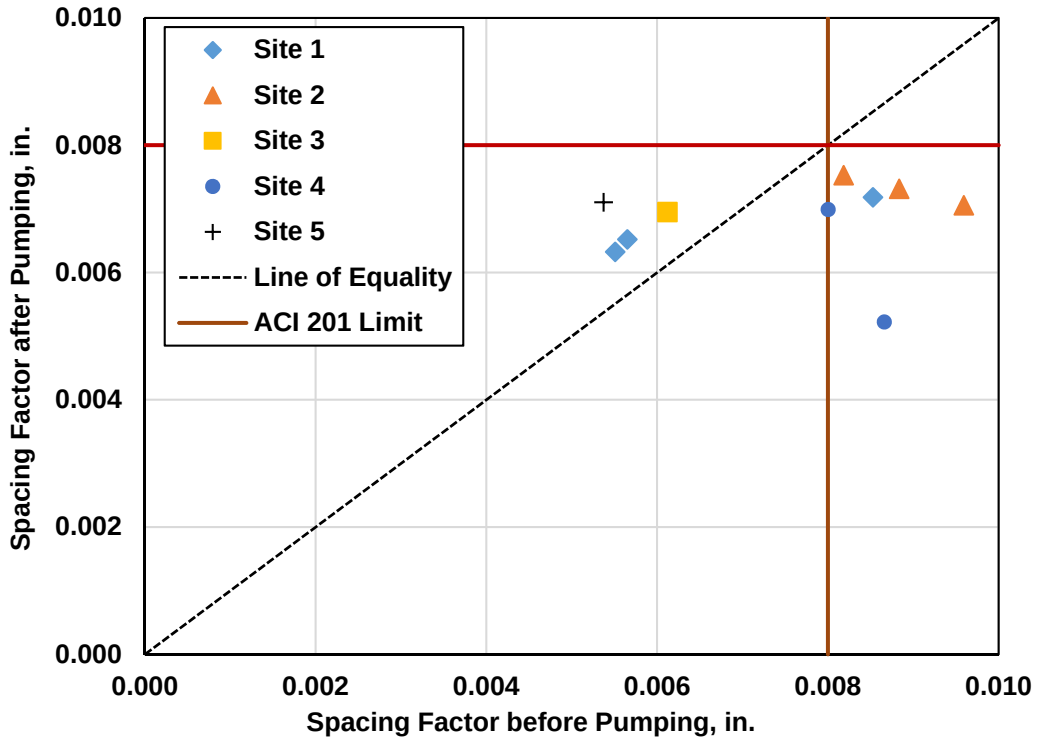

Figure 6.7 – Spacing factor before and after pumping – field investigation

Results of the SAM testing are shown in Figure 6.8. It is apparent from the results that in 5 out of 11 cases, the SAM number increased after pumping whereas in 6 cases, a decrease in the SAM value was recorded. Additionally, the complete set of data for the SAM testing from both

the full-scale pumping experiment and field investigation is shown in Figure 6.9. The SAM test was always conducted in parallel with measuring the fresh air void content, always before and after pumping. This test is proposed by the manufacturer of the device as a replacement of the hardened air void analysis for quality control and assurance in the field. As per the manufacturer's recommendation, the SAM value of 0.20 should be used as concrete acceptance limit for freeze-thaw durability. A total of 35 SAM tests were performed; 15 SAM tests for concrete before pumping and 20 tests for pumped concrete. Out of the 15 tests performed on concrete before pumping, in 11 cases (73.3% of the data set), the SAM number agreed with the hardened air void analysis, i.e. the spacing factor value was less than 200 μm and the SAM number was less than 0.20, or vice versa. In 2 cases (13.3%), false-negative result of the SAM test was generated (i.e. spacing factor less than 200 μm and SAM number larger greater than 0.20) and in 2 instances (13.3% of the data set), a false-positive result was generated (i.e. spacing factor greater than 200 μm and SAM number less than 0.20). Based on the obtained results, it can be concluded the SAM tests have shown good agreement with the hardened air void analysis when performed on fresh concrete before pumping. However, for the pumped concrete, 10 out of the 20 tests (50% of the data set) generated a false-negative result, 2 tests (10% of the data set) resulted in a false-positive result and only 8 tests (40% of the data set) showed an agreement between the SAM number and the hardened air void analysis. Therefore, if the SAM test was used as a quality tool in the field for pumped concrete, 60% of mixtures would be either accepted while exceeding the upper limit value of the spacing or rejected while compliant with the spacing factor limit. Based on the obtained data, it is apparent that further research and validation of this test method is needed before employing the SAM test as a quality control tool for pumped concrete.

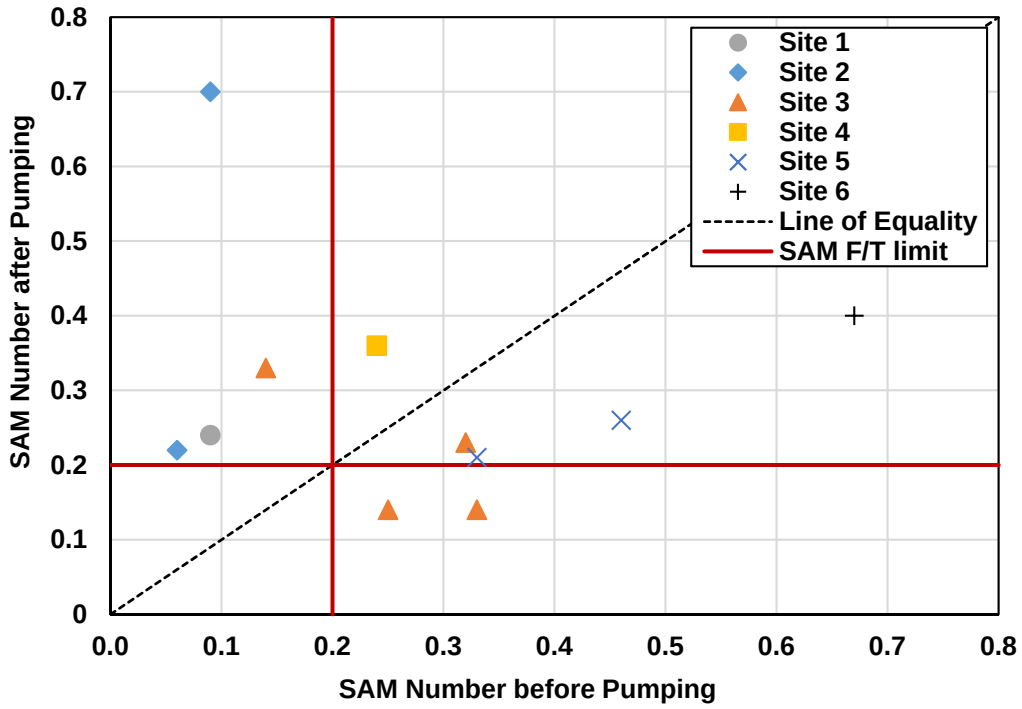

Figure 6.8 – SAM number before and after pumping – field investigation

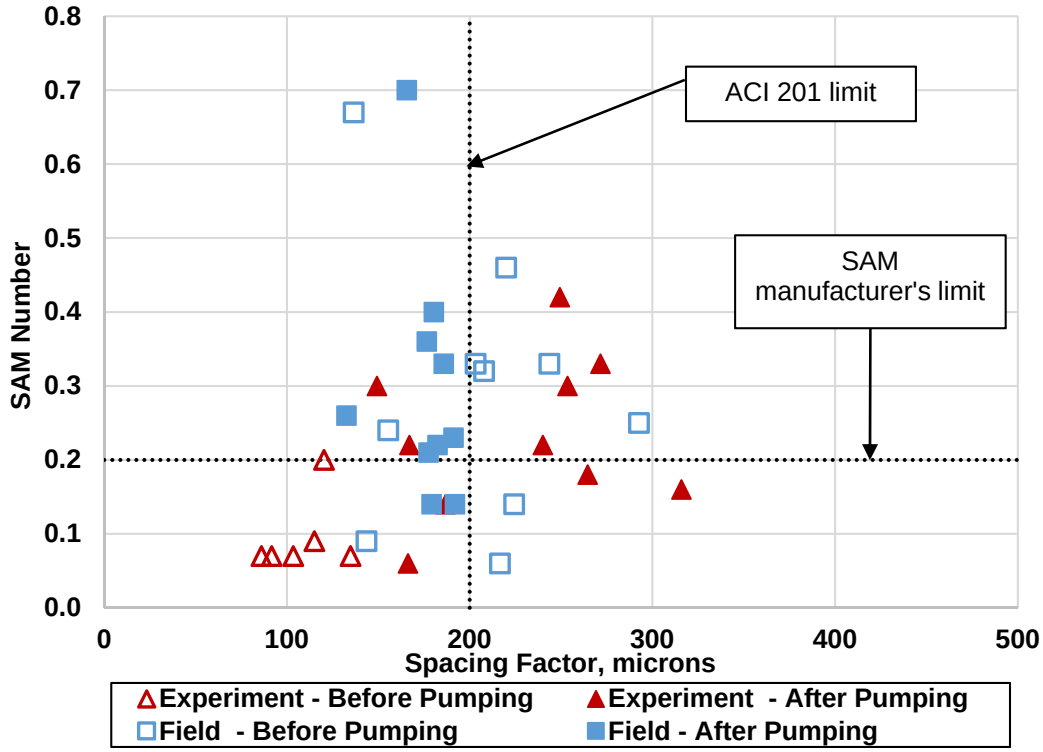

Figure 6.9 – SAM number before and after pumping – full-scale experiment and field investigation

Figure 6.10, Figure 6.11 and Figure 6.12 show yield stress, plastic viscosity and viscous constant, respectively, before and after pumping. No particular trend was observed in terms of a property change for yield stress, plastic viscosity or viscous constant due to pumping. Similarly, to changes observed during the full-scale experiment described in Chapter 5, it is likely that the magnitude of change for rheological properties depends on the time from mixing, aggregate moisture content before mixing, pumping pressure, and admixtures used. The value of yield stress remained the same or decreased for all but two mixes, whereas the plastic viscosity and viscous constant decreased in approximately half of the cases. Additionally, the precision and accuracy of conducted rheological testing was reduced in the field conditions. As two sets of concretes (before and after pumping) had to be tested at the same time, concrete after pumping was generally tested 10 to 15 minutes after the test on concrete before pumping was conducted. This could have possibly resulted in slightly changed rheological properties of pumped concrete due to the stiffening effect caused by structural build-up and concrete hydration.

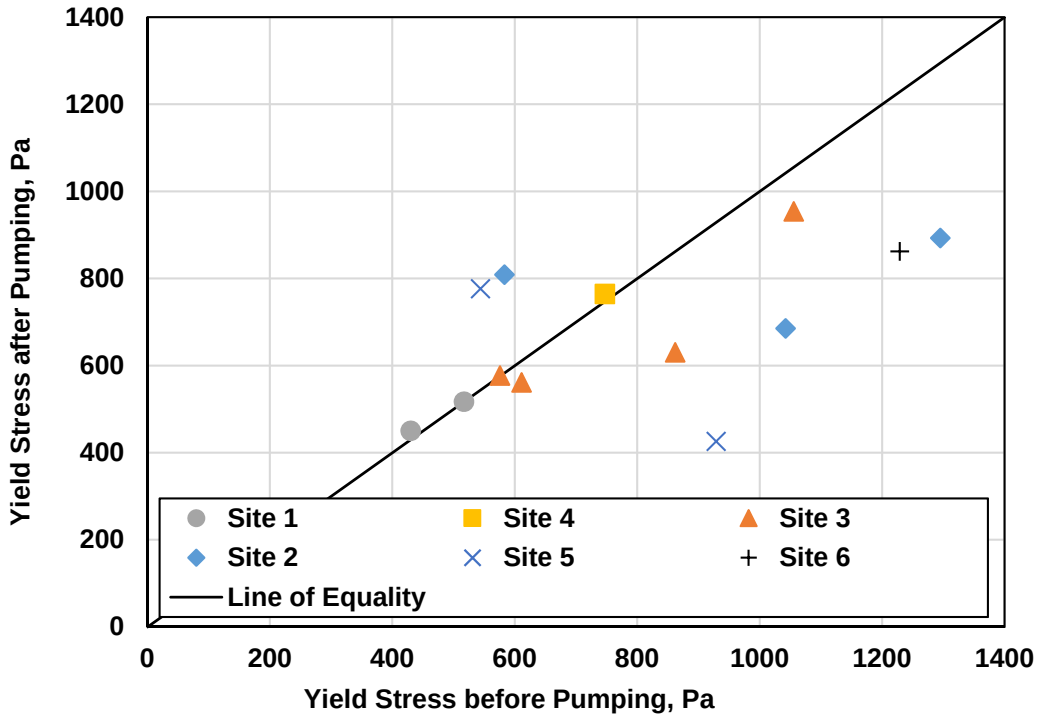

Figure 6.10 – Yield stress before and after pumping – field investigation

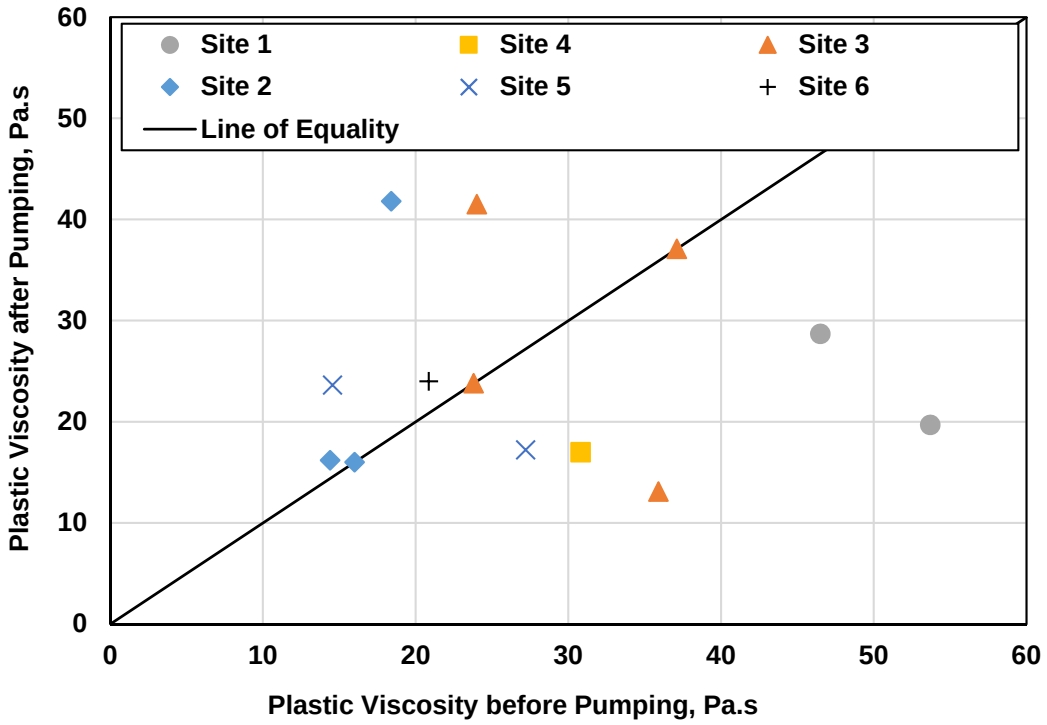

Figure 6.11 – Plastic viscosity before and after pumping – field investigation

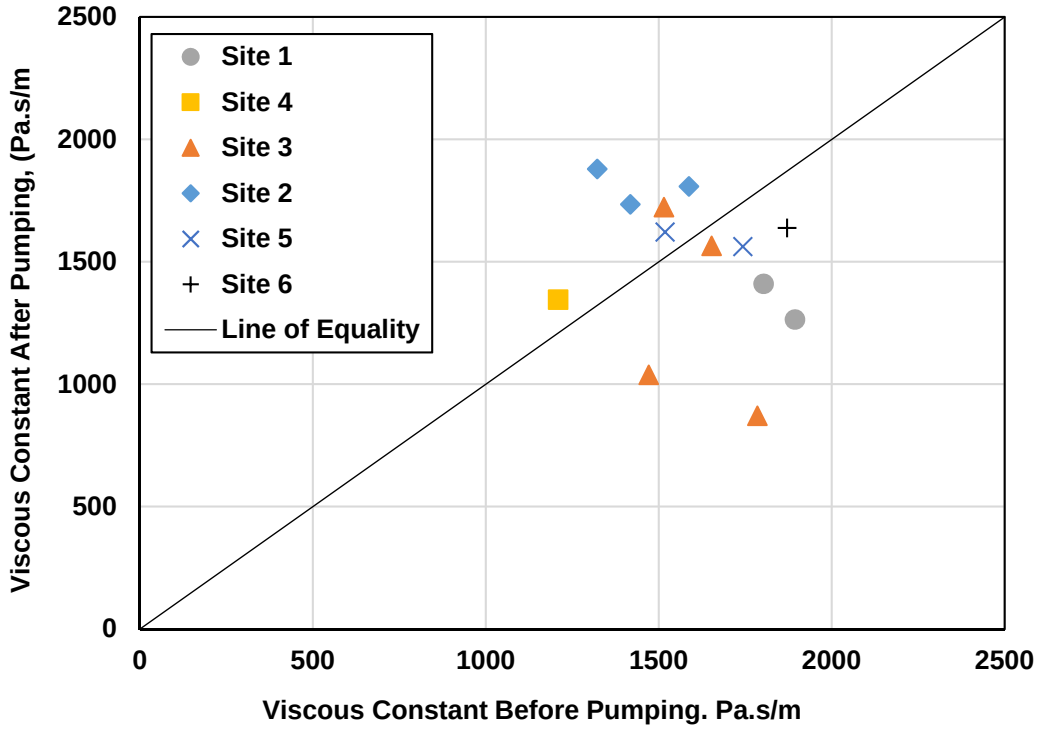

Figure 6.12 – Viscous constant before and after pumping – field investigation

6.4 Conclusions

In this chapter, a field investigation study on concrete pumping was described. As part of this study, six construction sites were visited during bridge deck placements and concrete before and after pumping was evaluated.

In all cases, workability of investigated concrete mixtures was changed due to pumping. Both increase and decrease in slump, yield stress and plastic viscosity of concrete after pumping was observed. No particular trends in workability changes were observed, hence it appears that the variables that affect workability changes due to pumping are complex and related to both particular concrete mixture proportions and pumping conditions.

Changes in the air void system due to pumping were dissimilar from changes observed during the full-scale experiment. Based on the analyzed data, it appears that the discharge conditions during concrete pumping, particularly the cushion effect of existing concrete in the formwork and the re-mixing effect due to flow of the discharged concrete, can both offset the air loss that occurs in the pipeline and entrain and entrap additional air bubbles in the mixture.

Lastly, the Super Air Meter was utilized to characterize the air void system of investigated CVC mixtures. Our results indicated that for significantly large number of tests, the SAM test produced either false-positive or false-negative results. Therefore, further research is needed before this test method can be implanted as a field quality control tool for pumped concrete.

Chapter 7 - Conclusions

A research program was conducted to improve the existing methodology of rheological characterization of the lubrication layer formed during pumping, evaluate the effect of concrete mixture constituents and proportioning on rheological properties of concrete and the lubrication layer, asses the effect of pumping and pumping pressure on concrete fresh properties and the air void system under controlled conditions, and to evaluate the effect of pumping on concrete fresh properties and the air void system in the field conditions. Based on the findings obtained from this research program, the following conclusions were made:

- The proposed correction procedure for interface rheology assessment was found to be a feasible way to determine the 3D flow effect caused by bottom of the interface rheometer cylinder during rheological characterization of the lubrication layer. The overall accuracy of the method was satisfactory, however, in several instances, the correction procedure delivered results (i.e. negative values of torque corresponding to the cylinder bottom contribution to the measurements) that did not agree with the physical sense of the method.
- The overall effect of the bottom of the cylinder on the values of viscous constant were relatively low, on average less than 10%.
- Limitations of the correction procedure were assessed, and it was concluded that stiffening of the concrete mixture during the correction procedure process, the accuracy and sensitivity of the torque sensor, and the accuracy of filling high measurements were the primary factors effecting precision of the correction method. Mitigation strategies to minimize these effects were proposed.
- No correlation between yield stress were found to affect the slope of the T-N curve, i.e. the magnitude of the torque attributed to the effect of the bottom of the cylinder. A weak

correlation was found between the T-N curve slope and plastic viscosity for interface rheometers with cone-shaped cylinders, however, further experimental evaluation is warranted to confirm the hypothesis that the cylinder bottom effect is direct relationship with concrete plastic viscosity.

- The consistency of interface rheology measurements and the correction procedure was better for cone-shaped cylinders. The angle between the horizontal plane of the cylinder and height of the conical part of the cylinder were found to have an influence on the overall magnitude of the cylinder bottom effect.
- Interface rheometer originally designed to be used primarily for SCC mixtures can be successfully employed for lubrication layer characterization of conventional concrete mixtures.
- A strong influence of air void content on rheological properties as well as properties of the lubrication layer was observed. Since air void content of concrete mixtures is not constant in the field, and typically varies within the specified range for different concrete loads, it is important to consider the effect of this variation when one attempts to measure rheological properties and characterize the lubrication layer of concrete mixtures, and especially when results are used for further analysis or modeling.
- In general, trends observed in rheological properties of the lubrication layer due to modifications of mixture proportions corresponded to changes that occurred in rheological properties of the whole mixture. This was true for all investigated mixture parameters (i.e. air void content, cement content, use of fly ash, water content, FA/CA ratio, use of VMA, and use of clay particles) except coarse aggregate shape.

- The overall magnitude of change in viscous constant and interface yield stress did not always correspond to the magnitude of change in the respective concrete rheological properties, i.e. plastic viscosity and yield stress. Presented results suggested that the rheological properties of the lubrication layer are not only influenced by the rheological changes of cement paste but also by the overall ability of the system to form the lubrication layer. It appears that changes in concrete constituents can result in changes in composition of the lubrication layer and its thickness. However, further research that would investigate true composition of the lubrication layer as well as an accurate technique for measuring lubrication layer thickness are needed.
- Measured rheological properties of the lubrication layer and concrete rheological properties can be utilized in pumping models to predict and evaluate adjustments in mixture proportions and their effect on concrete pumpability. In this work, Kaplan's pumping model was used to evaluate various mixture modifications. It was found that changes in predicted pumping pressures ranging from 5% up to 50% can be achieved by adjusting one individual parameter of concrete mixture.
- It is not recommended to rely on increasing the air void content of fresh concrete to reduce the pumping pressure since the behavior of the air void system under pressure is not well understood. Therefore, it is not entirely clear as to what is the real effect of the air content on rheological properties of concrete during the pumping operation.
- It was demonstrated that the use of stain gauges as an indirect method of monitoring pumping pressure is a viable option for standard job site concrete pumps. Furthermore, it has been shown that a linear relationship exists between pumping pressure and the flow rate of pumped concrete. Based on obtained pumping pressure values, it was determined that the

pumping pressure for a constant flow rate of concrete will be higher when the pump boom is oriented in the "flat" configuration, i.e. with the boom in a full horizontal extension.

- Pumping can significantly affect concrete fresh properties. During this testing program, decrease in slump, air content, increase in plastic viscosity, and both increase and decrease in yield stress was observed after pumping.
- No relationship between the air loss and pumping pressure or flow rate was detected. Moreover, the results of the total air void measurements in both plastic and hardened state were in general agreement, proving that nearly all air dissolved during the pumping process reappears rapidly after the pressure is relieved.
- The spacing factor increased after pumping. It was determined that the change in the spacing factor is primarily driven by the air loss, and that the air void system structure, in terms of air void size distribution, was not significantly affected by the pumping process. Moreover, significant amount of air voids with diameter less than 50 μm was detected in after-pumping hardened air void samples. Results of the experiment suggests that the changes induced in the air void system, such as total air loss (or gain) and spacing factor change, are not significantly affected by the pumping process and its parameters (pumping pressure, flow rate, boom configuration) but are rather reliant on the characteristics of individual concrete mixture.
- The Super Air Meter was utilized to characterize the air void system of investigated mixtures. The results indicated that for significantly large number of tests, the SAM test produced either false-positive or false-negative results for pumped concrete. Therefore, further research is needed before this test method can be implanted as a field quality control tool for pumped concrete.

References

[1] United States Geological Survey, “Mineral Commodity Summaries 2017,” 2017.

[2] ACI Committee 304, “Guide for Measuring, Mixing, Transporting, and Placing Concrete,” *ACI 304R-00*. American Concrete Institute, Farmington Hills, MI, p. 49, 2000.

[3] R. Sonnenberg, “From the Handcart to the Concrete Pump – Development of Readymix Concrete Conveying,” *Putzmeister Post - 50 Years of Putzmeister*, Aichtal, Germany, p. 72, 2008.

[4] C. A. Cornell and S. E. McKee, “Concrete Pump,” 1 093 916, 1914.

[5] ACI Committee 304, “Placing Concrete by Pumping Methods,” *304.2R-96*. American Concrete Institute, Farmington Hills, MI, p. 25, 1996.

[6] T. H. Cooke, *Concrete Pumping and Spraying: A Practical Guide*. Thomas Telford, 1990.

[7] B. Orchard, “New Heights Reached in Concrete Pumping,” *World Pumps*, no. September, pp. 18–19, 2009.

[8] Wam, “Dubai breaks Guinness record for largest continuous concrete pour,” *Emirates247.com*, 2017. [Online]. Available: http://www.emirates247.com/news/emirates/dubai-breaks-guinness-record-for-largest-continuous-concrete-pour-2017-09-12-1.658935. [Accessed: 01-Jan-2018].

[9] ACI Committee 304, “304.2R-17: Guide to Placing Concrete by Pumping Methods.” American Concrete Institute, Farmington Hills, MI, 2017.

[10] S. Jacobsen, L. Haugan, T. A. Hammer, and E. Kalogiannidis, “Flow conditions of fresh mortar and concrete in different pipes,” *Cem. Concr. Res.*, vol. 39, no. 11, pp. 997–1006, Nov. 2009.

[11] R. Khatib, “Analysis and Prediction of Pumping Characteristics of High-Strength Self-

Consolidating Concrete, PhD thesis," Universite de Sherbrooke, 2013.

[12] Putzmeister, "World's Largest Concrete Boom Pump Reaches Success on Historic Project," *Company Website*, 2009. [Online]. Available: http://www.putzmeisteramerica.com/news/job-stories/Worlds-Largest-Concrete-Boom-Pump-Reaches-Success-on-Historic-Project.

[13] D. Feys, K. H. Khayat, and R. Khatib, "How do concrete rheology, tribology, flow rate and pipe radius influence pumping pressure?," *Cem. Concr. Compos.*, vol. 66, 2016.

[14] T. S. Fisher, "How A Concrete Pump Works," *Publication #C940629*. The Aberdeen Group, 1994.

[15] Schwing America, "Rock Valve," *Trademark*. 1998.

[16] F. C. Wilson, "Ball-valve concrete pumps." The Aberdeen Group, 1988.

[17] Construction Forms Inc, "Conforms Catalog." Conforms, Port Washington, WI, p. 55, 2014.

[18] Putzmeister, "Catalogue 2017/2018." Putzmeister, Aichtal, Germany, p. 74, 2017.

[19] American Concrete Pumping Association, "Double S-Bend Elbow or 'Rams Horn' Can Be Deadly…," 2009.

[20] The British Society of Rheology, "Definitions." [Online]. Available: http://www.bsr.org.uk/definitions.asp. [Accessed: 01-May-2018].

[21] M. Reiner, "The Deborah Number," *Phys. Today*, vol. 17, no. 1, p. 62, Jan. 1964.

[22] P. Banfill, "Rheology of fresh cement and concrete," *Rheol. Rev.*, vol. 2006, pp. 61–130, 2006.

[23] P. Coussot, "Introduction to the Rheology of Complex Fluids," in *Understanding the Rheology of Concrete*, N. Roussel, Ed. Cambridge, UK: Woodhead Publishing, 2012, pp.

3–22.

[24] H. A. Barnes and J. F. Hutton, *An Introduction to Rheology*. Elsevier, 1989.

[25] J. E. Wallevik, "Relationship between the Bingham parameters and slump," *Cem. Concr. Res.*, vol. 36, no. 7, pp. 1214–1221, Jul. 2006.

[26] A. D. McNaught and A. Wilkinson, *Compendium of Chemical Terminology: IUPAC Recommendations*. Blackwell Science, 1997.

[27] P. Coussot, *Rheometry of Pastes, Suspensions, and Granular Materials*. Hoboken, NJ, USA: John Wiley & Sons, Inc., 2005.

[28] D. Feys, R. Verhoeven, and G. De Schutter, "Why is fresh self-compacting concrete shear thickening?," *Cem. Concr. Res.*, vol. 39, no. 6, pp. 510–523, 2009.

[29] A. Yahia, "Shear-thickening behavior of high-performance cement grouts - Influencing mix-design parameters," *Cem. Concr. Res.*, vol. 41, no. 3, pp. 230–235, 2011.

[30] H. Li, F. Huang, Y. Xie, Z. Yi, and Z. Wang, "Effect of water–powder ratio on shear thickening response of SCC," *Constr. Build. Mater.*, vol. 131, pp. 585–591, 2017.

[31] E. C. Bingham, "An investigation of the laws of plastic flow," *Bull. Bur. Stand.*, vol. 13, no. 2, p. 309, 1916.

[32] W. H. Herschel and R. Bulkley, "Konsistenzmessungen von Gummi-Benzollösungen," *Colloid Polym. Sci.*, vol. 39, no. 4, pp. 291–300, 1926.

[33] R. E. Robertson and H. A. Stiff, "An Improved Mathematical Model for Relating Shear Stress to Shear Rate in Drilling Fluids and Cement Slurries," *Soc. Pet. Eng. J.*, vol. 16, no. 01, pp. 31–36, 1976.

[34] A. Yahia and K. H. Khayat, "Analytical models for estimating yield stress of high-performance pseudoplastic grout," *Cem. Concr. Res.*, vol. 31, no. 5, pp. 731–738, 2001.

[35] W. Casson, “A flow equation for pigment-oil suspensions of the printing ink type,” in *Rheology of disperse systems*, 1959, p. 21.

[36] D. Quemada, P. Flaud, and P. H. Jezequel, “Rheological Properties and Flow of Concentrated Disperse Media I - Modelling of Steady and Unsteady Behavior,” *Chem. Eng. Commun.*, vol. 32, no. 1–5, 1985.

[37] W. Vom Berg, “Influence of specific surface and concentration of solids upon the flow behaviour of cement pastes,” *Mag. Concr. Res.*, vol. 31, no. 109, pp. 211–216, 1979.

[38] J. Harris, *Rheology and Non-Newtonian Flow*. Longman, 1977.

[39] G. Ovarlez, “Introduction to the rheometry of complex suspensions,” in *Understanding the Rheology of Concrete*, N. Roussel, Ed. Cambridge, UK: Woodhead Publishing, 2012, pp. 23–64.

[40] G. Heirman, L. Vandewalle, D. Van Gemert, and Ó. Wallevik, “Integration approach of the Couette inverse problem of powder type self-compacting concrete in a wide-gap concentric cylinder rheometer,” *J. Nonnewton. Fluid Mech.*, vol. 150, no. 2–3, pp. 93–103, Apr. 2008.

[41] J. E. Ferraris, C. F.; Brower, L. E.; Banfill, P.; Beaupre, D.; Chapdelaine, F.; deLarrard, F.; Domone, P.; Nachbaur, L.; Sedran, T.; Wallevik, O.; Vallevik, “Comparison of Concrete Rheometers: International Tests at LCPC (Nantes, France) in October 2000.,” Springfield, VA, 2001.

[42] J. E. Wallevik, “Rheology of Particle Suspension: Fresh Concrete, Mortar and Cement Paste with Various Types of Lignosulfonates,” The Norwegian University of Science and Technology, 2003.

[43] C. W. Macosko, *Rheology: principles, measurements, and applications*. New York, NY:

VCH, 1993.

[44] O. H. Wallevik, D. Feys, J. E. Wallevik, and K. H. Khayat, “Avoiding inaccurate interpretations of rheological measurements for cement-based materials,” *Cem. Concr. Res.*, vol. 78, pp. 100–109, 2015.

[45] M. Reiner and R. Riwlin, “Die Theorie der Strömung einer elastischen Flüssigkeiten Couette-Apparat,” *Colloid Polym. Sci.*, vol. 43, no. 1, 1927.

[46] D. Feys, J. E. Wallevik, A. Yahia, K. H. Khayat, and O. H. Wallevik, “Extension of the Reiner–Riwlin equation to determine modified Bingham parameters measured in coaxial cylinders rheometers,” *Mater. Struct.*, vol. 46, no. 1–2, pp. 289–311, Jul. 2013.

[47] J. E. Wallevik, “Rheological properties of cement paste: Thixotropic behavior and structural breakdown,” *Cem. Concr. Res.*, vol. 39, no. 1, pp. 14–29, Jan. 2009.

[48] J. Punkki, J. Golaszewski, and O. E. Gjørv, “Workability loss of high-strength concrete,” *ACI Mater. J.*, vol. 93, no. 5, pp. 427–431, 1996.

[49] E. Koehler and D. Fowler, “Development of a Portable Rheometer for Fresh Portland Cement Concrete,” 2004.

[50] G. H. Tattersall and P. F. G. Banfill, *The rheology of fresh concrete*. Pitman Advanced Pub. Program, 1983.

[51] D. Beaupre, “Rheology of High Performance Shotcrete,” University of British Columbia, 1994.

[52] D. Feys, “Rheological Properties and Pumping of Self-Compacting Concrete,” Ghent University, 2009.

[53] F. De Larrard, C. Hu, T. Sedran, and J. Szitkar, “A new rheometer for soft-to-fluid fresh concrete,” *ACI Mater. J.*, no. 94, 1997.

[54] E. Koehler and D. Fowler, “A New, Portable Rheometer for Fresh Self-Consolidating Concrete,” *ACI Spec. ...*, pp. 1–21, 2006.

[55] R. Browne and P. Bamforth, “Tests to establish concrete pumpability,” *ACI J. Proc.*, no. 74, pp. 193–203, 1977.

[56] T. Binns, “Pumped concrete,” in *Advanced Concrete Technology 3: Processes*, J. Newman and B. S. Choo, Eds. Butterworth-Heinemann, 2003, p. 704.

[57] L. Hamill, *Understanding Hydraulics*, 3rd ed. Basingstoke, UK: Palgrave Macmillan, 2011.

[58] RILEM TRechnical Committee 222-SCF, “Simulation of Fresh Concrete Flow,” 2014.

[59] D. Feys, G. De Schutter, and R. Verhoeven, “Parameters influencing pressure during pumping of self-compacting concrete,” *Mater. Struct.*, vol. 46, no. 4, pp. 533–555, Jul. 2012.

[60] S. P. Sutera and R. Skalak, “The History of Poiseuille Law,” *Annu. Rev. Fluid Mech.*, vol. 25, p. 1, 1993.

[61] E. Buckingham, “On Plastic Flow through Capillary Tubes,” *ASTM Proc.*, vol. 21, pp. 1154–1157, 1921.

[62] D. Feys, “Understanding the pumping of conventional vibrated and self-compacting concrete,” in *Understanding the Rheology of Concrete*, N. Roussel, Ed. Cambridge, UK: Woodhead Publishing, 2012, pp. 351–363.

[63] F. Chapdelaine, “Etude Fondamentale et Pratique sur le Pompage du Beton,” University of Laval, 2007.

[64] D. Kaplan, “Pompage des Bétons,” Laboratoire Central des Ponts et Chausees, Paris, 2001.

[65] D. Kaplan, F. De Larrard, and T. Sedran, “Design of Concrete Pumping Circuit,” *ACI Mater. J.*, vol. 102, no. 2, pp. 110–117, 2005.

[66] D. Feys, K. H. Khayat, A. Perez-Schell, and R. Khatib, “Development of a tribometer to characterize lubrication layer properties of self-consolidating concrete,” *Cem. Concr. Compos.*, vol. 54, pp. 40–52, Nov. 2014.

[67] S. Kwon, C. Park, J. Jeong, S. Jo, and S. Lee, “Prediction of Concrete Pumping: Part I—Development of New Tribometer for Analysis of Lubricating Layer,” *ACI Mater. J.*, no. 110, pp. 647–656, 2013.

[68] C. F. Ball, “Concrete By Pump And Pipeline,” *ACI J. Proc.*, no. 333, pp. 333–349, 1936.

[69] S. Morinaga, “Pumpability of concrete and pumping pressure in pipelines,” in *RILEM Seminar - Fresh concrete: Important properties and their measurement*, 1973, p. 7.1-1 to 7.3-39.

[70] M. Choi, N. Roussel, Y. Kim, and J. Kim, “Lubrication layer properties during concrete pumping,” *Cem. Concr. Res.*, vol. 45, pp. 69–78, Mar. 2013.

[71] S. D. Jo, C. K. Park, J. H. Jeong, S. H. Lee, and S. H. Kwon, “A computational approach to estimating a lubricating layer in concrete pumping,” *Comput. Mater. Contin.*, vol. 27, no. 3, pp. 189–210, 2012.

[72] T. Sedran and F. DeLarrand, “Mix design of Self Compacting Concrete,” in *Proceedings of the International RILEM Conference on Production Methods and Workability of Concrete*, 1996, pp. 439–450.

[73] V. Mechtcherine, V. N. Nerella, and K. Kasten, “Testing pumpability of concrete using Sliding Pipe Rheometer,” *Constr. Build. Mater.*, vol. 53, pp. 312–323, 2014.

[74] M. S. Choi, Y. J. Kim, and S. H. Kwon, “Prediction on pipe flow of pumped concrete

based on shear-induced particle migration," *Cem. Concr. Res.*, vol. 52, pp. 216–224, Oct. 2013.

[75] T. T. Ngo, E. H. Kadri, R. Bennacer, and F. Cussigh, "Use of tribometer to estimate interface friction and concrete boundary layer composition during the fluid concrete pumping," *Constr. Build. Mater.*, vol. 24, no. 7, pp. 1253–1261, Jul. 2010.

[76] C. T. Mai, E. H. Kadri, T. T. Ngo, A. Kaci, and M. Riche, "Estimation of the pumping pressure from concrete composition based on the identified tribological parameters," *Adv. Mater. Sci. Eng.*, vol. 2014, 2014.

[77] G. De Schutter and D. Feys, "Pumping of Fresh Concrete: Insights and Challenges," *RILEM Tech. Lett.*, no. 1, pp. 76–80, 2016.

[78] J. F. Best and R. O. Lane, *Testing for Optimum Pumpability of Concrete*, vol. 2, no. 10. 1980, pp. 9–17.

[79] D. Kaplan, F. De Larrard, and T. Sedran, "Avoidance of blockages in concrete pumping process," *ACI Mater. J.*, vol. 102, no. 2, pp. 183–191, 2005.

[80] S. Jacobsen, J. H. Mork, S. F. Lee, and L. Haugan, "Pumping of Concrete and Mortar – State of the Art," *sintefgroup.com*, p. 46, 2008.

[81] K. E. von Eckardstein, *Pumping Concrete and Concrete Pumps*. Herne, Germany: Friedrich Wilh. Schwing GmbH, 1983.

[82] M. Choi, C. F. Ferraris, N. S. Martys, D. Lootens, V. K. Bui, and H. R. T. Hamilton, "Metrology Needs for Predicting Concrete Pumpability," *Adv. Mater. Sci. Eng.*, vol. 2015, p. 10, 2015.

[83] M. S. Choi, Y. S. Kim, J. H. Kim, J. S. Kim, and S. H. Kwon, "Effects of an externally imposed electromagnetic field on the formation of a lubrication layer in concrete

pumping," *Constr. Build. Mater.*, vol. 61, pp. 18–23, 2014.

[84] ACI Committee 238, "Report on Measurements of Workability and Rheology of Fresh Concrete," Farmington Hills, MI, 2008.

[85] J. E. Gray, "Laboratory Procedure for Comparing Pumpability of Concrete Mixtures," *ASTM Proceeding*, vol. 62, pp. 964–971, 1962.

[86] "ASTM C173 / C173M - 16 Standard Test Method for Air Content of Freshly Mixed Concrete by the Volumetric Method." ASTM International, West Conshohocken, PA, 2016.

[87] N. Yazdani, M. Bergin, and G. Majtaba, "Effect of pumping on properties of bridge concrete," *J. Mater. Civ. Eng.*, no. 08, pp. 212–219, 2000.

[88] N. Ghafoori and H. Diawara, "Pumping influence on fresh properties of self-consolidating concrete," in *Concrete Solutions*, 2011, pp. 233–236.

[89] ACI Committee 301, "301-16 Specifications for structural concrete." American Concrete Institute, Farmington Hills, MI, p. 64, 2016.

[90] American Concrete Pumping Association, "A guide to understanding the qualities of concrete and how they affect pumping." p. 8, 2008.

[91] K. Hover, "Investigating Effects of Concrete Handling on Air Content," *Concr. Constr.*, no. September, pp. 745–750, 1995.

[92] R. Pleau, M. Pigeon, A. Lamontagne, and M. Lessard, "Influence of Pumping on Characteristics of Air-Void System of High-Performance Concrete," *Transp. Res. Rec.*, no. 1478, pp. 30–36, 1995.

[93] J. Yingling, G. M. Mullings, and R. D. Gaynor, "Loss of Air Content in Pumped Concrete," *Concr. Int.*, no. October, pp. 57–61, 1992.

[94] R. V. Macha, D. G. Zollinger, and R. Szecsy, “Examination of Air Entertainment Stability Factors of Pumped Concrete,” Texas Transportation Institute, Austin, TX, 1994.

[95] Tennessee Department of Transportation, “Evaluation Of The Changes In Air Content In Concrete Due To Pumping,” Nashville, TN, 2003.

[96] C. F. Scholer and J. Grossman, “Controlling Air Content in Concrete That is Being Pumped, A Synthetis Study,” 1998.

[97] D. A. Whiting and M. A. Nagi, *Manual on Control of Air Content in Concrete*. Skokie, Illinois: Portland Cement Association, 1998.

[98] M. Pigeon, J. Marchand, and R. Pleau, “Frost Resistant Concrete,” *Constr. Build. Mater.*, vol. 10, no. 5, pp. 339–348, 1996.

[99] M. Jolin, D. Burns, B. Bissonnette, F. Gagnon, and L. Bolduc, “Understanding the Pumpability of Concrete,” in *Proceedings Shotcrete for Underground Support XI*, 2009.

[100] M. . Dyer, “An investigation of concrete pumping and effects of pressure on the air void systeme of concrete,” University of Washington, 1991.

[101] W. Elkey, D. J. Janssen, and K. C. Hover, “Concrete Pumping Effects on Entrained Air Voids,” Washington State Transportation Center (TRAC), Seattle, WA, 1994.

[102] H. Kwon, C. K. Park, J. H. Jeong, S. D. Jo, and S. H. Lee, “Prediction of Concrete Pumping : Part II — Analytical Prediction and Experimental Verification,” *ACI Mater. J.*, no. 110, 2014.

[103] D. Feys, G. De Schutter, K. H. Khayat, and R. Verhoeven, “Changes in rheology of self-consolidating concrete induced by pumping,” *Mater. Struct. Constr.*, vol. 49, no. 11, pp. 4657–4677, 2016.

[104] A. C. Rust and M. Manga, “Effects of bubble deformation on the viscosity of dilute

suspensions," *J. Nonnewton. Fluid Mech.*, vol. 104, pp. 53–63, 2002.

[105] "ASTM C1611 / C1611M-14, Standard Test Method for Slump Flow of Self-Consolidating Concrete." ASTM International, West Conshohocken, PA, 2014.

[106] "ASTM C192 / C192M-14, Standard Practice for Making and Curing Concrete Test Specimens in the Laboratory." ASTM International, West Conshohocken, PA, 2014.

[107] C. F. Ferraris and N. S. Martys, "Relating fresh concrete viscosity measurements from different rheometers," *J. Res. Natl. Inst. Stand. Technol.*, vol. 108, no. 3, p. 229, May 2003.

[108] "ASTM C150 / C150M-15, Standard Specification for Portland Cement." ASTM International, West Conshohocken, PA, 2015.

[109] "ASTM C618-15, Standard Specification for Coal Fly Ash and Raw or Calcined Natural Pozzolan for Use in Concrete." ASTM International, West Conshohocken, PA, 2015.

[110] "ASTM C260 / C260M-10a(2016), Standard Specification for Air-Entraining Admixtures for Concrete." ASTM International, West Conshohocken, PA, 2016.

[111] "ASTM C494 / C494M-16, Standard Specification for Chemical Admixtures for Concrete." ASTM International, West Conshohocken, PA, 2016.

[112] S. Kawashima, M. Chaouche, D. J. Corr, and S. P. Shah, "Influence of purified attapulgite clays on the adhesive properties of cement pastes as measured by the tack test," *Cem. Concr. Compos.*, vol. 48, pp. 35–41, 2014.

[113] "ASTM C143 / C143M-15a, Standard Test Method for Slump of Hydraulic-Cement Concrete." ASTM International, West Conshohocken, PA, 2015.

[114] ASTM C231/C231M – 10, Ed., "Standard Test Method for Air Content of Freshly Mixed Concrete by the Pressure Method," ASTM International, West Conshohocken, PA, 2010.

[115] "ASTM C138 / C138M-16, Standard Test Method for Density (Unit Weight), Yield, and Air Content (Gravimetric) of Concrete." ASTM International, West Conshohocken, PA, 2016.

[116] "ASTM C1064 / C1064M-12, Standard Test Method for Temperature of Freshly Mixed Hydraulic-Cement Concrete." ASTM International, West Conshohocken, PA, 2012.

[117] G. H. Tattersall, *Workability and Quality Control of Concrete*. London: E & FN Spoon, 1991.

[118] O. H. Wallevik and J. E. Wallevik, "Rheology as a tool in concrete science: The use of rheographs and workability boxes," *Cem. Concr. Res.*, vol. 41, no. 12, pp. 1279–1288, Dec. 2011.

[119] L. Geiker, M., Brandl, M., Thrane, L., and Nielsen, "On the Effect of Coarse Aggregate Fraction and Shape on the Rheological Properties of Self-Compacting Concrete," *Cem. Concr. Aggregates*, vol. 24, no. 1, pp. 3–6, 2002.

[120] J. Hu and K. Wang, "Effect of coarse aggregate characteristics on concrete rheology," *Constr. Build. Mater.*, vol. 25, no. 3, pp. 1196–1204, 2011.

[121] R. S. Szecsy, "Concrete Rheology," University of Illinois at Urbana, 1997.

[122] K. C. Hover and R. J. Phares, "Impact of concrete placing method on air content, air-void system parameters, and freeze-thaw durability," no. 1532, pp. 1–8, 1996.

[123] J. Aldred, "Burj Khalifa – a new high for high-performance concrete," *Proc. Inst. Civ. Eng. - Civ. Eng.*, vol. 163, no. 2, pp. 66–73, 2010.

[124] "Schwing pumps concrete for the tallest building in the world," *Schwing Stetter News*, 2015. [Online]. Available: http://www.schwing-stetter.co.uk/Pages/NewsStory.aspx?id=7. [Accessed: 15-Nov-2015].

[125] Kansas Department of Transportation, *Standard Specifications for State Road & Bridge Construction*. 2015.

[126] "ASTM C33 / C33M-16, Standard Specification for Concrete Aggregates." ASTM International, West Conshohocken, PA, 2016.

[127] "AASHTO TP 118-15, Standard Method of Test for Characterization of the Air-Void System of Freshly Mixed Concrete by the Sequential Pressure Method." American Association of State Highway and Transportation Officials, Washington, DC, 2015.

[128] "ASTM C457 / C457M-16, Standard Test Method for Microscopical Determination of Parameters of the Air-Void System in Hardened Concrete." ASTM International, West Conshohocken, PA, 2016.

[129] J. Vosahlik, K. A. Riding, A. Esmaeily, R. Billinger, and H. McLeod, "Effects of Air Void Clustering on Concrete Compressive Strength," *ACI Mater. J.*, vol. 113, no. 6, 2016.

[130] K. Riding, A. Esmaeily, and J. Vosahlik, "Air Void Clustering," Topeka, KS, 2015.

[131] T. C. Powers and T. F. Willis, "The Air Requirement of Frost Resistant Concrete," *Proceedings, Highw. Res. Board, Res. Dev. Lab. Portl. Cem. Assoc.*, vol. 29, no. 33, pp. 184–211, 1949.

[132] Kansas Department of Transportation, "South Lawrence Trafficway - Project Construction Phasing Fact Sheet," 2013. [Online]. Available: https://www.ksdot.org/Assets/wwwksdotorg/bureaus/TopekaMetro/pdf/K-10 SLT Project Construction Phasing Fact Sheet.pdf. [Accessed: 18-Oct-2017].

[133] M. Reiner, "The de Waele–Ostwald Law," *Colloid Polym. Sci.*, vol. 65, no. 1, pp. 44–62, 1933.

[134] W. Ostwald, "Uber die Geschwindigkeitsfunktion der Viskosit at disperser Systeme. I.,"

Colloid Polym. Sci., no. 36, pp. 99–117, 1925.

[135] A. de Waele, "Viscometry and plastometry," *J. Oil Colour Chem*, vol. 6, pp. 33–69, 1923.

[136] R. S. Rivlin, "The hydrodynamics of non—Newtonian fluids Part 1," *Proc. R. Soc. A*\, no. 193, pp. 260–281, 1948.

[137] M. Reiner, "A Mathematical Theory of Dilatancy," *Am. J. Math.*, vol. 67, no. 3, pp. 350–362, 1945.

[138] G. Stokes, "n the Effect of the Internal Friction of Fluids on the Motion of Pendulums," *Trans. Cambridge Philos. Soc.*, vol. 9, p. 8, 1851.

[139] B. Bhushan, *Principles and applications of tribology*. John Wiley, 1999.